Theoretical Notes
Note 347

AFWL-TR-82-40
EMPTD-3-MRC-010
December 1981

TN 347

ELECTROMAGNETIC PULSE TECHNOLOGY DEVELOPMENT PROGRAM

BURIED CONDUCTOR STUDIES

V. A. J. van Lint

J. W. Erler

Prepared For
AIR FORCE WEAPONS LABORATORY
Kirtland Air Force Base, New Mexico 87117

Prepared By
MISSION RESEARCH CORPORATION
1400 San Mateo Blvd. S.E. Suite A
Albuquerque, New Mexico 87108
Contract F29601-78-C-0082

Subtask 03-08, "Buried Conductor Studies"

MRC
LuTech-EMA-RI

UNCLASSIFIED

SECURITY CLASSIFICATION OF THIS PAGE (When Data Entered)

REPORT DOCUMENTATION PAGE		READ INSTRUCTIONS BEFORE COMPLETING FORM
1. REPORT NUMBER AFWL-TR-82-40	2. GOVT ACCESSION NO.	3. RECIPIENT'S CATALOG NUMBER
4. TITLE (and Subtitle) BURIED CONDUCTOR STUDIES		5. TYPE OF REPORT & PERIOD COVERED Final
		6. PERFORMING ORG. REPORT NUMBER MRC/SD-R-93;EMPTD-3-MRC-010
7. AUTHOR(s) Victor A.J. van Lint James W. Erler		8. CONTRACT OR GRANT NUMBER(s) F29601-78-C-0082
9. PERFORMING ORGANIZATION NAME AND ADDRESS MISSION RESEARCH CORPORATION 5434 Ruffin Road San Diego, California 92123		10. PROGRAM ELEMENT PROJECT, TASK AREA & WORK UNIT NUMBERS
11. CONTROLLING OFFICE NAME AND ADDRESS Air Force Weapons Laboratory/NTYET Kirtland Air Force Base New Mexico 87117		12. REPORT DATE December 1981 13. NUMBER OF PAGES 221
14. MONITORING AGENCY NAME & ADDRESS(if different from Controlling Office)		15. SECURITY CLASS (of this report) Unclassified 15a. DECLASSIFICATION DOWNGRADING SCHEDULE

16. DISTRIBUTION STATEMENT (of this Report)

17. DISTRIBUTION STATEMENT (of the abstract entered in Block 20, if different from Report)

18. SUPPLEMENTARY NOTES

19. KEY WORDS (Continue on reverse side if necessary and identify by block number)

Earth breakdown
High voltage

20. ABSTRACT (Continue on reverse side if necessary and identify by block number)

The response of various earth samples to high electric fields was measured in cylindrical geometry. Threshold for electric breakdown, streamer development, and propagation were measured.

DD FORM 1 JAN 73 1473 EDITION OF 1 NOV 65 IS OBSOLETE

UNCLASSIFIED

SECURITY CLASSIFICATION OF THIS PAGE (When Data Entered)

ILLUSTRATIONS

Figure		Page
1	PI experiment sample holder	13
2	McAir experiment sample holder	16
3	McAir Conducting cylinder experiment	17
4	1 mR sample chamber	18
5	Resistor string	20
6	Screen box	22
7	Voltage probe calibration probe C	26
8	Voltage probes installed in 2 m-diameter sample holder	27
9	Voltage profile, 140 VAC, 1500 Ωm sand	37
10	Voltage profile, 1700 Ωm sand	39
11	Voltage profile, 300 Ωm sand mix	40
12	Voltage profile, 140 VAC, 300 Ωm sand mix	41
13	Voltage profile, 300 Ωm sand mix	42
14	Voltage profile, 140 VAC, SDF soil	44
15	Voltage profile, 1200 Ωm SDF soil	45
16	Voltage profile, 140 VAC, MX-B	46
17	Voltage profile, 140 Ωm MX-B soil	47
18	Voltage profile, 140 VAC, MX-B	48
19	Streamer development, 350 Ωm sand mix	50
20	Streamer development, 350 Ωm sand mix	51
21	Streamer development, 350 Ωm sand mix	52
22	Streamer initiation times vs geometry	53
23	Streamer initiation times vs ρ	54
24	Electric field for t_i = 10 μs	56
25	Streamer intiation time vs soil type	57
26	Initial current vs applied voltage, 300 Ωm mix	58
27	Voltage profile, 350 Ωm sand mix	60
28	Voltage profile, 350 Ωm sand mix	61
29	Voltage profile, 350 Ωm sand mix	62
30	Voltage profile, 350 Ωm sand mix	63

CONTENTS

Section		Page
I	INTRODUCTION	7
II	EXPERIMENT DESIGN	11
	1. EXPERIMENTS AT PHYSICS INTERNATIONAL	12
	a. Sample Geometry	12
	b. Pulser	14
	c. Recording	15
	2. MCAIR EXPERIMENTS	15
	a. Sample Geometries	15
	b. Pulsers	19
	c. Recording	21
	3. VOLTAGE PROBES	23
	4. VOLTAGE PROFILES AND STABILITY CONSIDERATIONS	28
	5. DATA PROCESSING	30
	6. EXPERIMENT SUMMARY	32
III	EXPERIMENTAL RESULTS	36
	1. CONDUCTION BELOW BREAKDOWN THRESHOLD	36
	2. STREAMER INITIATION	49
	3. APPARENT CONDUCTANCE AT HIGH FIELDS	59
	4. STREAMER STRUCTURE	98
	a. Azimuth/Axial Voltage Profiles	101
	b. Decoration of Plastic Sheets	115
	c. Conducting Rod Profiles	119
	5. COMBINED STRESS EXPERIMENTS	156
	6. OSCILLATORY BEHAVIOR	164
	7. DEPENDENCE ON SOIL TYPE	173
	8. DEPENDENCE ON EXPERIMENT GEOMETRY	184
	APPENDIX A. CIRCUITS USED AT PI AND MCAIR	217
	APPENDIX B. VOLTAGE PROBE RESPONSE TIME	218

ILLUSTRATIONS (Continued)

62	Normalized resistance profile, Shot 591, 80 kV applied	116
63	Conducting plastic decoration	117
64	Hole in conducting plastic	120
65	Conducting plastic decorated by arcs	121
66	Conducting cylinder geometry	122
67	Cylinder voltages, Shot 417	123
68	Azimuthal resistance profile with conducting rods	125
69	Azimuthal resistance profile with conducting rods	126
70	Azimuthal resistance profile with conducting rods	127
71	Azimuthal resistance profile with conducting rods	128
72	Azimuthal resistance profile with conducting rods	129
73	Azimuthal resistance profile with conducting rods	130
74	Azimuthal resistance profile with conducting rods	131
75	Azimuthal resistance profile with conducting rods	132
76	Azimuthal resistance profile with conducting rods	133
77	Azimuthal resistance profile with conducting rods	134
78	Azimuthal resistance profile with conducting rods	135
79	Azimuthal resistance profile with conducting rods	136
80	Azimuthal resistance profile with conducting rods	137
81	Azimuthal resistance profile with conducting rods	138
82	Azimuthal resistance profile with conducting rods	139
83	Azimuthal resistance profile with conducting rods	140
84	Azimuthal resistance profile with conducting rods	141
85	Azimuthal resistance profile with conducting rods	142
86	Azimuthal resistance profile with conducting rods	143
87	Azimuthal resistance profile with conducting rods	144
88	Azimuthal resistance profile with conducting rods	146
89	Azimuthal resistance profile with conducting rods	147
90	Azimuthal resistance profile with conducting rods	148
91	Azimuthal resistance profile with conducting rods	149
92	Azimuthal resistance profile with conducting rods	150
93	Azimuthal resistance profile with conducting rods	151

ILLUSTRATIONS (Continued)

31	Voltage profile, 350 Ωm sand mix	64
32	Voltage profile, 350 Ωm sand mix	65
33	Voltage profile, 350 Ωm sand mix	66
34	Voltage profile, 350 Ωm sand mix	67
35	Voltage profile, 350 Ωm sand mix	68
36	Voltage profile, 350 Ωm sand mix	69
37	Voltage profile, 350 Ωm sand mix	70
38	Voltage profile, 300 Ωm sand mix	72
39	Arc-over times, 300 Ωm sand mix	74
40	Voltage profile, 300 Ωm sand mix	77
41	Voltage profile, 300 Ωm sand mix	79
42	Voltage profile, 300 Ωm sand mix	81
43	Voltage profile, 300 Ωm sand mix	83
44	Voltage profile, 300 Ωm sand mix	85
45	Voltage probe records	87
46	Voltage probe records	88
47	Voltage probe and current records, Shot 285	92
48	Voltage profile, 130 Ωm MX-B soil	93
49	Voltage profile, 130 Ωm MX-B soil	94
50	Arc-over characteristics, Shot 544	95
51	Arc-over characteristics, Shot 547	96
52	Azimuthal resistance profile, 130 Ωm MX-B soil	102
53	Azimuthal resistance profile, 130 Ωm MX-B soil	104
54	Azimuthal resistance profile, 130 Ωm MX-B soil	105
55	Azimuthal resistance profile, 130 Ωm MX-B soil	106
56	Azimuthal resistance profile, 130 Ωm MX-B soil	108
57	Azimuthal resistance profile, 130 Ωm MX-B soil	109
58	Azimuthal resistance profile, 130 Ωm MX-B soil	110
59	Resistance profiles at 0.15 mR, 140 VAC applied	111
60	Resistance profiles at 0.15 m, 30 kV applied	113
61	Resistance profile, Shot 591, 80 kV applied	114

ILLUSTRATIONS (Concluded)

125	Voltage profile, 200 Ωm sand	197
126	Voltage profile, 300 Ωm sand mix	199
127	Voltage profile, 300 Ωm sand mix	202
128	Voltage profile, 2000 Ωm sand	205
129	Voltage profile, 3400 Ωm sand	206
130	Voltage profile, 5500 Ωm sand	208
131	Voltage profile, 2800 Ωm sand	209
132	Voltage profile, 7700 Ωm sand	210
133	Voltage profile, 3300 Ωm sand	211
134	Voltage profile, 350 Ωm sand mix	213
135	Voltage profile, 350 Ωm sand mix	215

LIST OF TABLES

Table		Page
1	Voltage probe types	24
2	Earth breakdown experiment at Physics International	33
3	Earth-insulator breakdown experiments at Physics International	34
4	Earth breakdown experiments at McAir	35
5	Shot 297 R_{EFF}	103
6	Conducting plastic shots at Physics International	118
7	Resistor voltage profile	164
8	Oscillatory behavior	167

ILLUSTRATIONS (Continued)

94	Metal cylinder geometry	152
95	Azimuthal-axial resistance profile with condutcting rods	153
96	Azimuthal-axial resistance profile with condutcting rods	154
97	Azimuthal-axial resistance profile with condutcting rods	155
98	Azimuthal-axial resistance profile with condutcting rods	157
99	Azimuthal-axial resistance profile with condutcting rods	158
100	Azimuthal-axial resistance profile with condutcting rods	159
101	Azimuthal-axial resistance profile with condutcting rods	160
102	Resistor voltages	162
103	Shot 584	165
104	Shot 560	168
105	Shot 38	169
106	Shot 40	170
107	Shot 578	172
108	Voltage profile, 7700 Ωm sand	174
109	Voltage profile, 1100 Ωm SDF soil	175
110	Voltage profile, 350 Ωm sand mix	176
111	Voltage profile, 170 Ωm sand	177
112	Voltage profile, 170 Ωm MX-B soil	178
113	Voltage profile, 130 Ωm MX-B soil, tamped	179
114	Arc-over time	182
115	Arc-over voltage for t_B - 100 μs	183
116	Voltage profile, 2800 Ωm sand	185
117	Voltage profile, 310 Ωm sand mix	186
118	Voltage profile, 170 Ωm sand	187
119	Voltage profile, 170 Ωm MX-B soil, untamped	188
120	Voltage profile, 130 Ωm MX-B soil, tamped	189
121	Apparent arc resistance	190
122	Voltage profile	192
123	Voltage profile, 200 Ωm sand	193
124	Voltage profile, 200 Ωm sand	195

The response of the earth to a conductor at high potential inserted into it can be approximated by considering the field distribution in cylindrical geometry. At low voltage the electric field falls off as 1/r, where r is the distance from the center of the conductor. As the voltage on the conductor is increased, electric breakdown is expected to proceed in the earth, starting at the surface of the conductor. The initiation of enhanced conductivity is expected to occur when the electric field at the surface of the conductor exceeds a critical value, E_i. Once initiated, such a breakdown streamer is expected to propagate outwards as long as the electric field at its tip exceeds a critical value which may be $\leq E_i$. The electric field existing at the tip of the streamer will be greater than the field that would exist at the same point if a sharp conducting line were not present; in other words, the presence of the conducting streamer produces field enhancement at its tip. Whether a streamer will continue to propagate or not may be characterized by the average field that exists in the vicinity of the streamer without taking into account enhancement due to the introduction of the streamer. One or more streamers are expected to continue to propagate as long as this average field is greater than a critical value, E_p. E_p may be a function of time. Since the breakdown streamers are not necessarily excellent conductors, the field within the streamer is characterized by a value, E_s. E_s is smaller than E_i or E_p. It is expected that E_s is a function of time and current flowing in the streamer.

Each of these parameters may be a function of the nature of the soil to which the electric field is applied. A primary dependence on the conductivity of the soil is expected, particularly since the energy deposition per unit volume at a given value of the electric field will be proportional to the conductivity. An additional dependence on soil type can exist because of the geometry of the conducting paths in the soil or the chemical nature of the conducting medium.

I. INTRODUCTION

The objective of the work presented in this report was to obtain experimental data on the electrical conduction in earth surrounding a long metallic conductor excited at a high voltage.

It has been established theoretically that a conductor in contact with the fireball of a nuclear explosion can achieve potentials of a few megavolts relative to distant earth. Such a conductor connected at some distance to a missile shelter complex could induce currents of hundreds of kiloamps onto it, potentially causing failure of the critical ground support equipment. Possible means to protect the missile and its essential launch equipment from such electric stresses include placing a resistive or dielectric link in series with the conductor. Typical cables used for power or communications in a missile field either have an outer conductor in electrical contact with the earth or are surrounded by an insulating jacket that will puncture upon application of such large potentials. Therefore, it is almost certain that electric stresses, sufficient to electrically break down the earth near such a conductor, will be produced. It is important to establish whether earth breakdown can produce a low impedance path that might shunt a resistive or dielectric link and negate its effectiveness. Stated another way, it is necessary to place an upper bound on the conduction through earth at high fields over long distances, so that a minimum standoff distance and a maximum electrical stress can be specified for isolation links so the earth will not negate their effectiveness.

in which breakdown streamers propagate from a central conductor outward into an ever-decreasing average field. This is representative of the actual situation for a buried conductor far away from the effective ground point. In addition to overall current and voltage measurements, extensive use was made of high-impedance voltage probes to measure the radial voltage profile and determine the region of earth near the central conductor in which the effective conductivity was increased by breakdown streamers.

Two major experimental programs were conducted. One used a 1 μF 100 kV pulser at PI to stress a 90° sector of earth with thickness between 0.1 and 0.3 m and outer radius between 0.5 and 1 m. These experiments served to check the dependence of streamer phenomena on sample geometry and to study the dependence of breakdown characteristics on soil type. The second experiment series utilized two pulsers at the McDonnell Douglas lightning test facility in St. Louis (McAir). Each pulser had a capability of being used as 1 through 5 stages with a capacitance of 230 μF per stage and a maximum charging voltage of 24 kV. Larger samples, including a 1-m-radius × 1-m-long cylinder, were driven with these pulsers to study the scaling of the streamer behavior with sample dimensions and to observe the effect of combined axial and radial electric fields. The experimental data will be organized according to the following general topics:

1. Conduction at fields below threshold for streamer initiation
2. Streamer initiation
3. Apparent conductance versus electric field and time at fields above streamer intiation
4. The streamer structure
5. The effects of combined axial and radial stress
6. Observations of oscillatory behavior
7. Dependence on soil type
8. Dependence on experiment geometry
9. Post arc-over behavior

One important characteristic of the voltage induced on long conductors by nuclear explosions is that, at the distances of interest from the explosion, the rise time of the voltage is relatively slow, measured in tens to hundreds of microseconds. This is a consequence of the inductance of the long conductor extending from the nuclear fireball voltage source to the point of interest. Even for soils having the lowest conductivity of interest (σ to 10^{-3} S/m), the effective dielectric relaxation time, ε/σ, is much shorter than the rise time of the electric field. This implies that the microscopic distribution of the electric field in the soil will be determined not by dielectric constants and displacement currents but by the conductivity profile and real current. In effect, the microscopic electric field distribution must be such as to produce continuity of real current.

This report will present the results of the experimental programs conducted by Mission Research Corporation (MRC) at Physics International (PI), San Leandro, California and McDonnell Douglas, St. Louis, Missouri. Implications of these results for modeling of the earth breakdown process have been reported separately (Ref. 1). These experiments were built on previous work by Jaycor on the earth breakdown threshold (Ref. 2) and complemented concurrent work by Jaycor on arc-over impedance (Ref. 3).

Section II of this report discusses the design of experiments to investigate earth conduction processes at high electric fields. The experiments are primarily in cylindrical geometry, and emphasize the circumstances

---

1. V.A.J. van Lint, J.L. Gilbert, "Soil Breakdown Modeling," Mission Research Corporation MRC/SD-N-75, San Diego, California (November 1981).

2. C.E. Mallon, et al., "Electrical Breakdown Characteristics of Soil Samples," AFWL-TR-81-213, Vol. 1, 2 & 3, La Jolla, California (January 1981.

3. C.E. Mallon, et al., "Electrical Breakdown Characteristics in 0.8 to 1.0 Meter MX Soil Samples," AFWL-TR-81-207, La Jolla, California, (September 1981).

1. EXPERIMENTS AT PHYSICS INTERNATIONAL

Experiments were performed at PI with relatively small samples of earth in 90° sectors, served to:

1. Check out experimental technique
2. Calibrate voltage probes
3. Characterize onset of non-linear behavior
4. Compare the behavior of different soils
5. Establish the dependence on sample geometry

a. Sample Geometry

The majority of the experiments at PI were performed in the sample holder shown in Figure 1. A 90° sector box was constructed with Plexiglas bottom and two sides. The center conductor, 0.01-m radius for most of the measurements, was placed at the intersection between the two side walls. A 90° circular sector copper sheet served as the outer electrode. The sample chamber was filled with soil samples to a depth of 0.1 m or 0.3 m for the different experiments. In the majority of the measurements, the outer electrode was placed at a radius of 0.5 m and the sample chamber was filled to a depth of 0.1 m.

In the initial experiments at the higher voltages, light flashes were observed at the surface of the Plexiglas in the vicinity of the center conductor. These apparent surface flash overs were subsequently inhibited by coating the Plexiglas surfaces near the center conductor with a thick layer of vacuum grease before filling the sample holder with soil.

II. EXPERIMENT DESIGN

Two general experiment configurations were used:

1. A cylindrical 90° sector, 0.1 to 0.3 m long, was driven by a 30-100 kV 0.9 μF pulser at PI.

2. A full cylindrical sample 1 m long was driven by one or two five-stage pulsers at the McDonnell Douglas lightning facility (McAir). Each Marx pulser is capable of being charged to 15 to 24 kV per stage and a net capacitance of 230 μF divided by the number of stages used.

The principal diagnostic techniques were measurement of the potential profile in the earth with high impedance voltage probes and measurement of the total current with a current transformer. Other techniques included decoration of conducting plastic sheets to observe the streamer geometry.

The experiment design will be discussed in this section according to the following organization.

1. Small-scale experiments at PI
2. Medium-scale experiments at McAir
3. Voltage probes
4. Voltage profiles and stabilities considerations
5. Data processing
6. Experiment summary

The following variations of sample geometry were investigated:

1. Outer electrode radius: 0.5 and 1 m
2. Soil sample height: 0.1 and 0.3 m
3. Sector angle: 30° and 90°
4. Center electrode radius: 0.0025 to 0.01 m

Figure 1 illustrates the locations of voltage probes during a typical radial profile measurement. For the experiments with 0.1-m-thick soil samples, the tips of the probes were inserted to a position 0.025 m below the top surface of the soil. In other experiments, some or all of the probes were placed along an azimuthal arc at a fixed distance from the center conductor. In another experiment series, the probes were located at a given radial distance but separated in both azimuth and vertical position. Finally, in the "rod" experiment, a set of 0.01-m-radius metal cylinders were placed along an azimuthal arc at a constant distance from the center conductor and the potential of each of these cylinders was monitored with a voltage probe. The significance of these experiment geometries and the data produced by them are discussed in Section III.

b. Pulser

For the PI experiments, a special pulser was configured and operated by PI personnel. It consisted of two 1.85-μF capacitors charged to a maximum of ± 50 kV and connected to each other by a triggered switch. The output of this pulser was connected through a 10-Ω copper sulfate series resistor to the center conductor of the sample holder in parallel with a 10,000-Ω shunt water resistor. The outer electrode of the sample holder was returned to pulser ground through a 0.15-Ω current-measuring resistor consisting of 60 10-Ω, 2-W resistors in parallel. For a few experiments at smaller currents a 1-Ω series resistor was used. In some of the experiments the arc current was limited by a 200-Ω resistor consisting of four 50-Ω

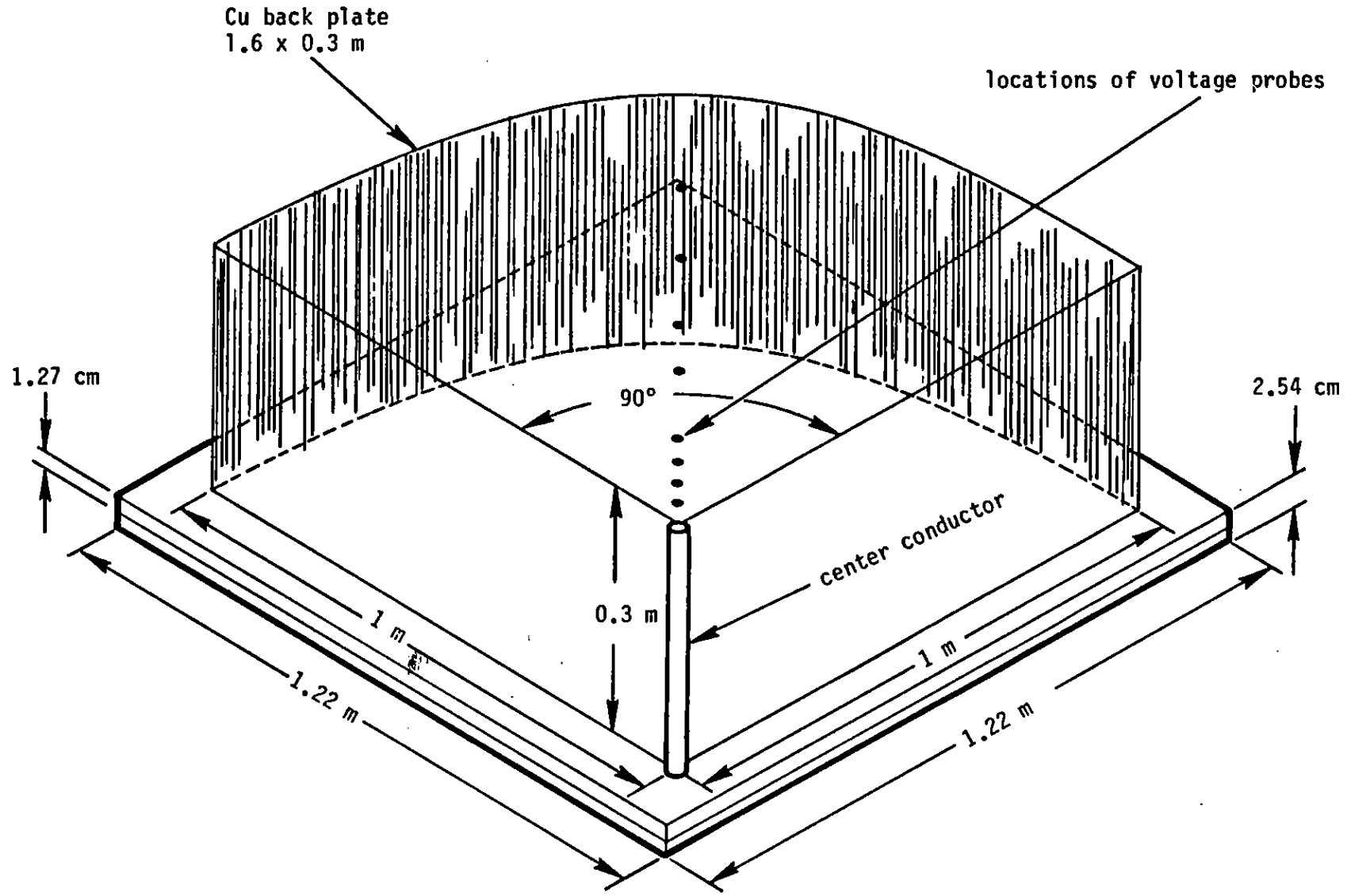

Figure 1. Physics International experiment sample holder.

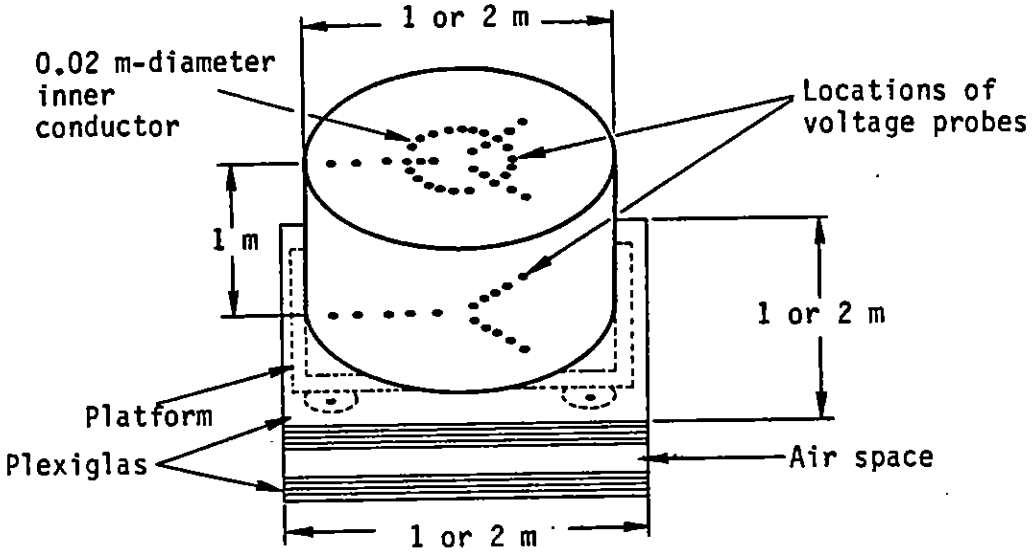

Figure 2. McAir experiment sample holder.

The two sample holders with the configuration shown in Figure 2 had permanently mounted voltage probes in the bottom at various radii from 0.05 m outward at three azimuths, arbitarily labeled 0°, 120° and 240°. The resistor strings associated with the voltage probe started from a position 0.05 m inside the earth sample, extended through the first 2.5 cm of Plexiglas under the sample chamber, turned through a 90° angle and proceeded radially outwards in the air space between the two Plexiglas layers. On the top side of the samples, a 1.3 cm-thick Plexiglas cover plate was drilled with holes in the pattern indicated, with both radial and azimuthal locations. Straight voltage probes were inserted into these holes as needed for the individual experimental measurements.

Figure 3 illustrates the use of the second 1 m-diameter sample holder with an array of 0.01-m-radius conducting cylinders to study the streamer structure. The array was constructed of copper tubes, linked with short sections of Plexiglas tubing to provide 0.01-m-separation between vertical segments. Along a vertical line there were 6 tubes. A total of 20 vertical lines of tubes were spaced around the circle at a radius of 0.15 m.

Carborundum, high-voltage resistors in series, connected between the outer electrode and the 0.15-Ω current-measuring resistor. The circuits used are shown in Appendix A.

c. Recording

During the PI experiments, data were recorded on both channels of the five Textronix type 555 oscilloscopes. The oscilloscopes were placed in a screen room near the sample holder. The cabling from the voltage and current probes to the screen room consisted of RG58 coax cables enclosed in an overall solid metal foil shield. The shield was connected to the shells of the cable connector both at the probes and at the screen room wall. Inside the screen room, RG58 jumper cables were used between the bulkhead feedthrough connectors and the oscilloscopes. The oscilloscope trigger was derived from a trigger-generator output on the pulser, carried to the screen room on RG58 cable and isolated with a pulse transformer at the screen room wall. In this geometry, any noise produced by the pulser was undetectable on the most sensitive scales used at 20 μs per division sweep speeds.

2. MCAIR EXPERIMENTS

a. Sample Geometries

Figure 2 illustrates the sample holder used during the McAir experiments. Three sample holders were constructed, one consisting of a 2-m-diameter by 1-m-long section of aluminum culvert placed with its end on two layers of 2.5-cm Plexiglas, separated by a space of ≈10 cm. Two other sample chambers consisted of 1-m-diameter by 1-m-long aluminum culverts. One of these was used in a configuration similar to that shown in Figure 2, the other did not have the air space between the two Plexiglas layers on the bottom. It was used exclusively for decorating the conducting plastic and the conducting rod experiment.

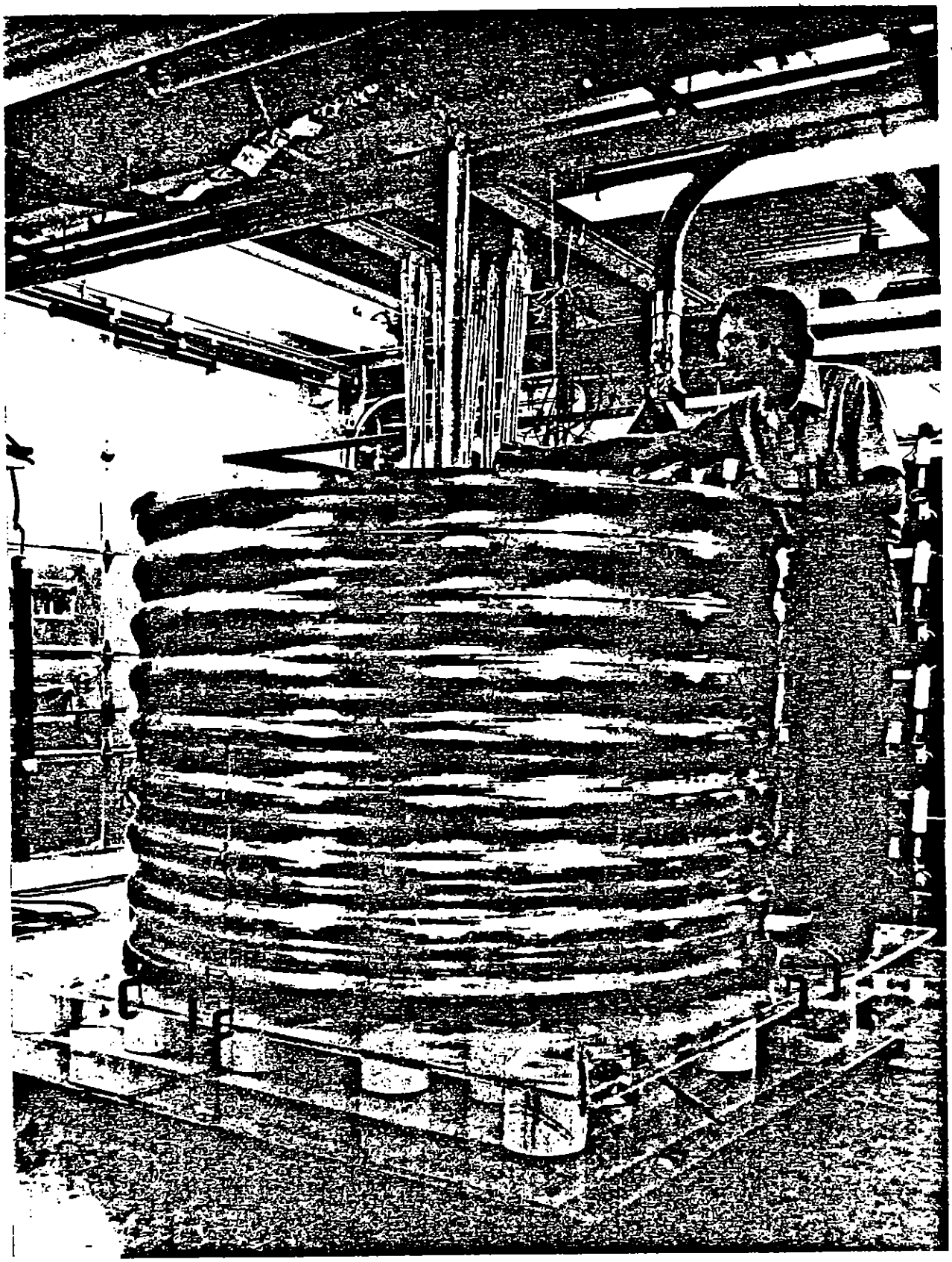

Figure 4. 1 mR sample chamber.

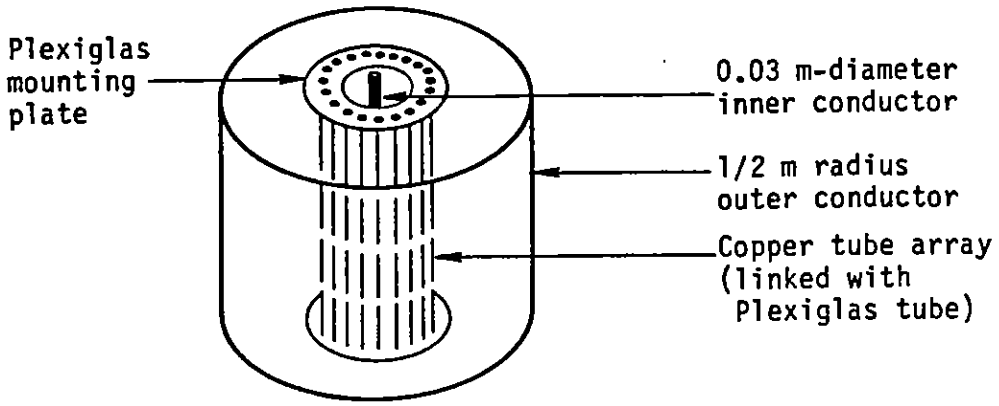

Figure 3. McAir conducting cylinder experiment.

In all cases, the soil sample was filled to a height of 1 m from the bottom Plexiglas plate to its top surface and was covered with a Plexiglas plate on top. The inner portions of both the bottom and top plates were coated with a thick layer of vacuum grease to inhibit surface arcovers. On disassembly of the sample holders after the experiments, no visible markings indicating surface flashovers were observed on any of the plastic surfaces. The inital experiments at PI, performed prior to treating the surfaces with vacuum grease, revealed marks on the Plexiglas at much smaller pulser currents. Therefore, it is safe to assume that the grease-coated, earth-plastic interface was not a preferential site for breakdown.

Figure 4 shows the 2-m-diameter sample chamber in the test cell at McAir. The pulser is connected to it by the foil at the top and metal sheet on the floor. Voltage probes are seen protruding axially from the top and radially out the bottom between the Plexiglas layers. Conduit for instrumentation cables to the screen box is shown at the rear.

The sample chamber shown in Figure 3 was also used to decorate two layers of conducting plastic. These layers were inserted into the earth at

bias was applied by connecting the pulser between the top (positive) and bottom of the resistor string, allowing the outer cylindrical conductor to float while measuring its voltage. In a self-bias configuration, the single pulser was applied between the top of the resistor string (positive) and the outside cylinder (ground). The bottom of the resistor string was allowed to float, while its voltage was measured with a voltage probe. In the third, axial/radial, configuration, two pulsers were used: a positive pulser applied to the top of the resistor string, and a negative-pulser output voltage applied to the cylindrical outer conductor. The ground return for both pulsers was connected to the bottom of the resistor string. In this configuration two current measurements were performed: the total current out of the bottom of the resistor string and the current returning to the radial pulser alone. Type 1049 current probes were used for both of these measurements. The circuit diagrams for the various configurations are shown in Appendix A.

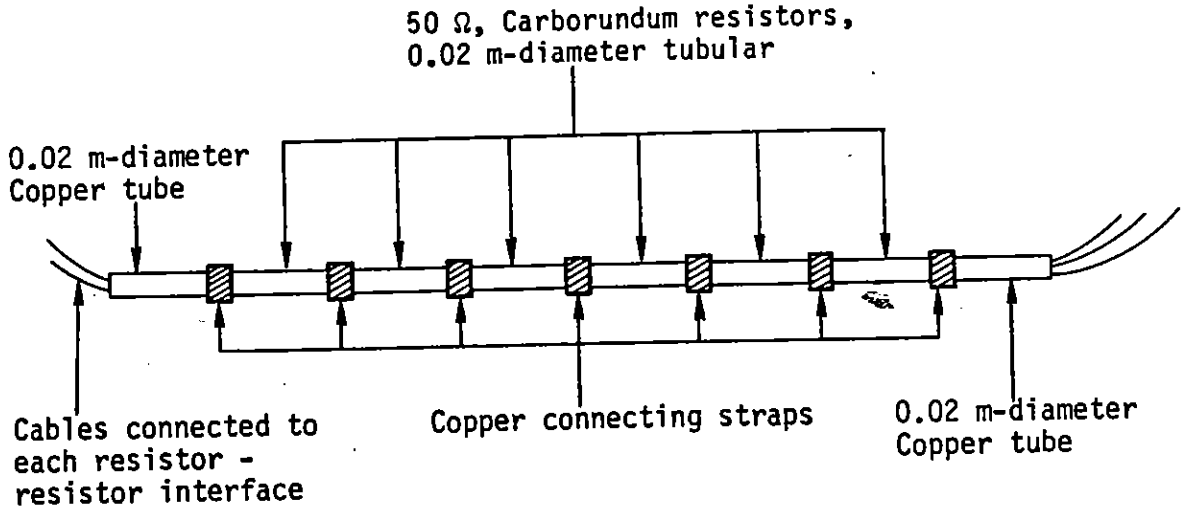

Figure 5. Resistor string.

radii of 0.08 and 0.15 m by gradually withdrawing supporting cylinders away from the plastic as dirt was filled in around it. This procedure was not only tedious and time consuming, but it also caused some physical damage to the plastic. This damage produced some ambiguity between marks produced by electrical arcing and those left behind by the emplacing procedure. It is clear that, in future attempts to decorate such plastic layers, a better holding and emplacing system will need to be devised.

b. Pulsers

Two pulsers were used during the McAir experiments, each consisting of a 1-to-5 stage Marx generator composed of 230 μF capacitance per stage and capable of being charged at 15 to 24 kV per stage. For example, a typical shot at 30 kV utilized two stages, resulting in a capacitance of 115 μF charged to 15 kV. At a nominal charge voltage of 20 kV the capacitor had the capability of delivering 4.6 C. The output of the pulser was connected to the top of the center electrode in the sample holder via a stainless steel, foil strip resistor with a nominal value near 4 Ω. The current was measured in the ground side of the pulser circuit with a type 1049 current probe, having a sensitivity of 0.002 V/A when connected to a terminated 50-Ω cable.

For the experiments with radial excitation alone, one pulser was used, since voltages above 100 kV could not be used without producing conductor-to-conductor arc-over early in the pulse. The single pulser was connected with its postive electrode to the center conductor, and the ground returned on the outer cylinder. The voltage at the center conductor was measured with a voltage probe similar to those used to measure the potential profile in the earth.

Three types of combined drive experiments were performed with the resistor string shown in Figure 5 on the axis of the sample holder. Axial

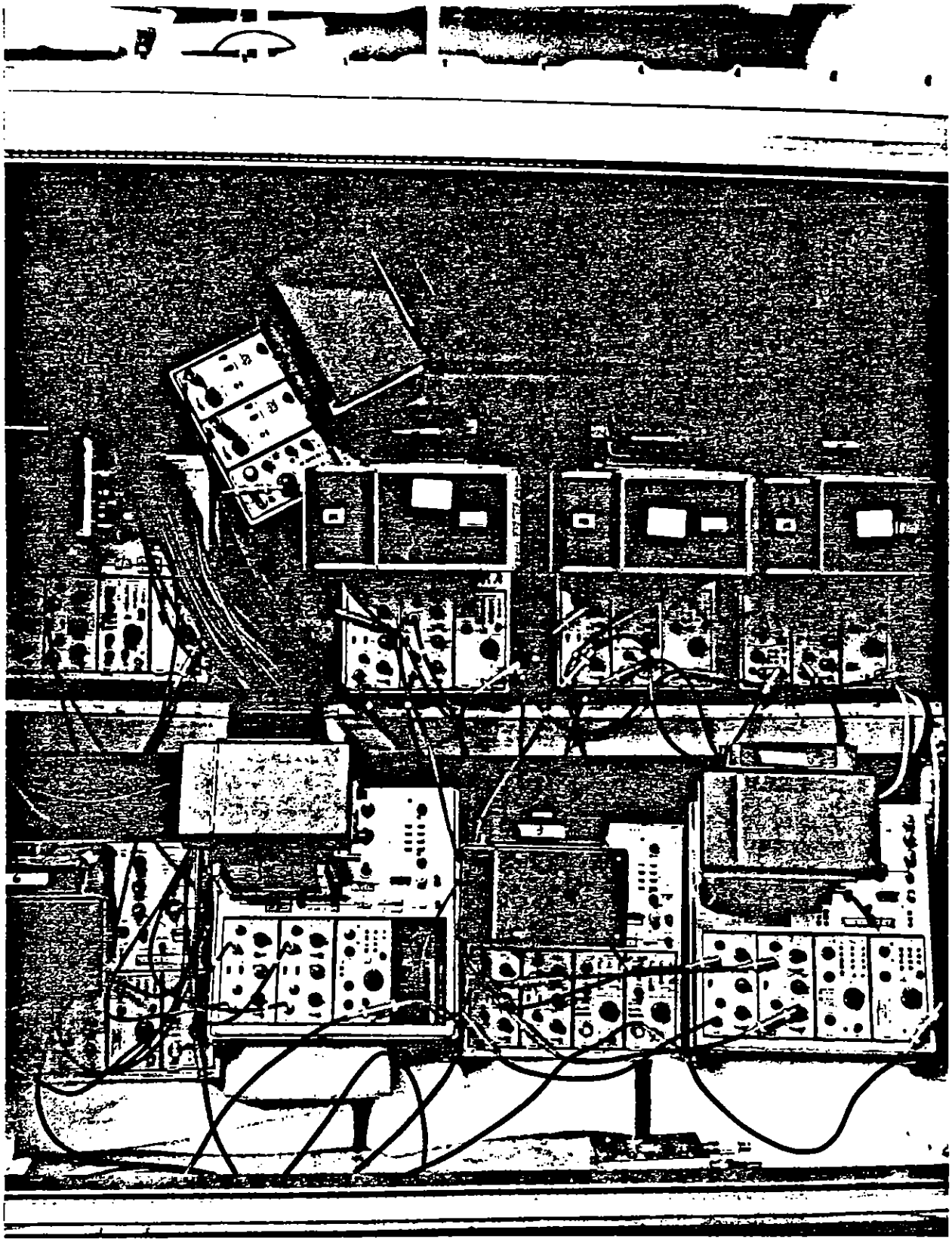

Figure 6. Screen box.

c. Recording

The cables from the voltage probes were routed close to the grounded outer cylinder of the sample holder into a 10 cm-diameter metal conduit that ended just above the sample holder at the 0° position. From there, the conduit proceeded along the ceiling of the test cell through a wall and was connected with metal foil to a screen box (Fig. 6). Nine oscilloscopes were placed within the screen box. Three Textronix type 7844, three Textronix type 7603, one Textronix type 7607 and two Textronix type 7704 using pre-amps type 7A16A, 7A18, and 7A26. The dual beam 7844 oscilloscopes used both pre-amplifiers in the chopped mode to produce four traces with two beams. Of the six single beam oscilloscopes, five of them were operated with both the mainframe and pre-amps chopped so that four traces were available. On the remaining oscilloscope, only the mainframe was chopped. This recording system produced a total of 34 oscilloscope records per data shot. These 34 traces were used to record the signals on 26 cables from the sample holder to the screen room. Two oscilloscopes were used to cover the later-time evolution of particularly interesting signals.

The oscilloscopes were triggered by a signal from the control console with ~10 μs delay prior to firing the Marx pulser. This provided on many of the records a short section of baseline prior to the recorded voltage transients. The trigger cable was isolated at the wall of the screen box by a pulse transformer.

While this system produced the maximum number of records with the available cabling and screen box facilities, it resulted in awkward postshot data reduction. Extreme care needs to be taken to maintain identity with four oscilloscope traces on each photograph, particularly when in some cases the pulser prefired and did not provide a preshot baseline on the record. The McAir operator was requested to provide a postshot trigger whenever a prefire occurred, but this was sometimes missed.

During the course of the PI experiments, a variety of probe configurations were tested to assess their voltage handling capabilities and response-time characteristics. Table 1 presents a listing of the probe types used during the PI and McAir experiments. The apparent exponential response time given in Table 1, together with Equation B6 from Appendix B yields an effective shunt capacitance per resistor in the probe of ≈0.5 pF It would be desirable to unfold the probe response from the fast-time data; however, this cannot be done with any confidence because the individual probes are not surrounded by a fixed potential environment. In a typical experiment a number of voltage probes protrude from the earth sample into the air above it. The effective termination point of the stray capacitance is then itself a time varying potential, depending upon the exact geometry of the probes and the relative voltages that they are measuring. Therefore no attempt was made to correct for probe response in the data. Instead, for the slower probes (type C) only data after 20 μs were used with confidence. On the faster probes (type E and F) earlier data can be used.

TABLE 1. VOLTAGE PROBE TYPES

Type	Number of Resistor	Resistor Value(Ω)	Resistor Type[a]	Epoxy Potted	Experiment	(μs)
A	21	240K	CC	Yes	PI	≈5
B	21	240K	CC	No	PI	≈4
C	50	100K	CC	No	PI, McAir	≈10
D[b]	50	100K	CF	No	PI	≈10
E	50	20K	CC	No	PI, McAir	≈3
F	20	100K	CC	No	McAir	≤2

[a] CC = Carbon composition
CF = Carbon film

[b] Calibration curve for CF resistors appears more linear at ≈100 μs but changes with time.

3. VOLTAGE PROBES

The principal technique by which the effective impedance of the earth was observed during these experiments involved the use of voltage probes to measure the potential profile as a function of radius, azimuth, and depth in the earth. The requirements on the voltage probes were:

1. That they operate in a calibratable matter (i.e., without breakdown or time dependent characteristics) up to the maximum expected voltages.

2. That they not perturb the current at the point in the earth's sample at which the voltage is being measured. This means that the impedance presented by the voltage probe must be large compared to the spreading resistance from the probe into the earth, and that the probe conductor in contact with the earth must be small compared to the distance scale on which the fields in the earth change.

3. That the response time of the probe must be able to follow the development of nonlinearities in the earth on a time scale of tens of microseconds.

Voltage probes were constructed by inserting a string of 2-W resistors into a Plexiglas tube and terminating the sensor part of the string in a small metal ball (~1 mm radius) and terminating the far end in a suitable current measuring resistor (typically 500 Ω). In order to assure high-impedance operation, the initial probes had a resistance of 5 MΩ, which is large compared to the spreading resistance even in the highest resistivity earth samples. Other probes with series resistance of 2 MΩ and 1 MΩ were used during the course of the experiments with lower resistivity materials, in order to have shorter response time. Appendix B presents the theory of the voltage probe response time and the trade-off in probe design between resistance, response time, and voltage handling capability.

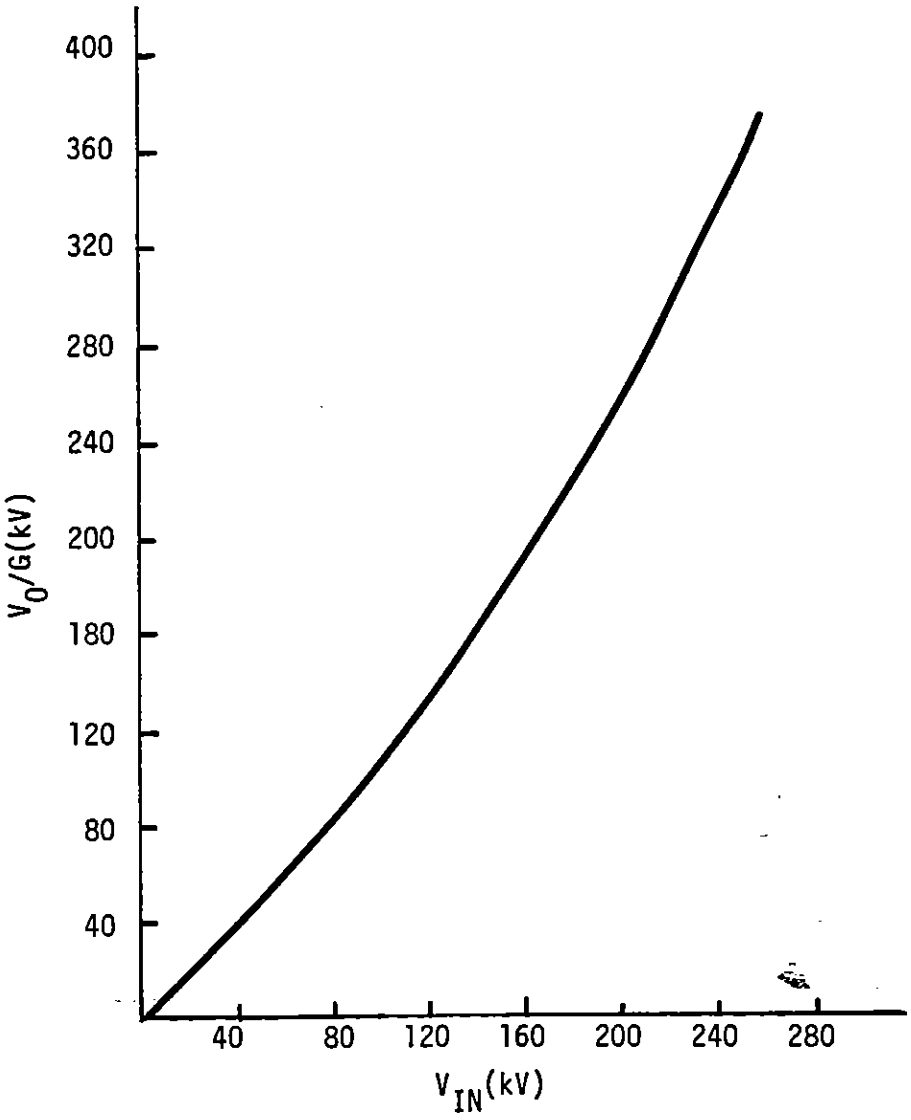

Figure 7. Voltage probe calibration probe C.

During the PI experiments, all of the probes were used and calibrated against the charging voltage of the pulser. The calibration curve of each probe used at PI was constructed from a calibration curve at 8 points betweeen 30 and 100 kV. This calibration curve was then fitted to a cubic polynominal by a least-squares process. In processing the data, the individual probe calibration curves were used to unfold the earth sample voltage from the measured oscilloscope voltage.

The probes used at McAir were selected on the basis of the PI experiments and were constructed after the PI experiments; therefore, they were not individually calibrated. Since it was expected that some of the McAir experiments would be conducted at voltages up to 200 kV, the bottom probes for the large sample chamber, as well as some of the movable top probes, were constructed as 50 element strings of 100 kΩ resistors. These exhibited the slowest response time. The lower probes of the smaller chamber on the 0.5-m-radius chamber were of type F, since less than 100 kV was expected to be applied to this chamber. The movable upper probes were mixed between type E and type C depending upon the expected application. Since the individual probes could not be calibrated during the McAir experiment, a generic calibration curve for the McAir probes was constructed by combining all data for probes composed of of 100 kΩ resistors and all data for probes composed of 20 kΩ resistors into two calibration curves normalized to the voltage per resistor. These generic calibration curves for probe types C, E, and F were used to unfold the McAir data. The data in Section III illustrate a greater scatter in the voltage probe data from McAir, which reflect this less accurate calibration. The probes, however, are still available and identified so that they can be calibrated individually in the future. As an example of the generic curve, the calibration for probe type C is shown in Figure 7.

Figure 8 shows a set of probes installed in an azimuthal configuration in the top of the 2-m-diameter sample holder at McAir.

4. VOLTAGE PROFILES AND STABILITY CONSIDERATIONS

In the majority of these experiments a voltage was applied between a center conductor and a coaxial cylindrical conductor, either in 360° or 90° geometry. The insulating boundary conditions at 90° and those at the top and bottom of the sample can be treated as if identical structures were replicated four times in angle and in axial distance at intervals equal to the length of the sample. In effect, the condition that current cannot flow across insulating boundaries is equivalent to having additional earth samples located with symmetries ensuring the same boundary conditions.

The purpose of the experiments was to observe, by measuring the voltage profile, the change in effective conductivity of the soil as a function of electric fields imposed on it. It was expected that one manifestation would be a rapid increase of conductivity with electric field, producing an effective negative resistance characteristic. This can create an instability, and will produce, as a natural consequence, discrete three-dimensional conducting structures and, possibly, runaway behavior. In plane-parallel geometry this characteristic results in almost immediate arc-over between electrodes once the conduction at any point in the sample area starts to increase (Ref. 2). In plane parallel geometry, the moment a streamer is nucleated, the field at the tip of the streamer is enhanced over the average field for two reasons:

a. the small radius of a conducting protrusion,
b. the distance from the end of the conducting protrusion to the other electrode, over which the voltage is now applied, is less than it is for the remaining electrode area.

In cylindrical geometry the instability may not occur as quickly. It is still true that a single conducting protrusion will produce an electric field at its head that is greater than the field that would be there in

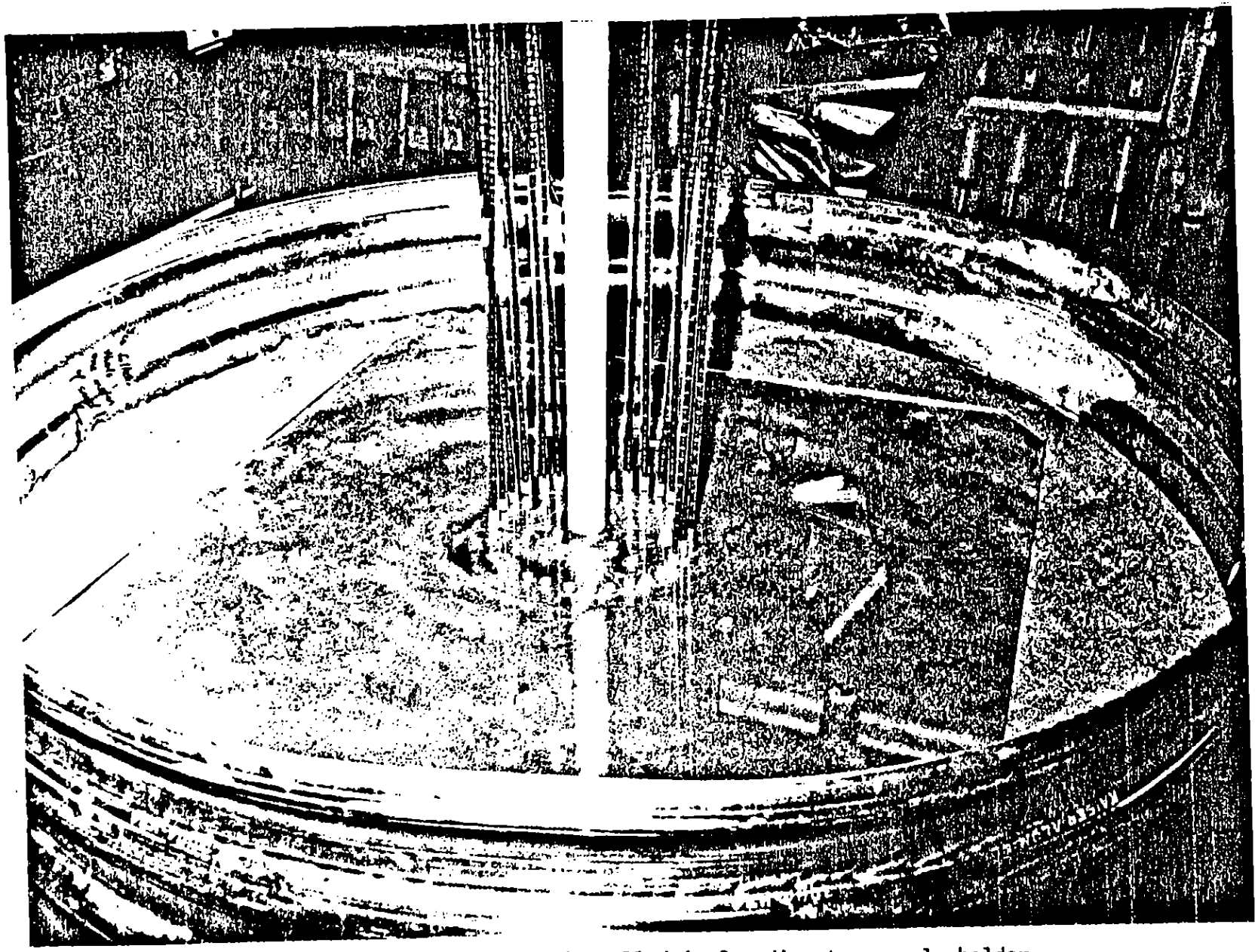

Figure 8. Voltage probes installed in 2 m-diameter sample holder.

In considering the expected behavior of the 90°-sector short samples in the PI experiments with the 360° longer samples at McAir, it can be expected that the PI experiments will come closer to satisfying the 1/e instability threshold than the McAir experiments. In effect, the images of the streamer structure produced by the close-in insulating boundary conditions serve to produce an apparent conductivity profile closer to the cylindrical one than the more limited number of actual streamers in the large geometry experiments. The fact that in the PI experiments increased conductivity extended slightly over the 1/e point is consistent with the measurement of a finite resistance for the streamers, at least at early times. The fact that instabilities occurred very quickly at McAir is the result of the greater influence of field enhancement at the tip of the streamer.

5. DATA PROCESSING

The majority of the data from both the PI and McAir experiments consisted of oscilloscope photographs of transient records from voltage probes and current probes. The total amount of information collected during the two experiment series is very large. At PI a total of 432 data shots were taken with 10 oscilloscope traces per shot. At McAir only 99 shots were attempted, but the data system generated up to 34 oscilloscope traces per shot. Therefore, there exist close to 8,000 useful oscilloscope records. Only a fraction of these records have been processed to date. These were chosen first to establish the validity of the method and, second, to generate the most urgently required data.

In most cases oscilloscope photographs have been translated into quantitative values for amplitude and inserted into digital computer data records for automatic data processing. Two types of digitizing were used, depending upon the nature of the analysis.

the absence of the intrusion. However, the field naturally falls off with distance away from the center conductor in cylindrical geometry. Therefore, it is no longer obvious that nucleation of a conducting streamer will produce a runaway arc-over between electrodes.

The effect of competition between a decreasing field (due to distance from the center conductor) versus increasing field (due to decreasing distance to the outer conductor) can be analyzed simply, if it is assumed that a sufficient density of conducting streamers occurs so that the end of the streamers can be represented as an equipotential. If, in addition, the conductivity within the streamers is very large compared to the conductivity in the soil between the ends of the streamers and the outer conductor, the value of the instability radius can be calculated to 1/e x the outer radius*. If the effective resistance of the streamer volume is significant, the instability radius is larger. In this same model the instability radius can also be increased by inserting a series resistance in the electrical circuit. The value of this resistance can be related to the resistance of the earth into which the conducting streamers have not penetrated. In effect, a certain amount of series resistance is necessary to provide stability; that resistance is provided either by the earth in the outer [(1-1/e) x R (R = radius of the outer conductor)] region, or a portion of the earth resistance is replaced by a discrete resistor.

The foregoing discussion assumes a uniform conductivity within the streamer volume out to a cylindrical surface. If this medium consists of relatively few conducting streamers, the instability radius will be less due to field enhancement at the tip of the streamers. Furthermore, replacing the outermost earth with an external resistor will be much less effective, because the increase in voltage drop across the resistor per unit increase in length of a discrete streamer is much less than for a uniformly expanding conducting cylinder.

*R.N. Carlisle, "A Geometrical Instability in a Soil-Filled Coaxial Structure," unpublished.

A different type of processing occurred in the analysis of the data from which azimuthal and axial profiles of the electric field were deduced, either with voltage probes alone or with probes connected to conducting cylinders. In this case, the records were digitized to produce the entire time history. The digitized data were reduced to an effective time dependent resistance, namely the voltage between the probe and the center conductor divided by the total sample current plotted as a function of time. Inspection of the resistance versus time records identified discrete times bracketing noticeable events, i.e., those at which the effective resistance associated with one or more probes changed suddenly. The data were then reprocessed to produce a resistance profile across the sample at these discrete times. Many of these data are presented in Section III, paragraph 4.

In a few cases the data were not digitized due to lack of time and resources and hand processing has been used to develop plots. This is particularly true of the axial voltage profile along the resistor string in the combined drive experiments at McAir, and in the time history of the voltage, current and resistance before and after arc-over from the McAir data.

6. EXPERIMENT SUMMARY

Table 2 presents a summary of the earth breakdown experiments performed at PI. These cover a large range of soil sample types and considerable variation in the sample geometry. Although the initial series of experiments, from shot 8 through 128, were conducted with a single sample of earth whose resistivity starts out at 1500 Ωm. subsequent data processing revealed that the resistivity gradually increased during the conduct of the experiment to almost 10,000 Ωm. The samples labeled MX-A and MX-B were recieved from St. Louis and consisted of the same material provided by the Ballistic Missile Office (BMO) and the Air Force Weapons Laboratory (AFWL) for the JAYCOR experiments (Ref. 3). MX-A is the fine silky sample, designated as MX-SVBO in the JAYCOR report. It includes extremely fine

1. The value of the recorded voltage was measured visually, at a few discrete times, on each of a number of oscilloscope records for a given shot. For example, in the PI data taken at 20 μs per division sweeps, measurements were usually performed at 20, 40, 70, 110, and 190 μs after the start of the applied voltage. For 200 μs/div sweep speeds, measurements were usually performed at 100, 200, 300, 500, 900, and 1900 μs.

2. When the detailed time evolution of a signal was required, the individual oscilloscope traces were digitized using a Textronix 4956 Graphics Tablet connected to a Textronix 4051 terminal.

In either case, the digitized data values were processed by computer to unfold the voltage probe calibration curve and generate a variety of data presentations. One form, used most frequently, generated a plot of probe voltage divided by total sample current versus the logarithm of the radius at which the probe was located. Curves correspond to different times after onset of the voltage pulse were presented, either on separate plots or overlaid. Numerous plots of this type are presented in Section III. The same data were also processed to generate other displays for convenient data interpretation. One version produced a log-log plot of the effective conductivity deduced from the ratio of adjacent voltage probes versus average electric field between voltage probes. Since this plot depended upon differences between voltage probe readings, it was more difficult to interpret than the voltage-versus-radius plots, but could be used to establish the electric fields at which nonlinear conductivity behavior appeared and the magnitude of the increase of effective conductivity. Another useful presentation of the same data was the radial electric field at the inner of two voltage probes versus the radius plotted in log-log form. Such a plot exhibits a 1/r slope ohmic region and an effective saturation or turndown due to conducting streamers close in.

particulate and can be compacted into an almost rigid structure by modest pressure. MX-B is a sand and gravel composite labeled MX-DWP-25 in the JAYCOR work. It is a loose material not significantly compacted by modest pressure. The sample from the Siege Development Facility (SDF) was received directly from AFWL at Kirtland AFB. All of these materials were used in the form in which they were received; no water was added or removed from the samples. They were stored in plastic bags as received until used in the experiment. The MX-B sample used at McAir was returned to plastic bags after use.

Table 3 is a summary of a few experiments performed at PI in which an insulator was placed around a center conductor in the cylindrical earth geometry. In general the earth characteristics were similar to those without the insulator when the insulator broke down. If the insulator was sufficiently thick, it did not break down and only short transient currents, resulting from displacement currents across the insulator, were observed in the voltage and current probes. These data have not been analyzed in this report.

Table 4 presents a summary of the earth breakdown experiments performed at McAir.

TABLE 3. EARTH-INSULATOR BREAKDOWN EXPERIMENTS AT PHYSICS INTERNATIONAL

Shot No.	Geometry[a]	Earth	V_0(kV)
110-111	Shrink tubing on 0.0025 mR rod	1500 Ωm sand	84
112-116	RG 223		84-100
117-122	RG 188		84-100
188	Shrink tubing on 0.01 mR rod	140 Ωm rod	70

[a]Radial profile unless otherwise stated.

TABLE 2. EARTH BREAKDOWN EXPERIMENTS AT PHYSICS INTERNATIONAL

Shot No.	Geometry[a]	Earth	V_0(kV)
8-23	90° × (0.01-1 m) R × 0.3 mL	1500 Ωm sand	30-100
29-31	Decorate paper		100
32-42	Add vacuum grease on dielectric surfaces		30-100
43-46	Decorate Mylar		100
47-51	90 × (0.01 - 1 m) R × 0.3 mL	"	30,100
52-58	90 × (0.01- 1 m) R × 0.1 mL		30,100
59-68	30 × (0.01 - 1 m) R × 0.1 mL		30,100
69-74	30 × (0.01 - 1 m) R × 0.3 mL		30,100
75-90	90 × (0.01 - 0.5 m) R × 0.1 mL		30,84,100
91-93	Decorate conduct plastic		30,84
123-128	90 × (0.005 - 0.5 m) R × 0.1 mL		80-84
129-140	90 × (0.01 - 0.5 m) R × 0.1 mL	500 Ωm sand	50-84
141-146	"	150 Ωm sand	50,55
147-167	"	SDF soil	30-75
168-174	"	140 Ωm sand	30-55
181-185	" + 200 Ω		30-70
186-187	Decorate conduct plastic		55,70
189-197	90 × (0.0025 - 0.5 m) R × 0.1 mL + 200 Ω	"	30-70
198-206	90 × (2 × 50 Ω - 0.5 m) R × 0.1 mL, outer 2 segments	"	30-60
207-223	90 × (0.01 - 0.5 m) × 0.1 mL + 200 Ω	1000 Ωm sand	30-50
234-247	"	MX-A loose[b]	30-95
248-260	"	MX-A tamped	30-100
261-272	"	MX-B loose	30-65
273-293	"	MX-B tamped	30-75
294-302	Azimuthal probes		30-75
303-328	Add radial 0.0025 mR rod	MX-B tamped	0.2,30-65
347-355	0.01 mR rods azimuthal, spaced 0.012 m		30-60
356-366	Repeat after stirring soil		50-65
367-373	Add 0.0025 mR radial rod		30-50
374-392	0.01 mR rods azimuthal, spaced 0.025 m		25-75
393-404	90° × (0.01 - 0.5 m) R × 0.1 mL + 200 Ω	350 Ωm mixed sand	30-65
405-417	0.01 mR rods azimuthal spaced 0.012 m	"	30-75
418-430	90° × (0.01 - 0.5 m) R × 0.3 mL + 200 Ω	"	30-75

[a] Radial profile unless otherwise stated.
[b] MX-A is silt, MX-B is sand/gravel.

III. EXPERIMENTAL RESULTS

The experimental results will be presented according to subject, independent of the experimental chronology. The subjects are:

1. Conduction below breakdown threshold
2. Streamer initiation
3. Apparent conductance at high fields
4. Streamer structure
5. Combined stress experiments
6. Oscillatory behavior
7. Dependence on soil type
8. Dependence on experiment geometry
9. Post arc-over behavior

1. CONDUCTION BELOW BREAKDOWN THRESHOLD

Measurements on conduction in the cylindrical earth samples below threshold for soil breakdown were performed during both the PI and McAir test series using 140 VAC excitation across the sample holder. For some of the materials, the lowest pulsed voltage available at PI, 30 kV, was below the threshold for streamer initiation. The results of these measurements will be discussed in this subsection.

Figure 9 displays a voltage profile measured with a high impedance AC voltmeter in a 0.3 mL, 90° sector of high resistivity sand (~1500 Ωm). The profile appears more or less ohmic from the first voltage probe out to the outer conductor, but exhibits a definite increased impedance near the

TABLE 4. EARTH BREAKDOWN EXPERIMENTS AT MCAIR

Shot #'s	V_0 (kV)	Probes[a] Top	Bottom
MX-B Soil	(0.01-0.5 m) R × 1 mL		
501-510 511-514	0.2, 20-60 30-40	3R	3R to 0.15 m
300 Ωm mixed sand	(0.01-1 m) R × 1 m		
515-524	0.2, 30-70	3R	1R
525-529	30-58	A @ 0.15 m	1R
530	30	1R A @ 0.15 m	1R
531	30	1R	1R
532-542	30-80	1R	3R
300 Ωm mixed sand	(0.003 - 1 m) R × 1 mL		
543-547	42-72	1R	3R
300 Ωm mixed sand	(0.01 - 0.5 m) R × 1 mL		
548	72 Decorate cond. plastic at 0.081 & 0.15 mR		
300 Ωm mixed sand	(0.01 m - 1 m) R × 1 mL, 200 Ω on axis		
549-552	20 kV axial	1R	3R
		Resistor voltage	
553-554	20 kV self bias	1R	3R
555-566	±20 kV combined	1R	3R
567-574	+20 kV axial	1R	3R
	-40 kV radial	1R	3R
575-578	36 to 60 kV self-bias	1R	3R
579-583	+20 kV axial	1R	3R
	-60 kV radial	1R	3R
584-585	80 kV self-bais	1R	3R
588-594	80 kV self-bias	Z/θ profile at 0.14 mR	
300 Ωm mixed sand	(0.01 m - 0.5 m) R × 1 mL, 0.01 mR rods at .15 mR		
595-611	20-40	4×5 Z × θ matrix	
612-625	32-60	θ only	

[a] R radial, A azimuthal

center conductor. Figure 10 displays voltages measured with the high-impedance probes under 30-kV pulsed excitation. A similar increase in apparent impedance near the center electrode is observed. However, the ohmic portion of the curve appears to have a resistivity larger than that measured at 140 VAC by approximately a factor of 1.3. This discrepancy is definitely outside the uncertainty of the measurement. An additional increase by ≈30% of the resistance near the center conductor with time is shown in Figure 10. It is also outside experimental uncertainty. These data appear to indicate a slight increase in bulk resistivity with increasing electric field, and an increased contact impedance with pulse duration at high fields. The latter is consistent with a partially blocking contact, for which the contact polarization builds up, with time, to an equilibrium value. After this, the current transported across the contact becomes continuous with the behavior of the bulk material.

Figure 11 presents similar profiles under a 30-kV pulse in 300-Ωm sand mix. In this case, enhanced conduction, presumably due to streamers, is observed near the center conductor. The small apparent change in contact impedance between 20 and 40 μs is not outside the experimental uncertainty due to the long response time of the probe used for this measurement. Additional data on 300-Ωm sand mix taken during the McAir experiments are shown in Figures 12 and 13. Figure 12 demonstrates some degree of inhomogeneity at 140 VAC in the material, both in azimuth at the top and between the top and bottom. The increase in impedance near the center conductor is again apparent. A set of profiles taken at 30 kV at the 0° azimuth on the bottom are shown in Figure 13. Some breakdown near the center conductor is evident. The apparent resistivity in the outer regions falls within the measurements of the various locations in Figure 12 and agrees particularly well with the 140-VAC measurements in the bottom at the 0° azimuth.

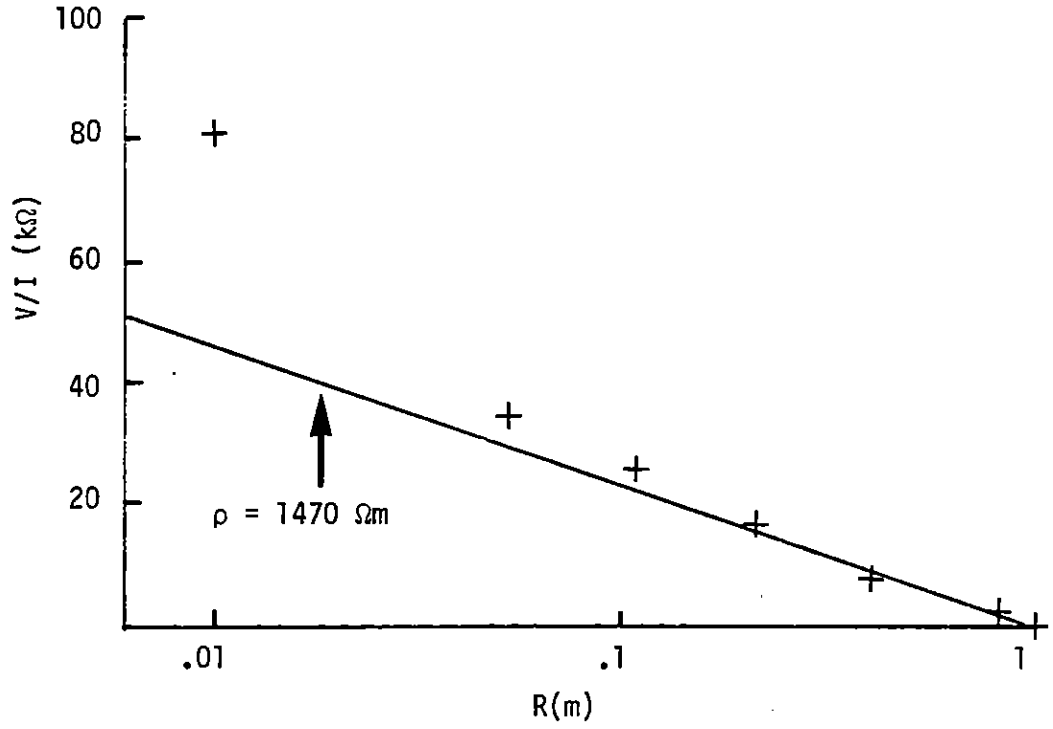

Figure 9. Voltage profile.
(140 VAC, 1500 Ωm sand
90° x 0.3 mL)

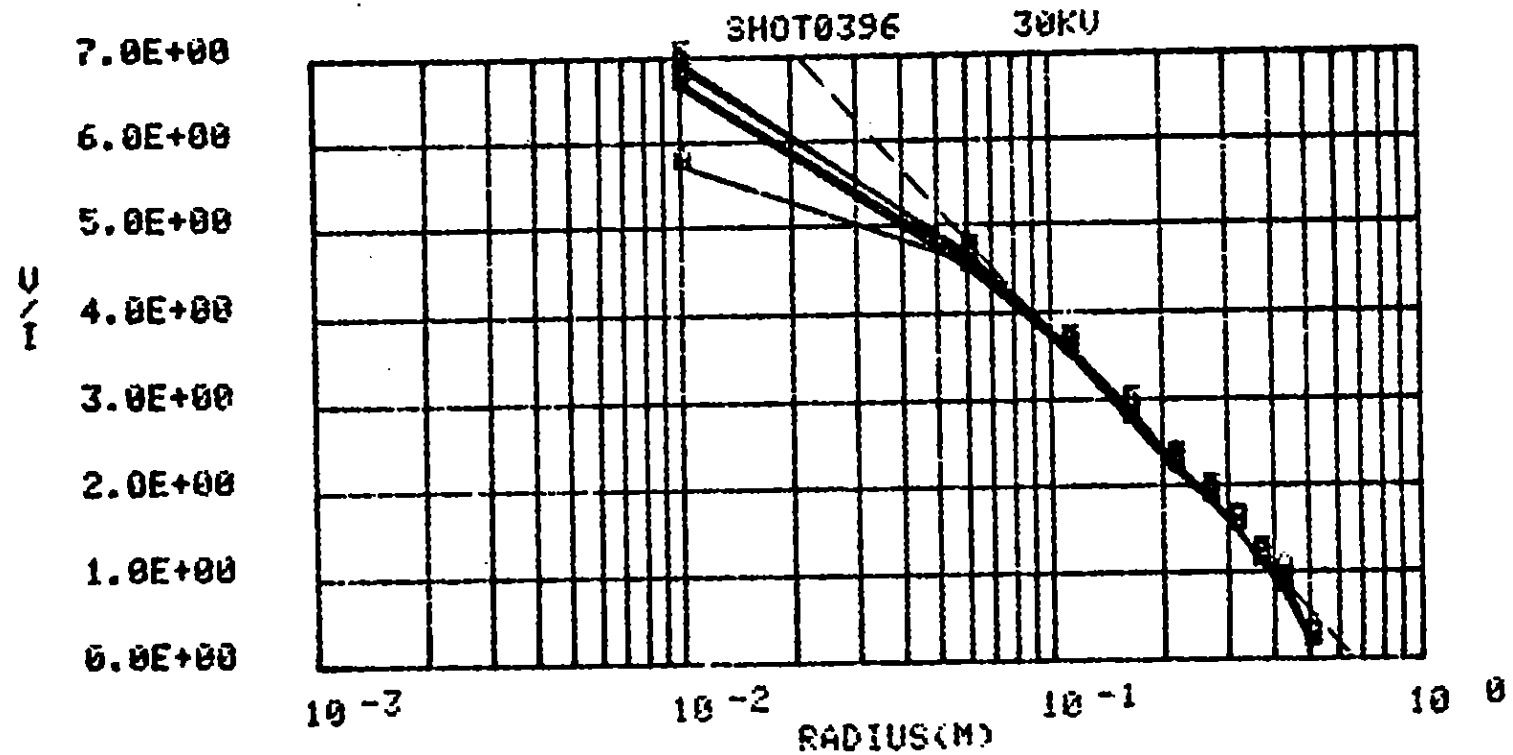

CODE	A	B	C	D	E
TIME	20 μs	40 μs	70 μs	110 μs	190 μs
CURRENT	5.3	5.0	4.8	4.5	4.4

Figure 11. Voltage profile.
(300 Ωm sand mix
PI, 90° x 0.1 m)

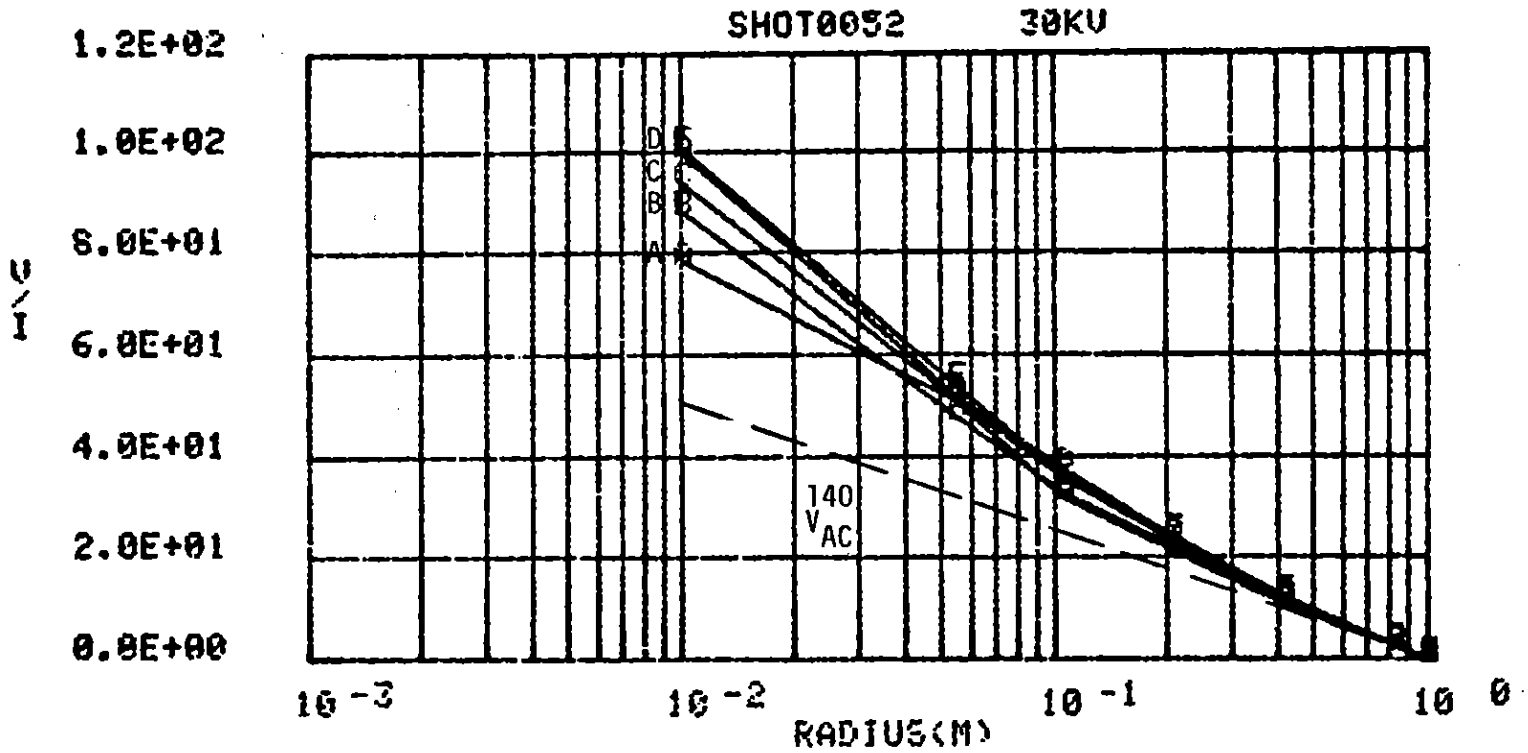

CODE	A	B	C	D	E
TIME	20 μs	40 μs	70 μs	110 μs	190 μs
CURRENT	0.4	0.4	0.4	0.3	0.3

Figure 10. Voltage profile.
(1700 Ωm sand)

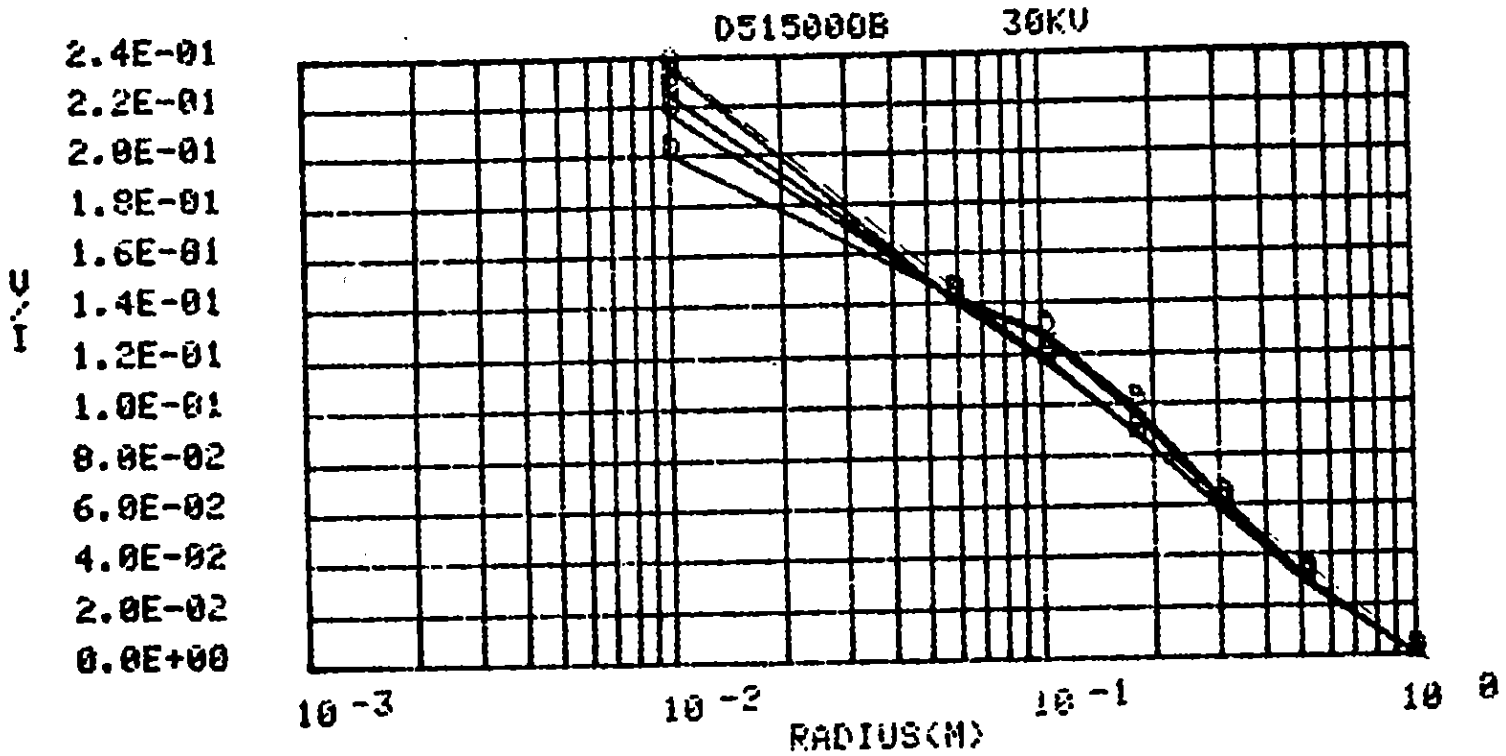

CODE	A	B	C	D
TIME	40 µs	80 µs	100 µs	180 µs
CURRENT	125.0	131.3	131.3	137.5

Figure 13. Voltage profile.
(300 Ωm sand mix
McAir, 360° x 1 m)

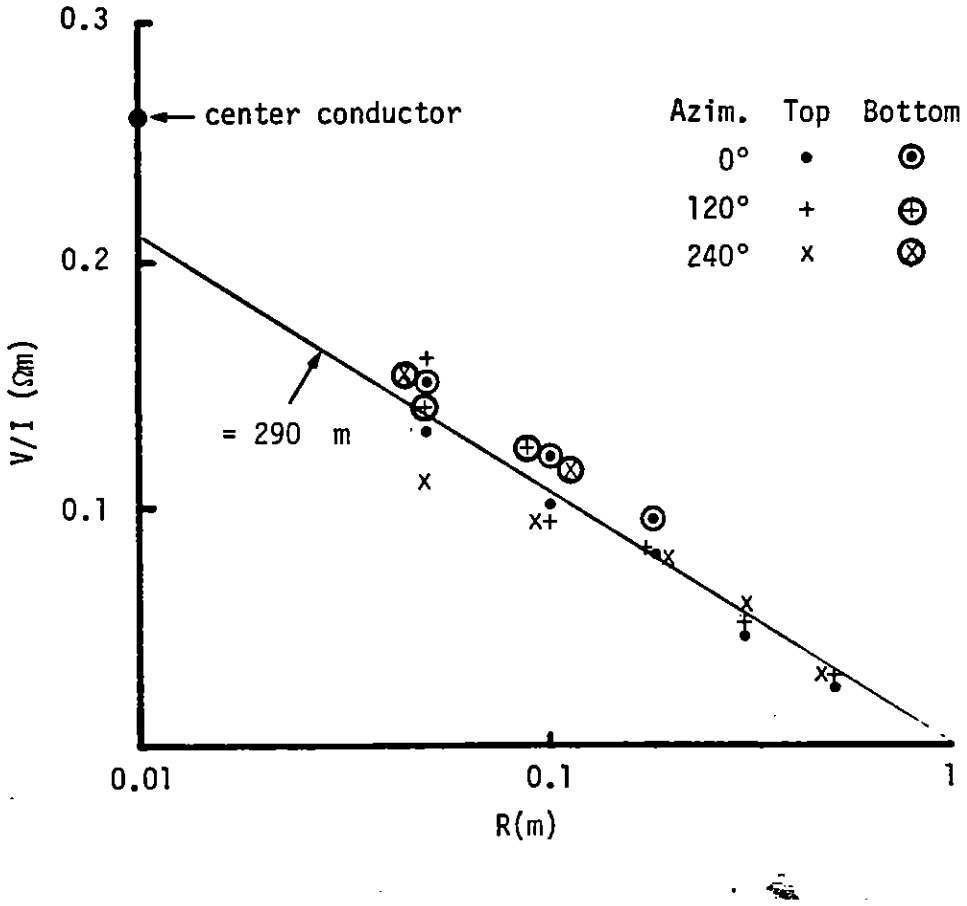

Figure 12. Voltage profile.
(140 VAC, 300 Ωm sand mix
360° x 1 mL)

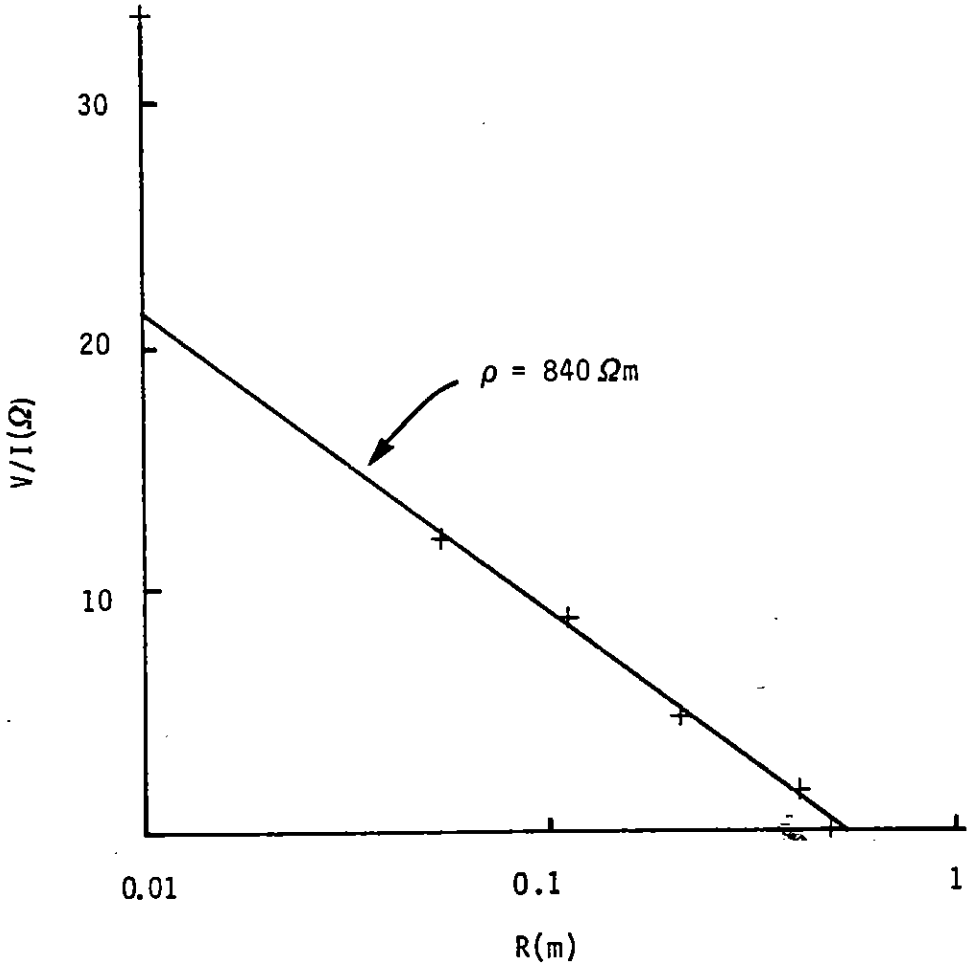

Figure 14. Voltage profile.
(140 VAC, SDF soil
90° x 0.1 mL)

Figures 14 and 15 compare profiles in SDF soil in 90° × 0.1 mL geometry under excitation with 140 VAC and a 30-kV pulse, respectively. Again, both exhibit enhanced impedance near the center rod. The resistivity in the outer regions of the sample appears to be 35% larger with 30-kV pulsed excitation than with 140 VAC. A small increase in contact impedance during the 30-kV pulse up to 190 μs is also apparent.

Figures 16 through 18 present similar comparisons with the MX-B soil. Figure 16 corresponds to 140-VAC excitation of a 90° × 0.1 mL sector. The shape of this curve is similar to the ones discussed before, although the magnitude of the contact impedance appears to be considerably less than in the higher resistivity sand samples. The current was not measured during this test so it is not possible to determine the absolute resistivity. Figure 17 presents the voltage profile observed with a 30-kV pulse. The decreased slope in close is undoubtedly the result of breakdown streamers between the center conductor and the first two voltage probes. The increased slope between the outermost probe at R = 0.41 m and the outer conductor is an apparent manifestation of contact impedance at the outer conductor. Figure 18 shows the voltage profile in the 360° × 1 mL MX-B soil sample at McAir with 140 VAC applied. There is a considerable difference in slope of the resistive portion between the top and the bottom, indicating that a more-than-proportionate fraction of the sample current is flowing through the bottom of the chamber, assuming the resistivity of the outermost material is independent of height in the chamber. A pulsed exposure of this sample was performed at 20 kV, but the data have not been reduced. The record of the current through the sample indicates an increase of a factor of 1.4 during the first 50 μs. This demonstrates that significant soil breakdown was occurring even with only 20 kV applied.

These data indicate that, in high resistivity soils, there is a small increase in effective resistivity with increase in current density, a small increase in impedance near the small diameter center electrode, particularly in the small geometries, and a small increase with time of the

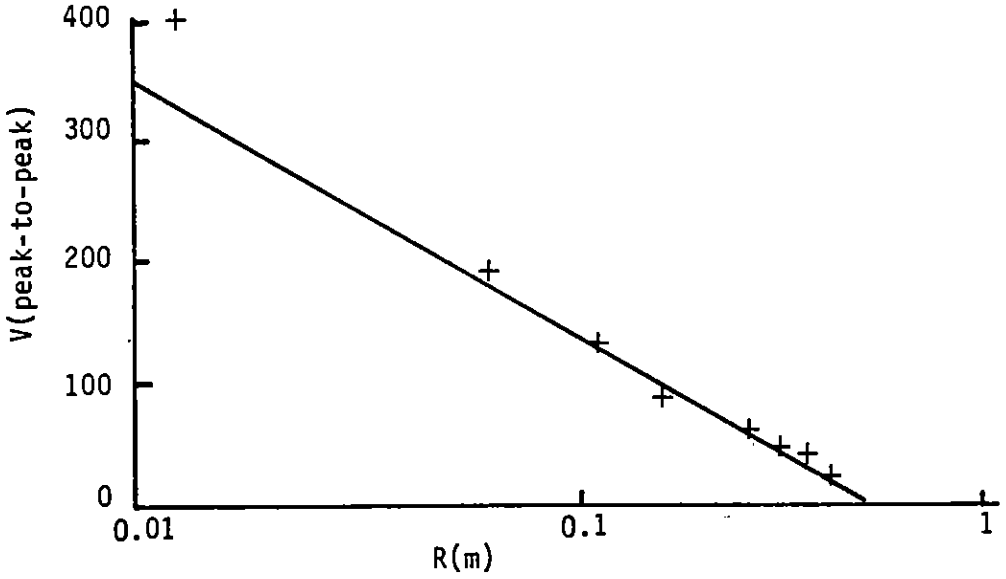

Figure 16. Voltage profile.
(140 VAC, MX-B
90° x 0.1 mL)

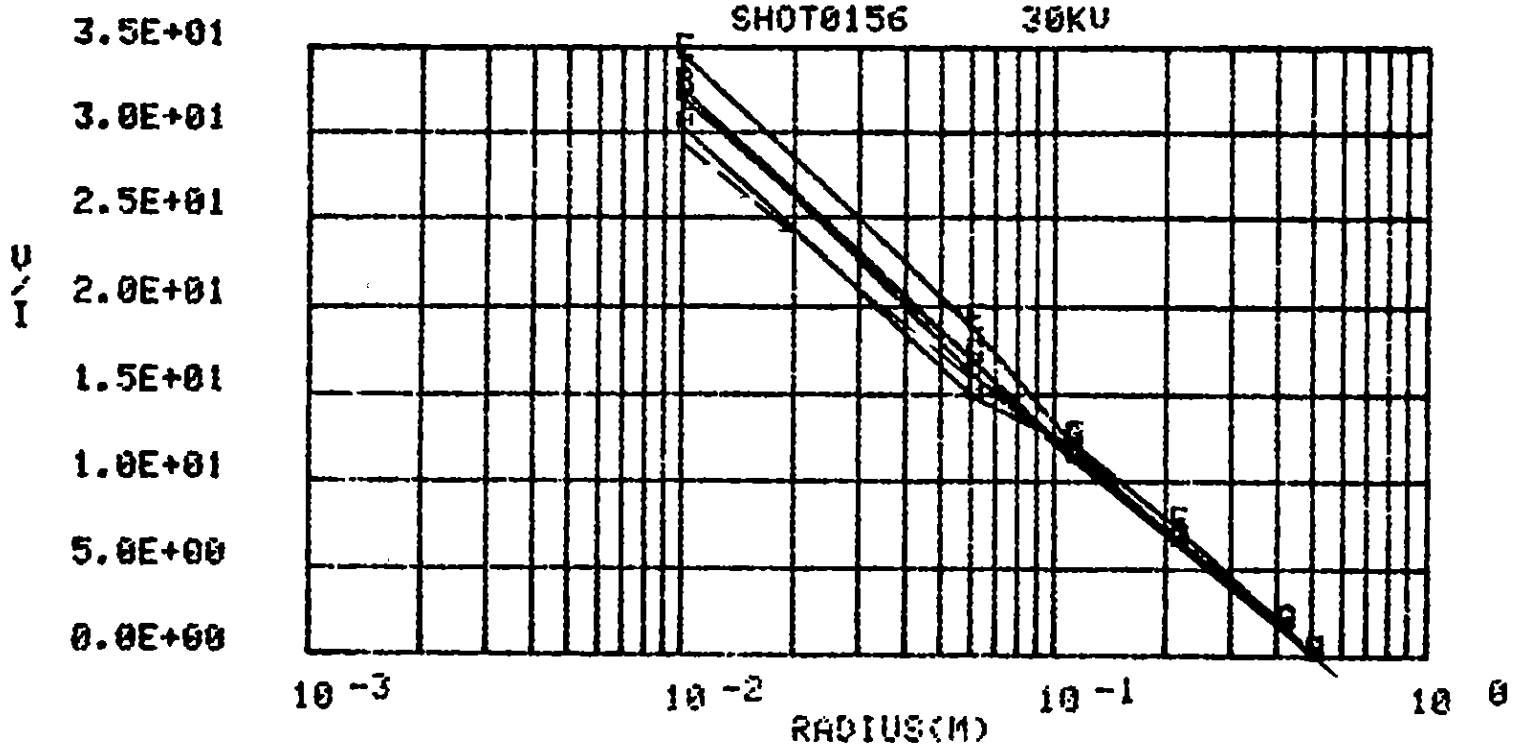

CODE	A	B	C	D	E
TIME	20 μs	40 μs	70 μs	110 μs	190 μs
CURRENT	1.1	1.0	1.0	1.0	0.9

Figure 15. Voltage profile.
(1200 Ωm SDF soil)

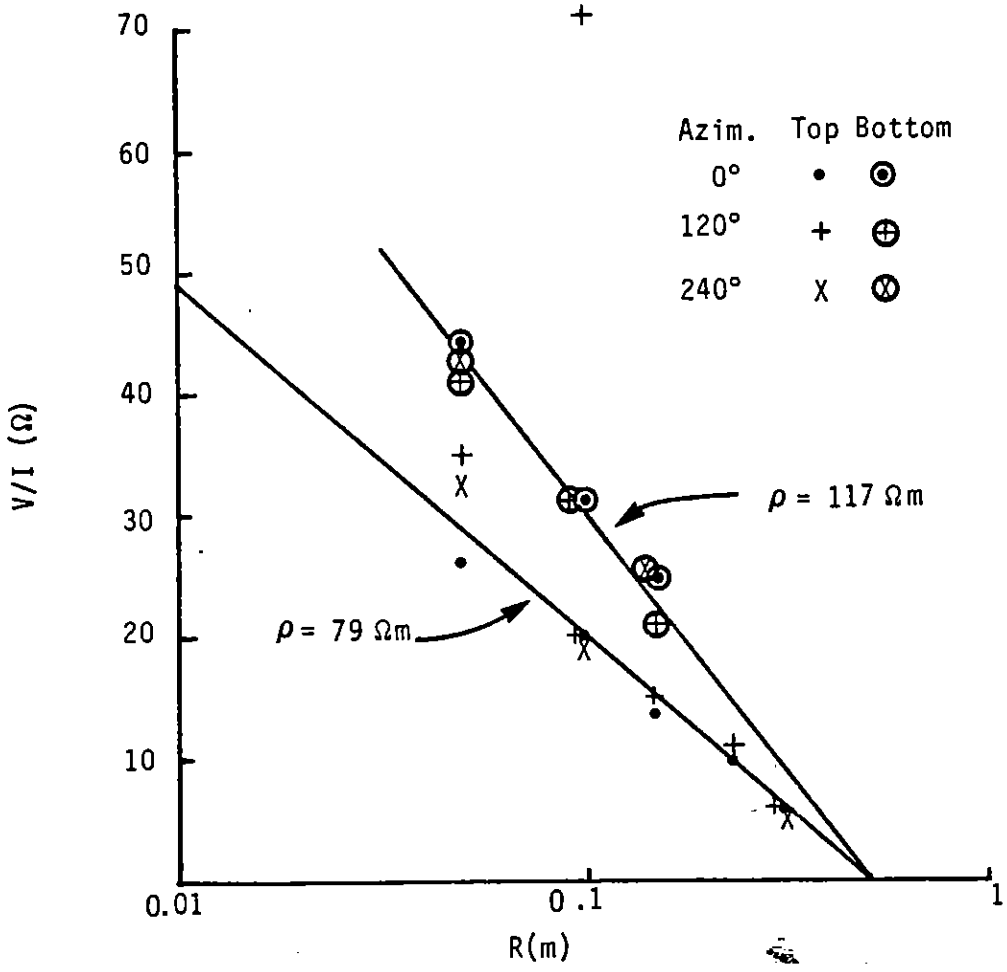

Figure 18. Voltage profile.
(140 VAC, MX-B
360° x 1 mL)

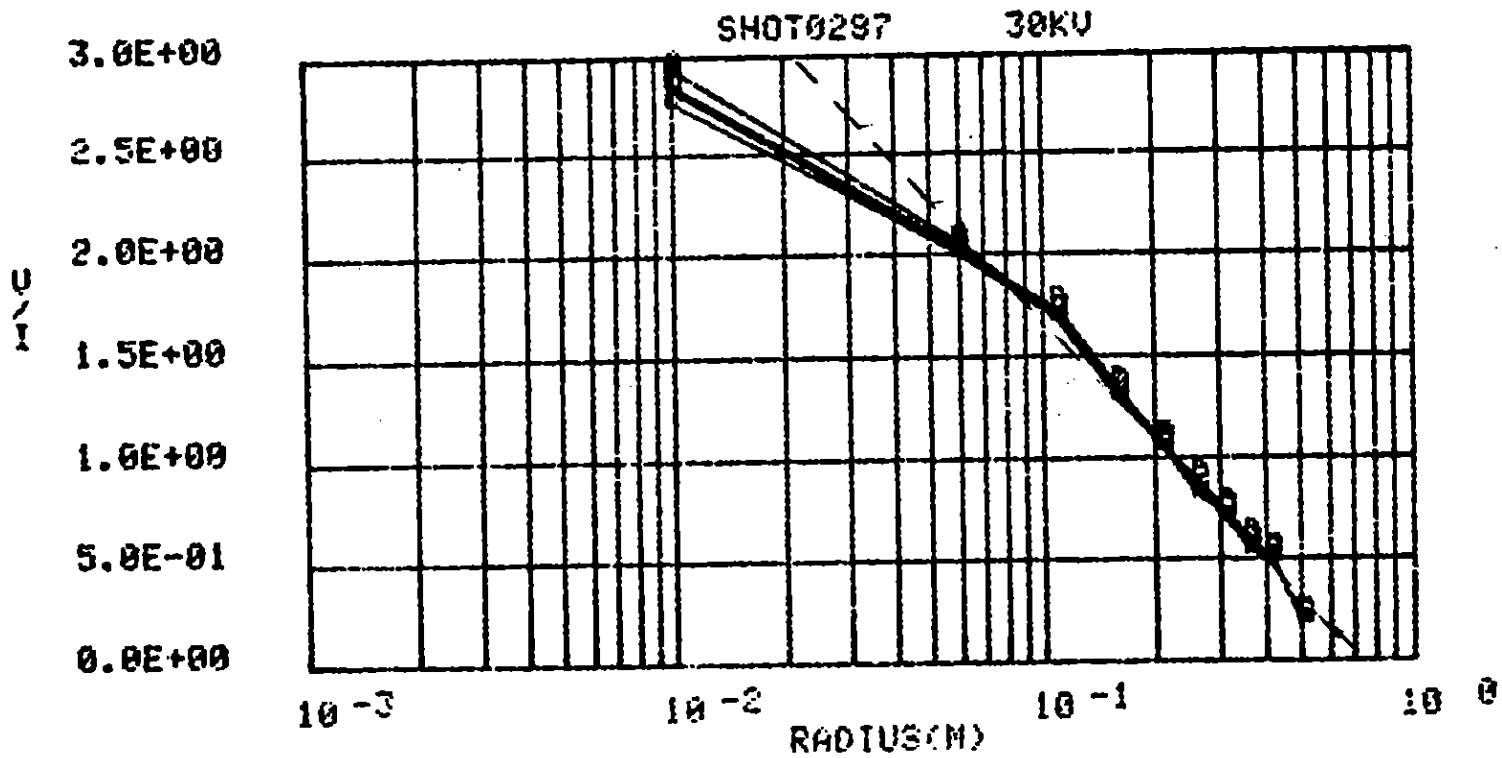

CODE	A	B	C	D
TIME	40 μs	70 μs	110 μs	190 μs
CURRENT	11.5	11.5	11.3	10.5

Figure 17. Voltage profile.
(140 Ωm MX-B soil)

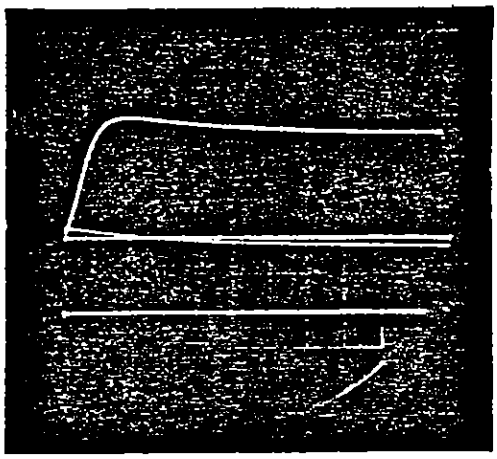

V_a = 30 kV

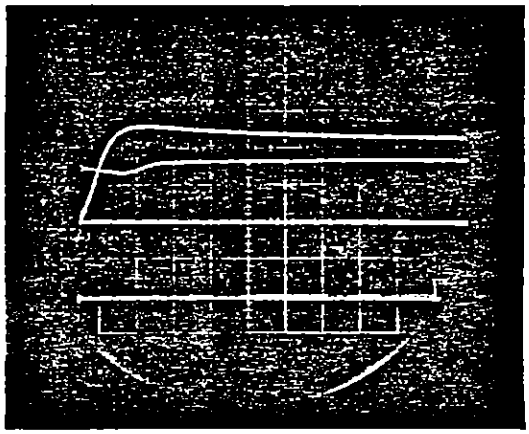

V_a = 45 kV

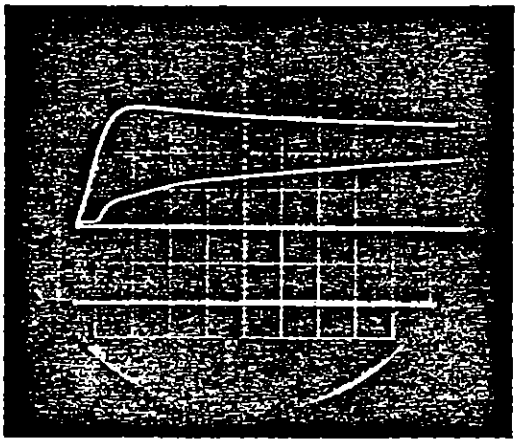

V_a = 55 kV

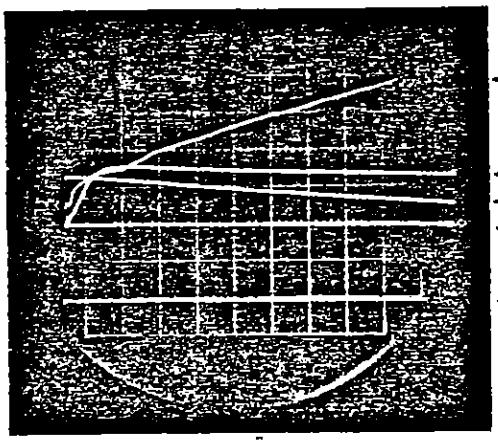

V_a = 64 kV

Upper = Voltage
Lower = Current
Sweep = 20 µs/div

Figure 19. Streamer development.
(350 Ωm sand mix
90° x 0.1 mL)

contact impedance under electric stresses below the threshold for streamer formation. While these effects are noticeable, their importance decreases under larger stresses which produce soil breakdown in the regions close to the central rod.

2. STREAMER INITIATION

As the pulsed field is increased beyond a threshold value, evidence for enhanced conduction near the central conductor appears in the 90° × 0.1 mL experiments (see Figure 1) after a time delay, which decreases with increasing electric field. Figure 19 presents four photographs of the sample current in the 300 Ωm sand mix in 90° × 0.1 mL geometry at increasing values of the applied voltage. At 30 kV the current immediately jumps to its ohmic value and decays slowly as a result of the buildup of contact impedance and the decay of the applied voltage. At 45 kV the current decays for approximately 20 μs along a similar curve, but then increases with some evidence of irregularity. At 55 kV the delay before the current increases is only ≈100 μs. At 64 kV the increase commences ≈4 μs after the application of the voltage.

A similar set of data for the same sand mixture in 90° × 0.3 mL geometry is shown in Figure 20. At corresponding voltages the initiation of the enhanced conduction appears to occur at slightly shorter times. Figure 21 illustrates the behavior of the same soil type in 360° × 1 mL geometry during the McAir experiments. Evidence of streamering with no observable delay time is apparent even at 30 kV. Figure 22 summarizes the measurements of streamer initiation times versus the electric field at the center conductor for these three geometries. Even though there is a considerable spread in values under the same conditions, it is obvious that the streamer initiation time decreases with increasing contact area. The dependence of streamer initiation time on resistivity of sand is illustrated in Figure 23. It is apparent that the electric field at which a given

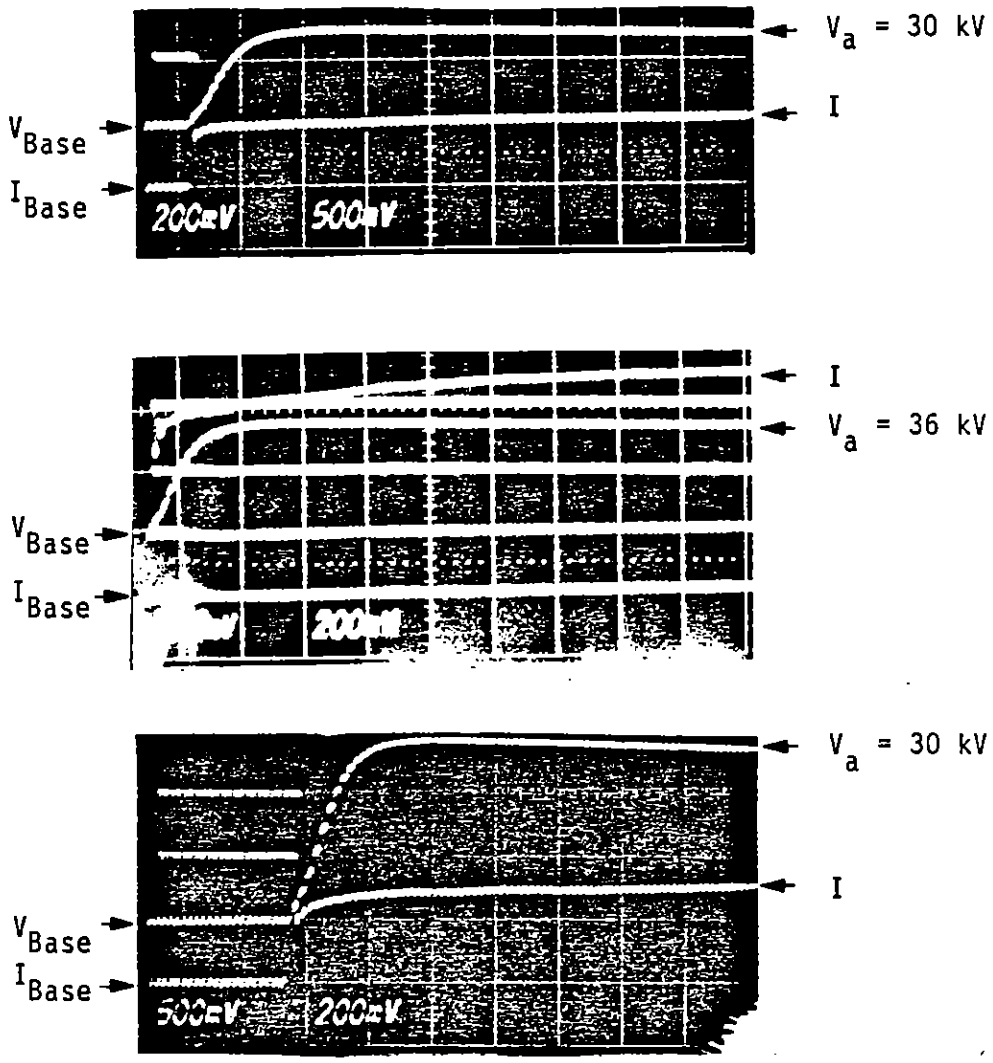

Figure 21. Streamer development.
(350 Ωm sand mix
360° x 1 mL)

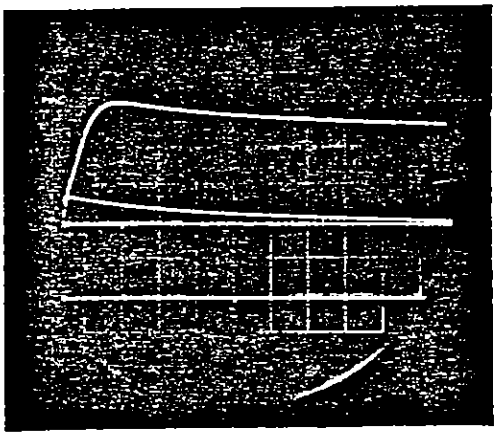

V_a = 30 kV

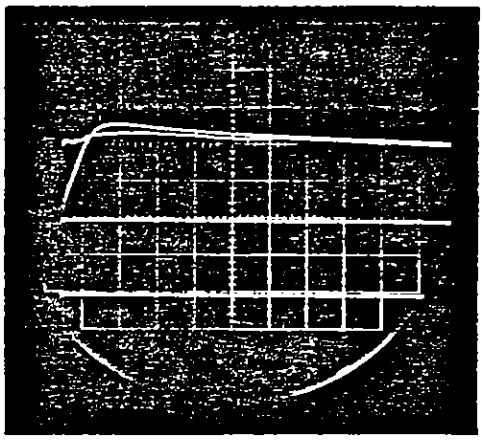

V_a = 45 kV

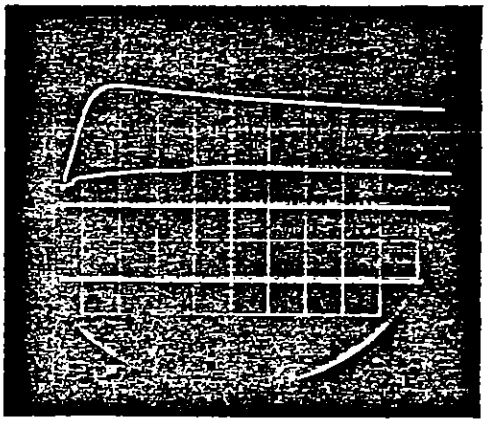

V_a = 55 kV

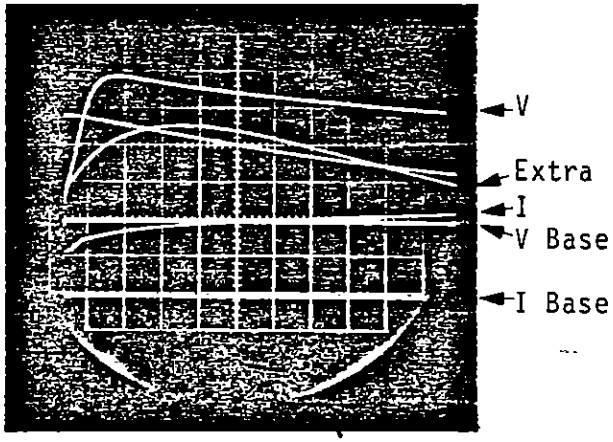

V_a = 65 kV
Upper - Voltage
Lower - Current
Sweep - 20 μs/div

Figure 20. Streamer development.
(350 Ωm sand mix
90° x 0.3 mL)

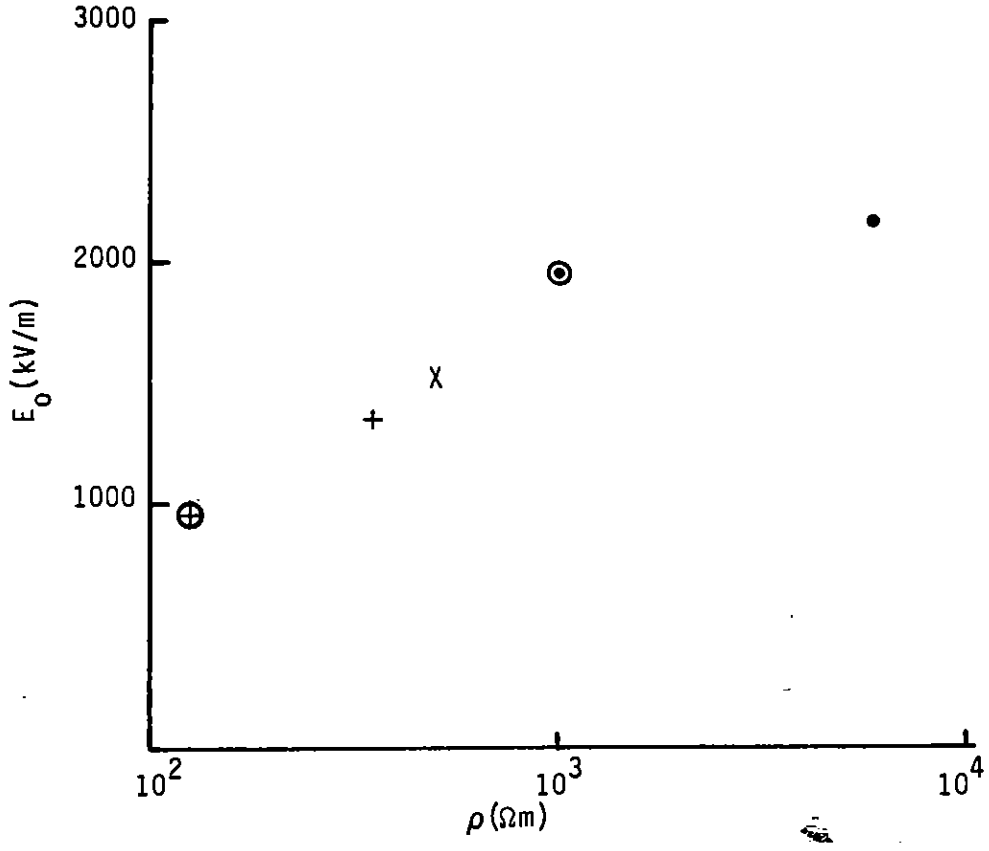

Figure 24. Electric field for t_i = 10 μs (Ref. 23).

initiation time is observed decreases with decreasing resistivity. The approximate electric field at which the initiation time is 10 μs is plotted versus the sample resistivity in Figure 24. A comparison of the streamer initiation times for two different soil types at a given resistivity is shown in Figure 25. There is no noticeable difference between the low resistivity sand and the MX-B soil, which is a mixture of mostly sand and small gravel with relatively little silt. No such comparison could be performed for the MX-A soil because its streamer initiation time was less than 1 μs even at 30 kV, and no sand of equivalent resistivity was tested.

Even though there was no measurable delay between the application of the electric field and initiation of streamers at any field in the 360° × 1 mL geometry or at the highest fields in the 90° × 0.1 mL and 90° × 0.3 mL geometries, the initial value of the current was proportional to the applied voltage over the entire range of applied voltages in both sets of experiments. This is illustrated by the McAir experiments in Figure 26. The apparent resistivity is 30% greater than the value measured from the voltage profiles (see Figs. 12 and 13), but this is a reflection of the additional impedance near the central rod.

These investigations lead to the following description of the manifestations of streamer initiation. At the time of application of a voltage pulse with a rise time ~1 μs, the current flowing through the sample appears to rise to a value proportional to the applied voltage. At sufficiently high electric fields, the conducting streamers develop from the central conductor outwards after a delay time that decreases with increasing electric field, and with increasing area of central electrode. The field at which a given delay time is observed increases with increasing soil resistivity.

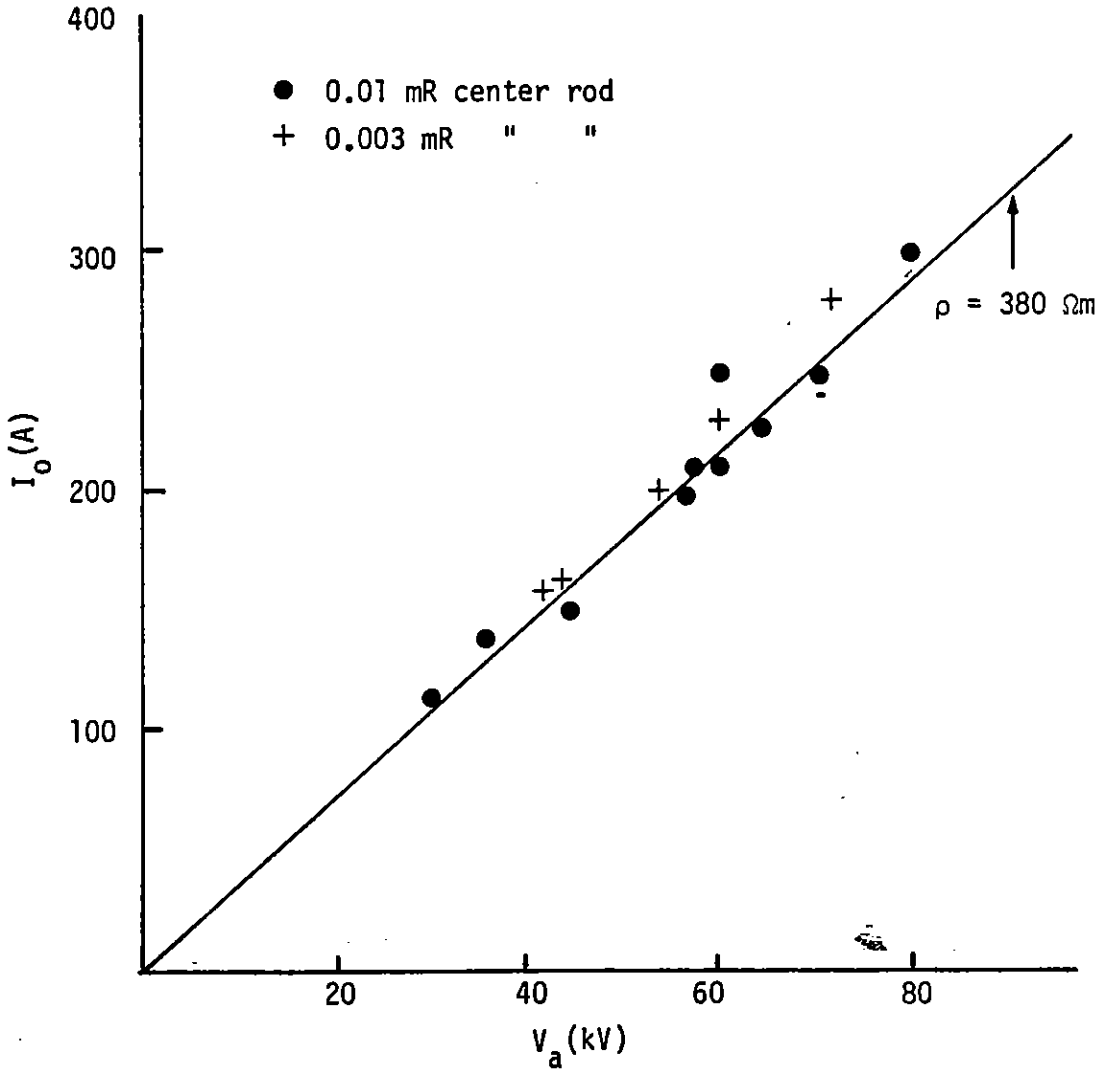

Figure 26. Initial current vs applied voltage.
(360° x 1 mL, 300 Ωm mix)

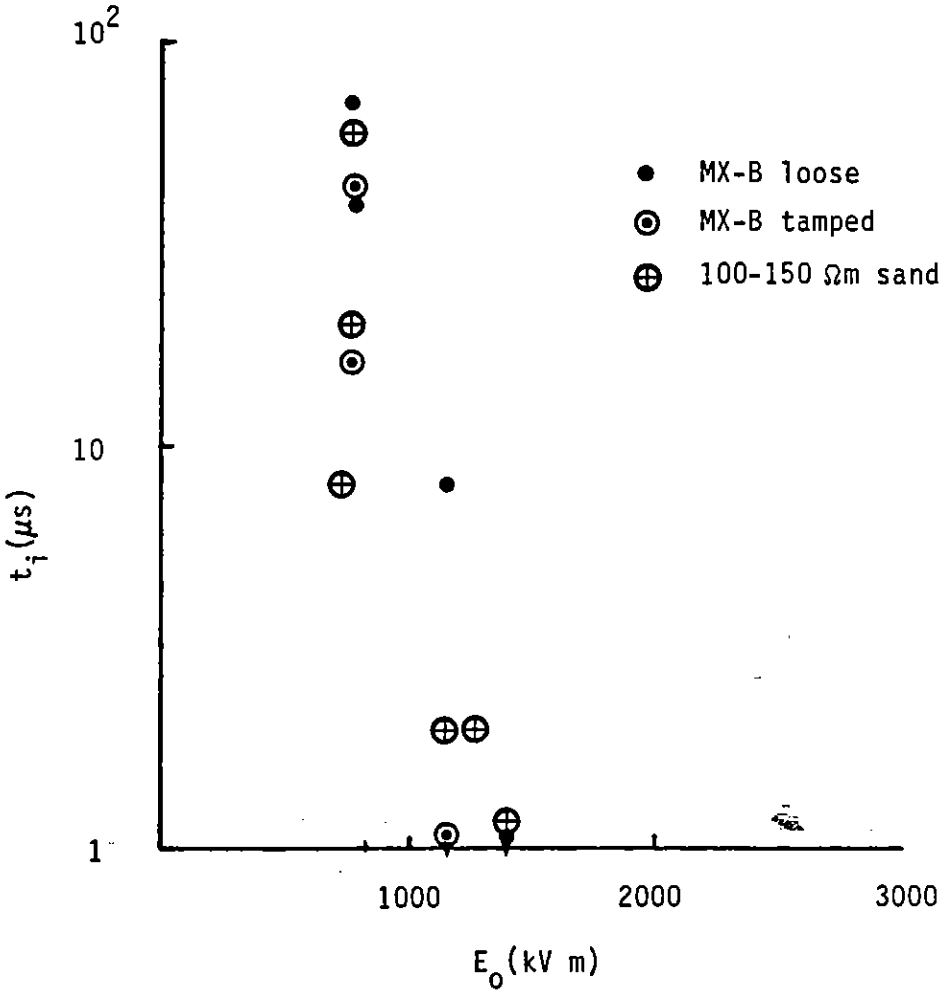

Figure 25. Streamer initiation times vs. soil type.

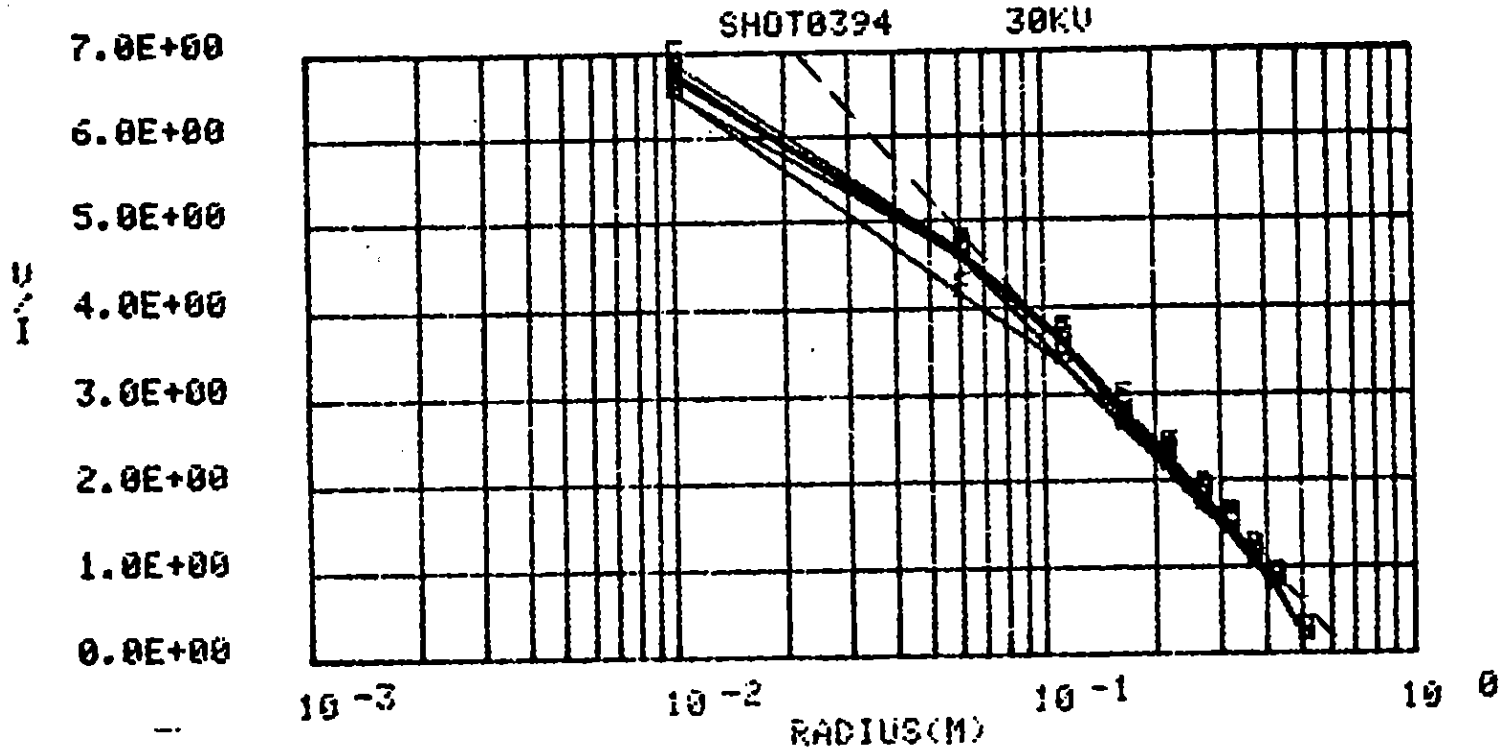

CODE	A	B	C	D	E	F
TIME	100 µs	200 µs	300 µs	500 µs	900 µs	1900 µs
CURRENT (A)	4.8	4.4	4.3	4.0	3.5	2.8

Figure 27. Voltage profile.
(350 Ωm sand mix
90° x 0.1 mL)

3. APPARENT CONDUCTANCE AT HIGH FIELDS

At electric fields above the threshold for streamer initiation at the center conductor, the conductance of the soil sample increases with increasing field and with time during the electrical pulse. The behavior of 300-Ωm sand mix will be used to illustrate the development and propagation of streamers leading up to a high enough applied voltage to arc-over between the central rod and outer conductor. Figures 27 through 30 illustrate the voltage profiles as a function of time for a selected range of applied voltages. At 30 kV (Fig. 27) the enhanced conduction is apparent out to ~0.1 m at 200 to 1900 μs. At 45 kV (Fig. 28) the conductance in the inner portions of the sample become slightly higher than at 30 kV. As a result of the greater charge loss from the pulser capacitor, the current at 1900 μs has decreased to a value comparable to earlier currents at 30 kV. At this point the close-in conductance appears to have increased to a value comparable to the 30-kV pulse value.

At 55 kV (Fig. 29) the conducting streamers extend beyond 0.2 m and the relaxation at late times is more apparent. At 65 kV (Fig. 30) the conducting streamers extend to approximately R = 0.3 m at 100 μs followed by arc-over at 140 to 160 μs. After arc-over the impedance in the arc continues to fall over a time greater than 100 μs. The data indicate that a significant fraction of the end-to-end resistance appears across the interfaces between earth and the electrodes, both inner and outer. The development of the arc resistance with time is shown in Figure 29, which represents, on a different scale, the voltage profile after arc-over for shot 403. There is an indication that the arc impedances increases when the current falls (curve D in Fig. 31).

The behavior of similar sand samples in a 90° × 0.3 mL geometry is illustrated in Figures 32 through 37. The general behavior is similar to that shown in Figures 27 through 31 for 90° × 0.1 mL geometry, but the threshold for arc-over appears to have increased by ≈10 kV.

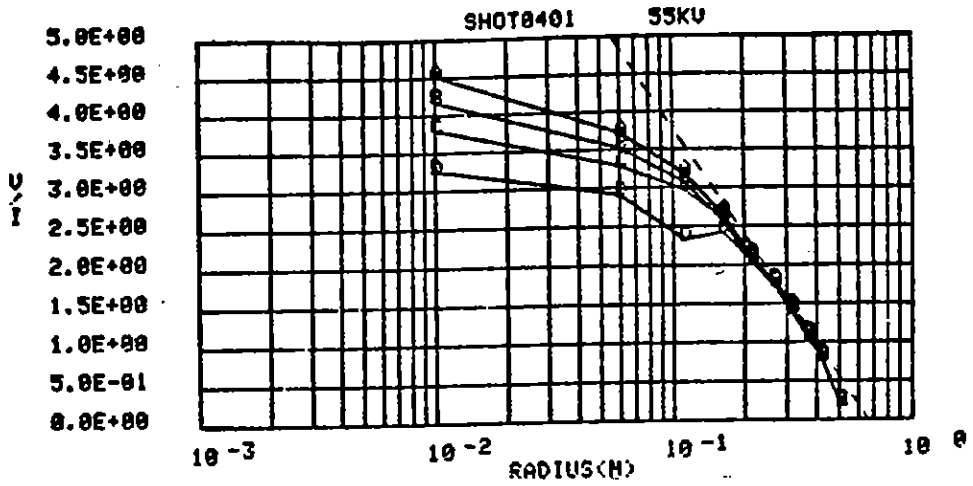

Code	A	B	C	D
Time	40 µs	70 µs	110 µs	190 µs
Current	13.50	14.25	15.25	16.75

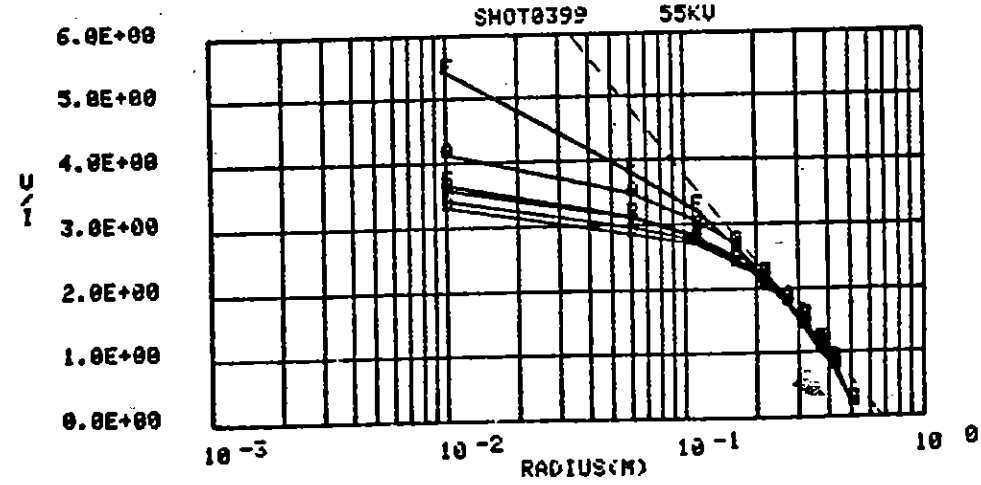

Code	A	B	C	D	E	F
Time	100 µs	200 µs	300 µs	500 µs	900 µs	1900 µs
Current	14.00	15.25	15.00	14.00	10.75	5.00

Figure 29. Voltage profile.
(350 Ωm sand mix
90° x 0.1 mL)

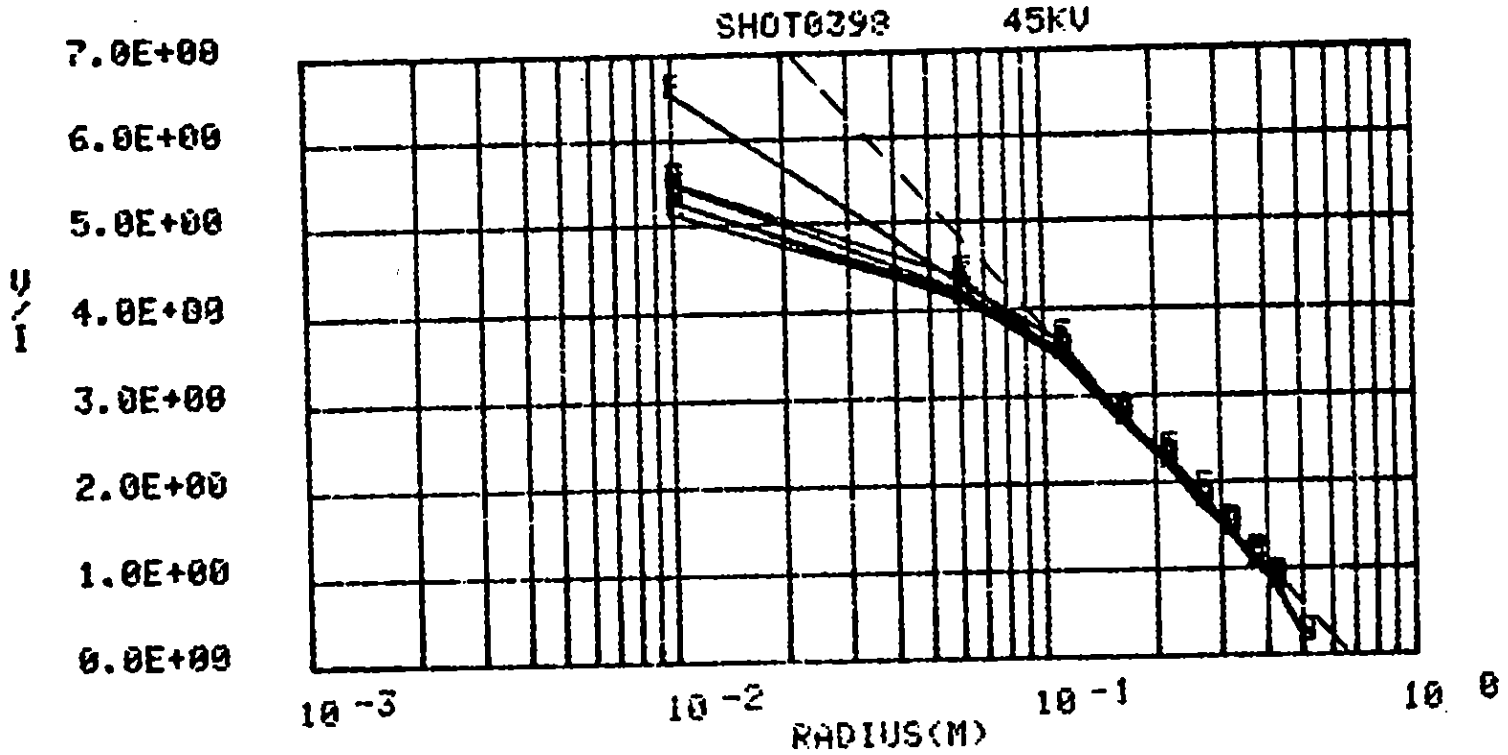

CODE	A	B	C	D	E	F
TIME	100 µs	200 µs	300 µs	500 µs	900 µs	1900 µs
CURRENT	8.8	8.6	8.5	7.8	6.5	4.0

Figure 28. Voltage profile.
(350 Ωm sand mix
90° x 0.1 mL)

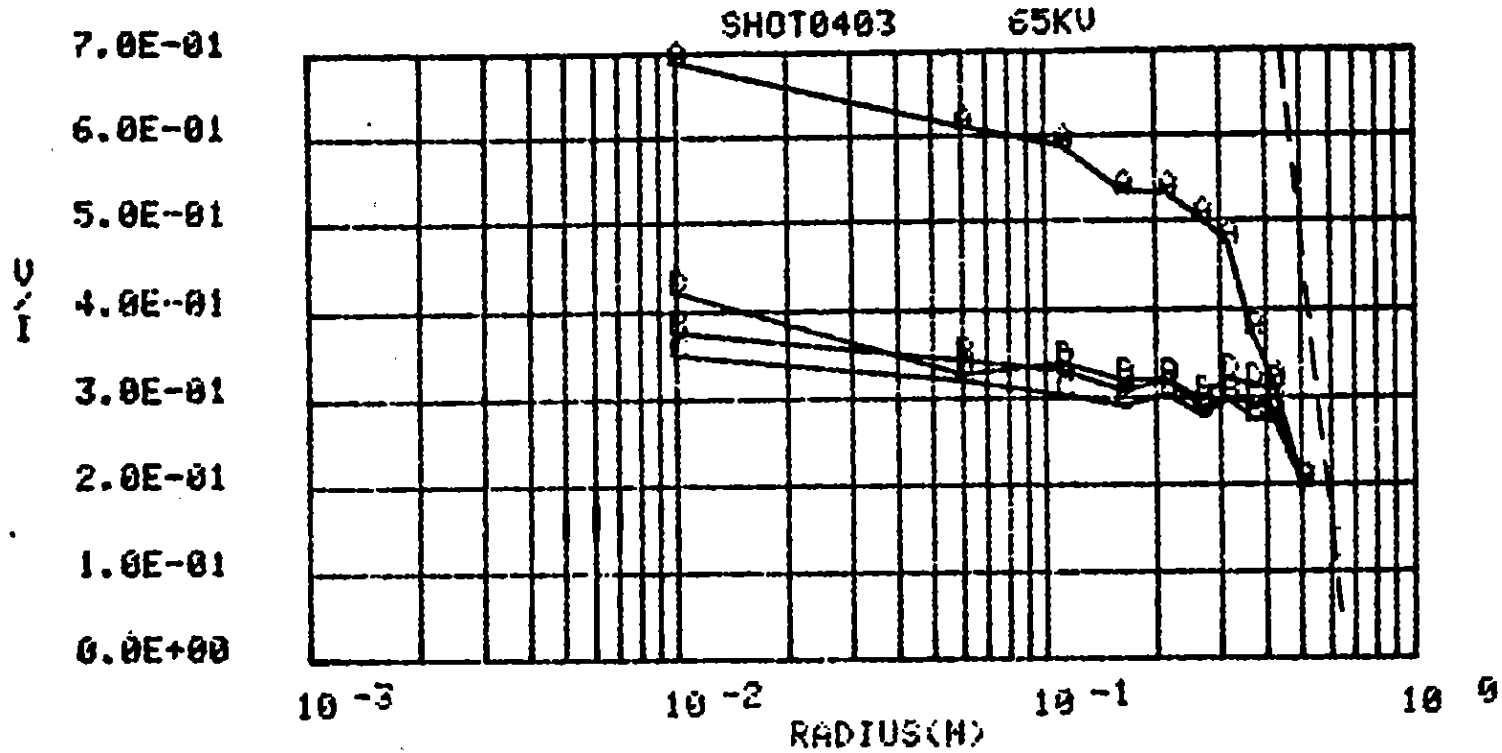

CODE	A	B	C	D
TIME	150 µs	200 µs	275 µs	475 µs
CURRENT	95.0	153.8	130.0	52.5

Figure 31. Voltage profile.
(350 Ωm sand mix
90° x 0.1 mL)

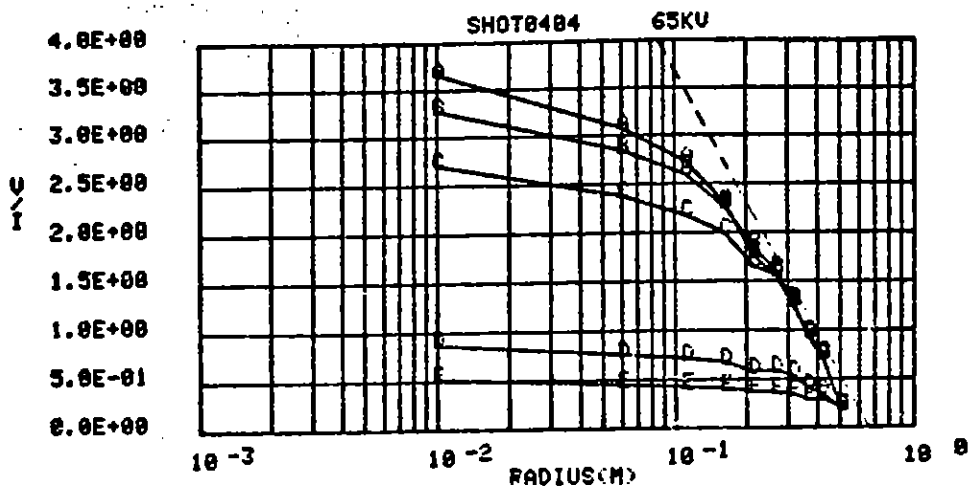

Code	A	B	C	D	E
Time	40 µs	70 µs	110 µs	170 µs	190 µs
Current	20.0	21.3	25.0	75.0	125.0

t_B = 165 µs

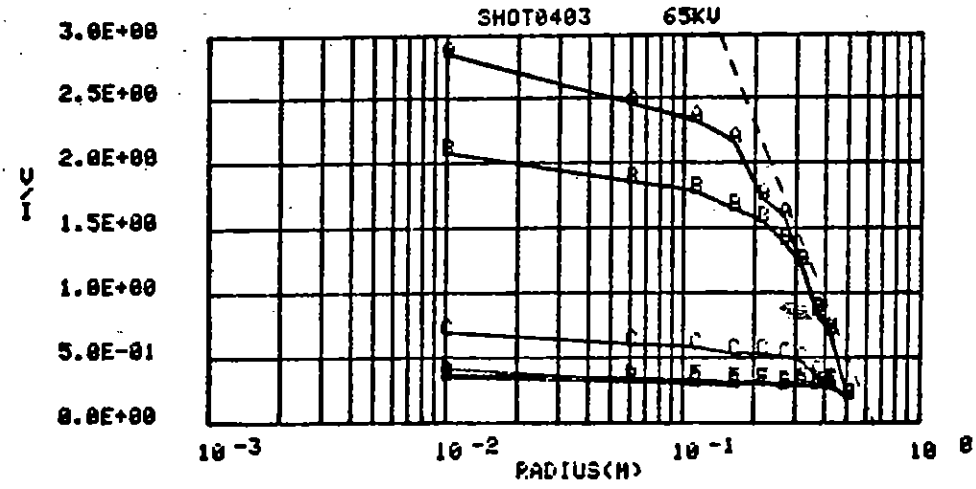

Code	A	B	C	D	E	F
Time	50 µs	100 µs	150 µs	200 µs	275 µs	475 µs
Current	25.0	32.5	95.0	153.8	130.0	52.5

t_B = 140 µs

Figure 30. Voltage profile.
(350 Ωm sand mix
90° x 0.1 mL)

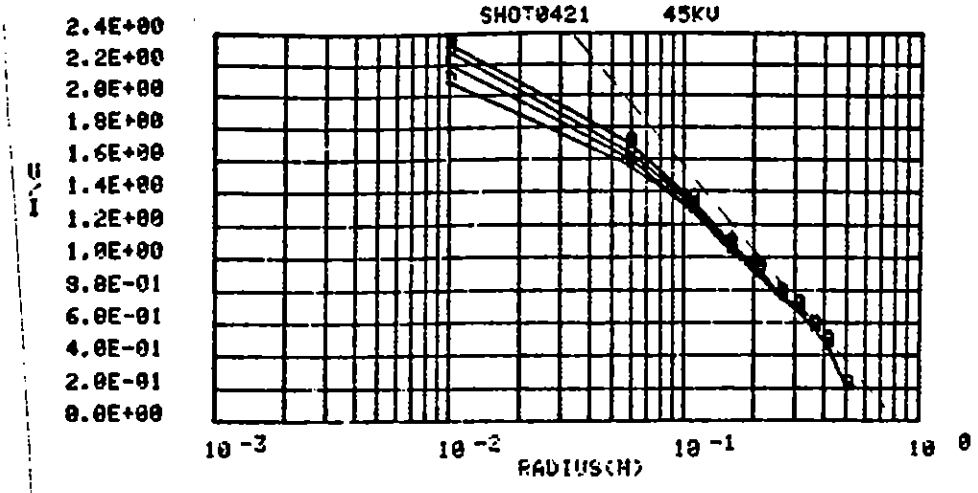

Code	A	B	C	D
Time	40 µs	70 µs	110 µs	190 µs
Current	21.3	21.0	21.0	20.5

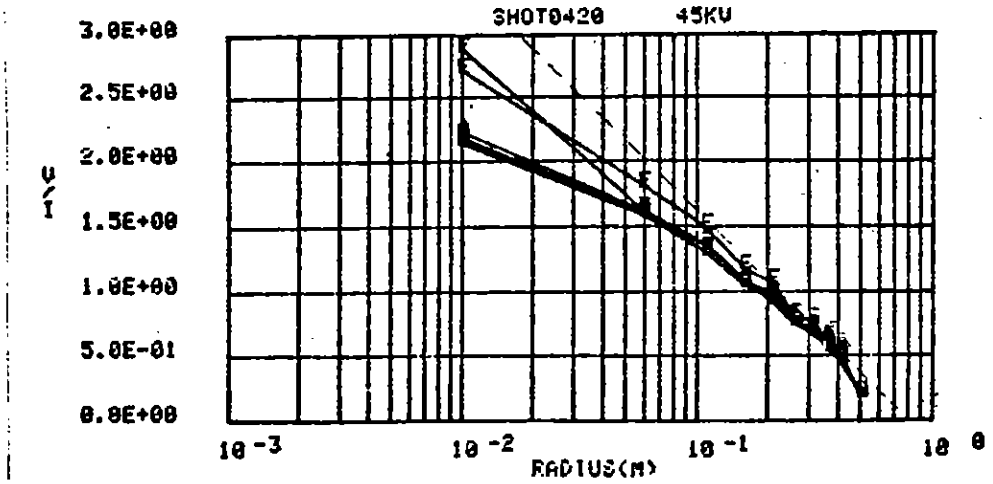

Code	A	B	C	D	E	F
Time	100 µs	200 µs	300 µs	500 µs	900 µs	1900 µs
Current	20.8	20.0	18.5	15.5	10.0	5.5

Figure 33. Voltage profile.
(350 Ωm sand mix
90° x 0.3 mL)

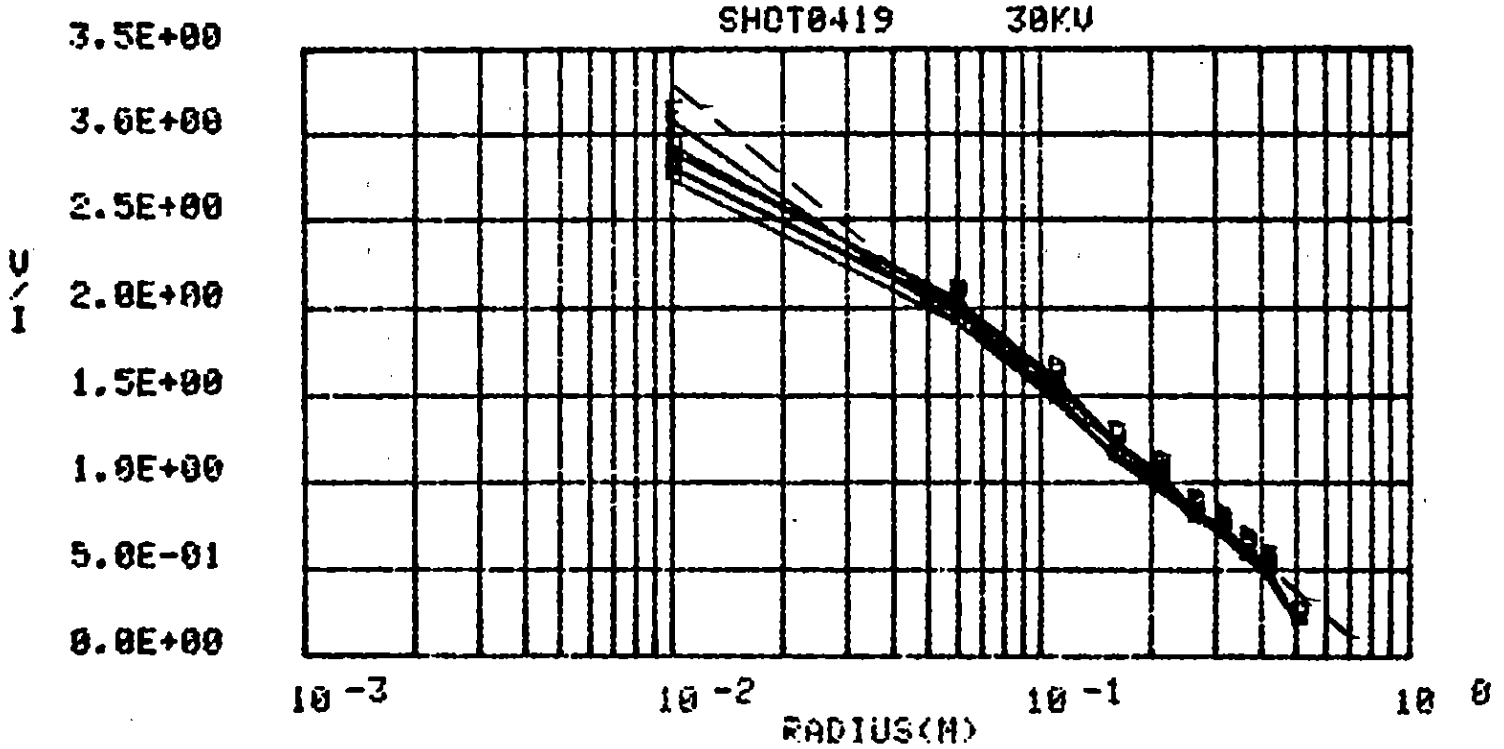

CODE	A	B	C	D	E	F
TIME	100 µs	200 µs	300 µs	500 µs	900 µs	1900 µs
CURRENT	11.0	10.0	9.5	8.0	6.5	3.8

Figure 32. Voltage profile.
(350 Ωm sand mix
90° x 0.3 mL)

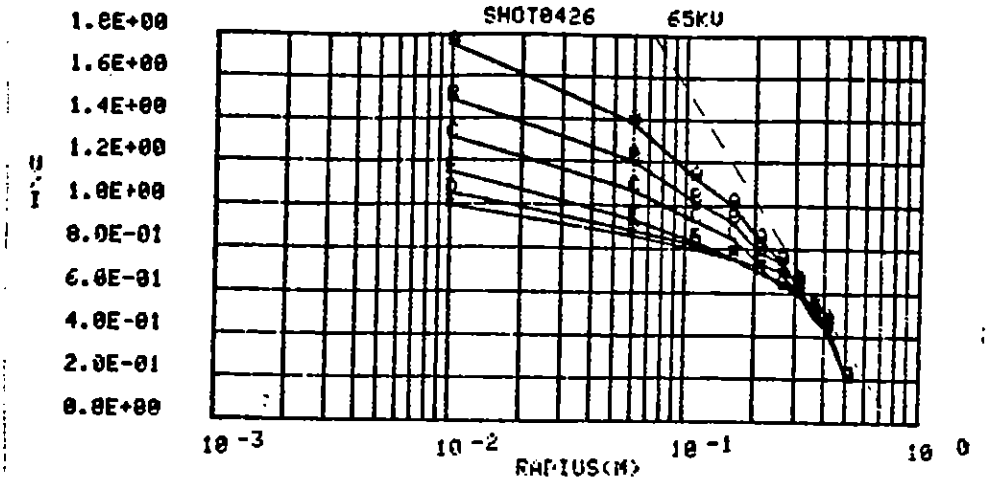

Code	A	B	C	D	E	F
Time	25 µs	50 µs	75 µs	175 µs	275 µs	475 µs
Current	40.0	45.0	50.0	55.0	50.0	35.0

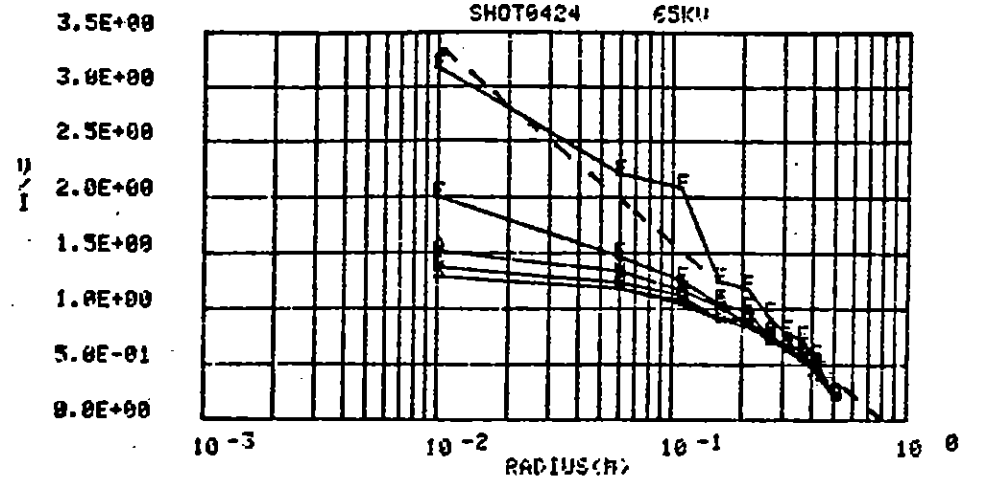

Code	A	B	C	D	E	F
Time	100 µs	200 µs	300 µs	500 µs	900 µs	1900 µs
Current	42.5	45.0	40.0	30.0	15.0	5.0

Figure 35. Voltage profile.
(350 Ωm sand mix
90° x 0.3 mL)

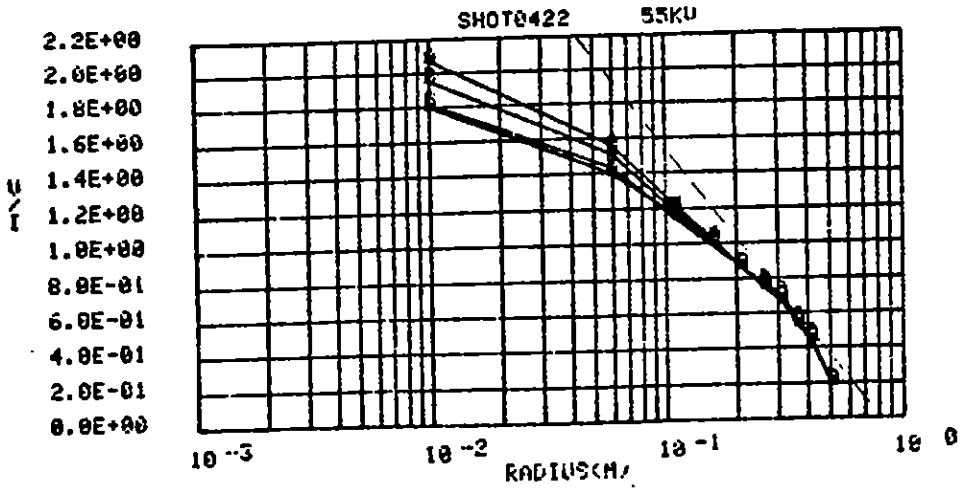

Code	A	B	C	D
Time	40 µs	70 µs	110 µs	190 µs
Current	29.0	29.5	30.0	28.5

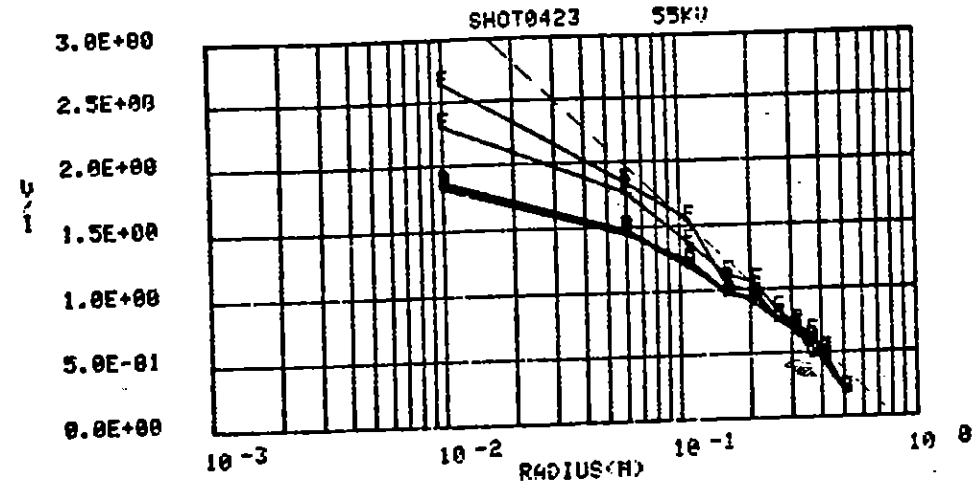

Code	A	B	C	D	E	F
Time	100 µs	200 µs	300 µs	500 µs	900 µs	1900 µs
Current	29.0	27.0	25.0	21.0	13.0	6.0

Figure 34. Voltage profile. (350 Ωm sand mix 90° x 0.3 mL)

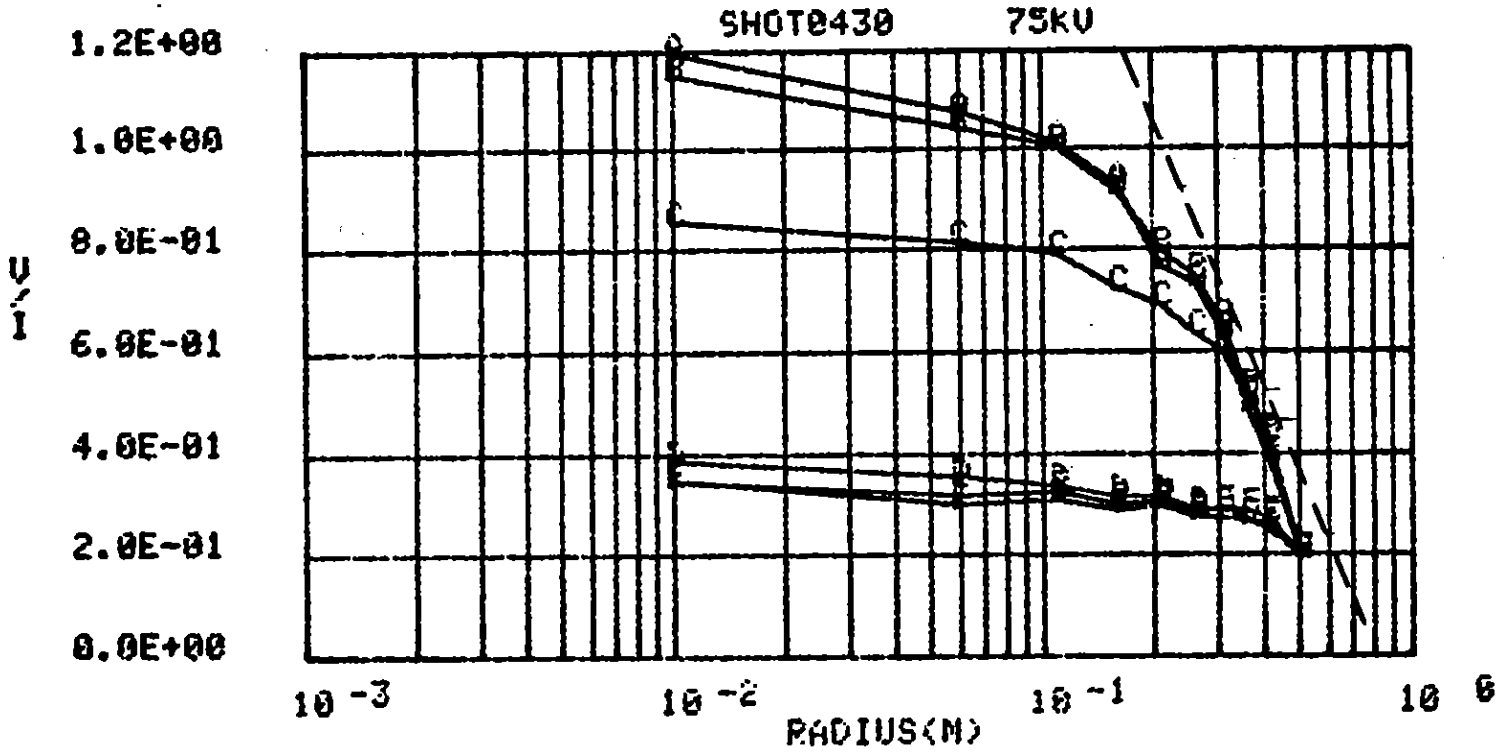

CODE	A	B	C	D	E	F	
TIME	50 μs	75 μs	175 μs	225 μs	275 μs	475 μs	t_B = 175 μs
CURRENT	65.0	65.0	75.0	150.0	140.0	70.0	

Figure 37. Voltage profile.
(350 Ωm sand mix
90° x 0.3 mL)

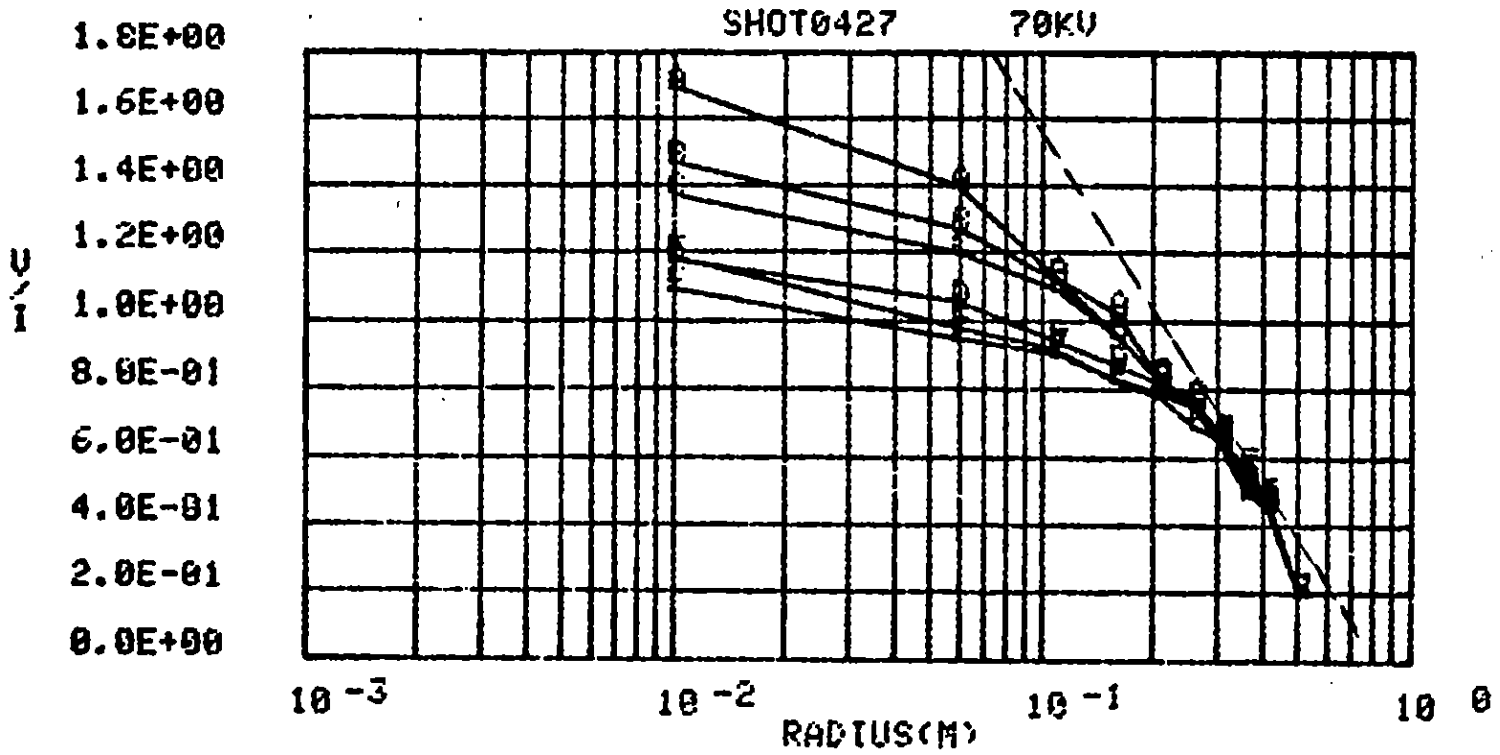

CODE	A	B	C	D	E	F
TIME	25 µs	50 µs	75 µs	175 µs	275 µs	475 µs
CURRENT	45.0	50.0	51.3	52.5	50.0	37.5

Figure 36. Voltage profile.
(350 Ωm sand mix
90° x 0.3 mL)

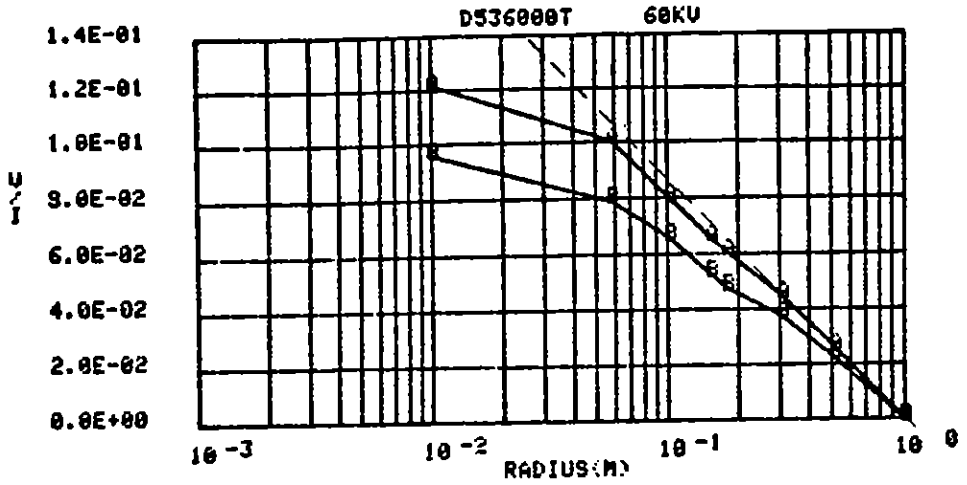

Code	A	B
Time	30 µs	50 µs
Current	500.0	625.0

(a) 0° top

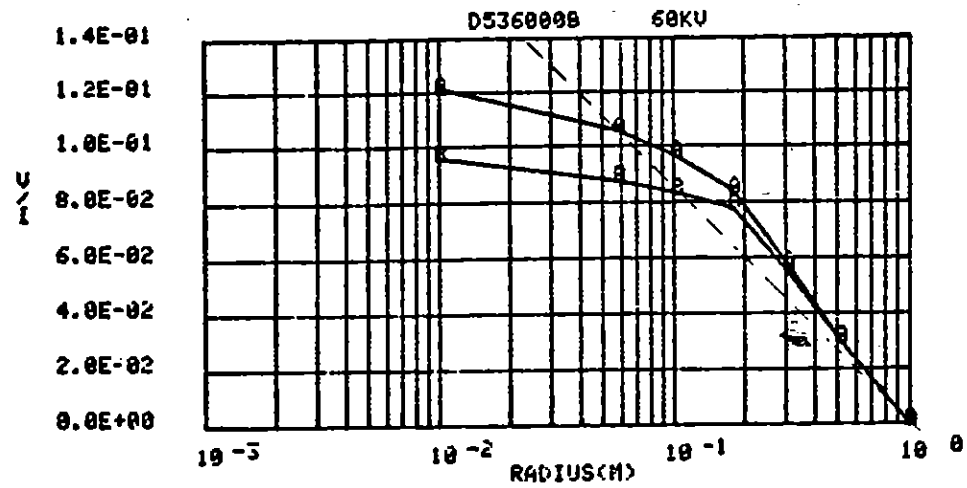

Code	A	B
Time	30 µs	50 µs
Current	500.0	625.0

(b) 0° bottom

Figure 38. Voltage profile. (300 Ωm sand mix, 360° x ± mL, t_B = 52 µs)

Figure 38 presents the early time profiles in the 300-Ωm mixed sand, using the 360° × 1 m geometry of the McAir experiments. Unfortunately, in these experiments, arc-over between inner and outer conductors occurred much quicker than in the smaller geometry experiments. For example, in shot 536, illustrated in Figure 38, arc-over occurred at 50 μs with 60 kV applied, even though in the 90° sector experiments it never occurred below 65 kV in the 0.1-m-long geometry or 70 kV in the 0.3-m-long geometry. As a matter of fact, in the 360° × 1 m experiments, arc-over occurred once at an applied voltage as low as 35 kV.

Figure 39 presents a summary of the arc-over times for the 300-Ωm sand mixture at various geometries. Again, there is a considerable spread in arc-over times at a given applied voltage. For example, in the 360° geometry, with a 0.01-m-radius center conductor, arc-over occurred once at an applied voltage of only 35 kV and twice at 45 kV, even though it did not occur on one shot each at 45, 52, and 60 kV. Similarly, with the 0.003-m-radius center conductor, arc-over occurred at one shot at 44 kV, but not on a shot at 54 kV. Nevertheless, some trends are apparent from Figure 39; namely,

1. The average arc-over occurs more readily with the larger diameter center conductor.
2. Arc-over occurs more readily in 360° × 1 mL geometry than in 90° × 0.1 mL or 90° × 0.3 mL geometry, both with 0.01-m-radius center conductors.
3. Arc-over in the 360° geometry with a 0.003-m-radius center conductor may occur at approximately the same time as in 90° geometry with a 0.01-m-radius center conductor.

As discussed in Section II, paragraph 4, arc-over is assumed to be a manifestation of an electrical instability in the experiment geometry, when the electric field at the tip of a conducting streamer increases as it

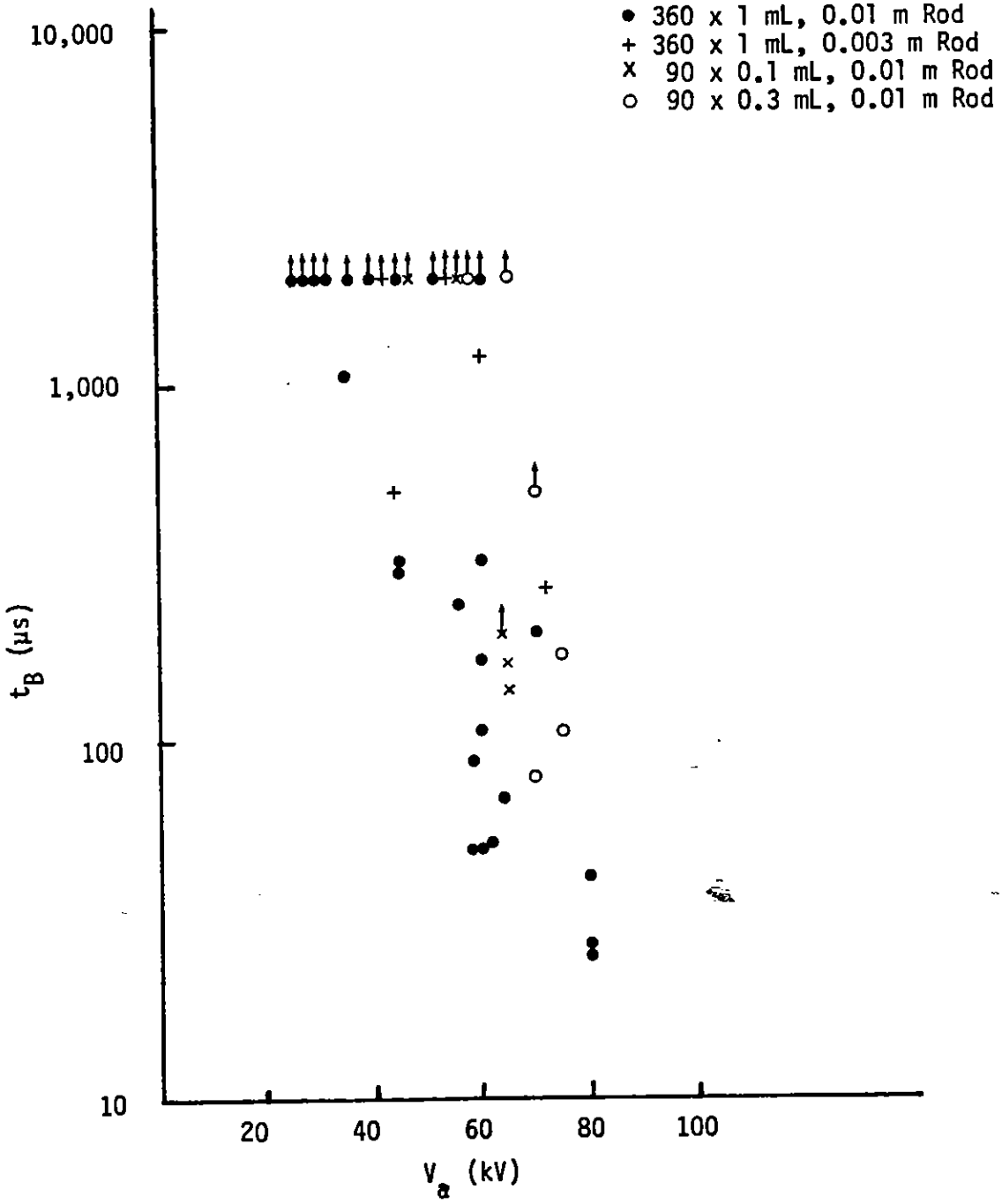

Figure 39. Arc-over times.
(300 Ωm sand mix)

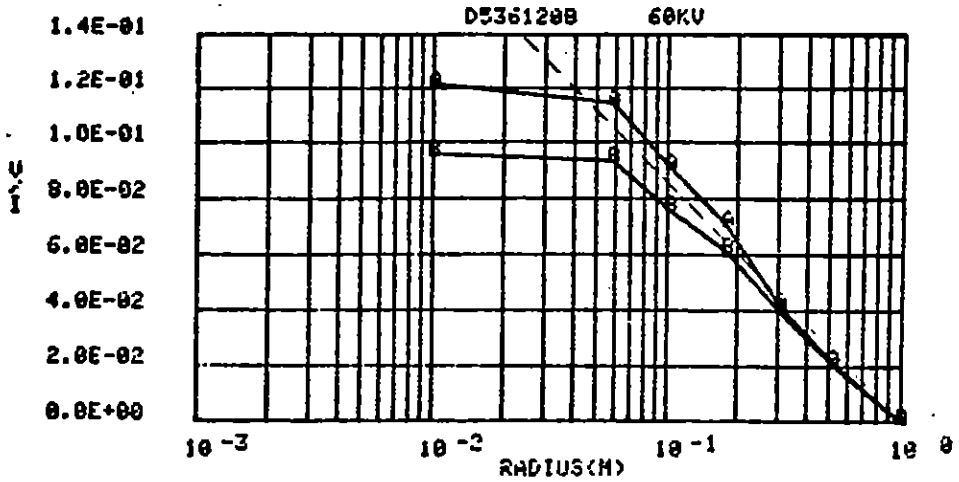

Code	A	B
Time	30 μs	50 μs
Current	500.0	625.0

(c) 120° bottom

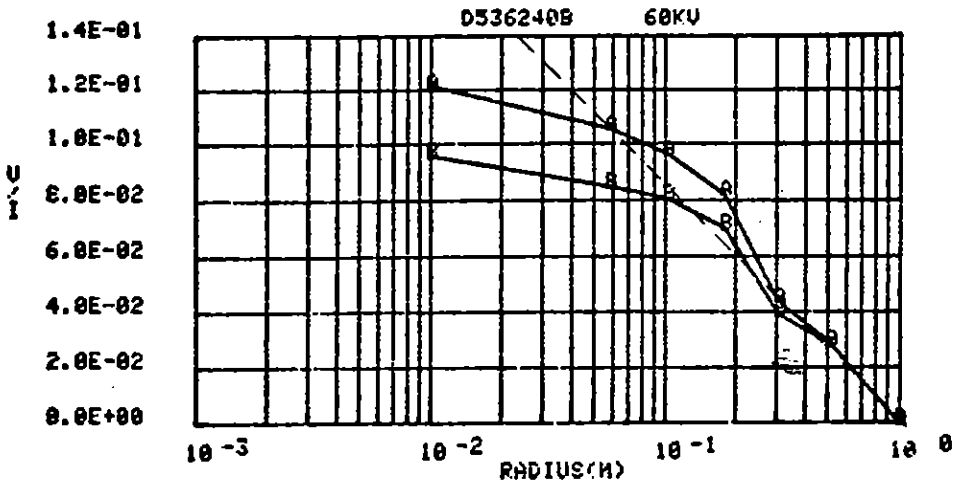

Code	A	B
Time	30 μs	50 μs
Current	500.0	625.0

(d) 240° bottom

Figure 38. Concluded.

Figures 40 through 44 present the voltage profiles at various applied voltages in the 360° × 1 mL geometry using a 0.003-m-radius center conductor. The strange looking point at early times at 0° on the top at a radius of 0.5 m is the result of a voltage record that has an obviously different time history, as shown in Figure 45. The top trace in each of these photos in this figure represents the voltage record for this probe. The other three traces are voltage records for probes located at 240° on the bottom. The top probe has a much faster time response than the bottom probes, as illustrated in the photo for shot 547. The differences in early time behavior in that photo are exclusively due to the different frequency response of the probes. Therefore, the anomalous behavior in the records of the same probe on shot 543 through 546 cannot be ascribed to its frequency response. The behavior of this probe in shot 542, which was the last shot prior to changing the center conductor, was also completely normal. A considerable amount of work was done to change the center conductor and it is possible that something was disturbed between shots 542 and 543. However, no changes were made during the sequence from shots 543 through 547. Only the number of stages in the power supply and its charging voltage were changed in proceeding from one shot to the next. The waveform on the same sequence of shots for the probes located at 0.05, 0.10, 0.18 and 0.30-m-radius at the 0° azimuth on the top are shown in Figure 46. These are also fast probes having the same frequency response as the top record in the photos of Figure 45. There is no evidence of unusual behavior in any of these traces, including the bottom trace, which is the probe closest to the anomalous record.

One suggestion of possible instrumentation malfunction is given by close examination of the second trace on each photograph in Figure 45. Although the general waveform of this trace is consistent with the response of probes on the bottom of the sample, there is evidence of a small amplitude oscillatory behavior having the same period and phase as the anomalous response in the upper trace. While these two traces are generated by voltage probes in totally different regions of the sample, they share a common

moves outward. This occurs when the streamer has expanded far enough that the increase, due to coming closer to the outer electrode, overtakes the decrease due to increasing radial distance from the central electrode. As discussed in Section II, paragraph 4, if one assumed that the streamer structure around the central electrode could be approximated by a perfectly conducting cylinder out to the ends of the streamer, the instability would occur when the radius of the cylinder equals 1/e of the radius of the outer conductor. In the limiting case of a single perfectly conducting small filament moving out from the center conductor, the instability could occur at a much shorter length. If the effective resistance per unit length of the conducting streamer is not negligible, the radius at which it becomes unstable will be larger. Using this model, we can interpret the behavior illustrated in Figure 39 in terms of the degree of uniformity of the streamer structure.

In the 90° geometry, the insulating boundary conditions at the edge of the 90° sector and at the top and bottom of the 0.1 or 0.3-m-long sample constrain the current flow. In effect, they produce an equivalent of 360° × 1-m-long geometry in which image streamers occur every 90° in azimuth and every 0.1 or 0.3 m in length, in order to satisfy the boundary conditions that no current crosses the boundaries of the smaller sample. This enforces a certain degree of uniformity on the apparent electric field profile, which promotes the ideal situation in which the streamers will propagate out to 1/e of the outer radius or farther as determined by the streamer resistance. In the 360° geometry with the smaller diameter center conductor, the electric field at the central rod was well above the streamer initiation threshold along its entire length. Therefore, one would expect a lot of streamers to be created around the central rod, again promoting a certain degree of axial and azimuthal uniformity. With the larger diameter central rod, relatively few streamers are initiated in the entire sample geometry, leading to a rather narrow window in applied voltage between the onset of streamers and arc-over. It was the observation of this different behavior at McAir, as contrasted to the previous PI experiments, that led to the addition of the measurements with the smaller diameter, separate conductor.

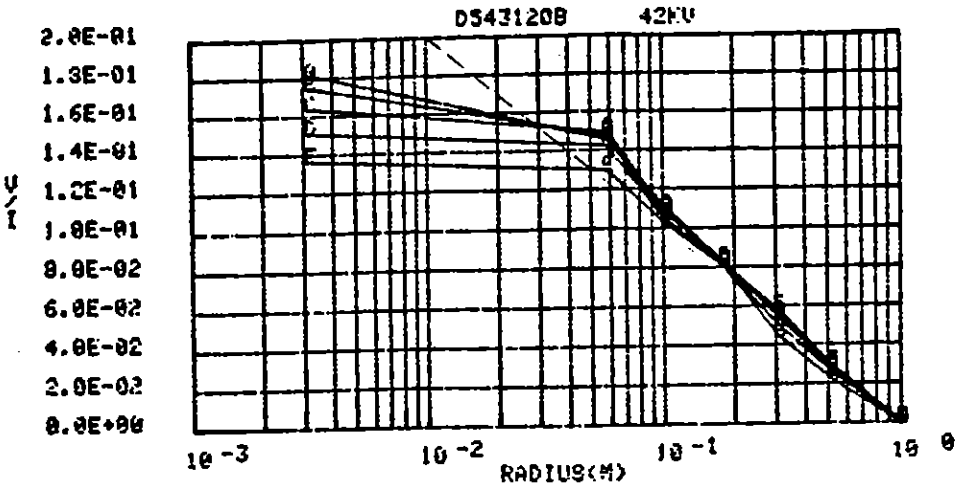

Code	A	B	C	D	E
Time	20 μs	40 μs	70 μs	110 μs	190 μs
Current	210.0	240.0	250.0	265.0	280.0

(c) 120° bottom

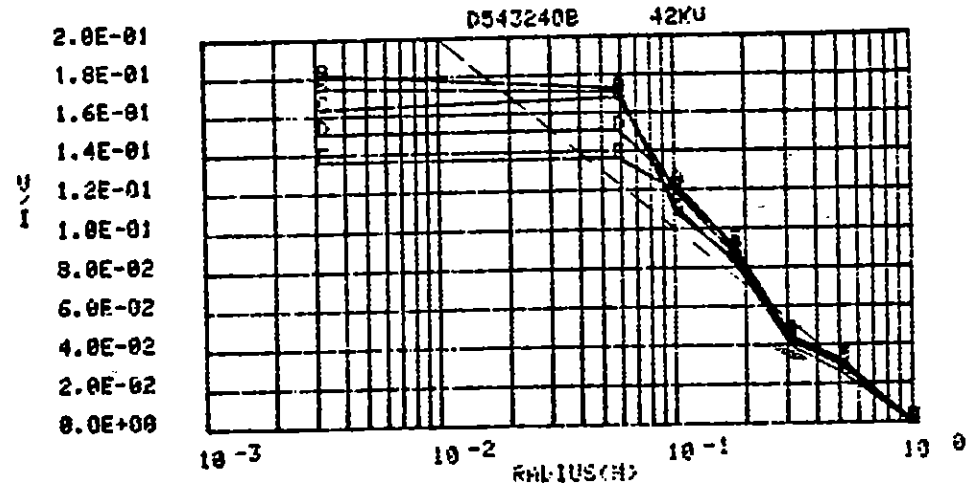

Code	A	B	C	D	E
Time	20 μs	40 μs	70 μs	110 μs	190 μs
Current	210.0	240.0	250.0	265.0	280.0

(d) 240° bottom

Figure 40. Concluded.

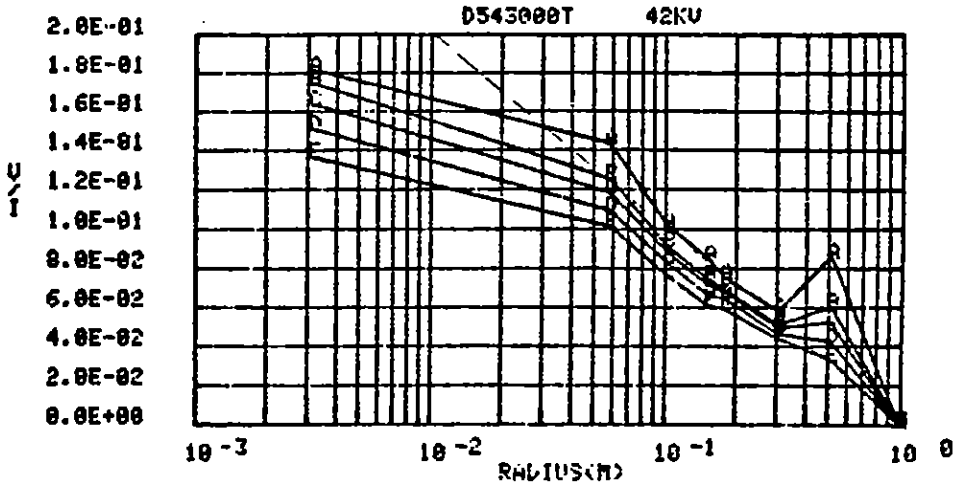

Code	A	B	C	D	E
Time	20 μs	40 μs	70 μs	110 μs	190 μs
Current	218.0	240.0	250.0	265.0	280.0

(a) 0° top

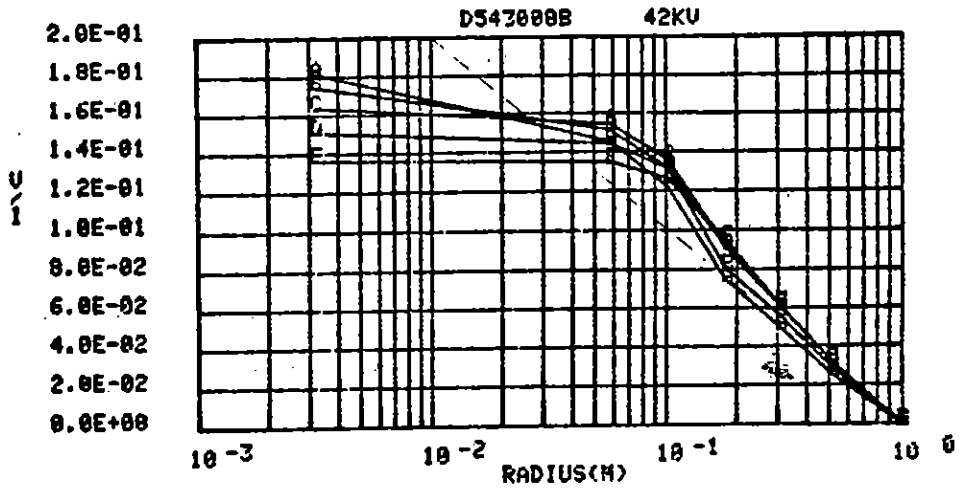

Code	A	B	C	D	E
Time	20 μs	40 μs	70 μs	110 μs	190 μs
Current	210.0	240.0	250.0	265.0	280.0

(b) 0° bottom

Figure 40. Voltage profile. (300 Ωm sand mix, 360° x 1 m x (0.003-1) mR)

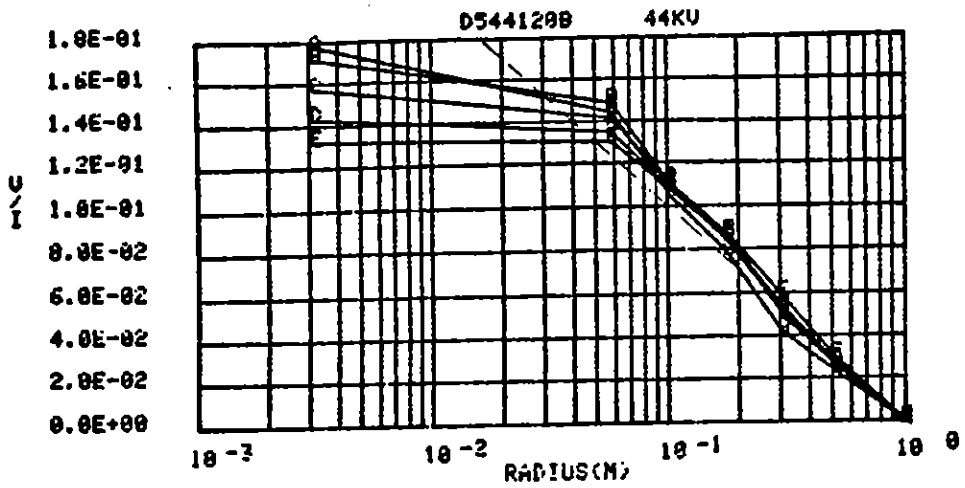

Code	A	B	C	D	E
Time	20 μs	40 μs	70 μs	110 μs	190 μs
Current	225.0	250.0	270.0	290.0	300.0

(b) 120° bottom

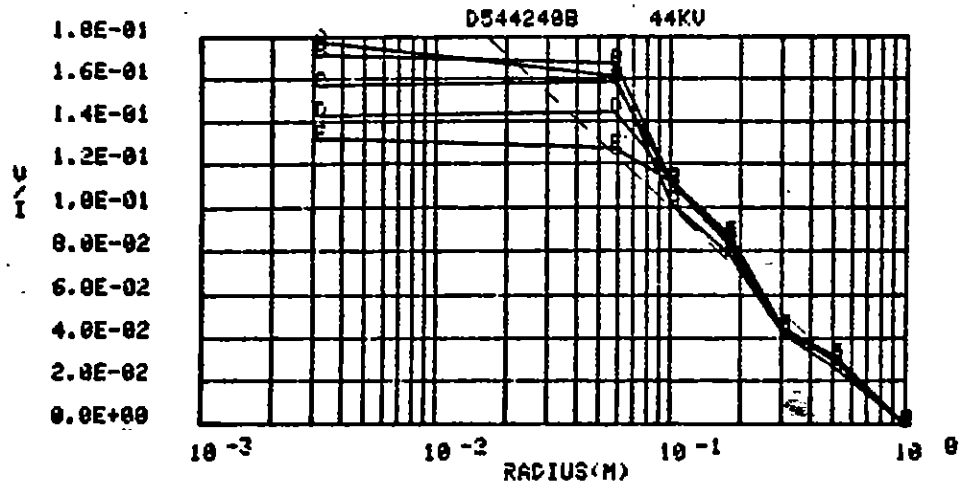

Code	A	B	C	D	E
Time	20 μs	40 μs	70 s	110 μs	190 μs
Current	225.0	250.0	270.0	290.0	300.0

(d) 240° bottom

Figure 41. Concluded.

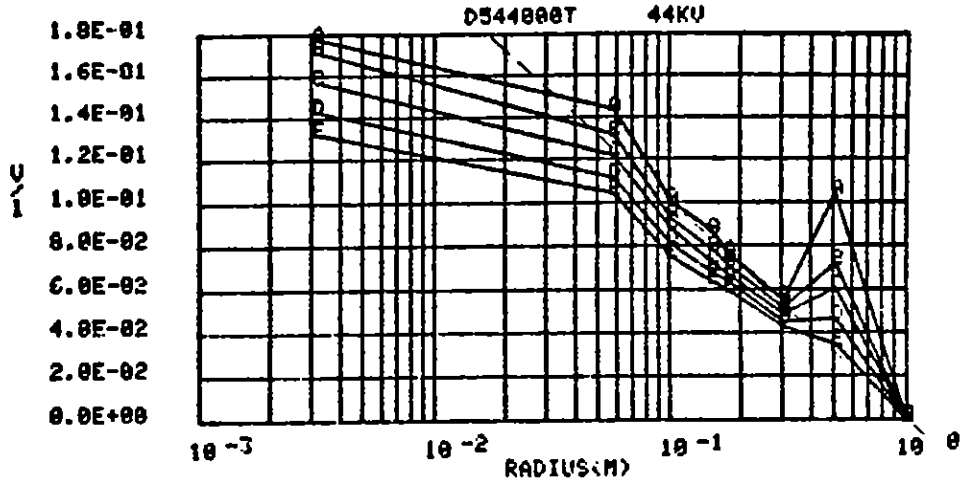

Code	A	B	C	D	E
Time	20 μs	40 μs	70 μs	110 μs	190 μs
Current	225.0	250.0	270.0	290.0	300.0

(a) 0° top

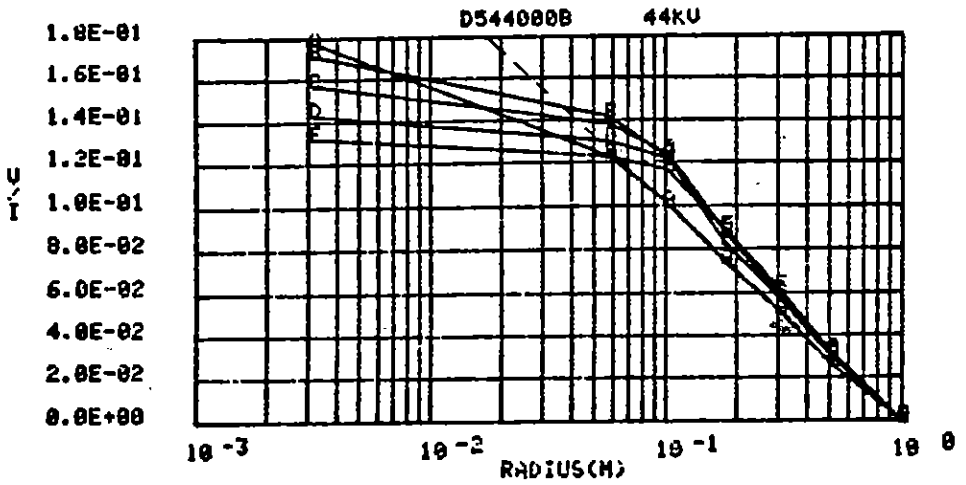

Code	A	B	C	D	E
Time	20 μs	40 μs	70 μs	110 μs	190 μs
Current	225.0	250.0	270.0	290.0	300.0

(b) 0° bottom

Figure 41. Voltage profile. (300 Ωm sand mix, 360° x 1 m x (0.003-1) mR, t_B = 500 μs)

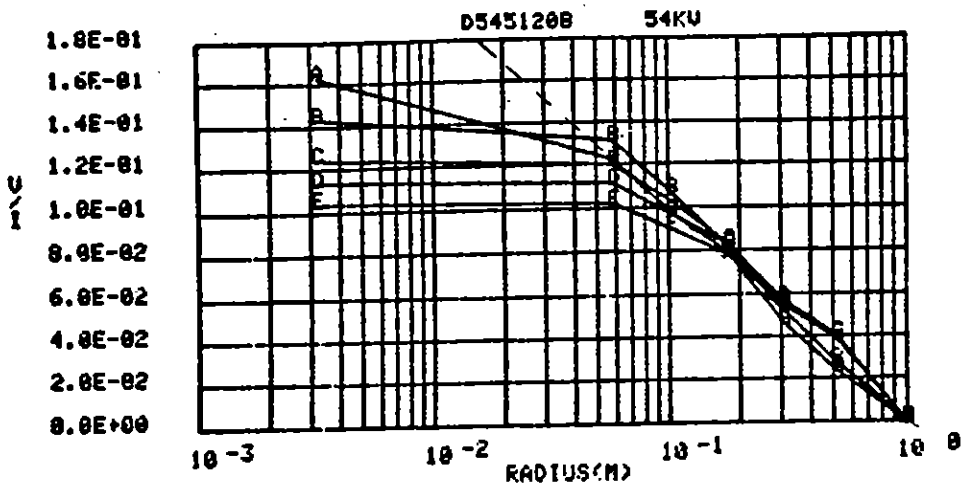

Code	A	B	C	D	E
Time	20 μs	40 μs	70 μs	110 μs	160 μs
Current	312.5	375.0	425.0	450.0	475.0

(c) 120° bottom

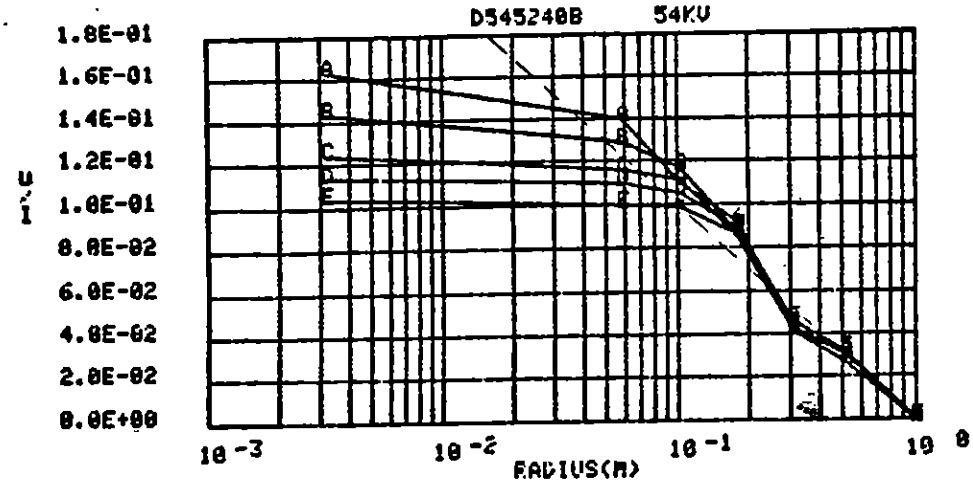

Code	A	B	C	D	E
Time	20 μs	40 μs	70 μs	110 μs	160 μs
Current	312.5	375.0	425.0	450.0	475.0

(d) 240° bottom

Figure 42. Concluded.

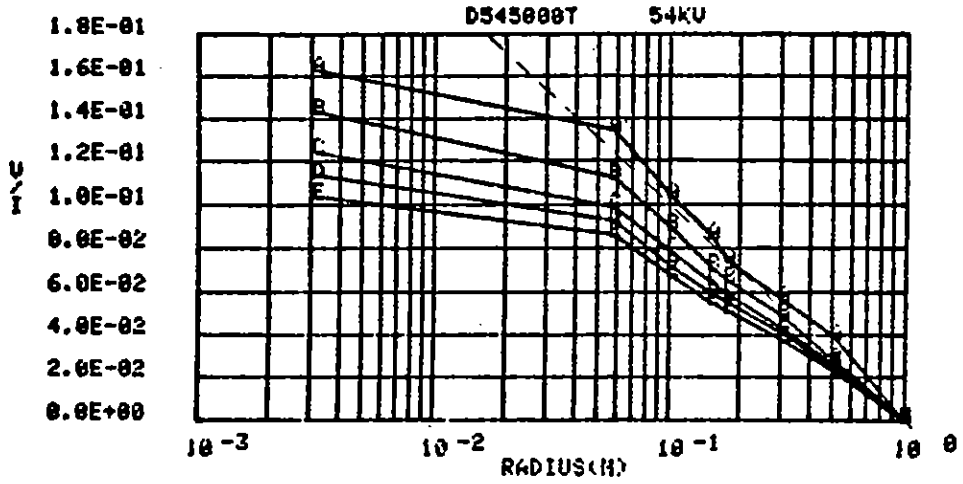

Code	A	B	C	D	E
Time	20 μs	40 μs	70 μs	110 μs	160 μs
Current	312.5	375.0	425.0	450.0	475.0

(a) 0° top

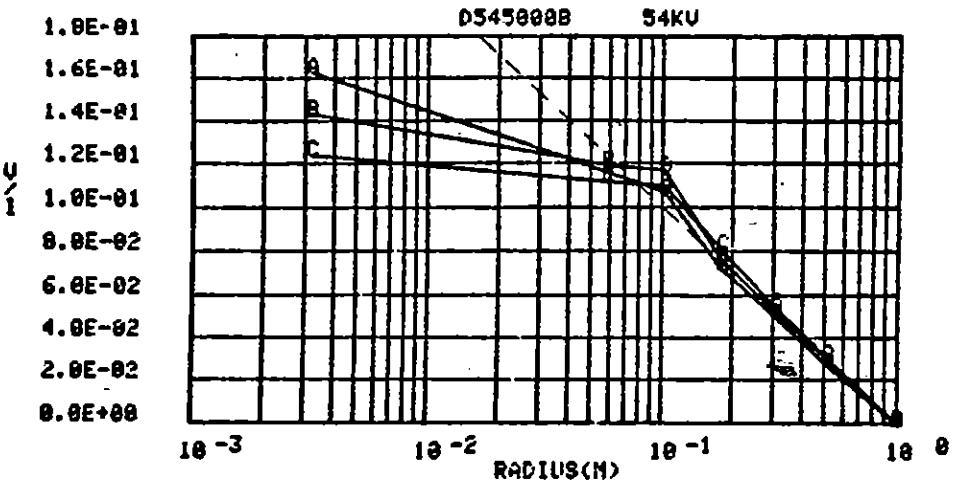

Code	A	B	C
Time	20 μs	40 μs	70 μs
Current	312.5	375.0	425.0

(b) 0° bottom

Figure 42. Voltage profile. (300 Ωm sand mix, 360° x 1 m x (0.003-1) mR)

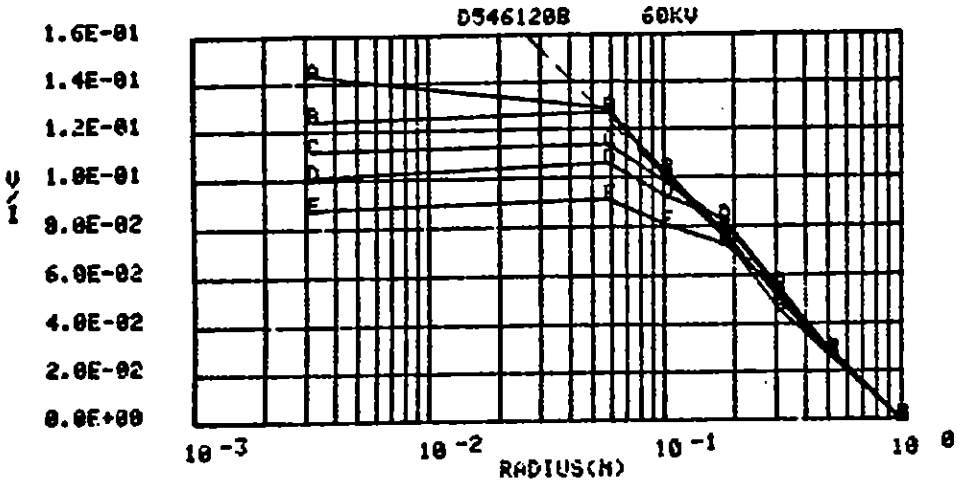

Code	A	B	C	D	E
Time	20 μs	40 μs	70 μs	110 μs	160 μs
Current	400.0	475.0	512.5	550.0	612.5

(c) 120° bottom

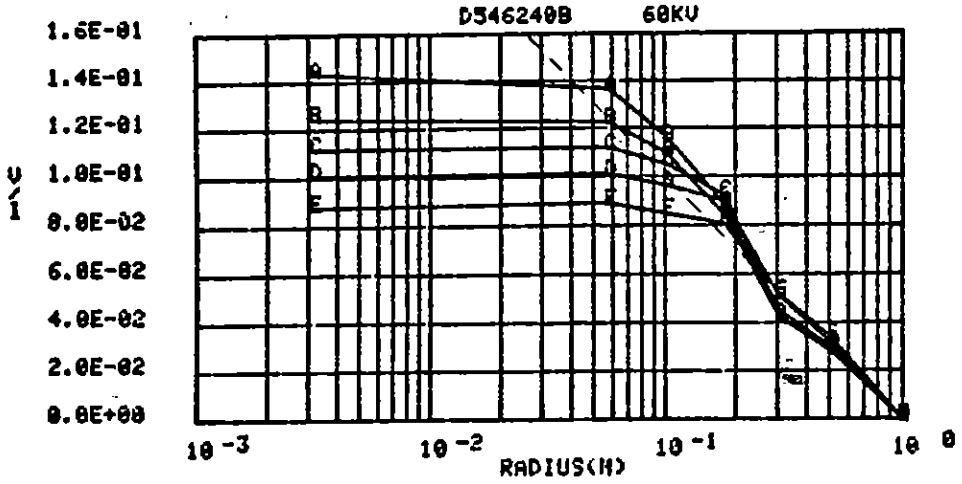

Code	A	B	C	D	E
Time	20 μs	40 μs	70 μs	110 μs	160 μs
Current	400.0	475.0	512.5	550.0	612.5

(d) 240° bottom

Figure 43. Concluded.

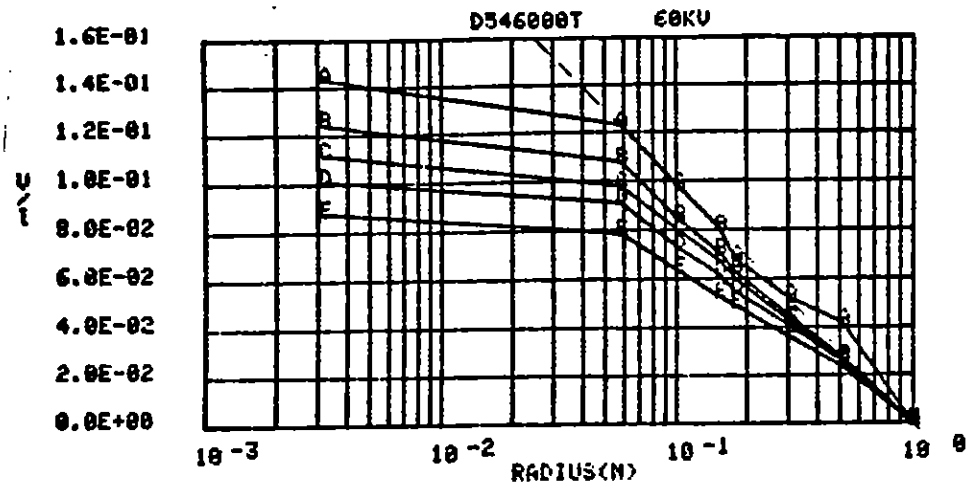

Code	A	B	C	D	E
Time	20 μs	40 μs	70 μs	110 μs	160 μs
Current	400.0	475.0	512.5	550.0	612.5

(a) 0° top

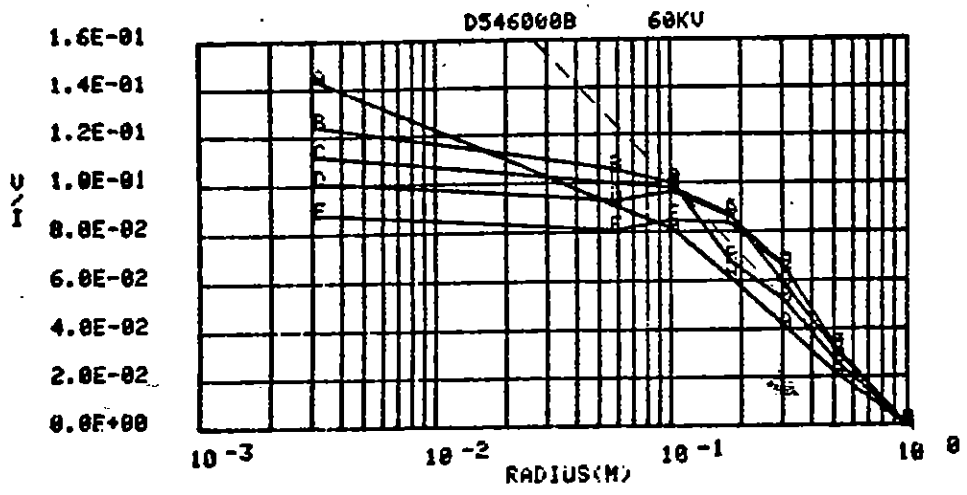

Code	A	B	C	D	E
Time	20 μs	40 μs	70 μs	110 μs	160 μs
Current	400.0	475.0	512.5	550.0	612.5

(b) 0° bottom

Figure 43. Voltage profile. (300 Ωm sand mix, 360° x 1 m x (0.003-1) mR, t_B = 1200 μs)

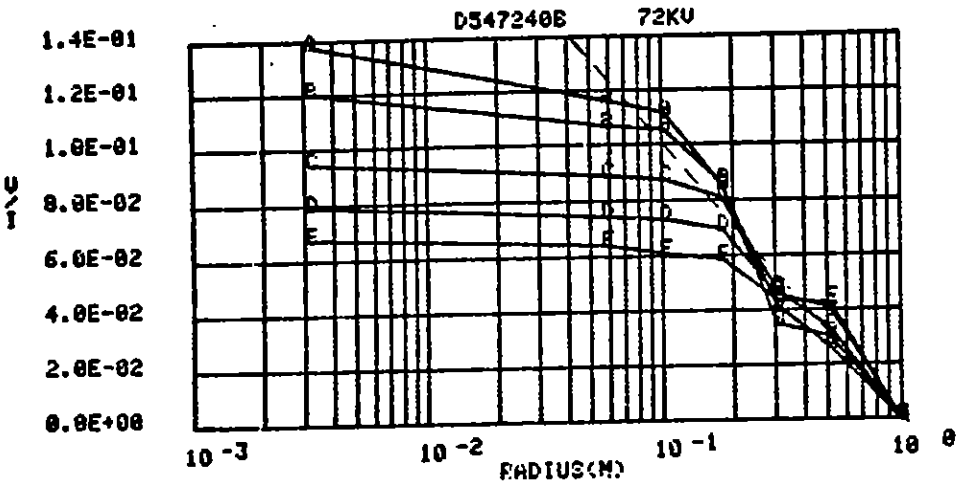

Code	A	B	C	D	E
Time	20 μs	40 μs	70 μs	110 μs	160 μs
Current	500.	625.	775.	900.	1025.

(c) 240° bottom

Figure 44. Concluded.

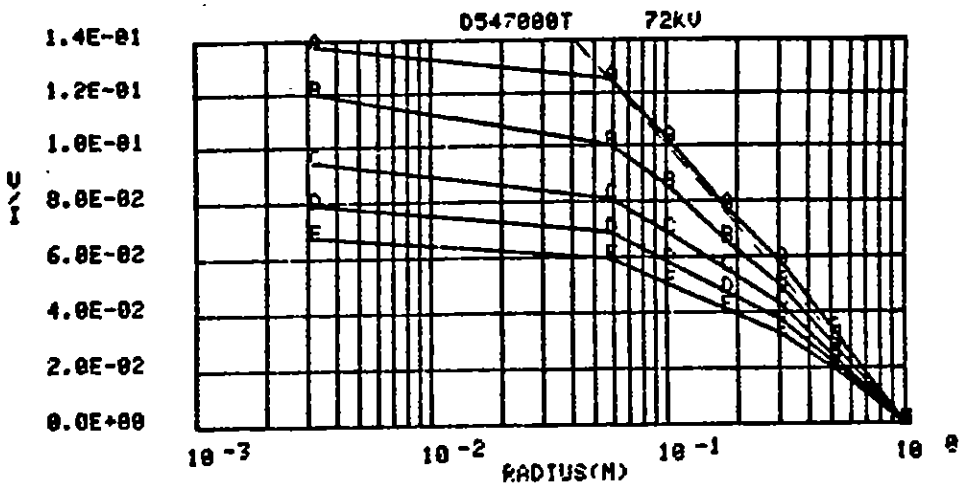

Code	A	B	C	D	E
Time	20 μs	40 μs	70 μs	110 μs	160 μs
Current	500.	625.	775.	900.	1025.

(a) 0° top

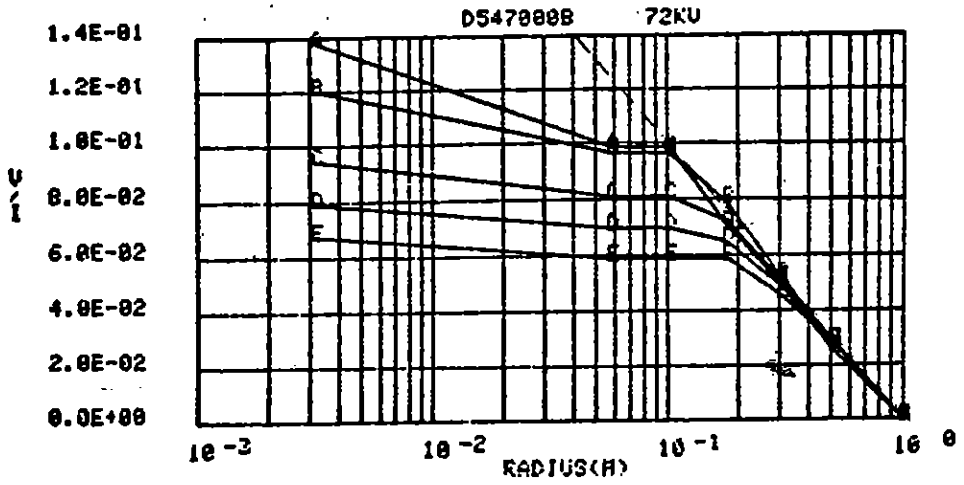

Code	A	B	C	D	E
Time	20 μs	40 μs	70 μs	110 μs	160 μs
Current	500.	625.	775.	900.	1025.

(b) 0° bottom

Figure 44. Voltage profile. (300 Ωm sand mix, 360° x 1 m x (0.003-1) mR, t_B = 270 μs)

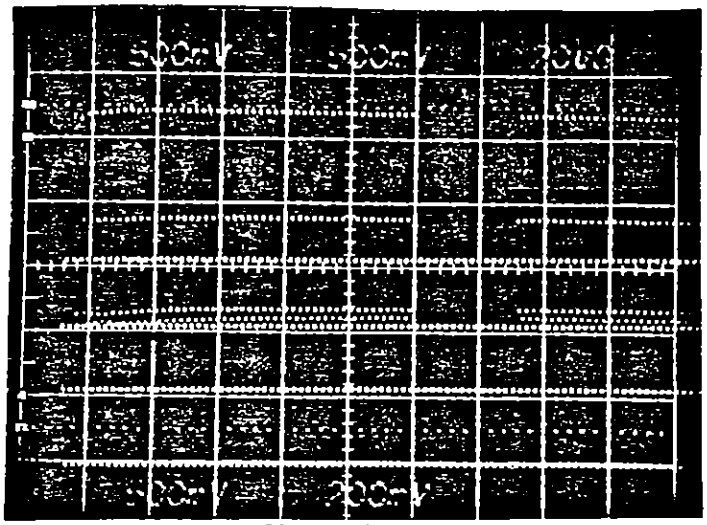

Trace (top to bottom)	Probe Location	Radius (m)
1	0° top	0.05
2	" "	0.10
3	" "	0.18
4	" "	0.30

Shot 543, Va = 42 kV

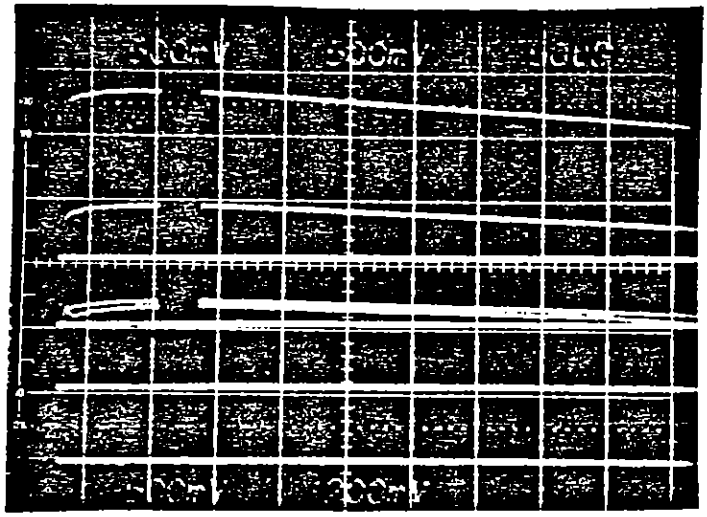

Shot 544, Va = 44 kV

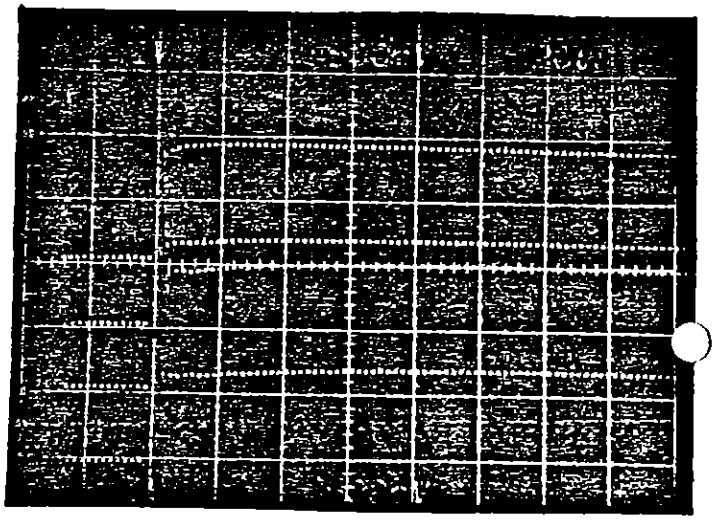

Shot 545, Va = 54 kV

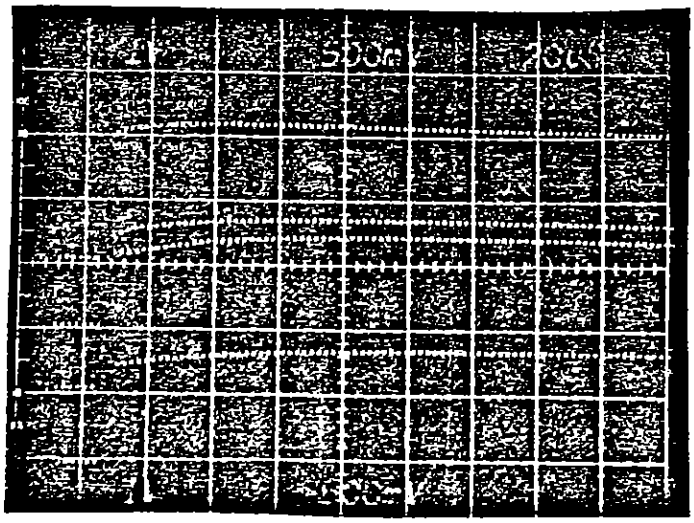

Shot 546, Va = 60 kV

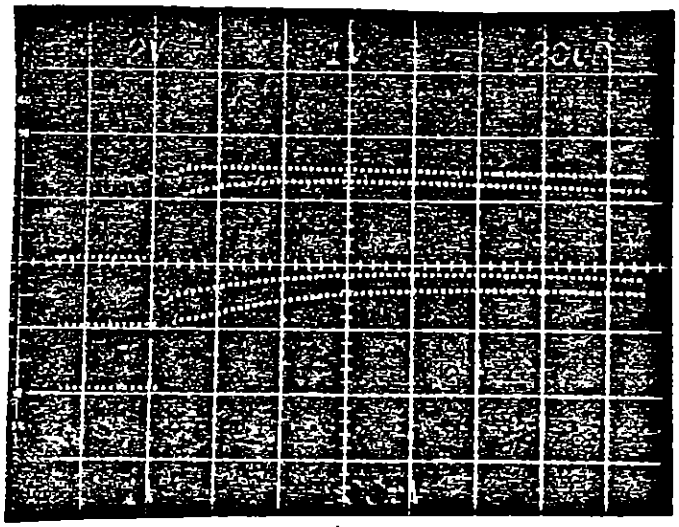

Shot 547, Va = 72 kV

Figure 46. Voltage probe records.

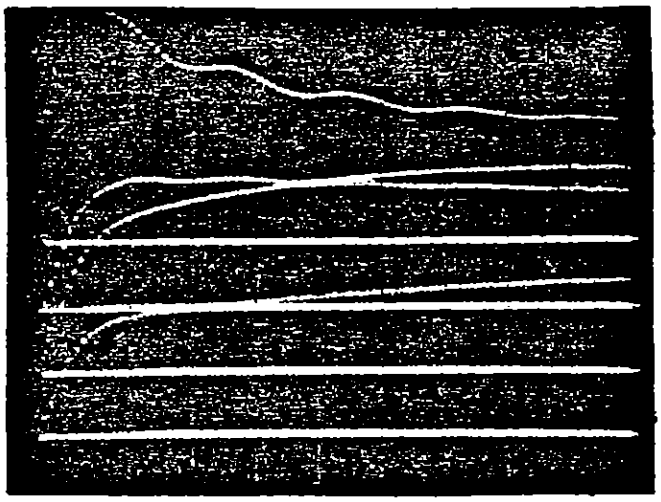

Trace (top to bottom)	Probe Location	Radius (m)
1	0° top	0.5
2	240° bottom	0.05
3	" "	0.1
4	" "	0.18

Shot 543, Va = 42 kV

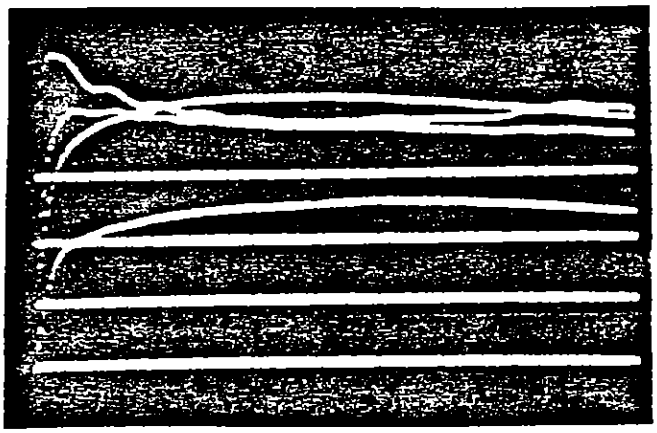

Shot 544, Va = 44 kV

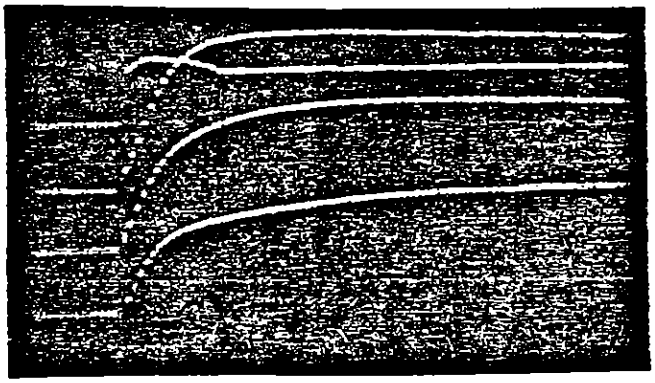

Shot 545, Va = 54 kV

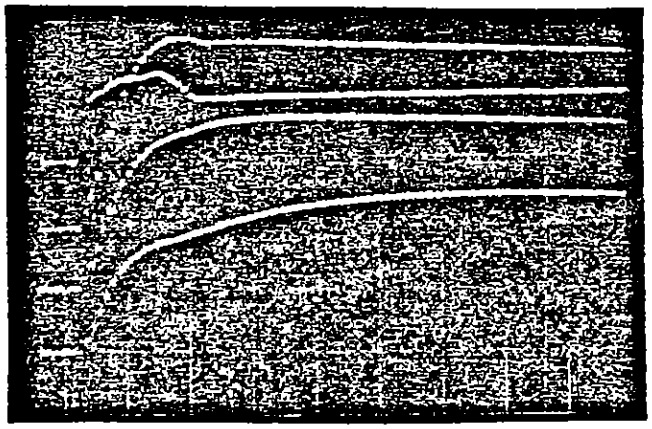

Shot 546, Va = 60 kV

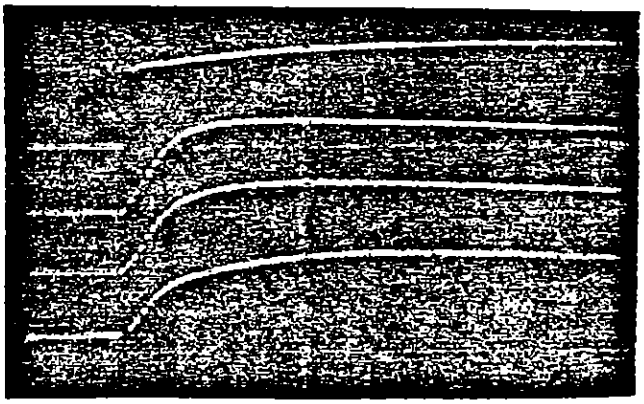

Shot 547, Va = 72 kV

Figure 45. Voltage probe records.

the 0° top sector carries less than its proportionate share of the current; the 0° and 240° bottom sectors carry more than their proportionate share; and the 120° bottom sector carries approximately its share of the total current. With this interpretation, the radius to which conducting streamers apparently extend falls between 0.05 and 0.10 m at 42 kV and extends out to at least 0.2 m at 72 kV. A crude estimate of the velocity at which the streamers move out can be deduced from the change in location of the break point in the voltage profiles at various times. This indicates that this point moves some tens of centimeters in times of tens of microseconds during the observation time. However, it is clear that the initial progression from the onset of streamering to the first voltage profile measurement occurs much faster, as does the development of arc-over between electrodes once the instability is achieved. Therefore, it is probable that the relatively slow velocity phase illustrated by these voltage profiles is characteristic of a gradual extension of the streamer radius in response to a gradual decrease of the voltage drop across the region in which the streamers have already been established. This decrease in apparent streamer impedance with time is apparent in Figures 40 through 44 as a decrease in slope of the inner portion of the voltage profile.

Many of the voltage profiles appear to have a transition region between the low-impedance streamers and the outer ohmic region in which the apparent resistivity is greater than the ohmic value. This behavior is expected from a model in which relatively few streamers dominate the late-time current flow. In effect, the voltage profile just beyond the end of a streamer will fall more rapidly than the ohmic value, because the current is constricted to flow away from the end of the streamer rather than being free to occupy the entire cross-sectional area of the sample.

Although data are available on the voltage profile during the onset and recovery of arc-over between electrodes in the McAir experiments,

oscilloscope pre-amp, which chops between these two records at a 500-kHz rate.

Therefore, in summary the situation is:

1. The anomalous record exhibited by the probe at 0.5-m radius on the 0° top azimuth is not reinforced by any other probe data..
2. No changes were made prior to or after the anomalous records that would explain the appearance and disappearance of the strange waveform.
3. If the voltage profile were as reflected by this record, it could be explained only by an arc or a streamer that passed very close to the voltage probe, creating a local high current density between the outer probe and the outer conductor. It would be difficult, but not impossible, to construct a situation in which the voltage on this probe was higher than that measured on the next inward probe.
4. There is some suggestion of crosstalk between the two records sharing a single oscilloscope pre-amp that may indicate a temporary pre-amp malfunction.

While this record might represent an interesting example of a streamer that accidentally passed almost directly by a voltage probe, the indication of crosstalk in the oscilloscope pre-amp weakens this interpretation.

Ignoring this one probe, the behavior of the streamers can be inferred from the remaining records illustrated in Figures 40 through 44. In all cases, enhanced conduction is revealed between the center conductor and the voltage probe at a 0.05-m radius, even at the earliest measurement time of 20 μs. The shape of the voltage profile indicates that at later times

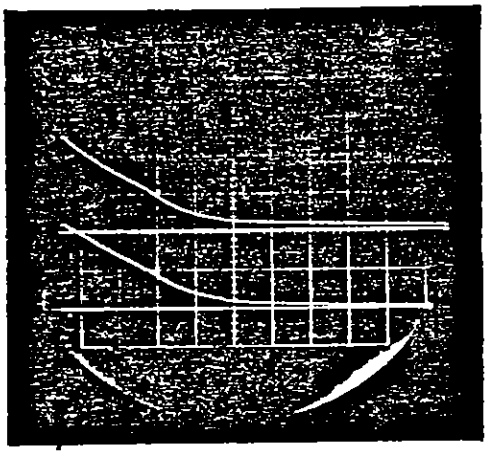

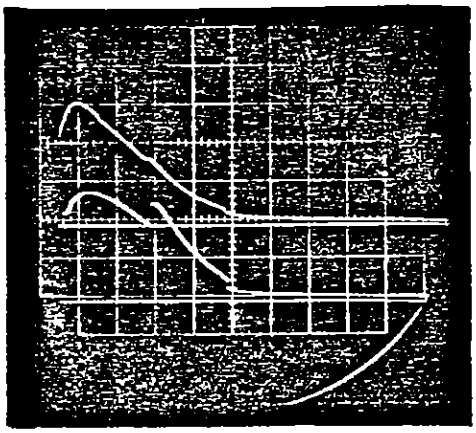

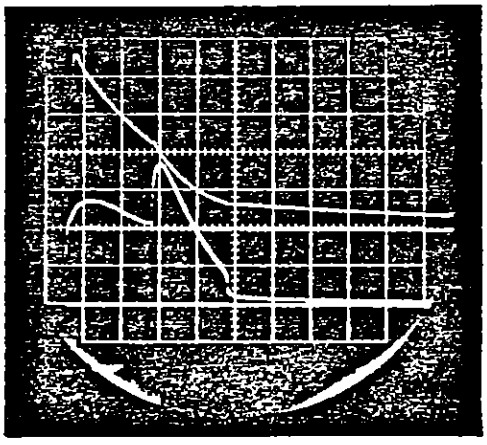

Sensitivity	Type of Probe and Position (if a voltage probe)
50 kV/div	Voltage 0.055 m radius
50 kV/div	Voltage 0.11 m radius
20 kV/div	Voltage 0.21 m radius
10 kV/div	Voltage 0.41 m radius
20 kV/div	Voltage central conductor
24 A/div	Current

Sweep - 200 μs/div

Figure 47. Voltage probe and current records. (Shot 285, Va = 75 kV)

these data have not yet been analyzed. Photographs also exist showing a sudden decrease in current upon extinguishing an arc in the PI data on the 300-Ωm mixed sand. These have not yet been processed. An example of such data showing the development and recovery from arc-over in MX-B soil is shown in Figures 47 and 48. The current record in Figure 47 exhibits the typical increase after a prompt ohmic value and then a gradual decrease as the applied voltage decays. At 440-μs, arc-over occurs and the peak current is limited by the sample resistance and the external 200-Ω series resistor. The current has fallen, 400 μs later, in response to the decreasing power supply voltage to a value at which the arc suddenly extinguishes, and the sample returns to a more or less ohmic behavior. The various voltage probes shown in the upper photos of Figure 47 and in Figure 48 reflect this behavior. The innermost voltage probes essentially follow the applied voltage throughout the record. The outer probes follow more nearly the current waveform. Figure 49 presents the history of the development of the streamers and arc-over in the same material at the same applied voltage with better time resolution. In general, the behavior is similar to that illustrated previously for the 300-Ωm material in the same geometry. Again, a significant fraction of the overall voltage drop appears to be concentrated at the inner and outer electrodes, particularly the outer electrode.

The slope of the voltage versus radius curves in the streamer region provides a lower limit to the streamer impedance. Since the voltage probes are not directly on the streamers, the actual streamer impedance could be less. The electric field near a streamer appears to vary from ≈100 kV/m at early times ($\lesssim$ 50 μs) at ≈50 A currents to $\lesssim$ 10 kV/m at later times (≈400 μs) and ≈100 A.

Very few of the post arc-over data have been analyzed. Two examples that have been processed by hand are shown in Figures 50 and 51. The characteristic reported by Jaycor (Ref. 3) are seen here; namely,

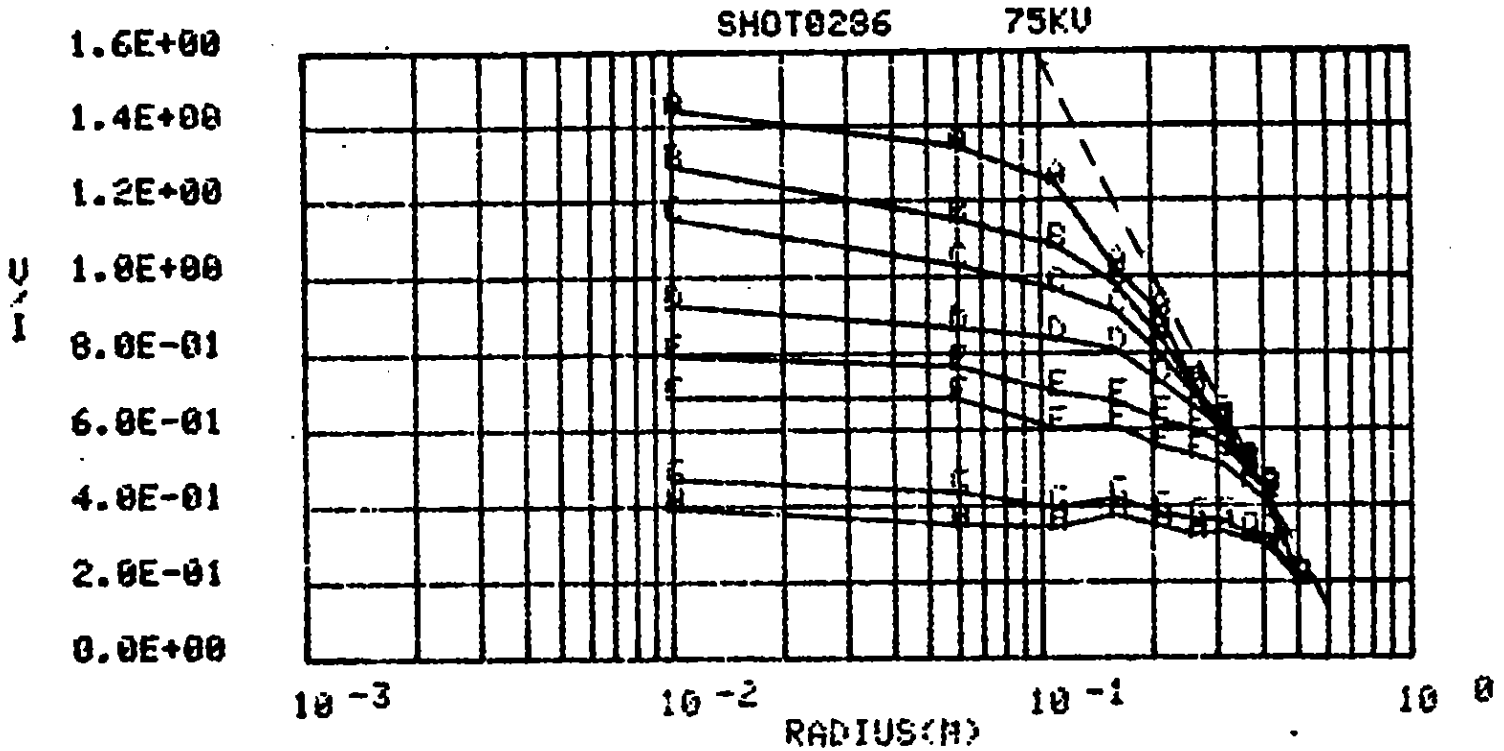

CODE	A	B	C	D	E	F	G	H
TIME	25 µs	50 µs	75 µs	175 µs	275 µs	410 µs	425 µs	475 µs
CURRENT	55.0	62.5	67.5	72.5	72.5	65.0	95.0	95.0

Figure 49. Voltage profile.
(130 Ωm MX-B soil
90° x 0.1 mL)

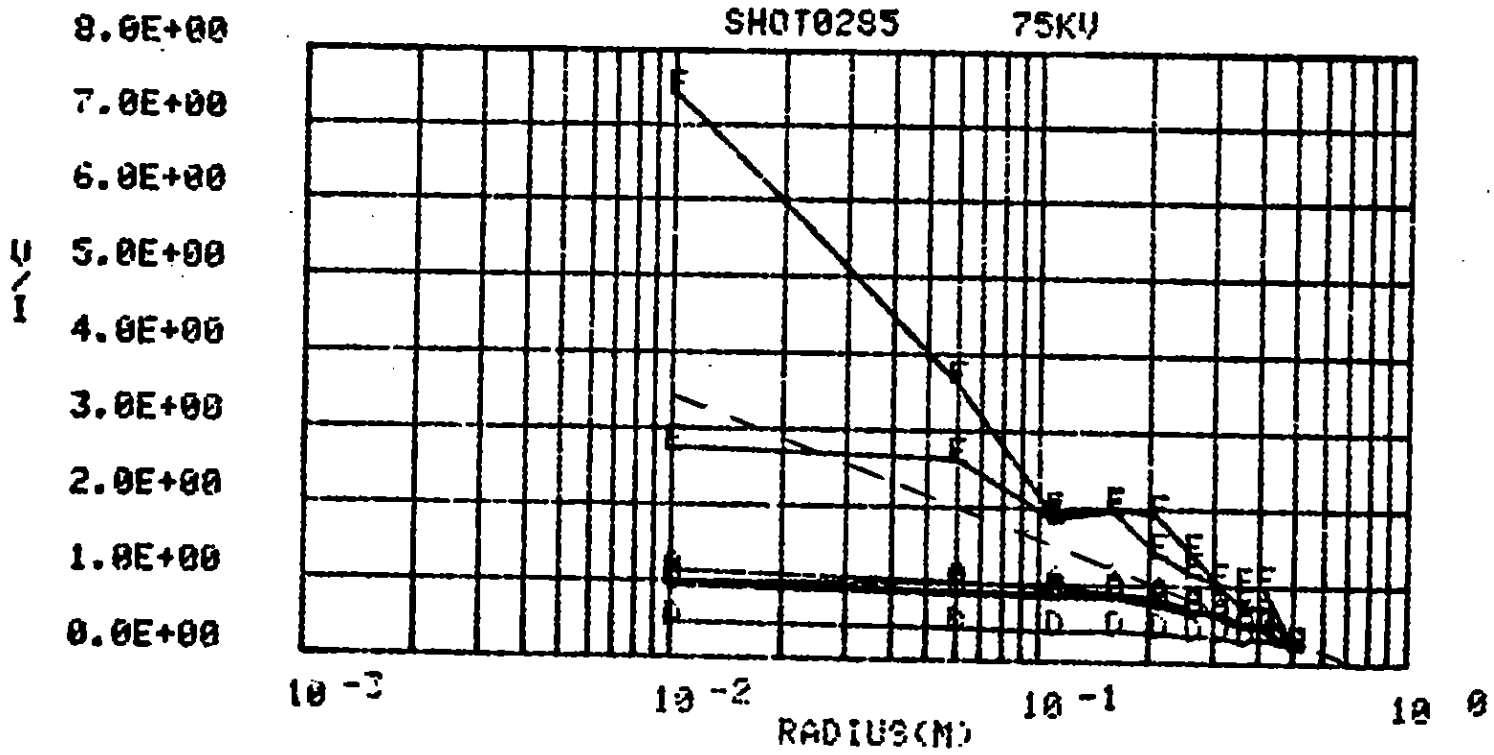

CODE	A	B	C	D	E	F
TIME	100 µs	200 µs	300 µs	500 µs	900 µs	1900 µs
CURRENT	67.5	66.3	61.3	92.5	5.0	1.3

Figure 48. Voltage profile.
(130 Ωm MX-B soil
90° x 0.1 mL)

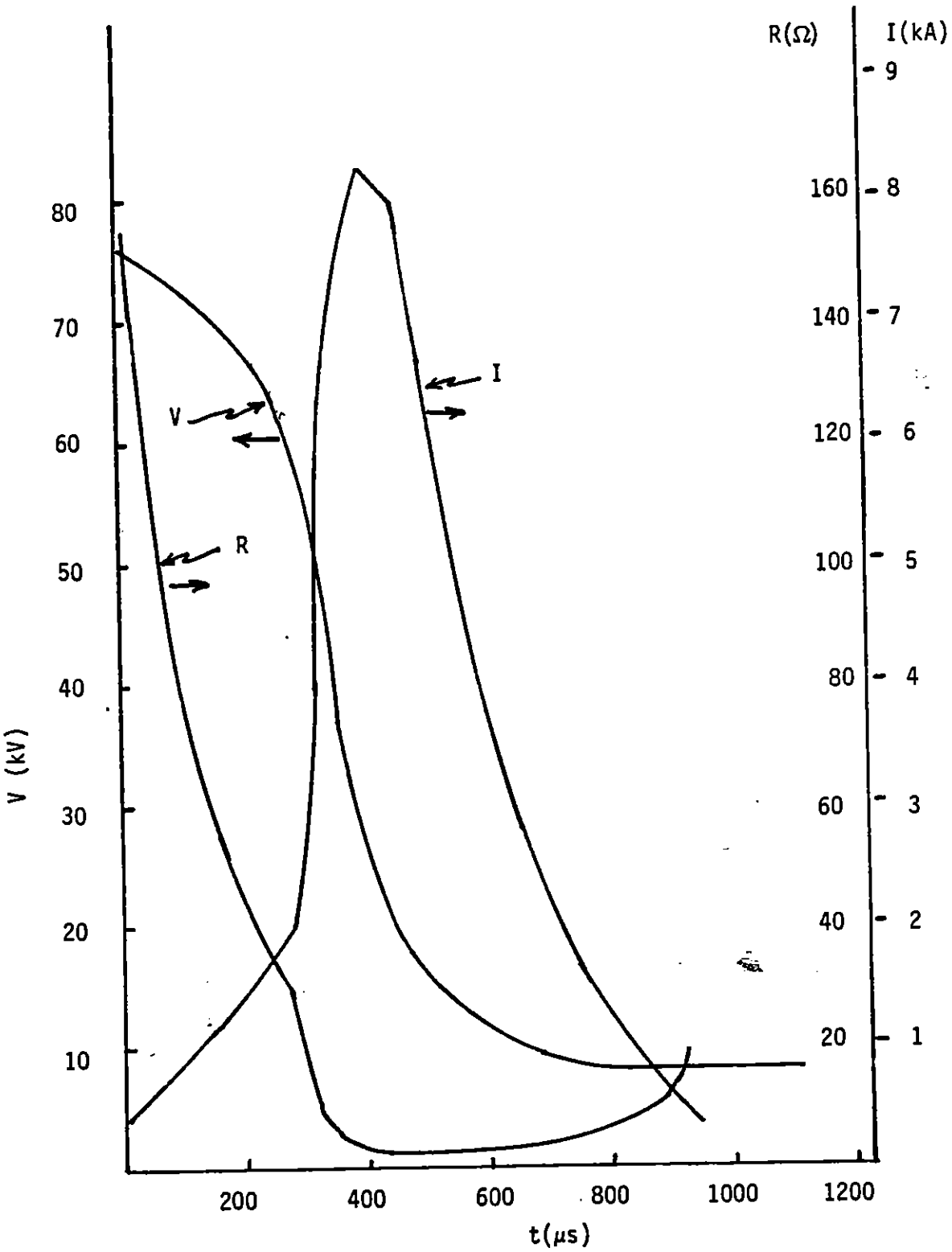

Figure 51. Arc-over characteristics shot 547, Va = 72 kV.

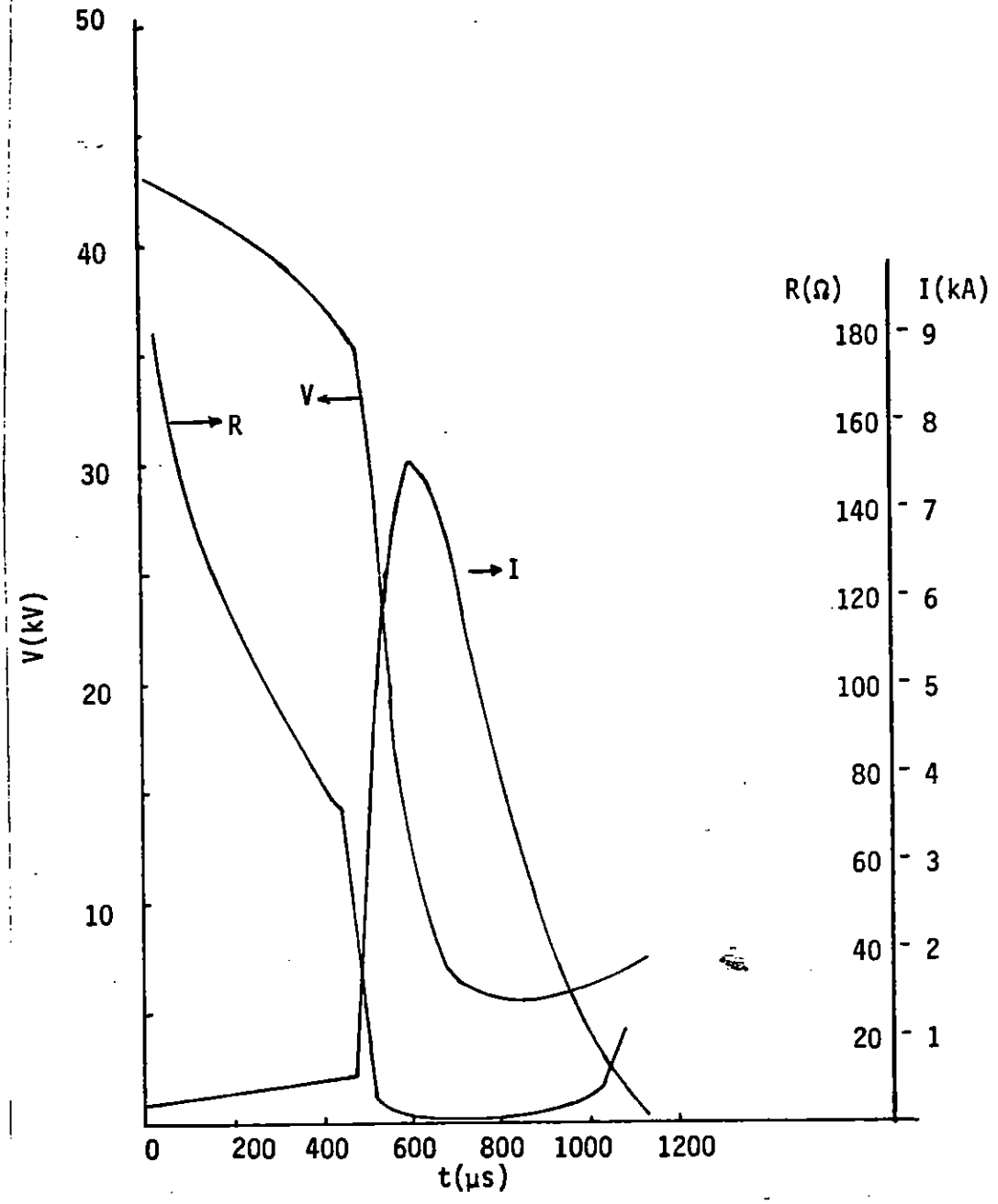

Figure 50. Arc-over characteristics shot 544, Va = 44 kV.

4. STREAMER STRUCTURE

It is apparent from the foregoing data that, as the voltage is increased from a subthreshold value to arc-over, the current flow changes from uniform ohmic flow to one or more streamers with noticeable inhomogeneity and then to arc-over. The nature of a low impedance arc, as well as the data presented in Reference 2 and 3, demonstrates that at arc-over a single conducting channel connecting the inner and outer electrodes dominates the sample current. It is not clear from the data presented above how many streamers exist in the intermediate voltage and time regime at which, at least temporarily, stable configuration of enhanced conduction in the inner region and ohmic conduction in the outer regions coexist. A number of techniques were used to illuminate this question during the PI and McAir experiment series:

1. Measuring voltage profiles at various points in azimuth and axial distance at a constant radius from the central conductor.
2. Measuring the potential on various metal rods placed at different azimuths and axial distances at constant radius from the center conductor.
3. Observing the decoration produced on a sheet of conducting plastic placed inside the earth sample at a given radius from the center conductor.

The advantages and disadvantages of each of these techniques are the following:

1. The measurement of the azimuthal/axial voltage profile provides a direct determination of the electric field around the streamers. The impedance of the voltage probes is sufficiently high that a negligible fraction of the earth current

1. Increasing current and decreasing resistance prior to arc-over.
2. Rapidly falling pulser voltage after arc-over.
3. Resistance continuing to decrease slightly beyond the time of peak in current.
4. Eventual rapid recovery of resistance when the current becomes low enough.

Another characteristic of the arc-over process is the rate at which the current increases immediately after the apparent onset of instability. At McAir the rate of increase of current was near 100-200 A/μs for all the shots with 0.01-mR center conductor. On shots 544 (V_a = 44 kV) and 547 (V_a = 72 kV) with a 0.003-mR center conductor, it was 60-80 A/μs. On shot 546 (V_a = 60 kV) it was only 4 A/μs, but the arc-over instability occurred extremely late (1200 μs), when the pulser voltage had already decayed to only 28 kV.

In the PI experiments, with a 200-Ω series resistor, the current increased a small amount suddenly (Fig. 47) and then increased to its maximum at a rate of ≈3 A/μs. On one shot (167, SDF soil, 90° × 0.1 mL geometry, V_a = 75 kV) with only the 10-Ω pulser series resistor, the current rose at a rate of ≈40 A/μs. The PI and McAir experiments indicate that, after the arc-over instability, the current rises at a rate

$$\frac{dI}{dt} \approx 500/R_s \quad A/\mu s$$

where R_s is the series resistance.

vicinity. Furthermore, since the cylinders introduce a local equipotential, they will inhibit the extension of the streamers beyond the plane at which the cylinders are inserted. However, this technique is useful for establishing the multiplicity of streamers approaching the cylinders from inside at applied voltages for which the streamers would not be likely to propagate beyond the position at which the cylinders are located.

3. The insertion of a sheet of conducting plastic at a given radius from the center conductor introduces the least perturbation into the current flow in the earth, but represents a difficult operational problem. The earth must be removed to both emplace and retrieve the conducting plastic. Various materials were tried during the PI experiment to achieve a reasonable combination of minimizing the perturbation introduced by the sheet, and achieving sensitivity for decoration of the sheet by streamers. Thin sheets of Mylar exhibited excellent marks, were relatively immune to mechanical damage during insertion, but were suspect because they introduced an insulating sheet into earth geometry. It is possible to estimate that the capacitance across such a sheet is sufficient to allow relatively uniform current flow up to the onset of streamer induced breakdown. However, once punch-through is achieved at a given location, it is clear that the remaining current from the entire earth segment will try to flow through that location. Therefore, other materials were sought. Various types of conducting paper were attempted, but no unambiguous marks were left on them by the streamers. Eventually, sheets of a conducting plastic that is normally used to wrap electronic devices sensitive to electrostatic discharges were tried and found to be successful. The plastic has a thickness of $\approx 10^{-4}$ m and a rated sheet resistivity

flows into them. The principal perturbation introduced by the voltage probe is the removal of a 1.6 cm cylinder of earth between the sensing position and the top of the sample by the insulating shaft around the voltage probe. This implies that the current flow in the earth must be redirected around the probe shaft, producing a small perturbation. However, the number of probes and recording channels available limit the number of voltage measurements that can be taken on a single shot, and therefore limit the combination of area coverage and the resolution achievable. It can be seen easily that, if streamers have characteristic dimensions of 1 mm or so, it is not likely a voltage probe would find itself close enough to the streamer to measure the actual streamer potential, as distinct from the field existing at many streamer radii away.

2. The use of voltage probes connected to conducting cylinders circumvents the problem of area coverage by placing conducting cylinders so as to intercept at least half the surface at a given radius from the center conductor, but it introduces noticeable perturbations in the potential profile. In particular, once a streamer comes near enough to such a conducting cylinder, it discovers that the impedance for current flow through the cylinder is significantly less than the spreading resistance from a streamer with a small area at its head. Therefore, even though the cylinders are not connected to low impedance equipment, each does introduce a micro-instability for streamers approaching them. Similarly, once a streamer has attached to a cylinder, the potential of the nearest cylinder will be drawn toward the potential of the center conductor, thereby inhibiting additional streamer growth in the

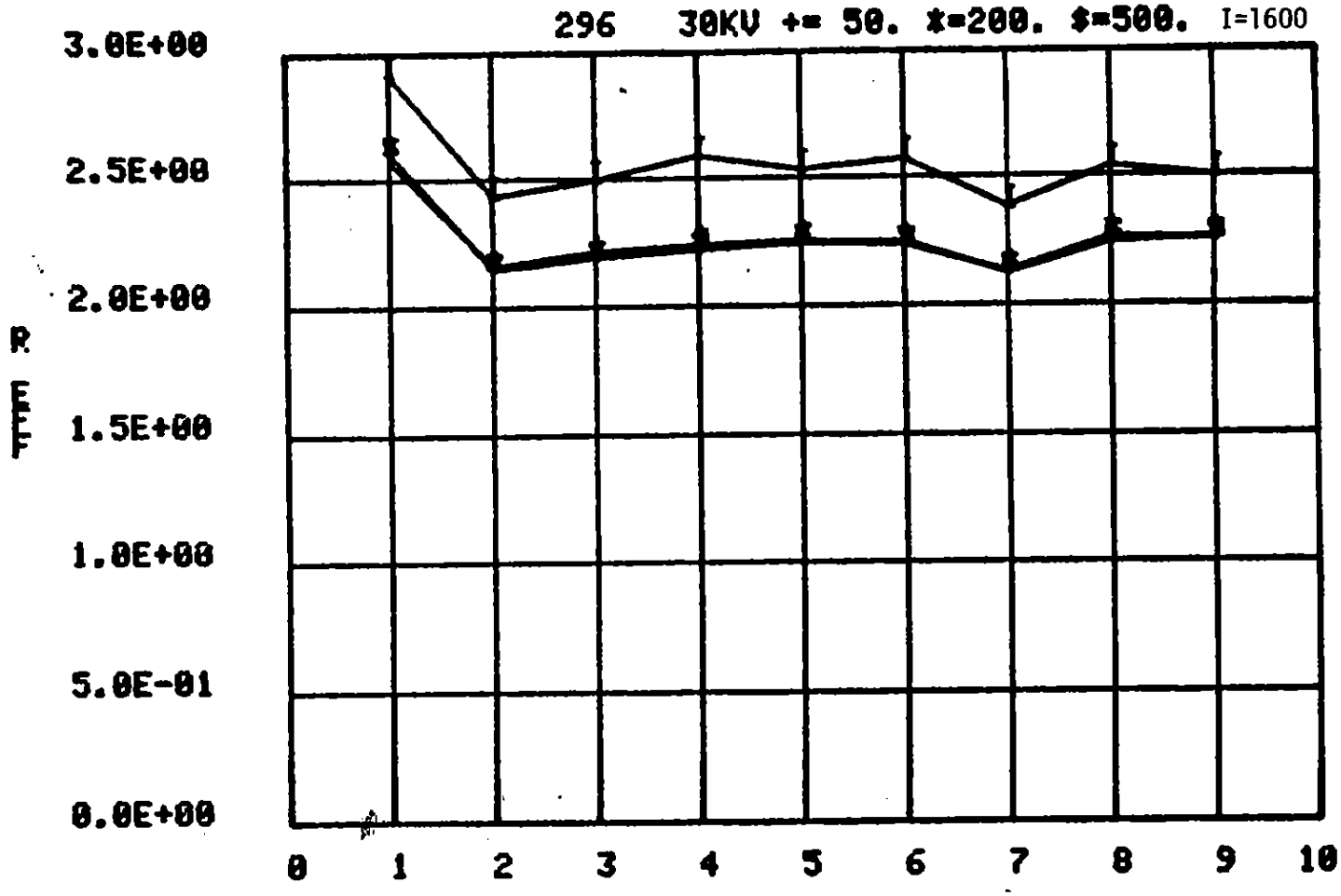

Figure 52. Azimuthal resistance profile.
(130 Ωm MX-B soil
90° x 0.1 mL)

of 3×10^4 Ω/sq. This translates into an effective volume resistivity of 3 Ωm. It is not obvious that this is the correct value of the resistivity for current flow through its thickness, since in the electronic circuit applications the most important characteristic is to promote equipotentials over the surface near electronic devices, rather than to equilibrate the potential between the inside and outside surfaces. The other disadvantage of the plastic is that mechanical damage during the emplacement and retrieval of the sheet can produce marks that can be confused with the decorations caused by conducting streamers.

All three of these techniques were used during both the PI 90° sector experiments and the McAir 360° measurements.

a. Azimuth/Axial Voltage Profiles

Figure 52 presents the measurements of the voltage profile in MX-B soil, 90° × 0.5 mL geometry at 30-kV applied voltage. Under these circumstances there was no evidence of streamer development in this sample (i.e., there is no increase in current beyond the initial value). The data in Figure 52 are plotted as an effective resistance which is calculated from the voltage difference between the probe and the center conductor divided by the total sample current. In other words, this would be the resistance of the material between the center conductor and the probe if the surface at the probe distance were an equipotential at the probe potential. If the current flow were uniformly diverging cylindrically from the center conductor, all probes would exhibit the same effective resistance as determined by the resistivity of the soil, the fraction of the solid angle represented by the sample geometry, the sample length, and the logarithm of the ratio of the probe position radius to the center conductor radius. For the MX-B material, which exhibited a volume resistivity of 130 Ωm in the voltage profiles, the corresponding value of R_{EFF} would be 2.3 kΩ. This is in reasonable

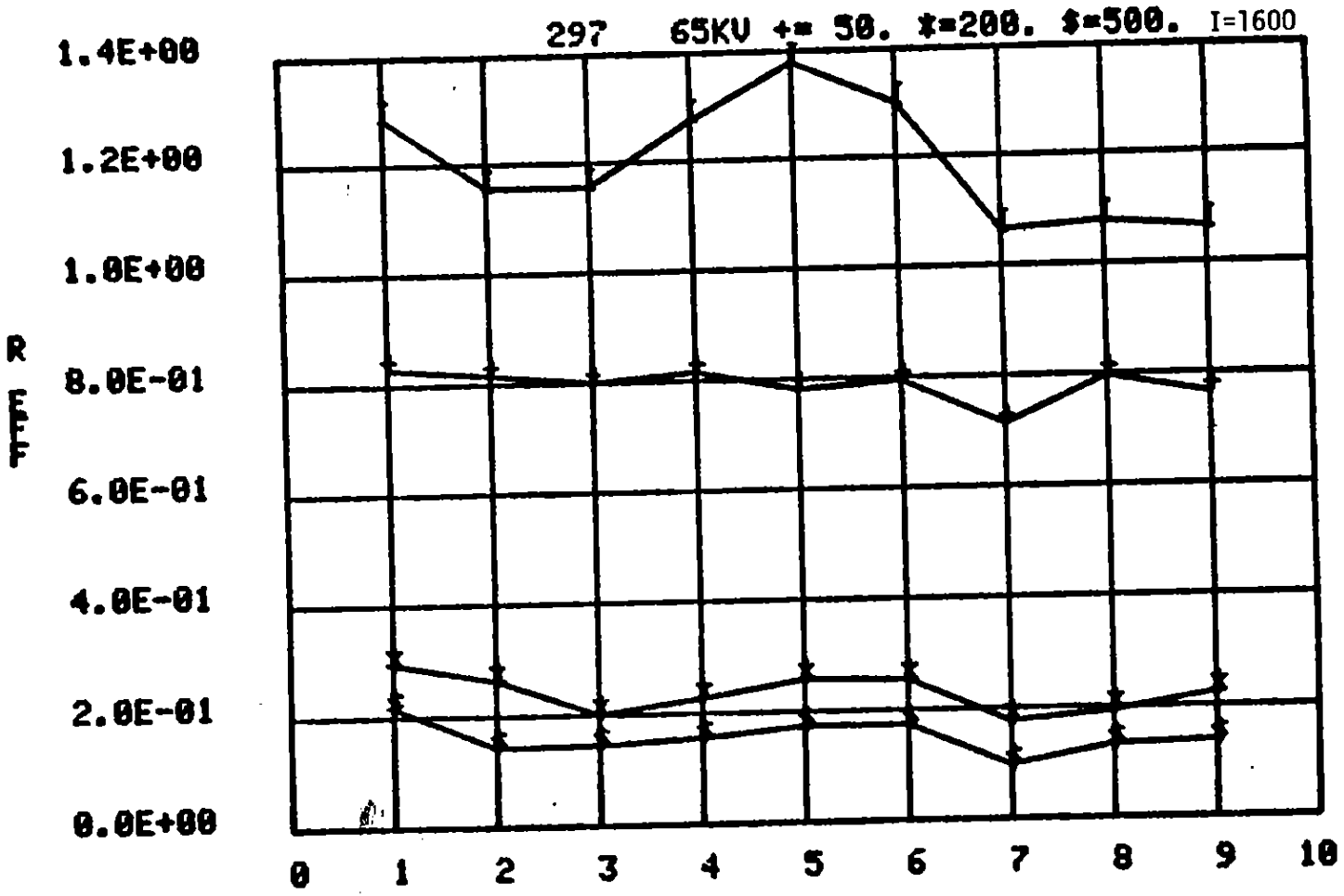

Figure 53. Azimuthal resistance profile.
(130 Ωm MX-B soil
90° x 0.1 mL)

agreement with the values shown in Figure 52. The values given in Figure 52 correspond to an average of 2.27 ± 0.13 kΩ. The spread is consistent with the accuracy of the voltage probe calibrations, which is approximately 5%. Figure 53 illustrates the voltage profile at various times after application of a 65-kV pulse. Even at the earliest times the effective resistance is considerably smaller than the ohmic value, indicating that streamers have proceeded out from the central conductor. At 200 and 500 μs there is a clear minimum in the R_{EFF} at probe position 7. The confidence in this conclusion can be reinforced by reference to Table 5, which presents a statistical analysis of these data. The points have been separated into two groups; one for probes 1 through 6 and 9, the other for probes 7 and 8. The mean values and standard deviations in the data and in the probe calibration have been used to evaluate the difference between the means in these two groups divided by the standard deviation in this difference, calculated by conventional techniques. This ratio is given in the last column of Table 5. The difference is outside one standard deviation for all four measurements, and is equal to almost three standard deviations at 200 μs.

TABLE 5. SHOT 297 R_{EFF}

		Points 1-6, 9			Points 7, 8		
t(μs)	I(A)	$\overline{Re}$	σ(Re)	$\sigma(\overline{Re})$	$\overline{Re}$	σ(Re)	ΔRe/σ(Δ)
50	32	0.80	0.024	0.009	0.76	0.02	1.8
200	40	0.247	0.031	0.012	0.18	0.02	2.9
500	35	0.170	0.022	0.008	0.12	0.02	2.3
1600	5	1.23	0.01	0.04	1.07	0.12	1.3

Figure 54 and 55 present the profiles from two other shots with 65 kV applied. There is clear evidence of one streamer in each profile. The location of the streamer varies between each shot and the next. In shot 299, (Fig. 55) the streamer appeared to be going closest to probe 4 at 100 μs, but produced a very small R_{EEF} for probe 3 at 160 μs. This appears to present evidence for a low impedance within the streamer itself. The apparent gradual decrease in impedance observed in the other experiments

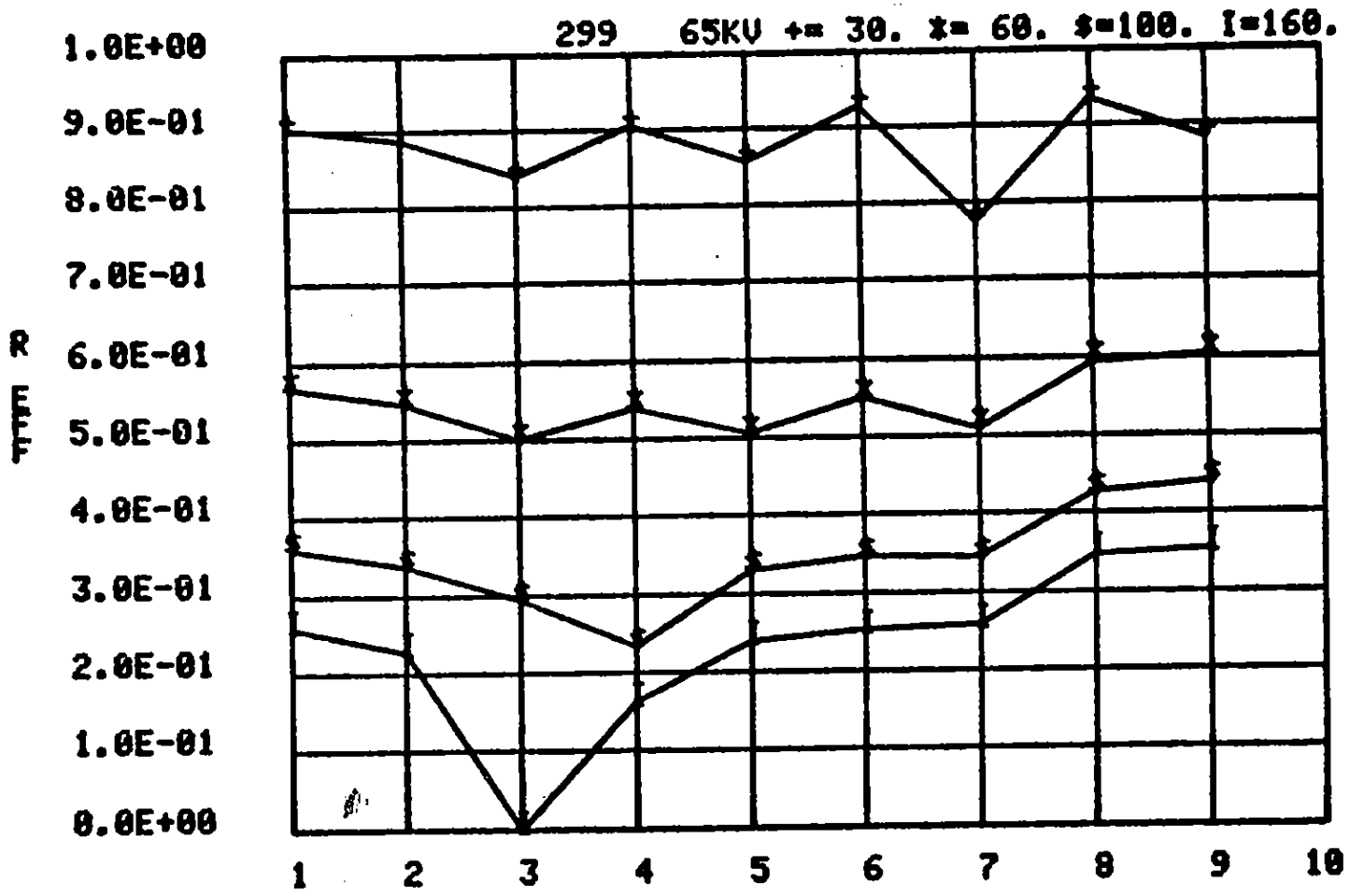

Figure 55. Azimuthal resistance profile.
(130 Ωm MX-B soil
90° x 0.1 mL)

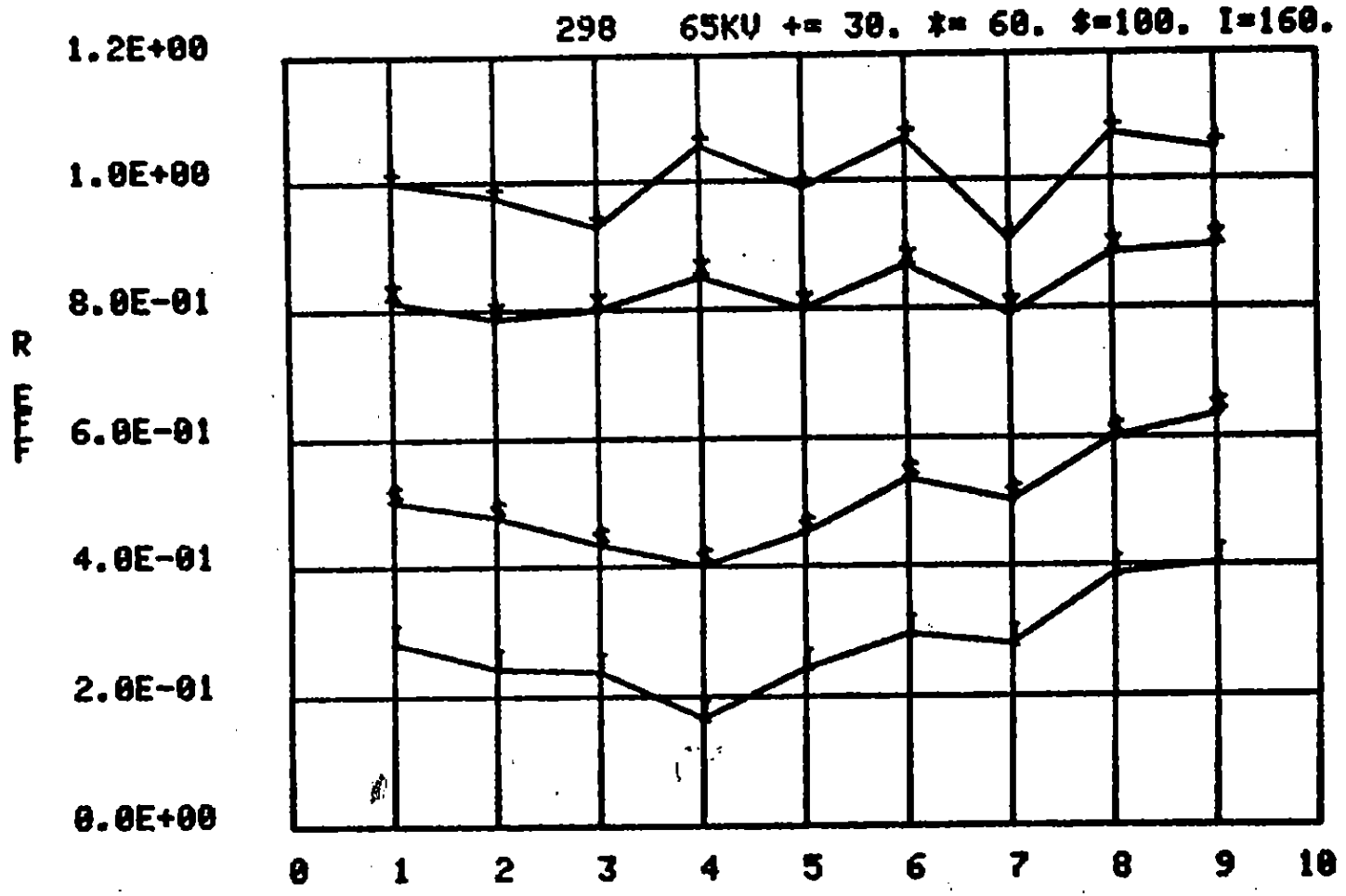

Figure 54. Azimuthal resistance profile.
(130 Ωm MX-B soil
90° x 0.1 mL)

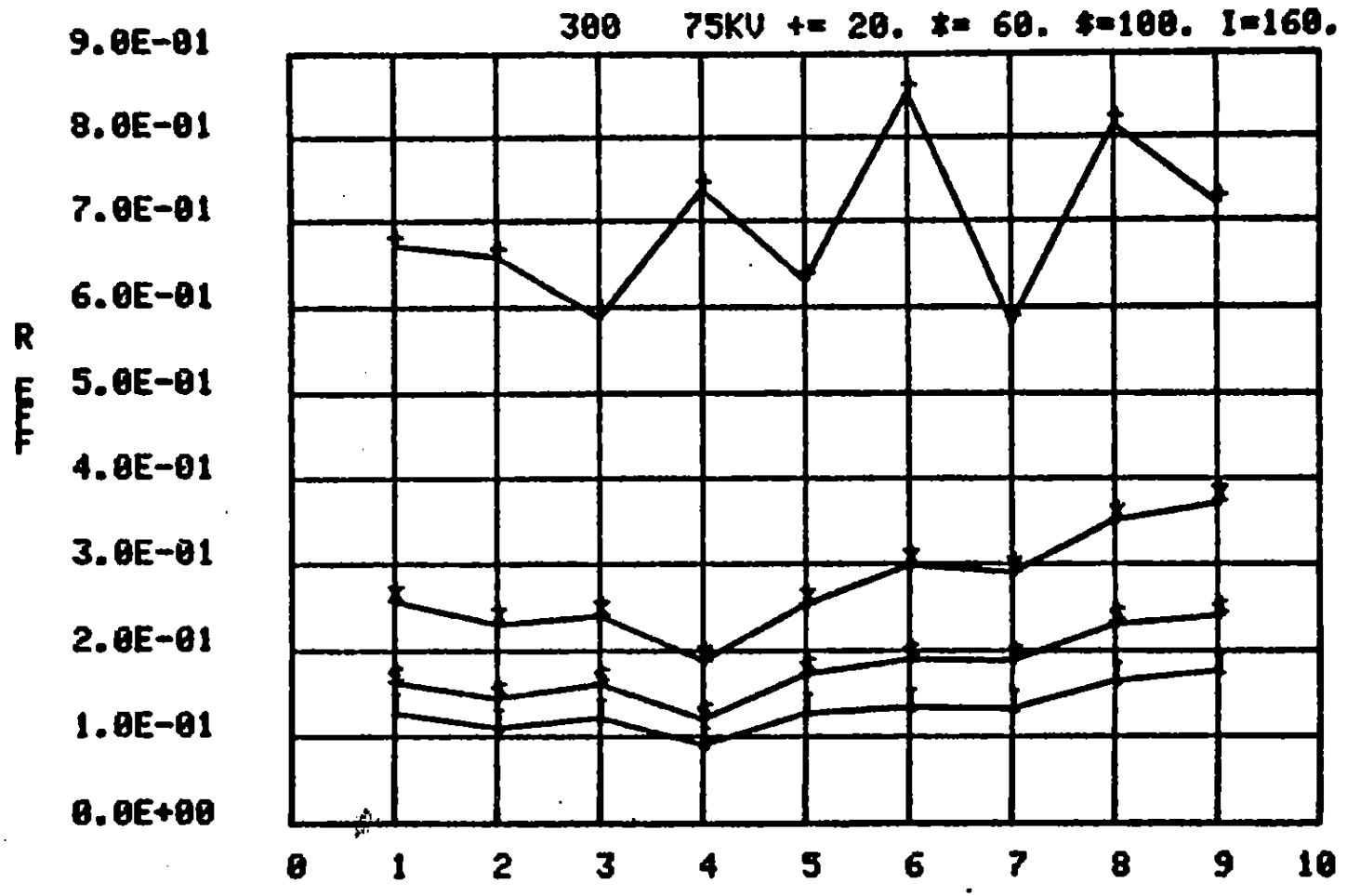

Figure 56. Azimuthal resistance profile.
(130 Ωm MX-B soil
90° x 0.1 mL)

could be a manifestation of a gradually expanding effective conducting radius around a well conducting central core. As long as the voltage probes are many radii away from such a structure, it will manifest a finite R_{EFF}.

Similar measurements on shots with 75 kV applied are shown in Figures 56 through 58. Again, the location of the streamer appears to be different for each shot. In Figure 58 the recovery of the impedance as the current decreases is observed. Within the accuracy of the measurements there is no noticeable difference in the impedance during the recovery between probes near which the streamer flowed and the others.

The relatively subtle differences in voltages observed by the various probes led to an experimental determination of the voltage profile measured by the same probes around a simulated highly conducting streamer, i.e., a 0.0025-m-diameter metal rod protruding radially outward from the center conductor. Figure 59 presents the results of profiles measured with 140 VAC applied to the sample. Statistical analysis of these data indicate that the effective resistance of the central five probes was less than that of the outer four by 0.007 ± 0.007 for the baseline experiment with no radial rod, 0.022 ± 0.011 with the rod protruding out to 10 cm, and 0.048 ± 0.008 with the rod protruding out to 0.15 m (i.e., out to the plane of the voltage probes). The relatively subtle differences are due at least to the relatively large spreading resistance from a small-diameter conductor into the resistive medium and could be augmented by an additional resistive barrier at the metal earth contact. Electrostatic profile calculations need to be performed to establish the degree of additional contact barrier required to explain these data. In any case, it is clear that the observed voltage profiles during high voltage excitation exhibit larger variations than those produced by the conducting rod alone. This would imply one of two conclusions: (a) if a barrier is required to explain 140 VAC results, the barrier may be considerably less around a streamer, and (b) the effective diameter out to which the high conductivity region is produced by a streamer may be considerably larger than 0.0025 m.

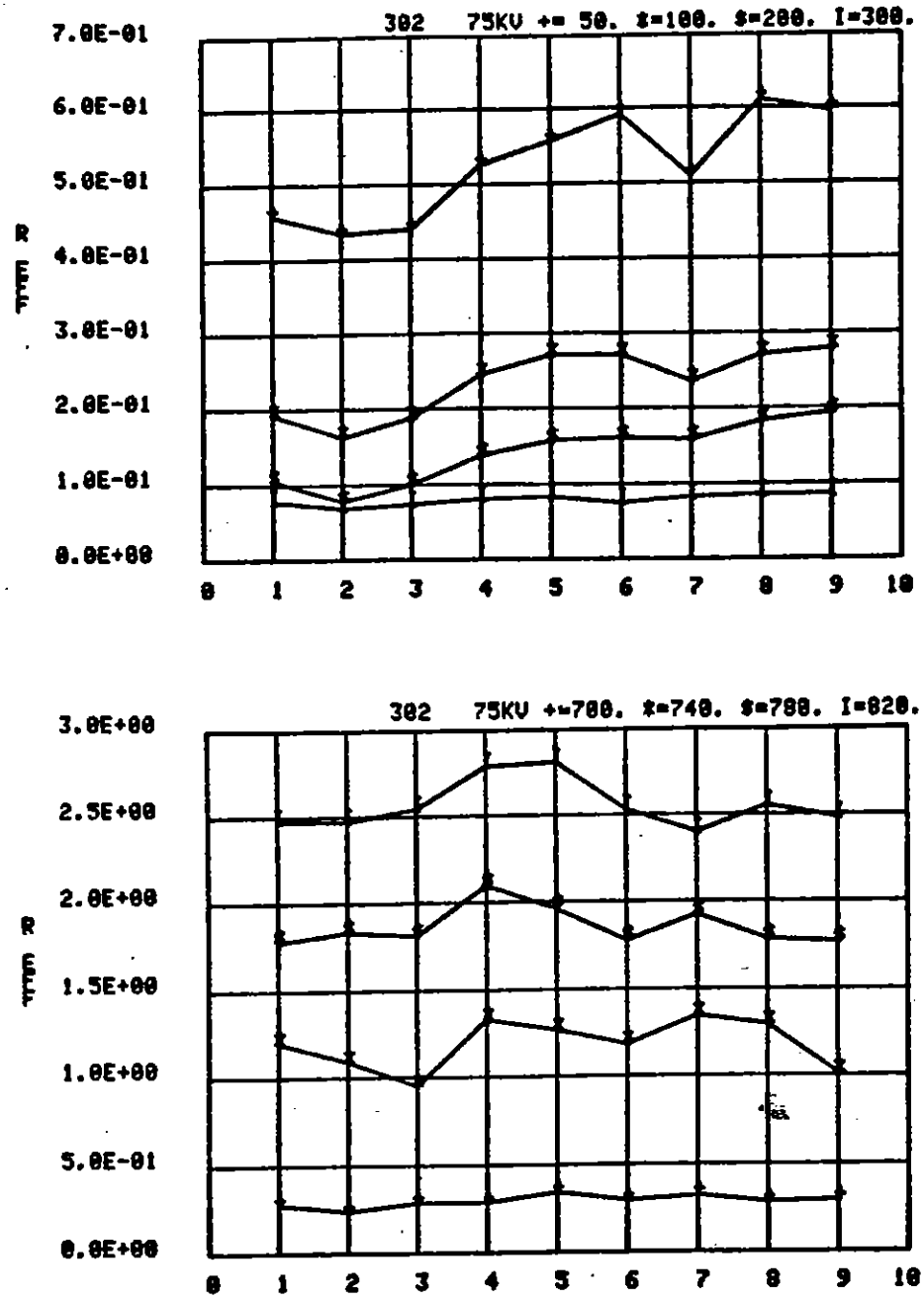

Figure 58. Azimuthal resistance profile.
(130 Ωm MX-B soil
90° x 0.1 mL)

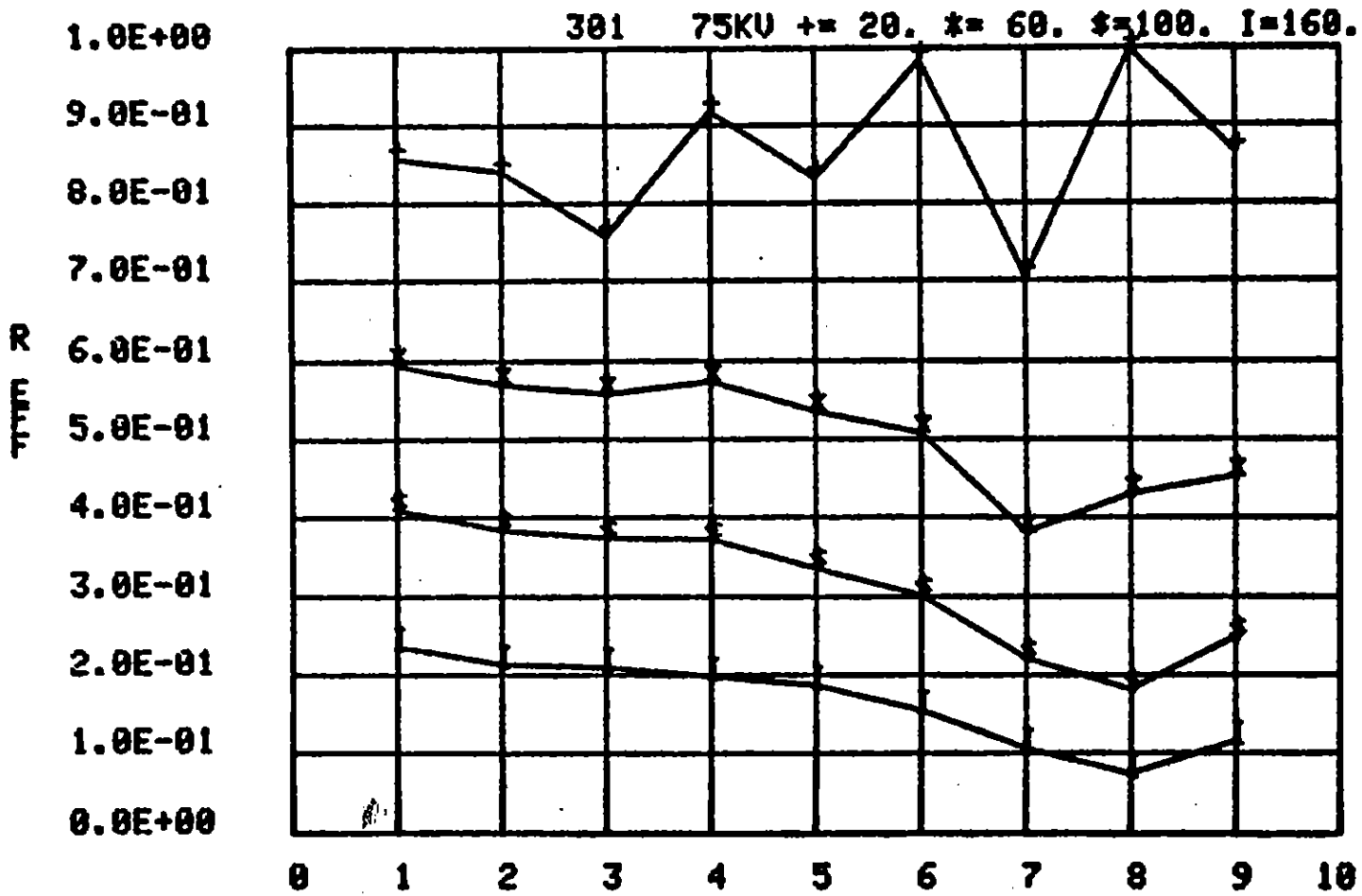

Figure 57. Azimuthal resistance profile.
(130 Ωm MX-B soil
90° x 0.1 mL)

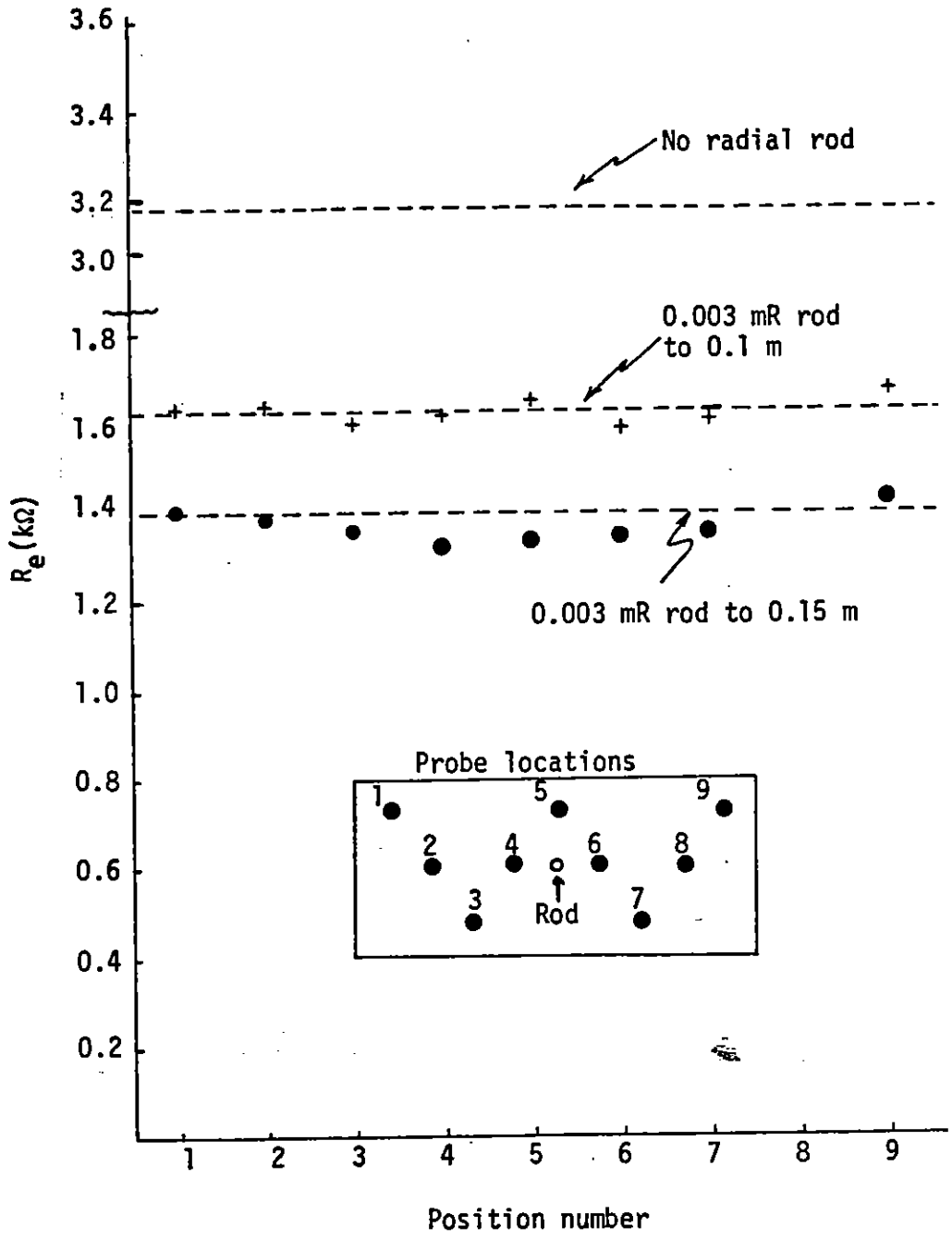

Figure 59. Resistance profiles at 0.15 mR, 140 VAC applied.

Figure 60 presents a comparison of similar voltage profiles with a 30 kV pulse applied. With no radial rod, the effective resistance is slightly less than that observed for 140 VAC, but exhibits no detectable azimuthal variation. This is the same profile previously presented in Figure 52. With a 0.003 mR axial rod protruding to a radius of 0.1 m there is a large decrease of the effective resistance compared to the 140 VAC value and a much greater depression in the middle, albeit a somewhat asymmetric one. When the rod protrudes to a radius of 0.15 m, i.e., with its end in the plane of the probes, the effective resistance in the middle is much less than out near the edges. The average value of R_E for the three central points is 0.07 kΩ, whereas for the four outermost points it is 0.29 kΩ. These data clearly illustrate that the effect of streamers, even at 30 kV, extends the potential of a small conductor out to distances of 0.02 to 0.03 m, whereas with only 140 VAC applied, the effect at equivalent distances is very subtle. Additional shots in these configurations were taken at higher applied voltages, but these data have not been reduced.

During the McAir experiments on 300-Ωm mixed sand, a similar voltage profile was measured by selecting a 90° sector out of the 360° geometry and placing probes at four heights within that sector. Figure 61 presents the voltage profile measured by these probes at four different times after applying an 80-kV pulse. Three comments apply to these data:

1. This experiment was performed with a 344-Ω axial resistor in the center of the sample under self-bias conditions (i.e., voltage was applied between the top of the axial resistor and the outside cylindrical conductor). The R_{EFF} data as presented in Figure 61 represent voltage differences between the probe and the top of the axial resistor string. This explains the gradual increase of R_{EFF} as one progresses to voltage probes farther down in the sample.

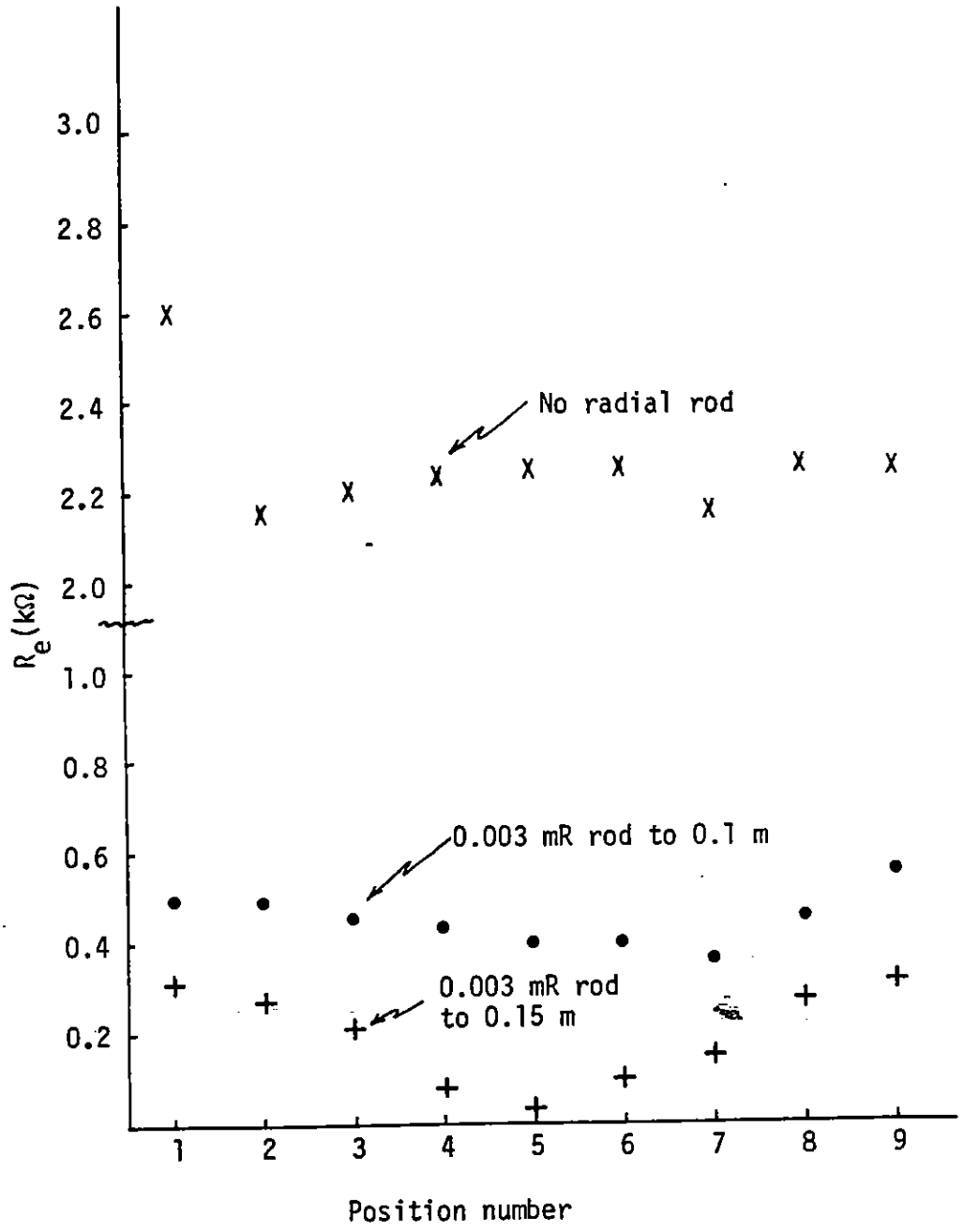

Figure 60. Resistance profiles at 0.15 mR, 30 kV applied.

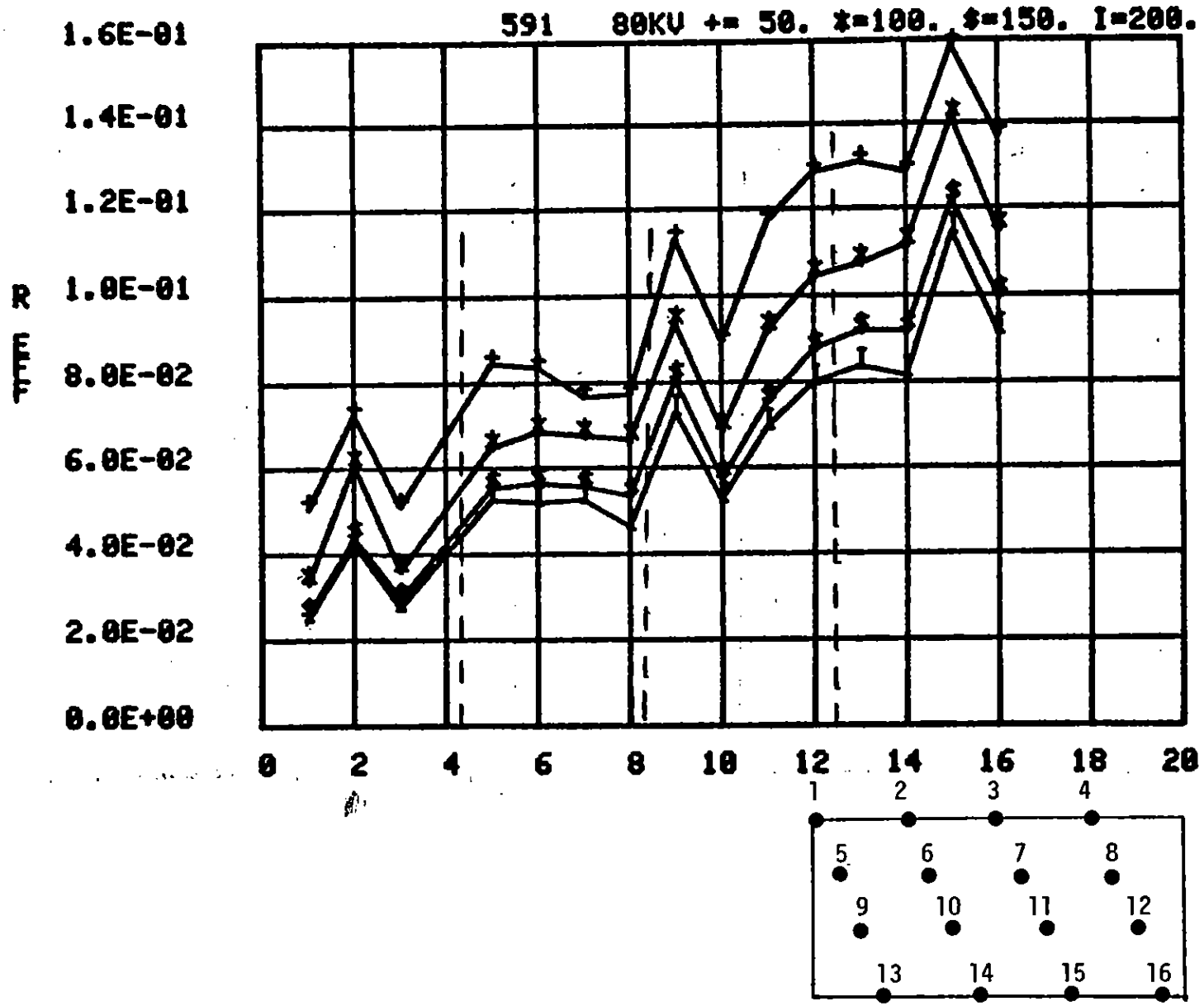

Figure 61. Resistance profile.
(Shot 591, 80 kV applied)

2. Since only a generic calibration curve was used for these voltage probes, rather than a probe-by-probe, specific curve as used for the PI data, there is considerably more variation from one probe to the next in R_{EFF}.
3. There is no obvious trend in these data, other than a general decrease of R_{EFF} with time. This may be due to two possible explanations: (a) a sector was selected in which there was no predominant streamer, or (b) with 80 kV applied, the more or less uniform streamers extended out to the radius of the voltage probes (0.14 m). These data have been replotted in Figure 62 after normalization to the effective resistance at 50 μs in an attempt to cancel out the individual probe calibrations and the bias produced by the axial resistor. Again, there is considerable scatter in the data, although there is a suggestion that the development of a lower impedance path in the vicinity of probe 10 at 100 μs extending to probe 11 at 150 μs, and to 14 at 200 μs.

There exist unprocessed data on 6 more shots, also taken at 80 kV. Shot to shot comparison of these data might reduce the apparent noise due to voltage probe calibration. Unfortunately, no data were taken with lower applied voltage, at which the non-uniformities in streamer behavior out to the radius at which the voltage probe were placed might be more apparent.

b. Decoration of Plastic Sheets

Conducting plastic sheets were decorated with streamers and arcs at both PI and McAir.

Figure 63 is a photograph of a part of a conducting plastic sheet placed at a radius of 0.05 m in 5600-Ωm sand with 90° × 0.1 mL geometry at V_a = 84 kV. While streamering was apparent in the current and voltage

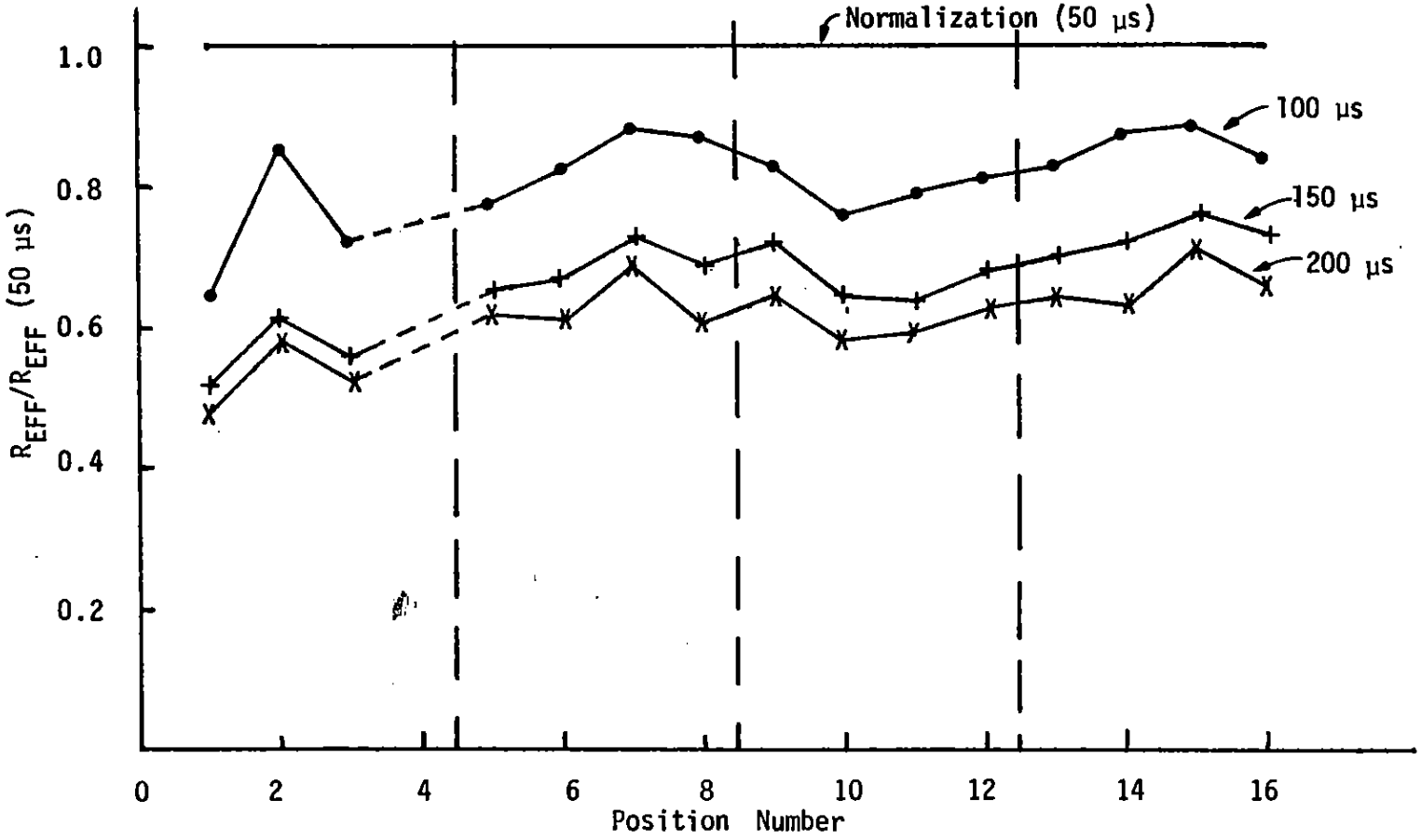

Figure 62. Normalized resistance profile.
(Shot 591, 80 kV applied)

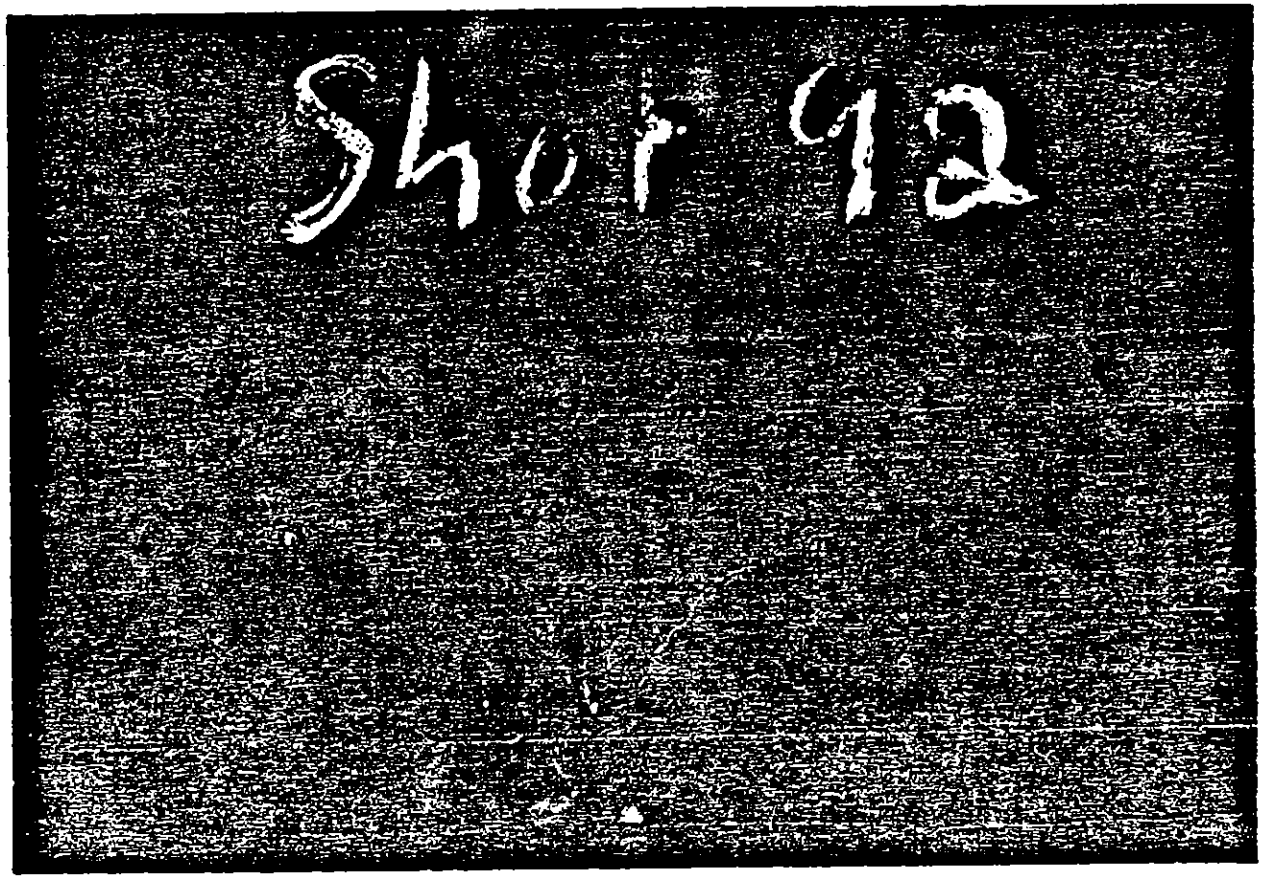

Figure 63. Conducting plastic decoration.
(V_a = 84 kV, R = 0.05 m, 5500 Ωm sand)

probe records, no arc-over occurred. Three small holes are close together ≈6 mm from the right-hand edge of the plastic (white spots at intersection of tree near bottom of photo in Figure 63). The Lichtenberg figure structure extending to a distance of ≈20 mm from the holes is apparent.

Similar structures of smaller lateral extent were produced in lower resistivity soil samples near the center conductor under non-arcing conditions and near the outer conductor under arc-over. Table 6 presents a summary of these results. On no occasion in the PI experiments was there more than one pattern on the plastic.

TABLE 6. CONDUCTING PLASTIC SHOTS AT PI

Shot No.	Soil Resistivity	Location	V_a (kV)	Arc-over	Observations
92	5600 Ωm	R = 0.05 m	84	No	Licht. Fig. ≈20-mm radius
93	"	"	84	"	" " " " "
186	140 Ωm	around center conductor	55	"	Dense Licht. Fig. ≈6-mm radius on outside of plastic
187	"	inside outer conductor	70	Yes	Dense Licht. Fig. ≈6-mm radius on inside of plastic

The central hole in the pattern is typically ≈0.3-mm diameter, even for ≈100 A arc (shot 187). On two shots in 5600-Ωm sand (#92, #93) with I ≈ 1 A, one produced three nearby holes, each ≈0.3-mm diameter; the other produced no visible puncture. Both produced dramatic Lichtenberg figures, as illustrated in Figure 63.

The conclusions drawn from these data are that:

1. In 90° × 0.1 mL geometry only one major streamer with high-current density concentrated in <0.3-mm diameter dominates the current flow from the center conductor outward.

2. The streamer is surrounded by a large radial electric field whose extent is greater in higher resistivity earth.

One shot at McAir was used to decorate two plastic sheets, one at a radius of 0.08 m, the other at 0.15 m. The 0.5-m radius × 1-mL sample of 350-Ωm sand mix was subjected to one radial pulse at 72 kV. Arc-over was observed in the voltage and current probes at 20 μs. The peak current after arc-over was ≈30 kA. The two sheets showed extensive handling damage as well as some electrically produced features. The inner sheet (R = 0.08 m) showed two large holes and a number of regions containing multiple small punctures. The outer sheet (R = 0.15 m) showed one large hole reasonably in line with one of the inner sheet holes. A small group of punctures is in line with the other inner sheet hole. Thermal damage to the plastic is evident by its change in texture. Figure 64 is a photo of the hole in the outer sheet. Its overall diameter is ≈30 mm.

The pattern of holes on both sheets is illustrated in Figure 65. Inspecting the plastic proves that some features are due to mechanical damage during installation (e.g., tear at top of Figure 65a and holes near top right of Figure 65b). However, there is no doubt about the major features, because they exhibit thermal damage to the plastic.

c. Conducting Rod Profiles

Figure 66 illustrates the geometry of an experiment with a 90° sample sector containing seven conducting cylinders placed at a radius of 0.10 m to measure the streamer structure. As discussed above, the cylinders will attract a streamer when it comes close enough, and there is a tendency to suppress propagation to adjacent cylinders. The records from this experiment geometry are typified by those shown in Figure 67. A step is observed in the voltage and current when a streamer approaches and attaches to a particular cylinder. Once a streamer has attached to a cylinder, subsequent attachments to other cylinders do not produce a significant voltage step in

Figure 64. Hole in conducting plastic.
(R = 0.2 m)

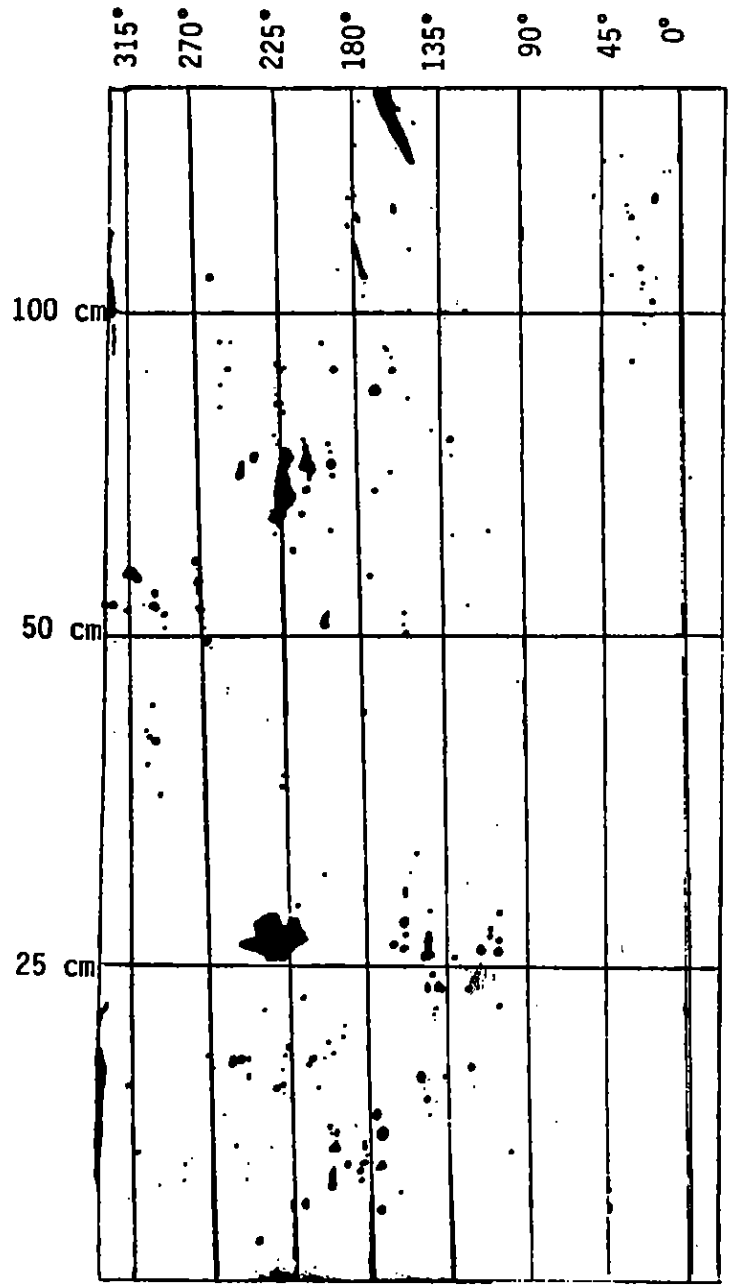

(a)

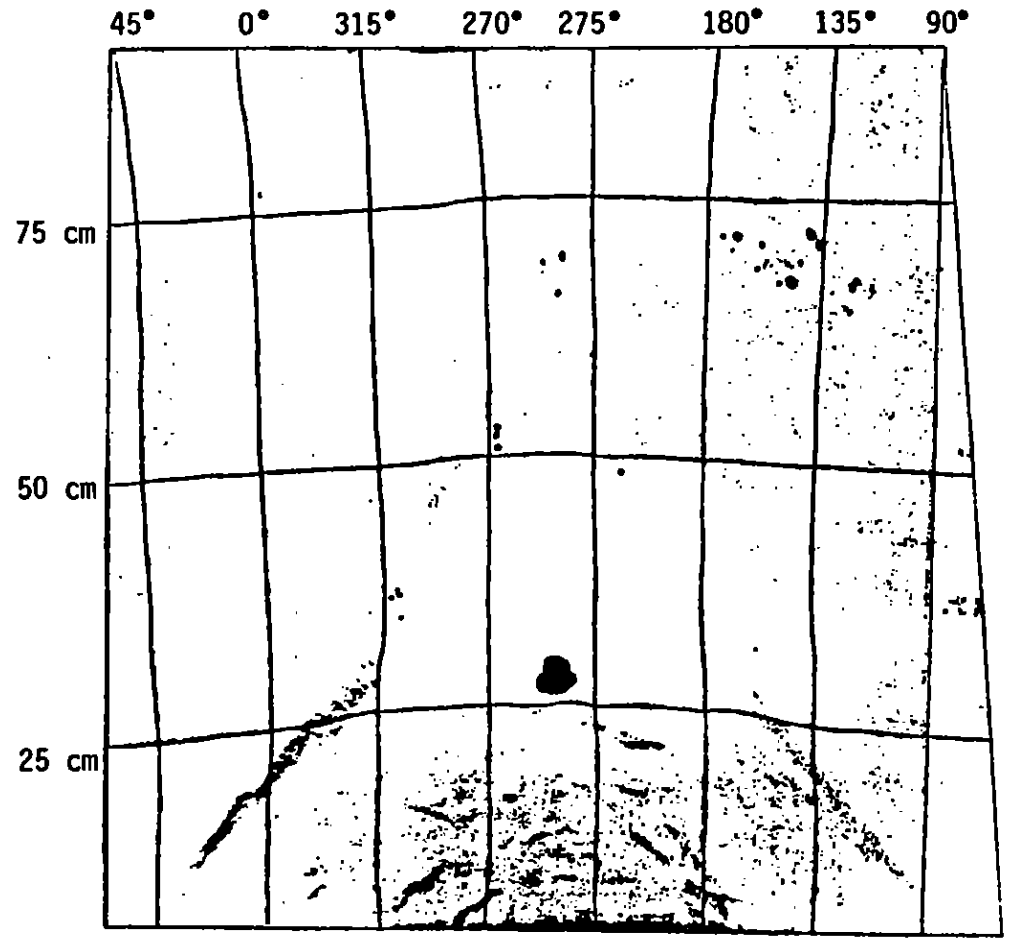

(b)

Figure 65. Conducting plastic decorated by arcs at: (a) 7.6 cm radius and, (b) 15 cm radius (including tears in the plastic).

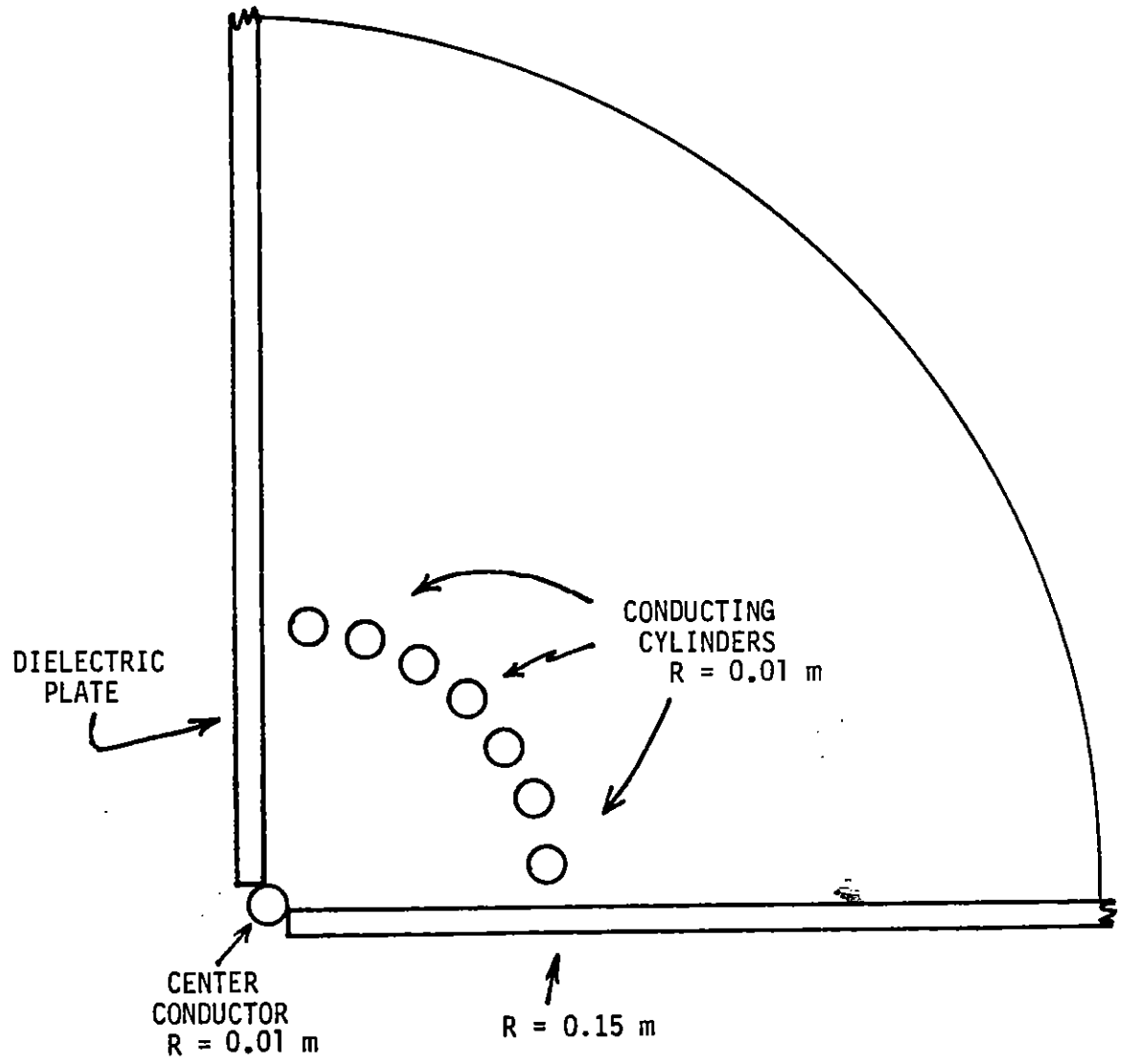

Figure 66. Conducting cylinder geometry.

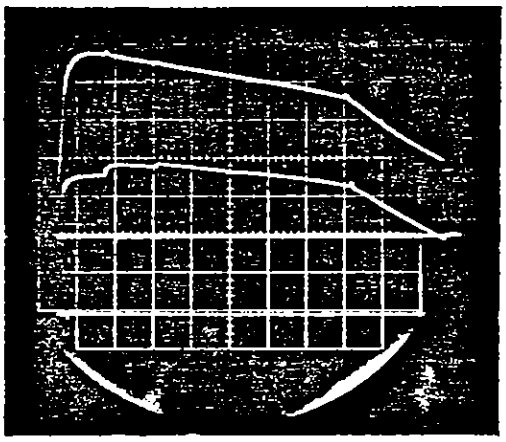

(a) Probe 2, 4

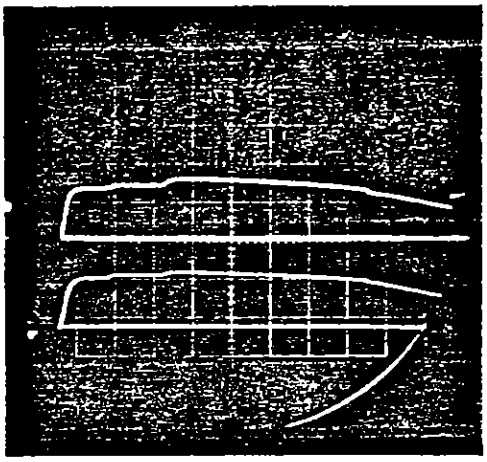

(b) Probe 7, 6

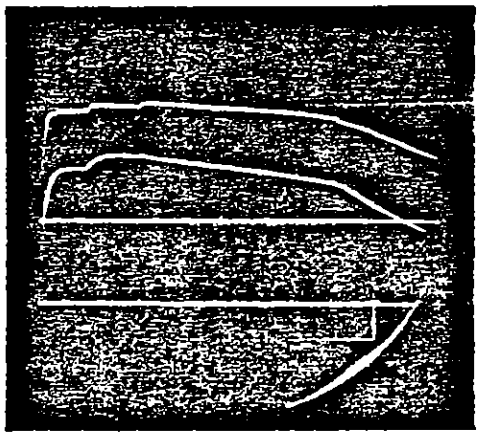

(c) Probe 5, 3

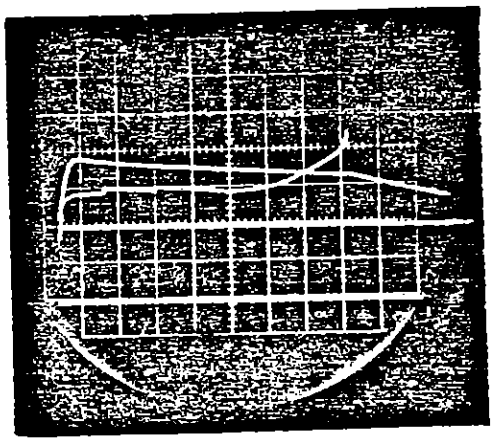

(d) Va, I

Figure 67. Cylinder voltages.
(Shot 417, Va - 75 kV)

the first one. The examples of the effective resistance profile observed with this geometry are presented in Figures 68 through 76. These profiles are all taken in the 300-Ωm sand mix. At 30 kV (Fig. 68), no significant deviations from ohmic behavior are observed. At 40 kV the effective impedance is decreasing as a function of time, indicating that streamers are moving out from the center. Apart from a hint of a decreased impedance in the vicinity of probe 6, no particular structure is evident. At 50 kV (Fig. 70) a streamer has clearly developed and attached to probe 4 at 230 μs. At 60 kV, Figures 71 and 72, strong evidence of a streamer is apparent, first on probe 7 (Fig. 71) and on the subsequent shot at probe 4 (Fig. 72). At 65 kV the same differences are observed on Figures 73 and 74. In both cases, the earliest records indicate streamers approaching both the center and the right hand edge. In shot 413 the one at the right-hand edge won out; in shot 414 the one in the middle attached first. The 70-kV shot (Fig. 75) illustrates the attachment of a streamer to probe 6 at 90 μs followed by a gradually decreasing R_{EFF} to probe 5. At 75 kV (Fig. 76) this effect is seen again, this time from probe 3, which is attached at 60 μs to probe 2. A similar set of records for the MX-B soil are shown in Figures 77 through 93. The ohmic resistance deduced from the slope of the radial voltage profile curve, would be 1.9 kΩ. The 30 kV values (Fig. 77) are near 1.7 kΩ, indicating a small amount of radial streamering. This evidence is supported by a small increase in current after the onset of the voltage. At 40 kV (Fig. 78) the effective resistance is decreasing with time but no structure is evident. At 50 kV in two successive shots (Figs. 79 and 80), a streamer branches from probe 2 to probe 3. In four successive shots, at 60 kV (Figs. 81 through 85), a variety of streamer behavior is observed. In the first two shots, the streamer attaches to probe 4 and branches to probe 5 (Figs. 81 and 82). In the third shot (Fig. 83) it attaches to probe 2. In the fourth shot (Fig. 84) it attaches to both probe 2 and probe 5, and finally, in the fifth shot (Fig. 85) it attaches only to probe 2. Returning to 50 kV after that sequence of shots at 60 kV, the streamer is observed first attached to probe 5 (Fig. 86), then to probe 2 (Fig. 87). At 65 kV

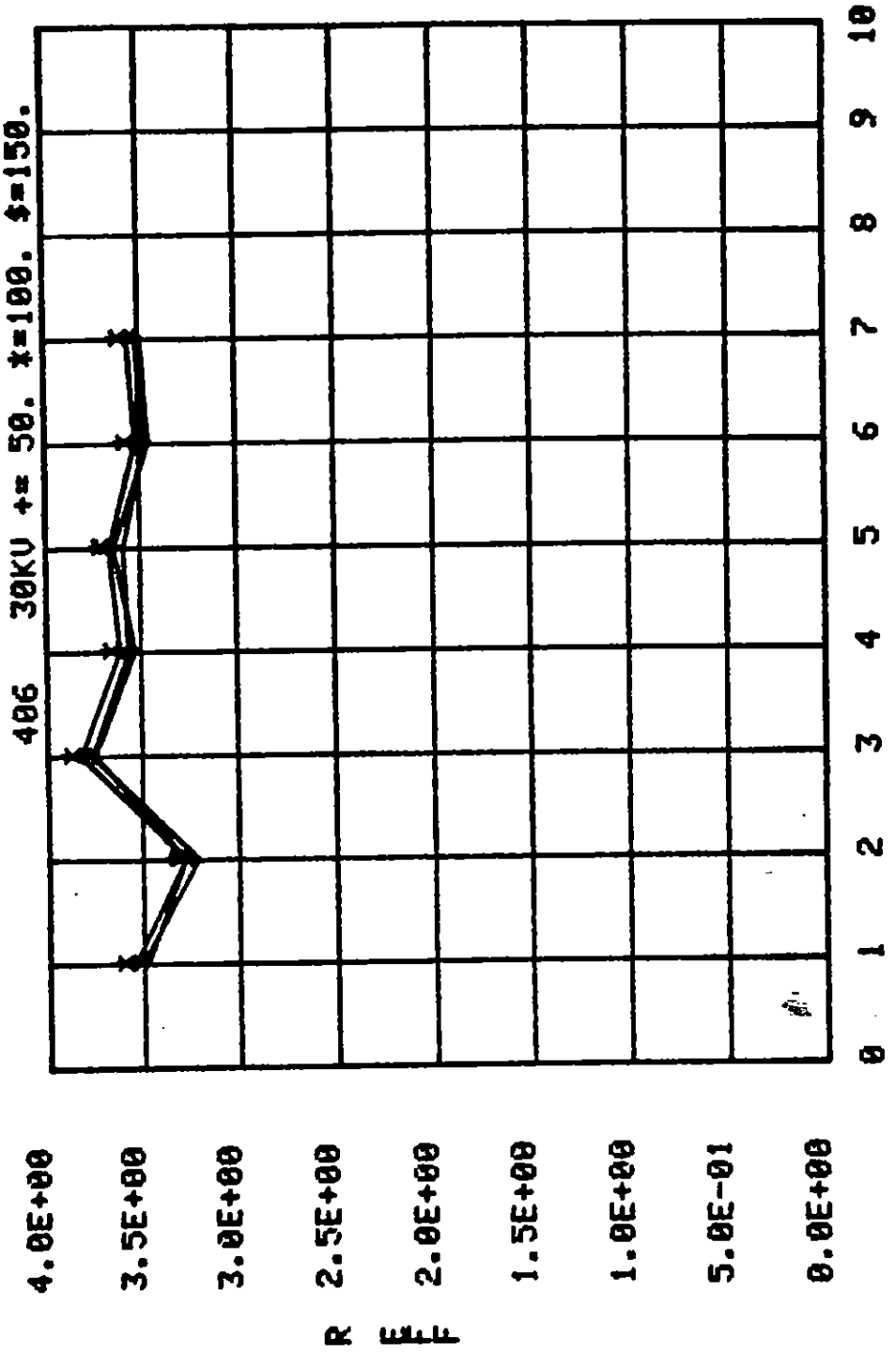

Figure 68. Azimuthal resistance profile with conducting rods. (350 Ωm sand mix 90° x 0.1 mL)

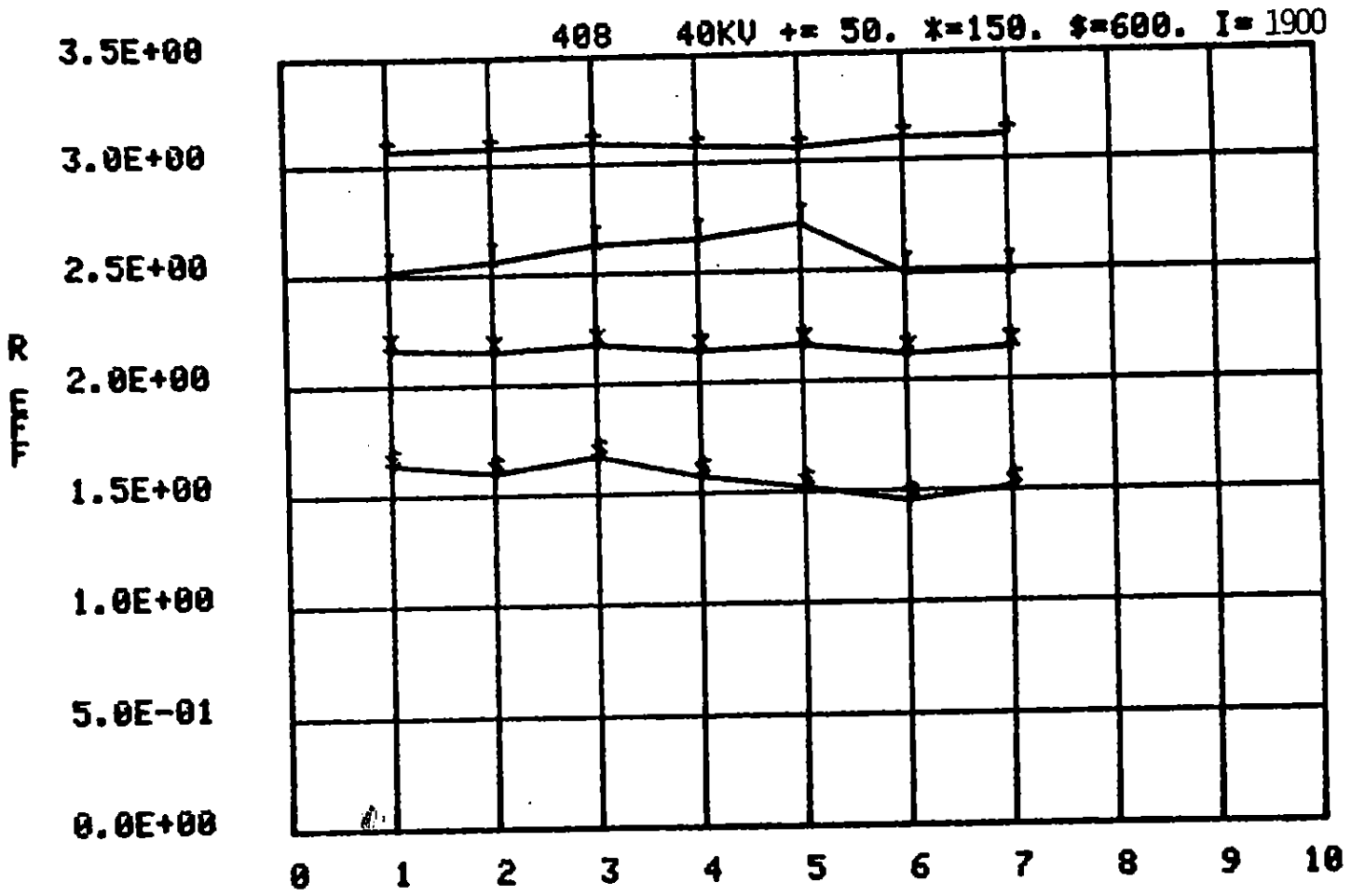

Figure 69. Azimuthal resistance profile with conducting rods. (350 Ωm sand mix 90° x 0.1 mL)

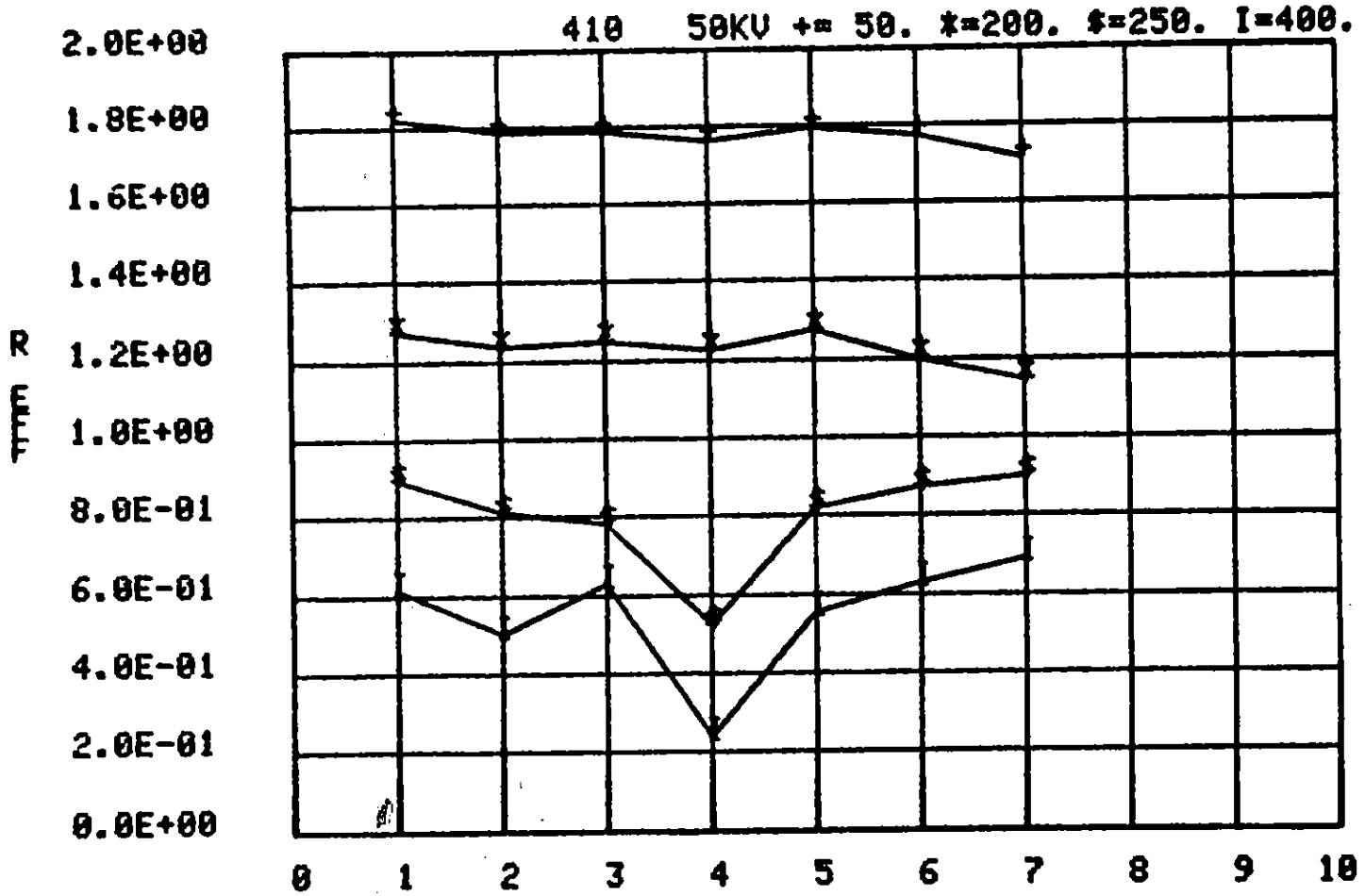

Figure 70. Azimuthal resistance profile with conducting rods. (350 Ωm sand mix 90° x 0.1 mL)

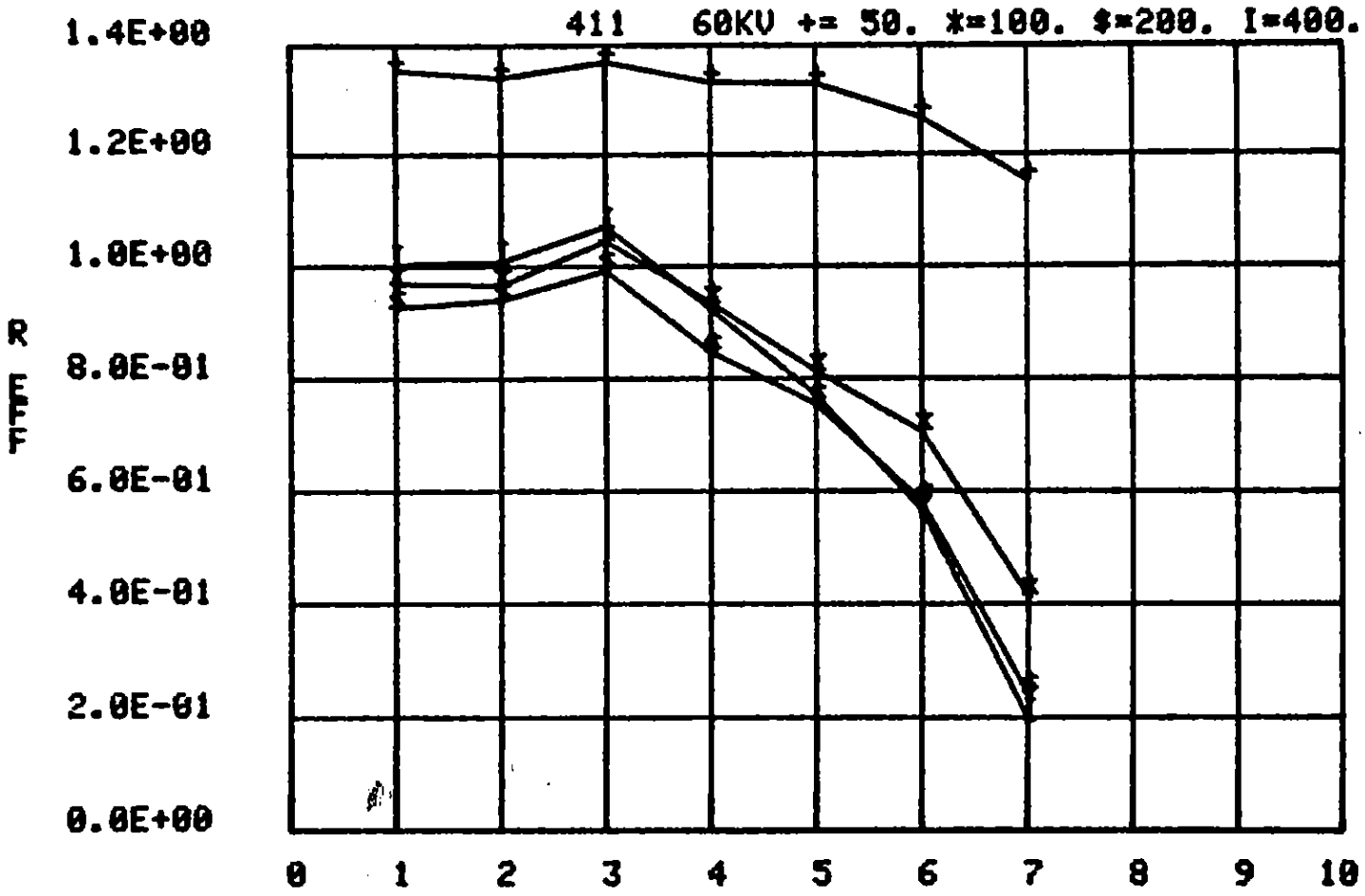

Figure 71. Azimuthal resistance profile with conducting rods. (350 Ωm sand mix 90° x 0.1 mL)

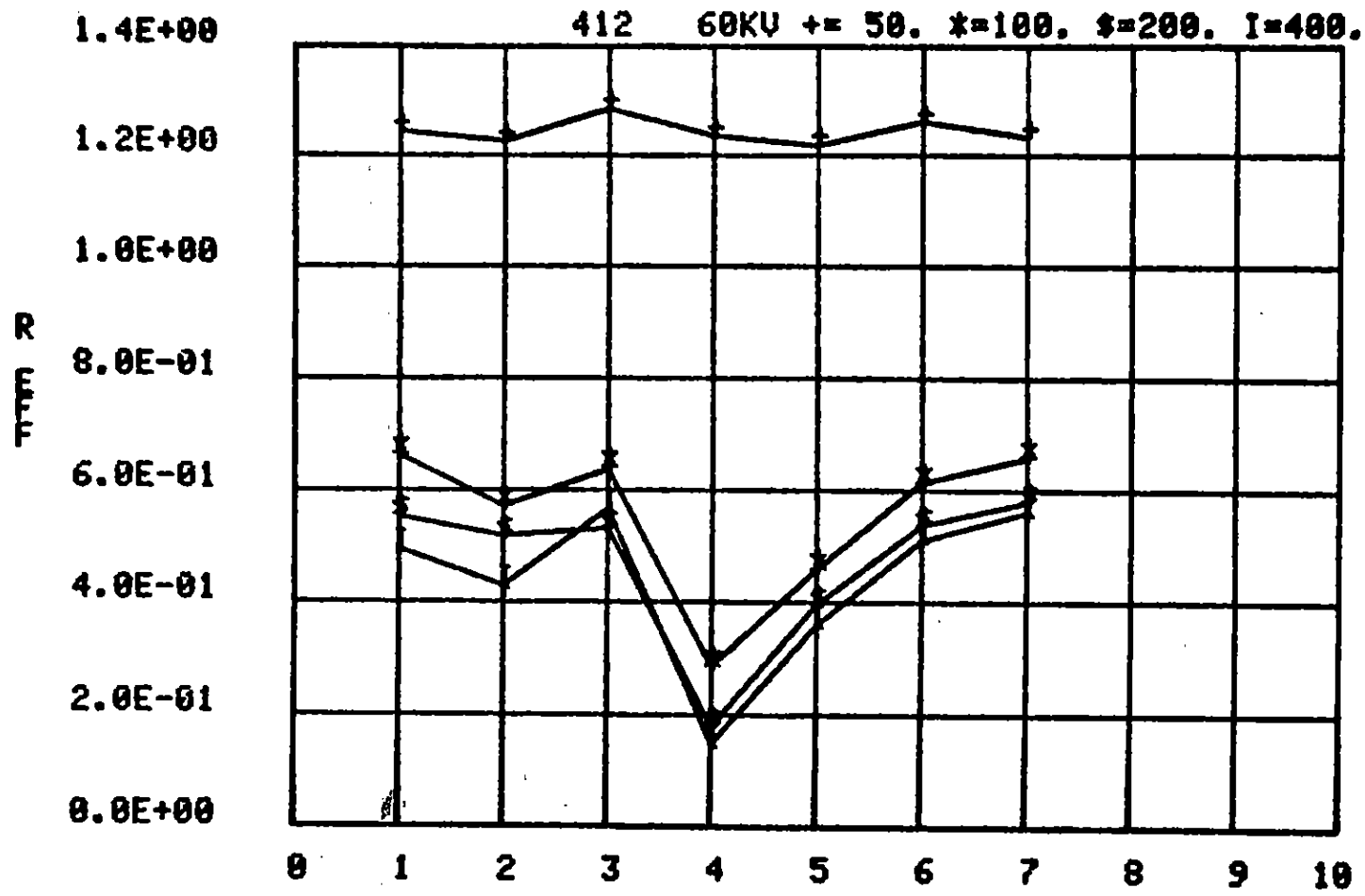

Figure 72. Azimuthal resistance profile with conducting rods. (350 Ωm sand mix 90° x 0.1 mL)

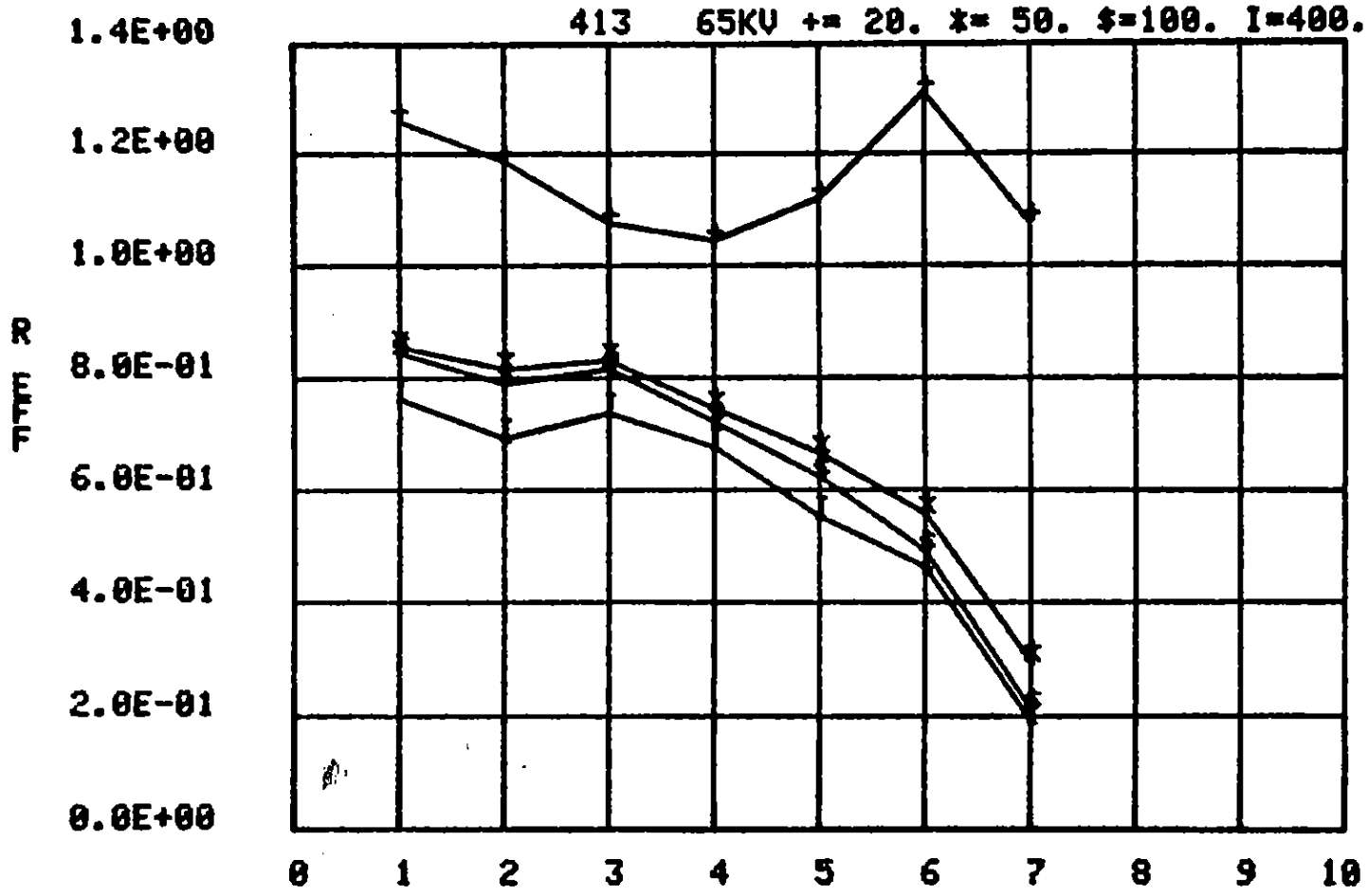

Figure 73. Azimuthal resistance profile with conducting rods. (350 Ωm sand mix 90° x 0.1 mL)

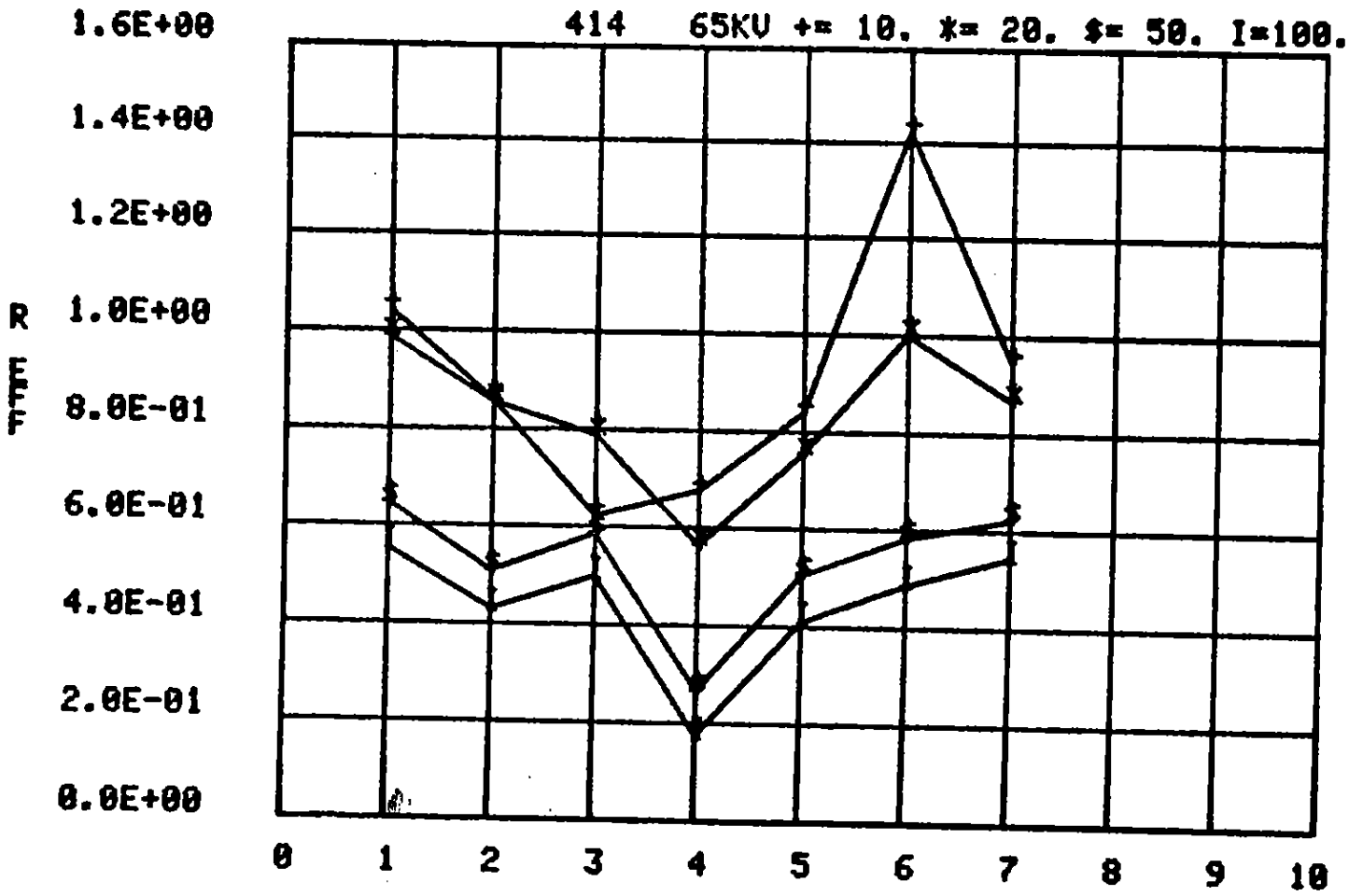

Figure 74. Azimuthal resistance profile with conducting rods. (350 Ωm sand mix 90° x 0.1 mL)

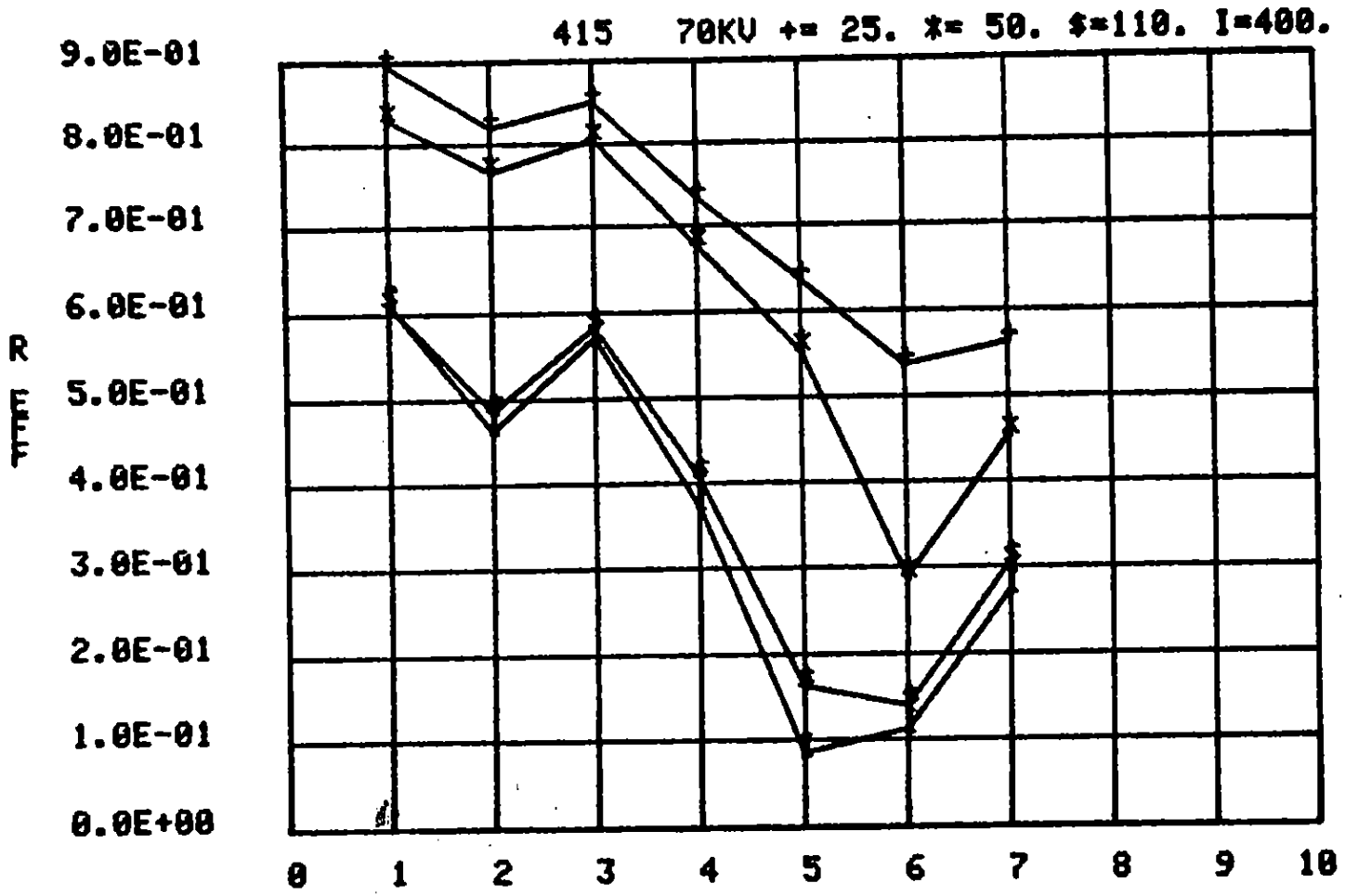

Figure 75. Azimuthal resistance profile with conducting rods. (350 Ωm sand mix 90° x 0.1 mL)

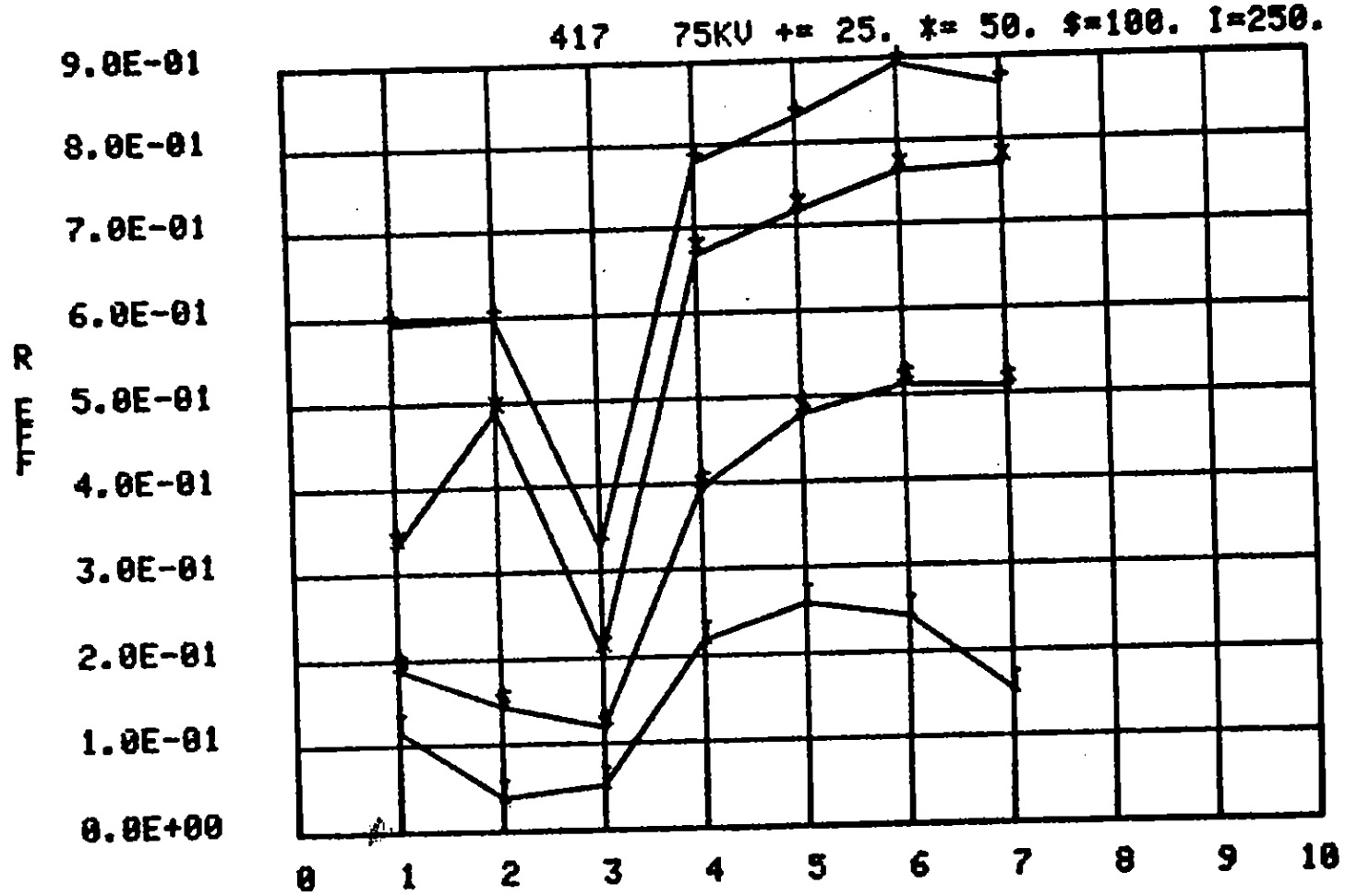

Figure 76. Azimuthal resistance profile with conducting rods. (350 Ωm sand mix 90° x 0.1 mL)

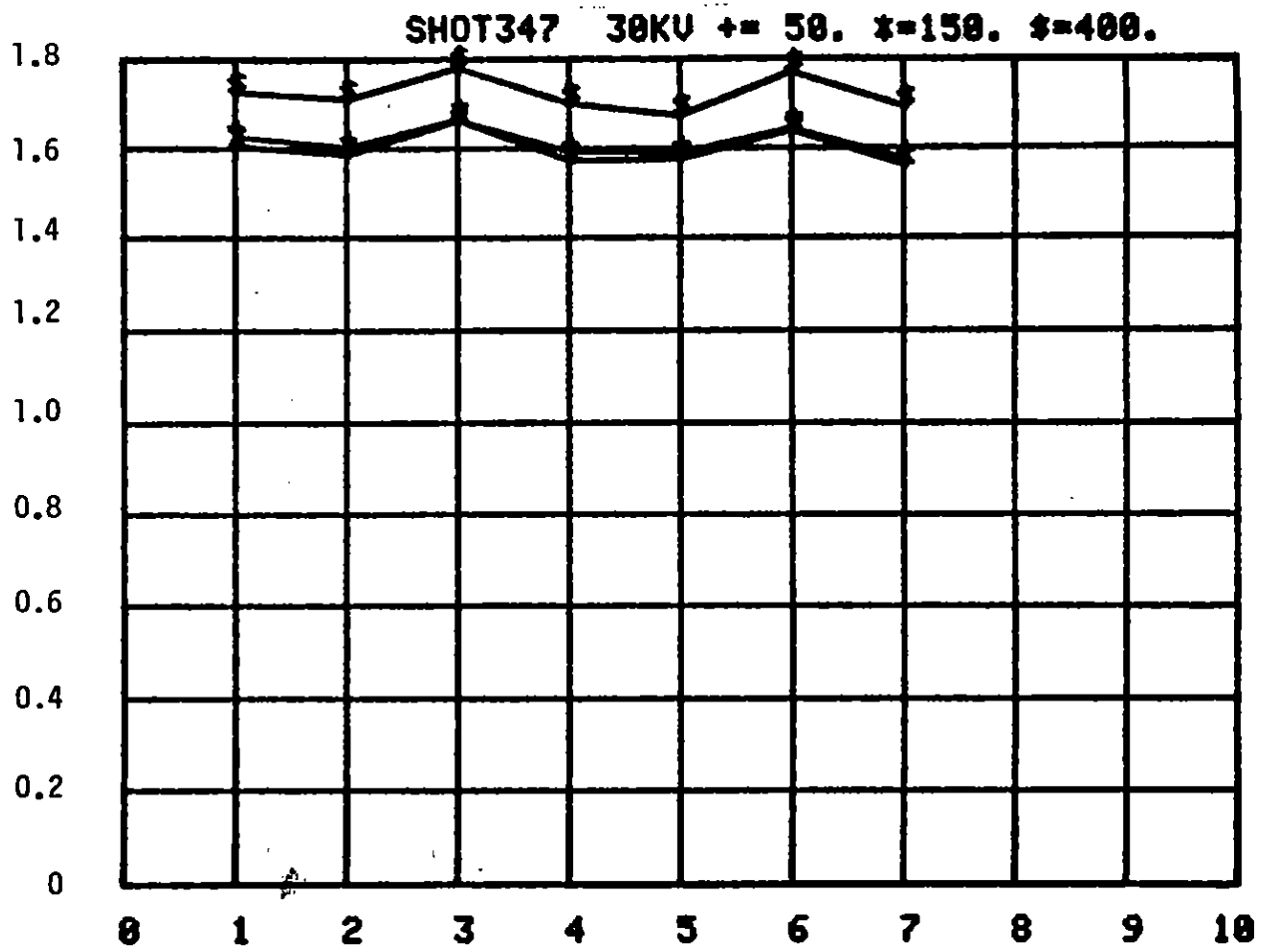

Figure 77. Azimuthal resistance profile with conducting rods. (130Ω m MX-B soil 90° x 0.1 mL)

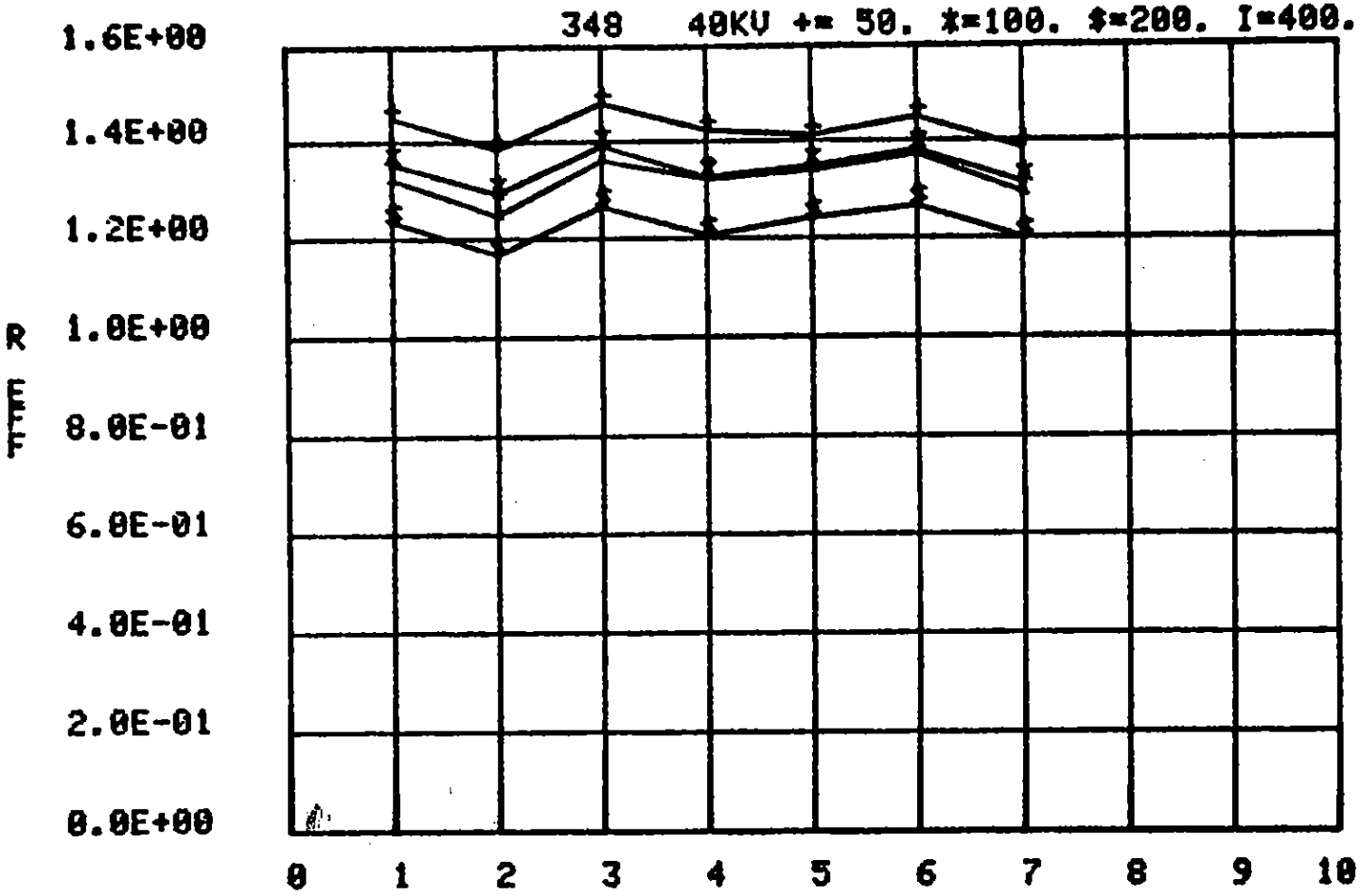

Figure 78. Azimuthal resistance profile with conducting rods. (130 Ωm MX-B soil 90° x 0.1 mL)

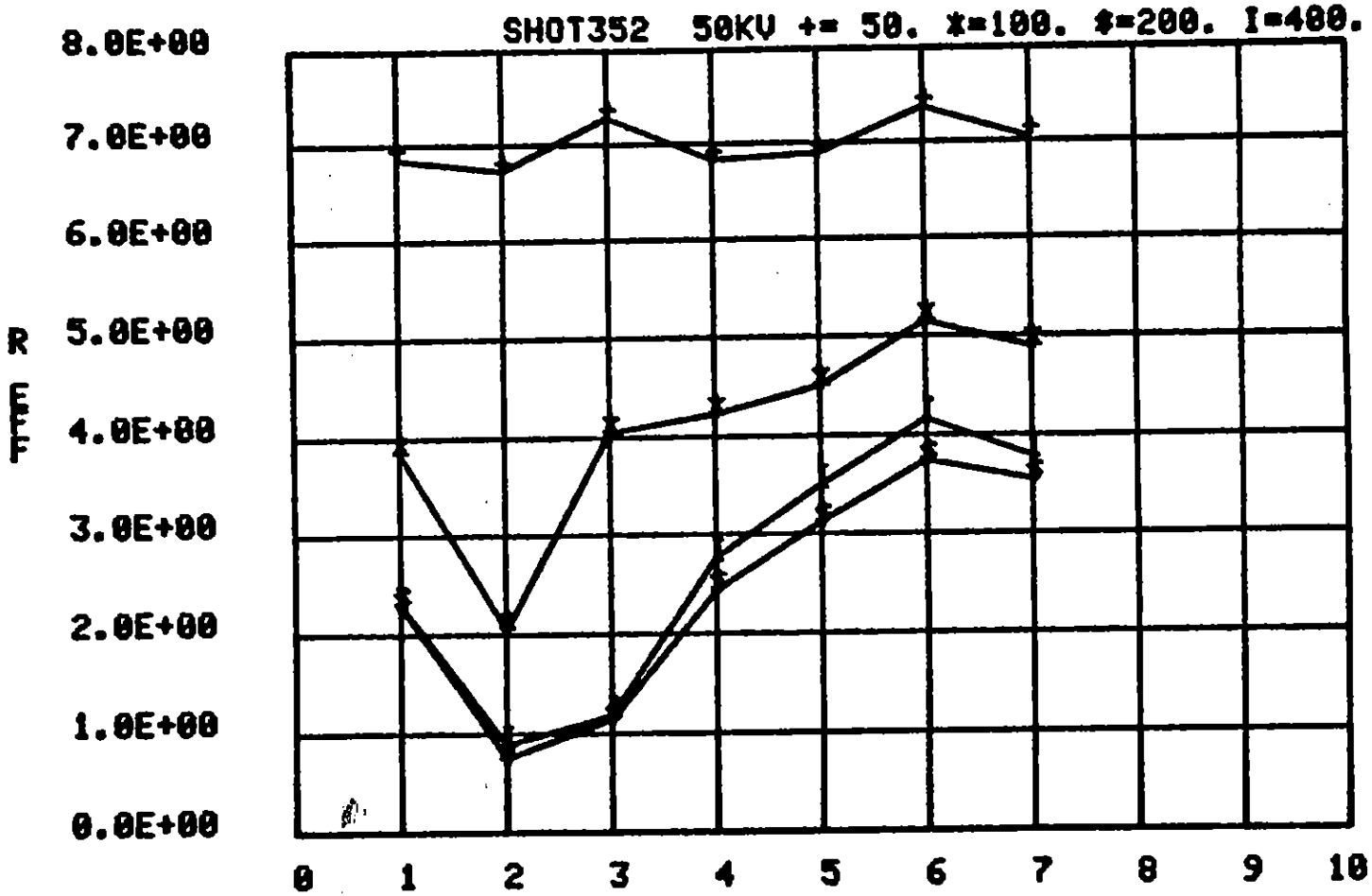

Figure 79. Azimuthal resistance profile with conductong rods. (130 Ωm MX-B soil 90° x 0.1 mL)

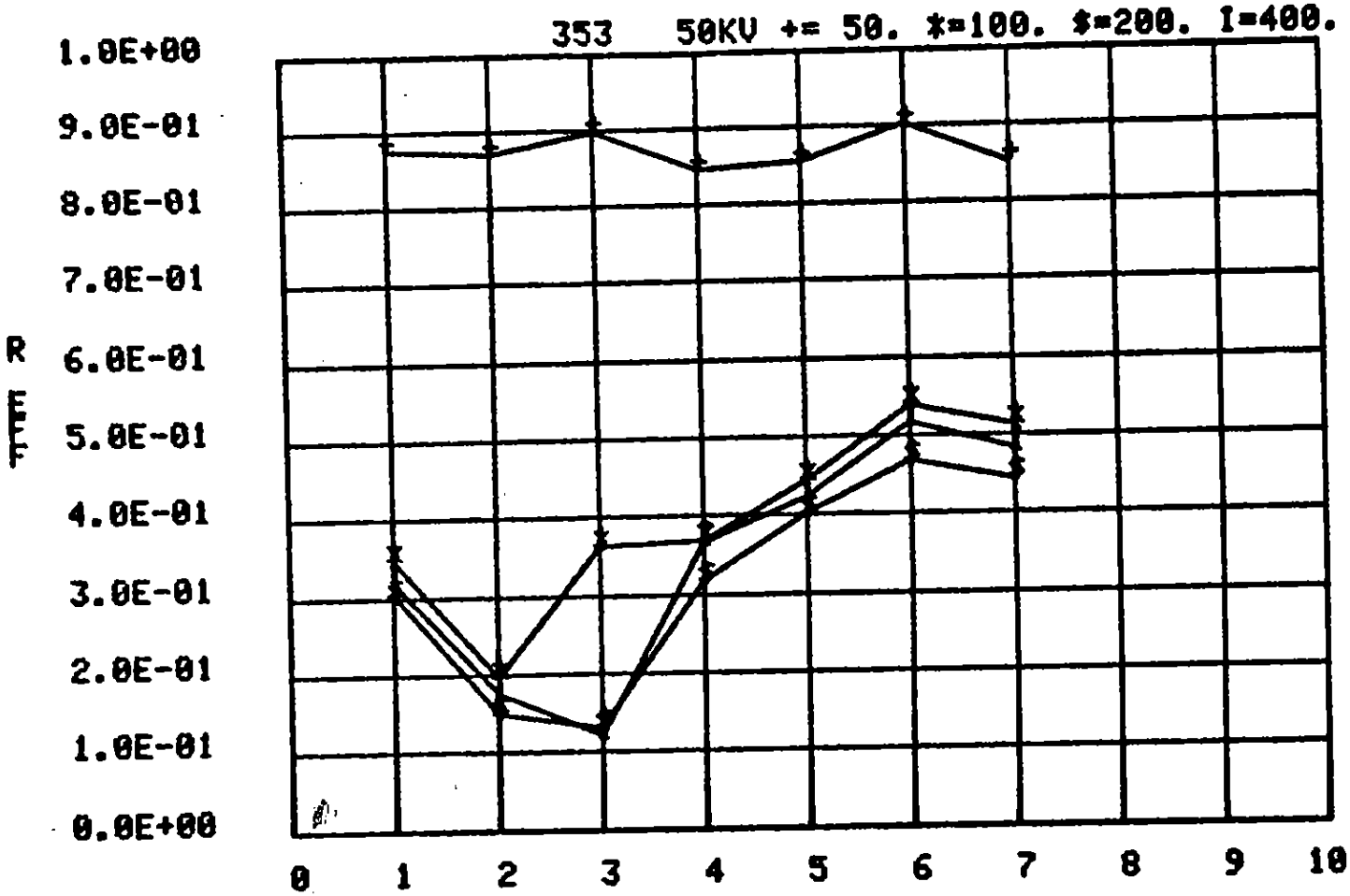

Figure 80. Azimuthal resistance profile with conducting rods. (130 Ωm MX-B soil 90° x 0.1 mL)

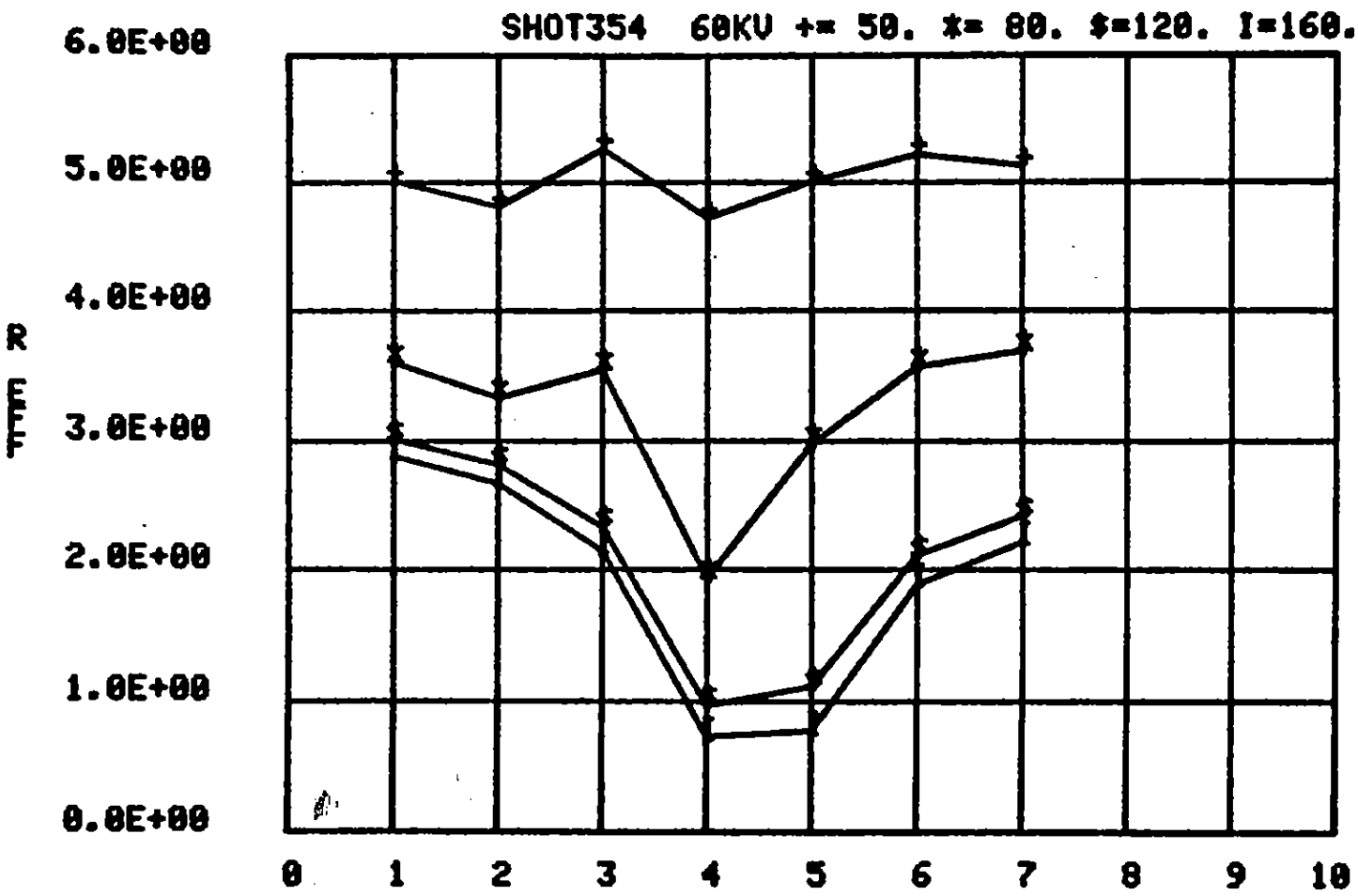

Figure 81. Azimuthal resistance profile with conducting rods. (130 Ωm MX-B soil 90° x 0.1 mL)

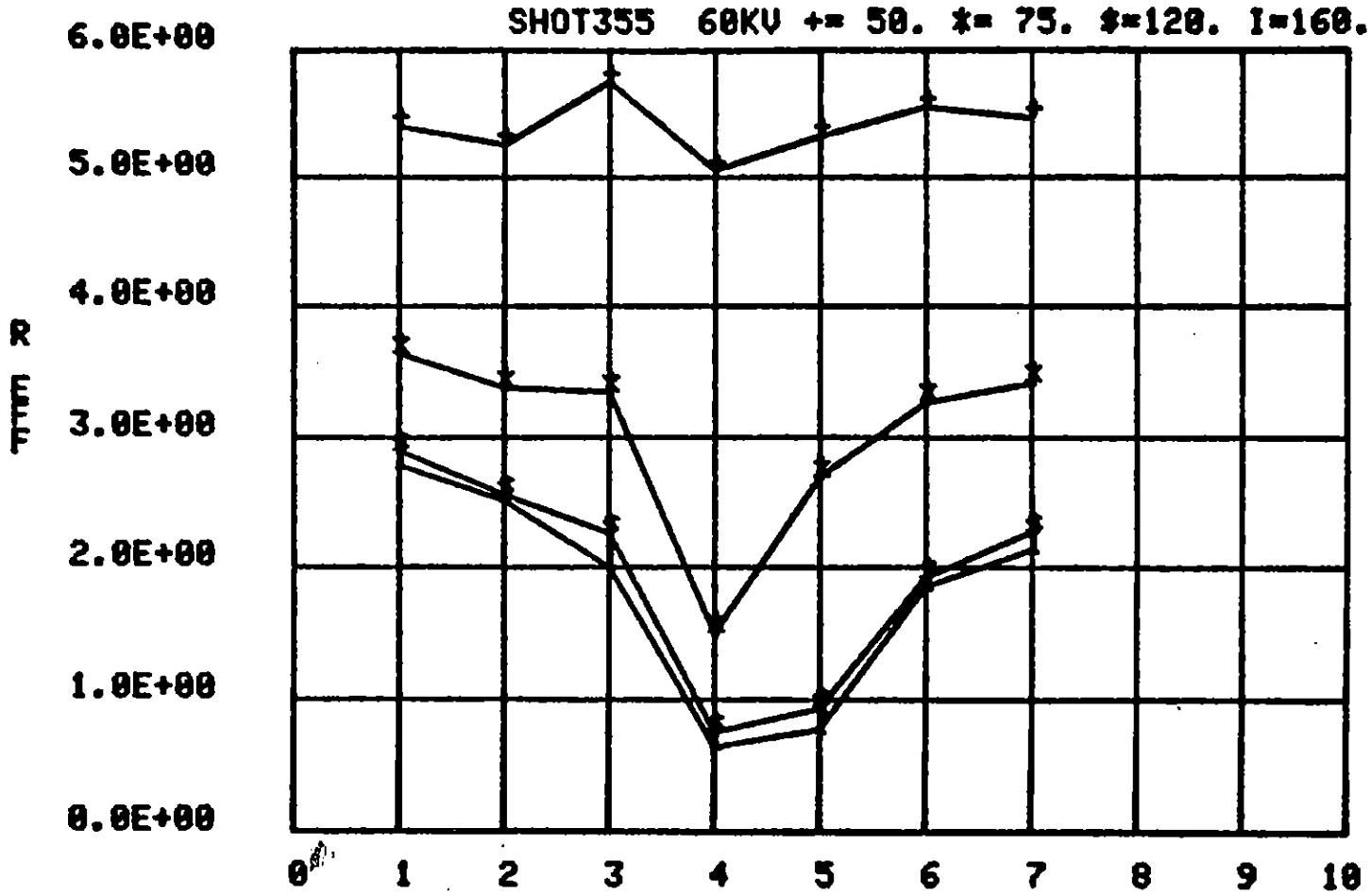

Figure 82. Azimuthal resistance profile with conducting rods. (130 Ωm MX-B soil 90° x 0.1 mL)

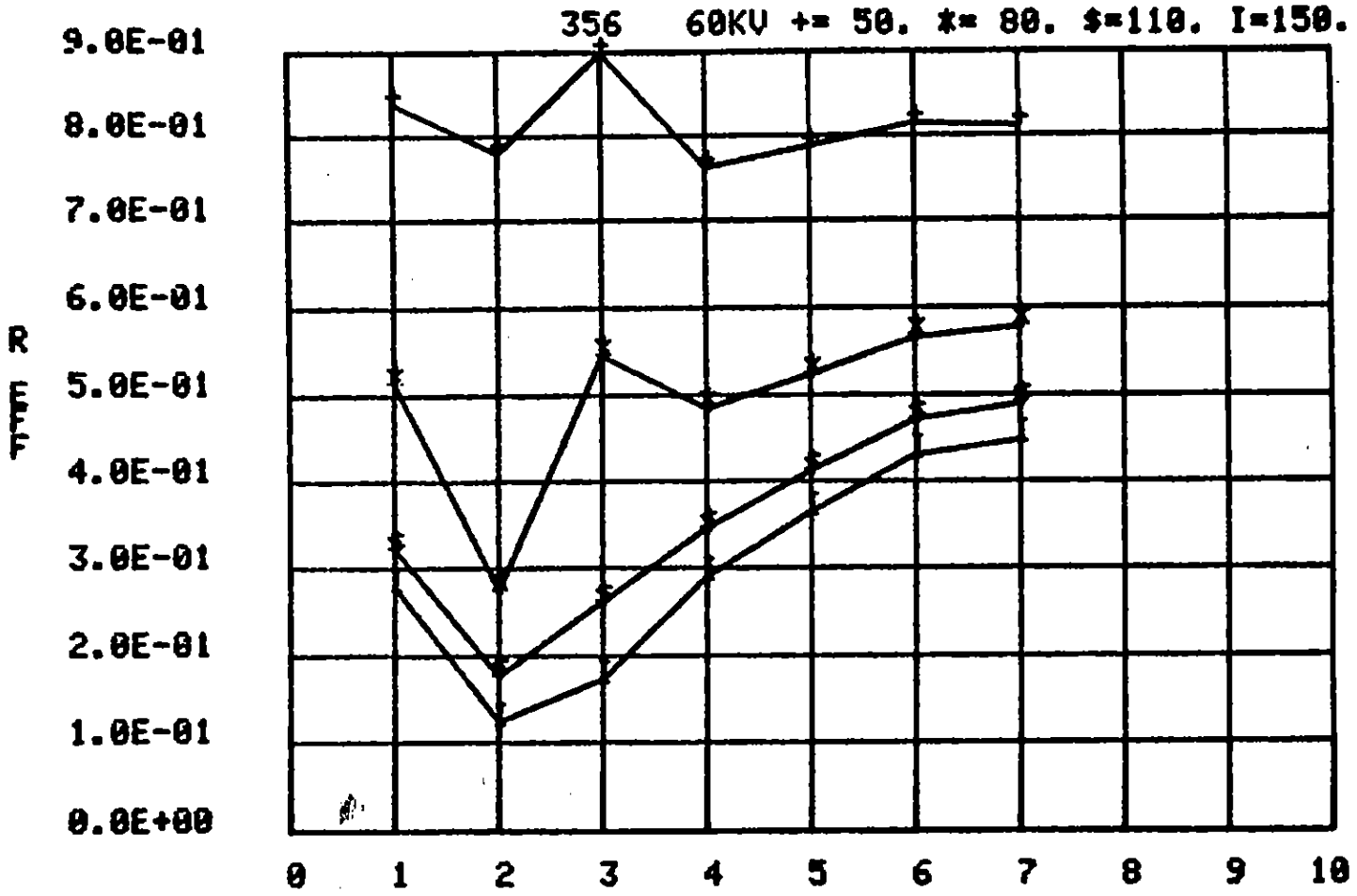

Figure 83. Azimuthal resistance profile with conducting rods. (130 Ωm MX-B soil 90° x 0.1 mL)

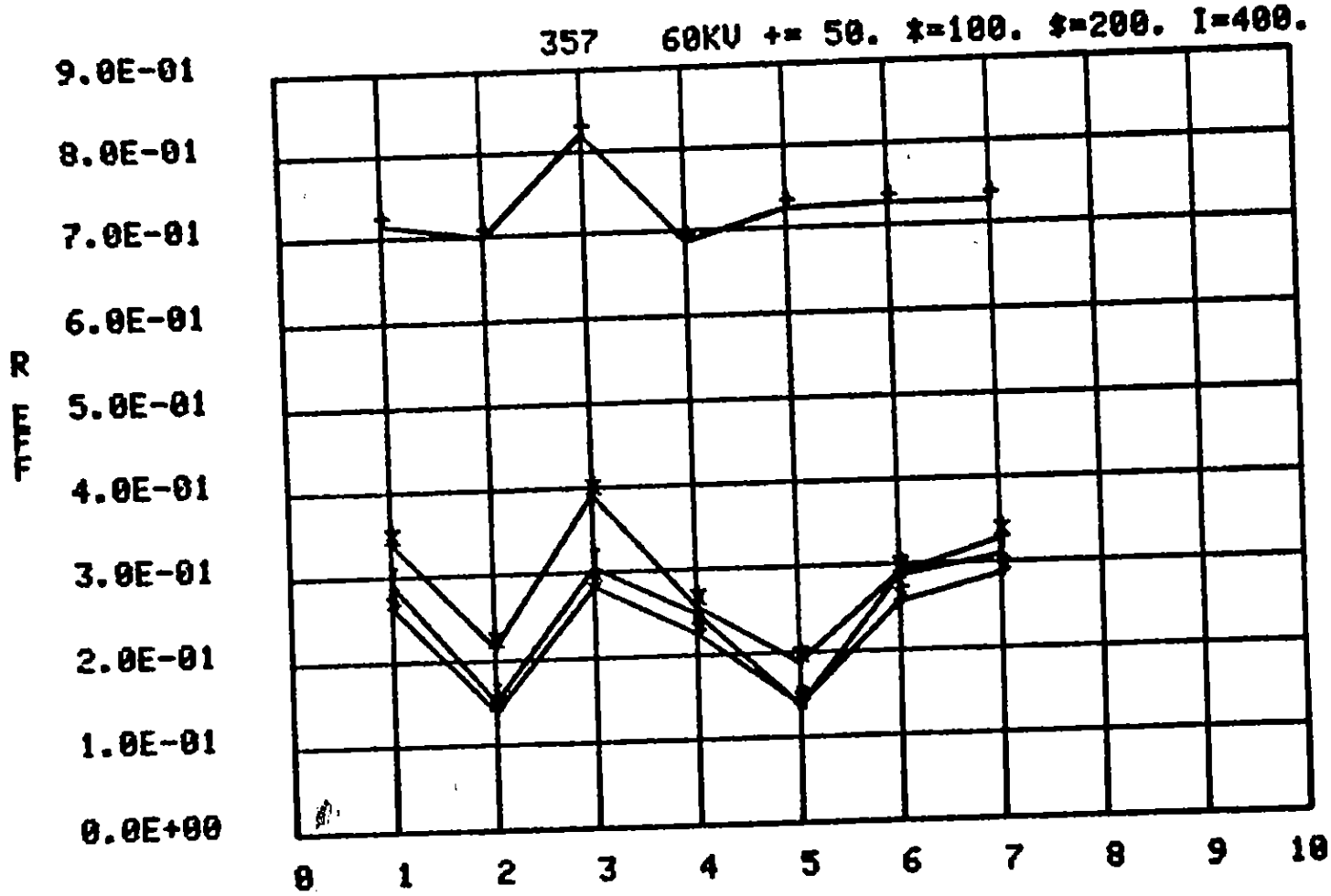

Figure 84. Azimuthal resistance profile with conducting rods. (130 Ωm MX-B soil 90° x 0.1 mL)

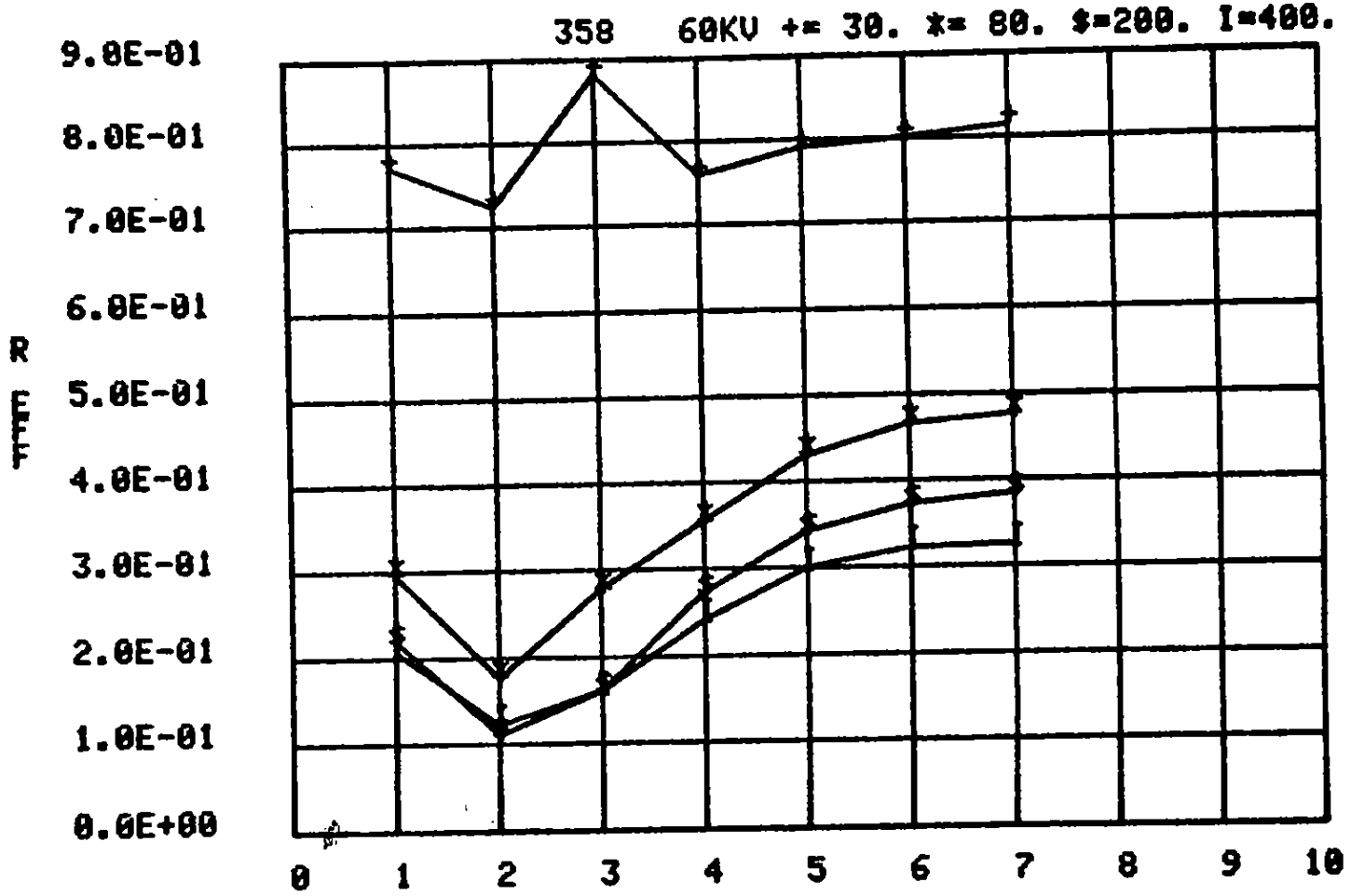

Figure 85. Azimuthal resistance profile with conducting rods. (130 Ωm MX-B soil 90° x 0.1 mL)

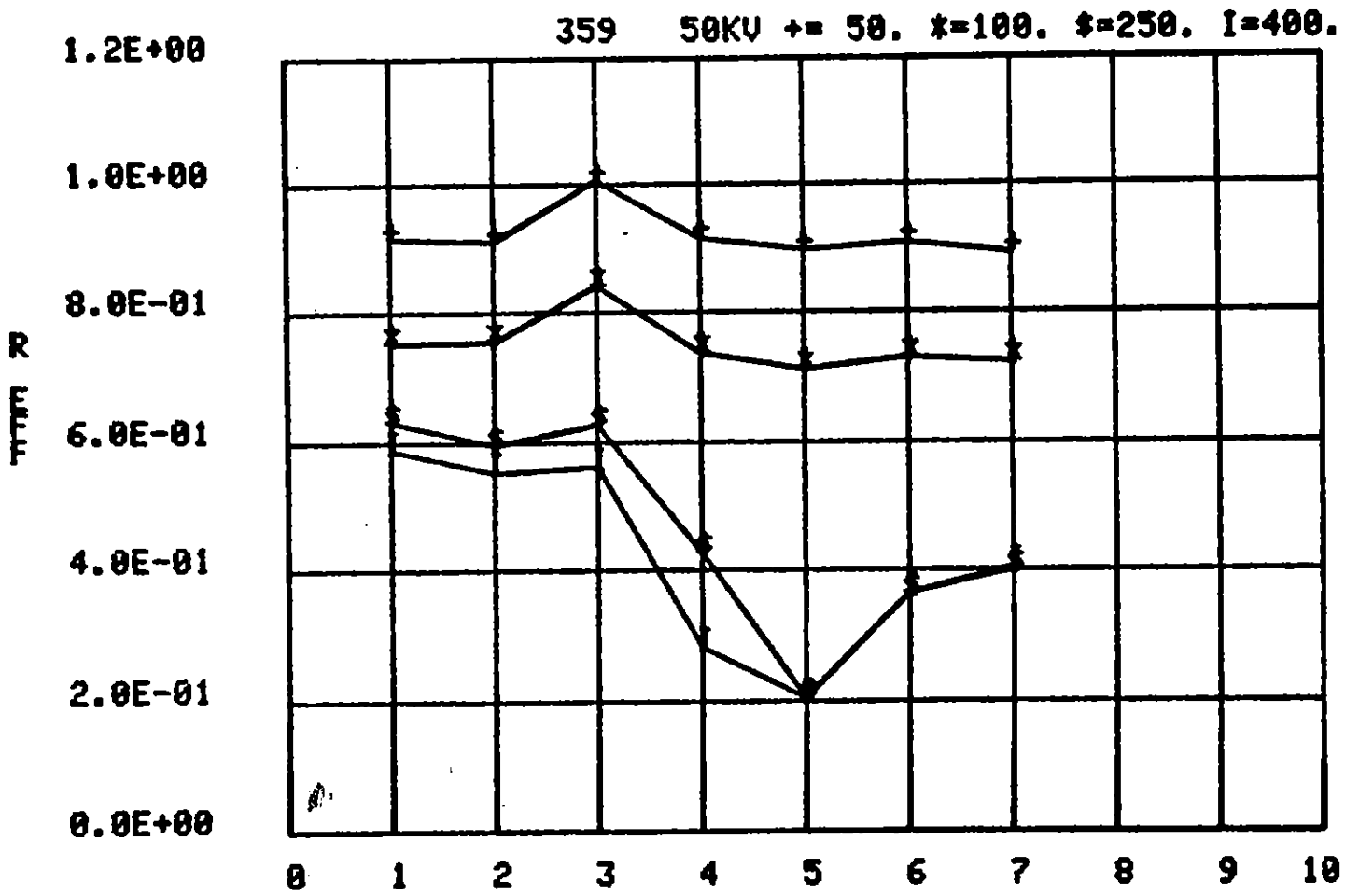

Figure 86. Azimuthal resistance profile with conducting rods. (130 Ωm MX-B soil 90° x 0.1 mL)

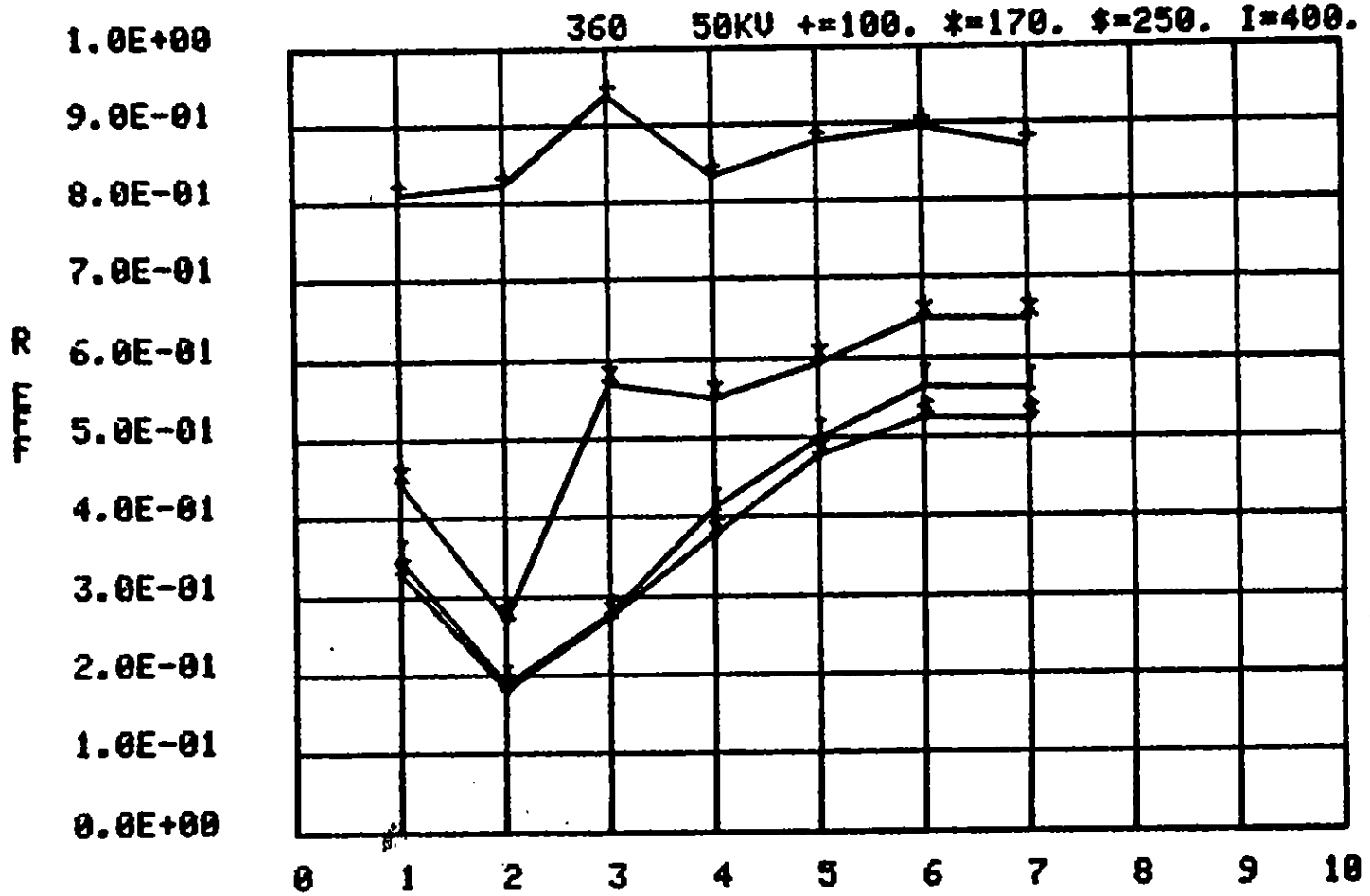

Figure 87. Azimuthal resistance profile with conducting rods. (130 Ωm MX-B soil 90° x 0.1 mL)

(Figs. 88 through 93) there appears to be a preference for branching from probe 4 to probe 5, although on the first shot (Fig. 78) it attaches to probe 2 and in the last two (Figs. 90 and 91) there is a tendency toward probe 2 as well. Returning again to 50 kV (Figs. 92 and 93) attachment to probe 2 is again observed.

Figure 94 illustrates the geometry of the metal rods in the McAir experiment. The indicated array of metal cylinders is continued for 20 rows around a circle at a radius of 0.15 m. In the initial experiments, all cylinders were insulated from each other and the indicated subset of 20 rods was measured with voltage probes. Results of these measurements are illustrated in Figures 95 through 97. The vertical dashed lines in these figures separate the different layers of voltage probes. At 30 kV (Fig. 95) no significant structure is observed, only a gradual decrease of effective resistance with time. The relatively large variation in reading from probe to probe must be a combination of probe calibration uncertainty and possibly oscilloscope trace identification problems. At 35 kV there is a hint of a streamer developing at position 20 between 300 and 400 μs and possibly also at position 5 between 400 and 500 μs. At 40 kV (Fig. 97) a streamer impacts position 18 at 90 μs, followed by a branching to position 13 (the next higher cylinder) at 125 μs, followed by a further branching to position 8 at 240 μs. Independently, a streamer develops at position 5 at 120 μs.

It is not beyond credibility that the observed vertical branching could be the result of electrical stresses at the end of a metal cylinder creating larger electrical fields between it and the adjacent one. During the PI experiments, a variety of lateral cylinder spacings between 0.003 and 0.02 m were tried. At 0.003 m, arc-over between adjacent cylinders became apparent, resulting in a succession of attachments. No differences were observed between the 0.01 m spacing finally selected and 0.02 m. However, no PI experiments were performed with rods above each other. The same 0.01-m spacing was used vertically and horizontally in the McAir experiments. However, the field enhancement at the ends of the metal rods is greater than

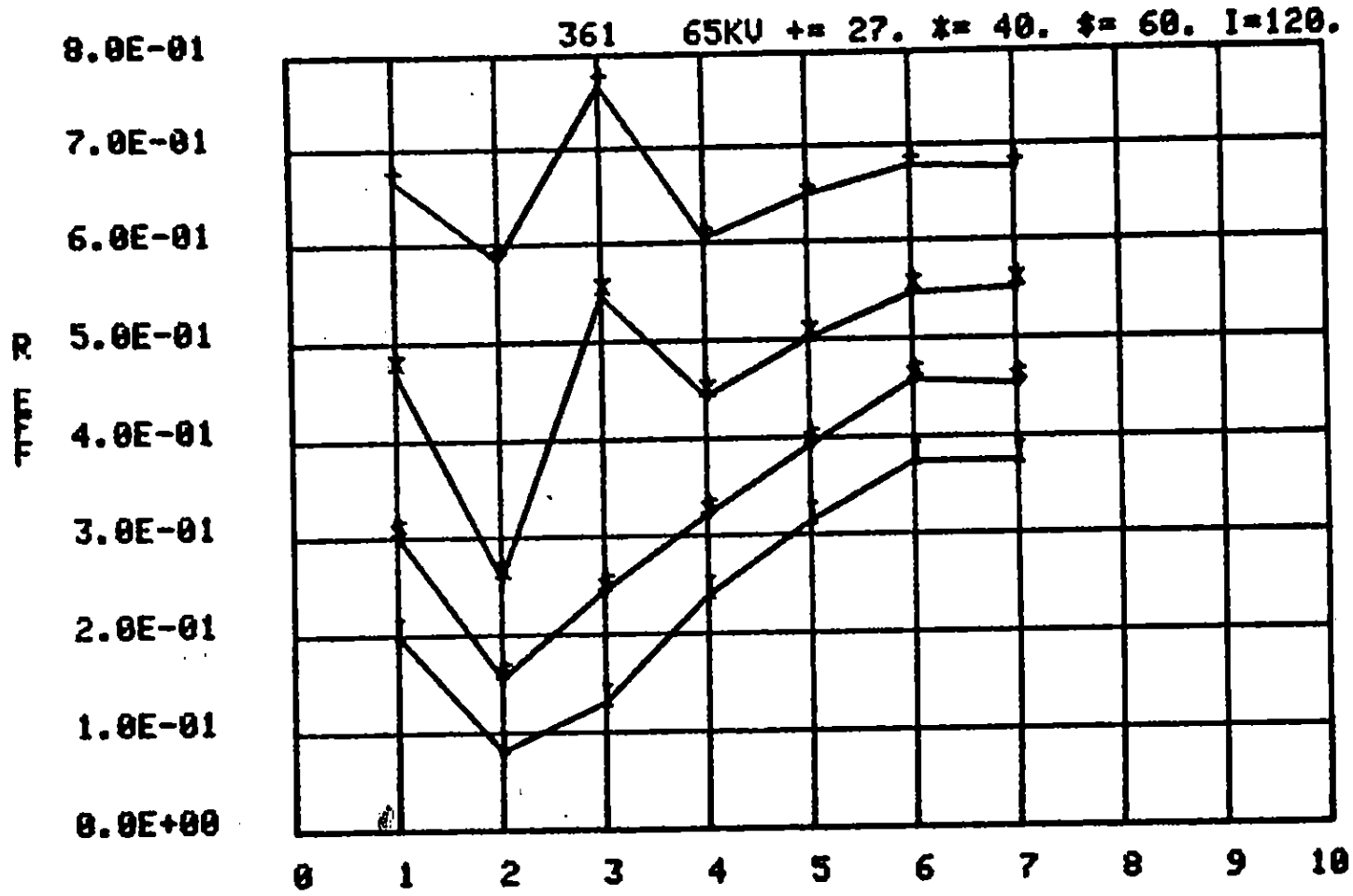

Figure 88. Azimuthal resistance profile with conductong rods. (130 Ωm MX-B soil 90° x 0.1 mL)

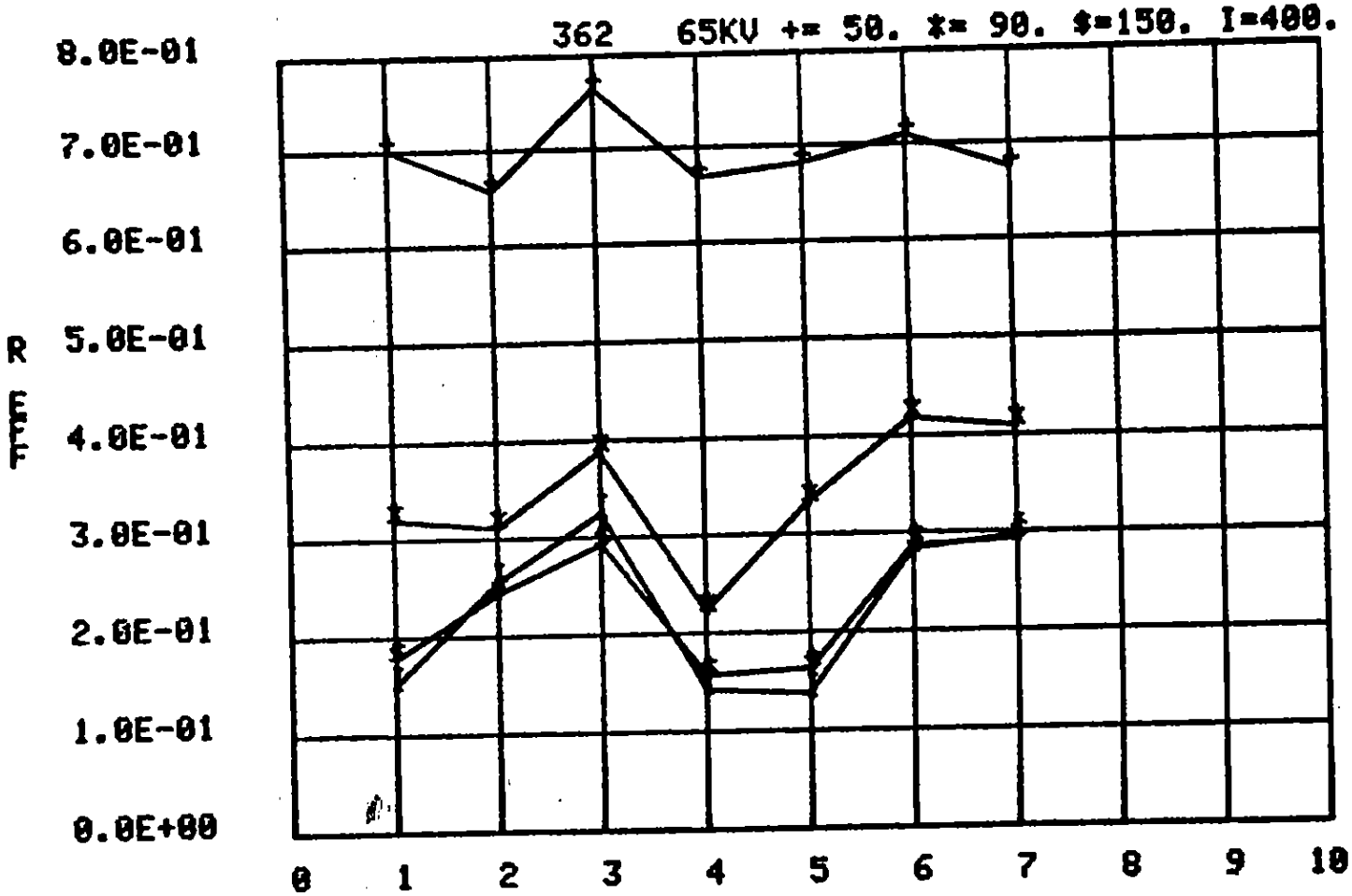

Figure 89. Azimuthal resistance profile with conducting rods. (130 Ωm MX-B soil 90° x 0.1 mL)

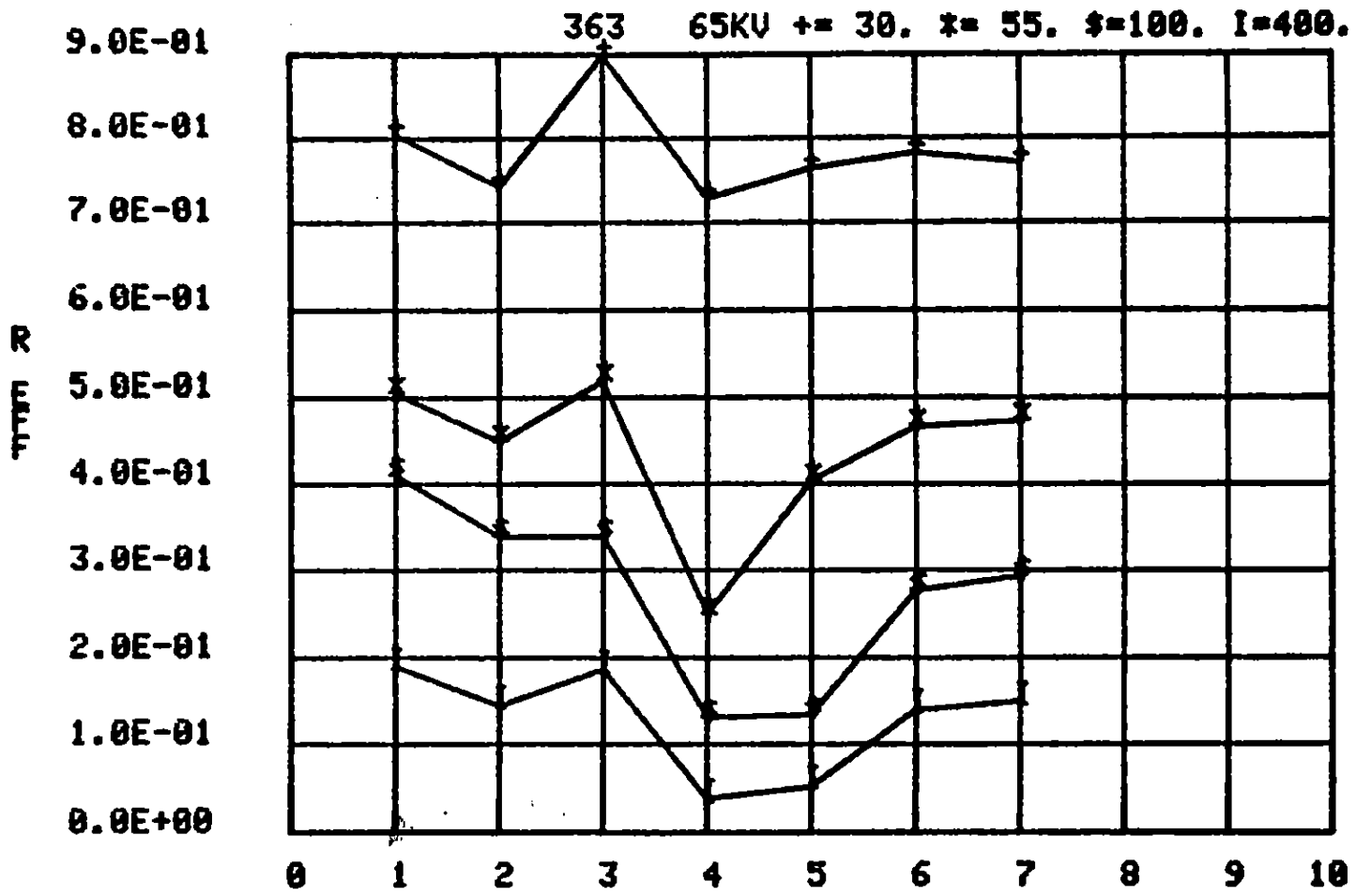

Figure 90. Azimuthal resistance profile with conducting rods. (130 Ωm MX-B soil 90° x 0.1 mL)

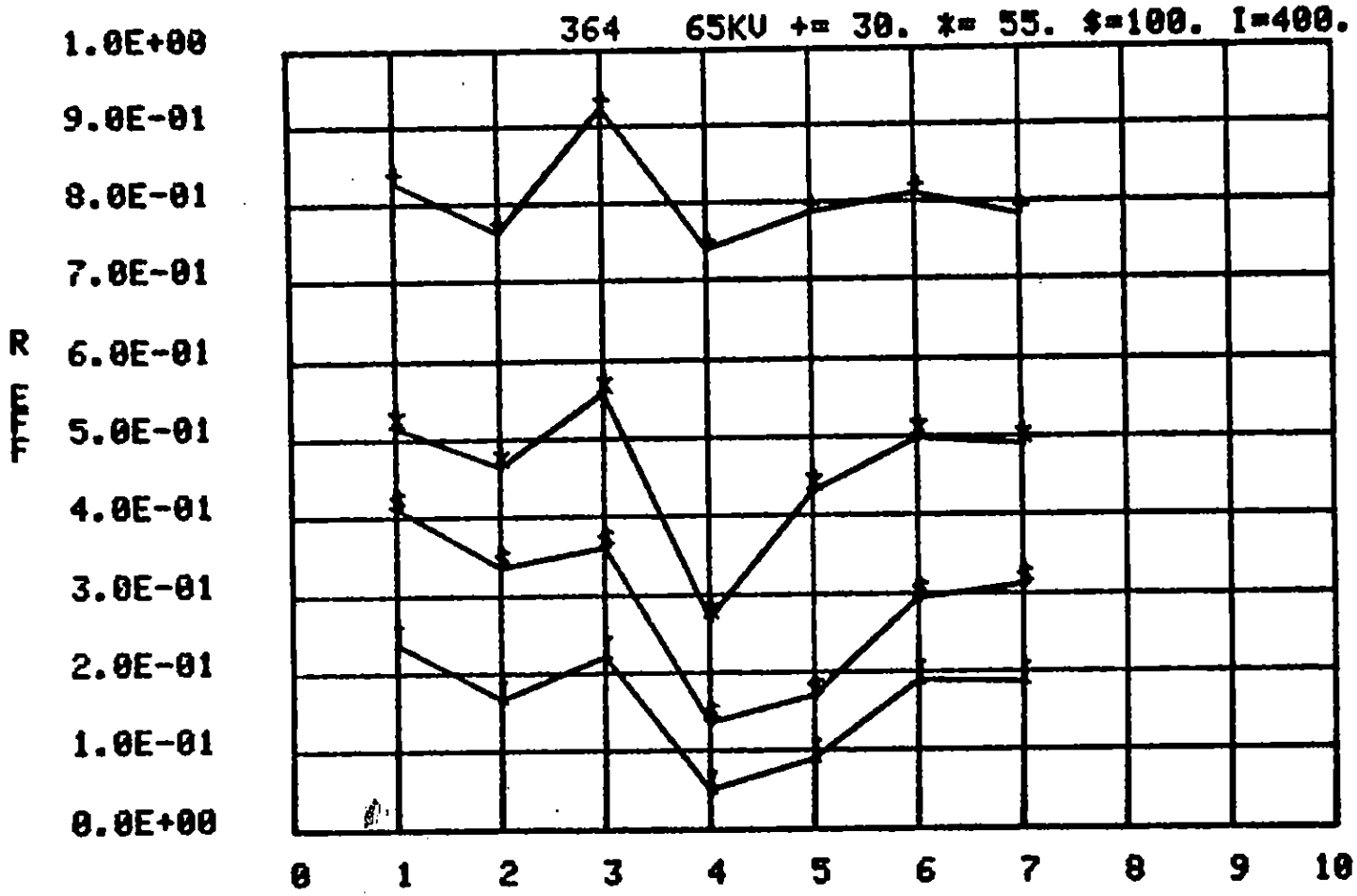

Figure 91. Azimuthal resistance profile with conducting rods. (130 Ωm MX-B soil 90° x 0.1 mL)

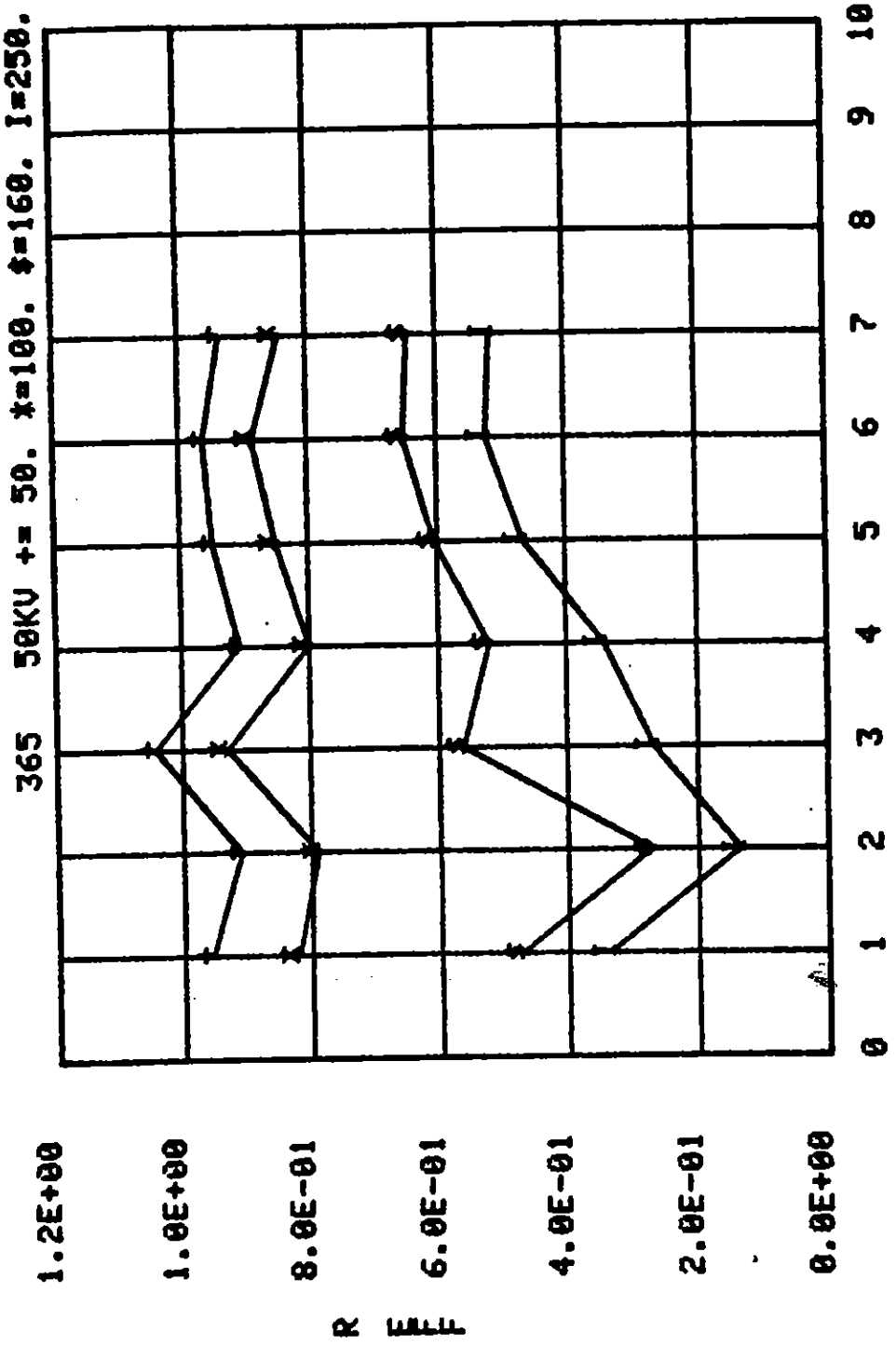

Figure 92. Azimuthal resistance profile with conducting rods. (130 Ωm MX-B soil 90° x 0.1 mL)

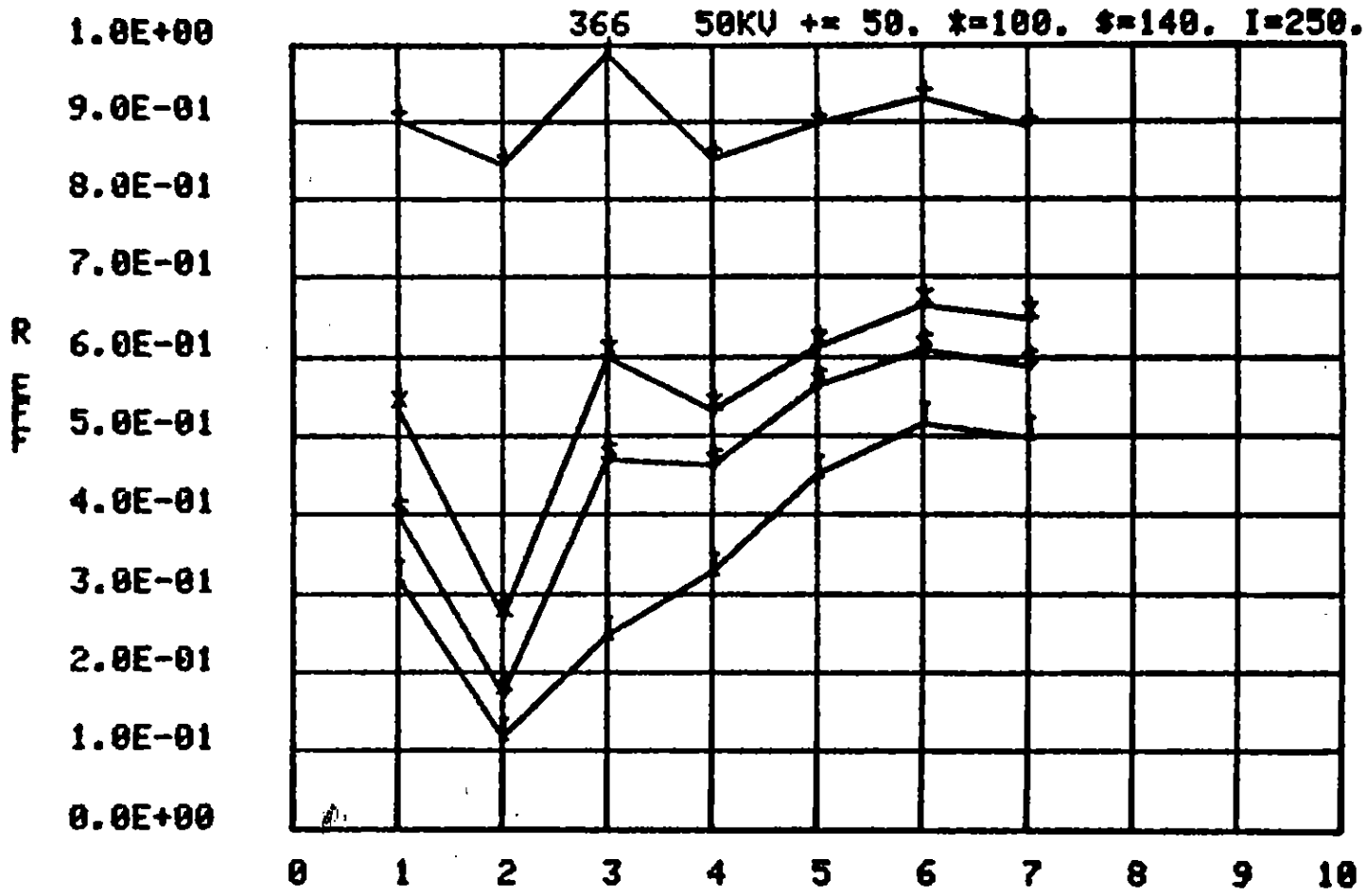

Figure 93. Azimuthal resistance profile with conducting rods. (130 Ωm MX-B soil 90° x 0.1 mL)

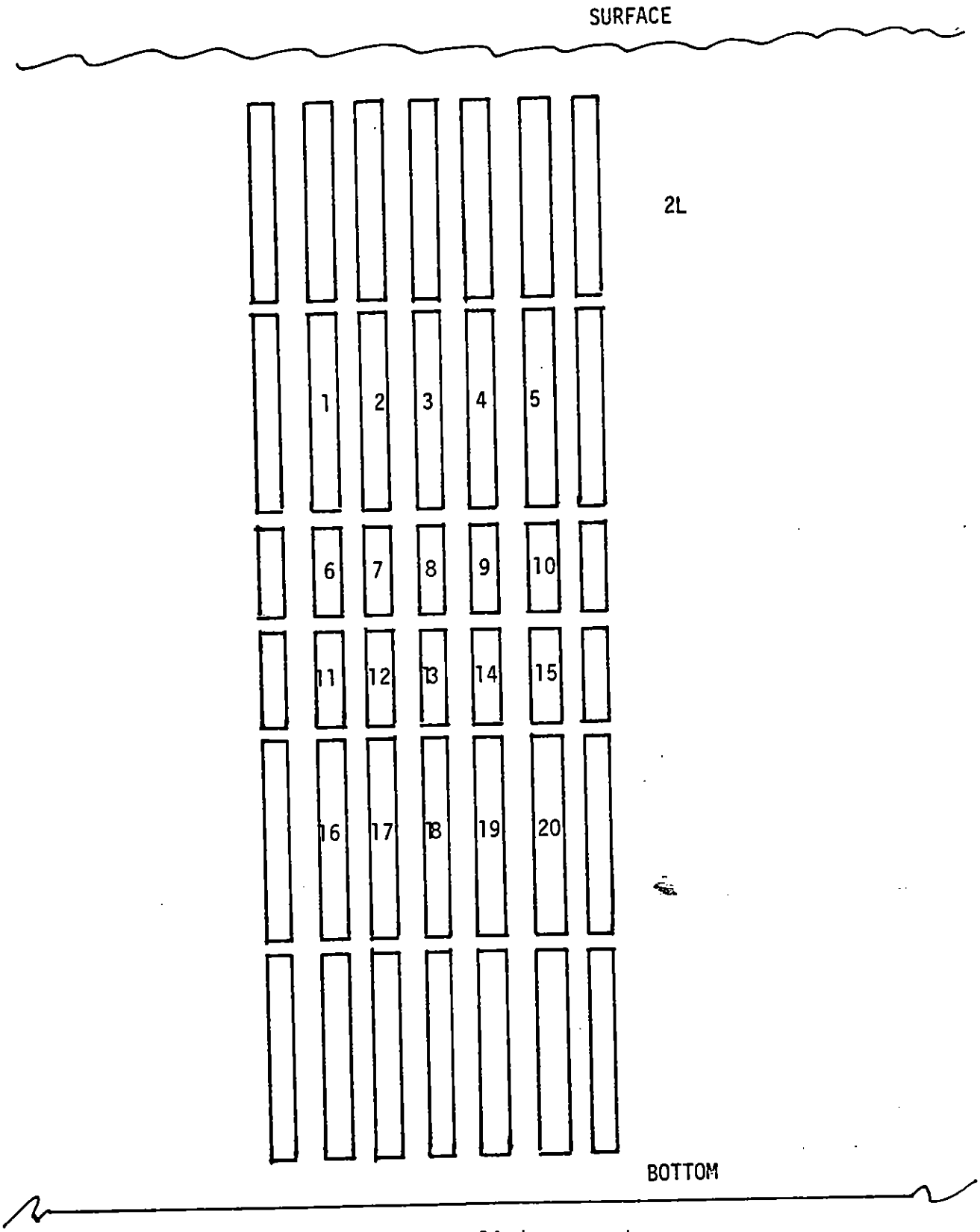

Figure 94. Metal cylinder geometry.

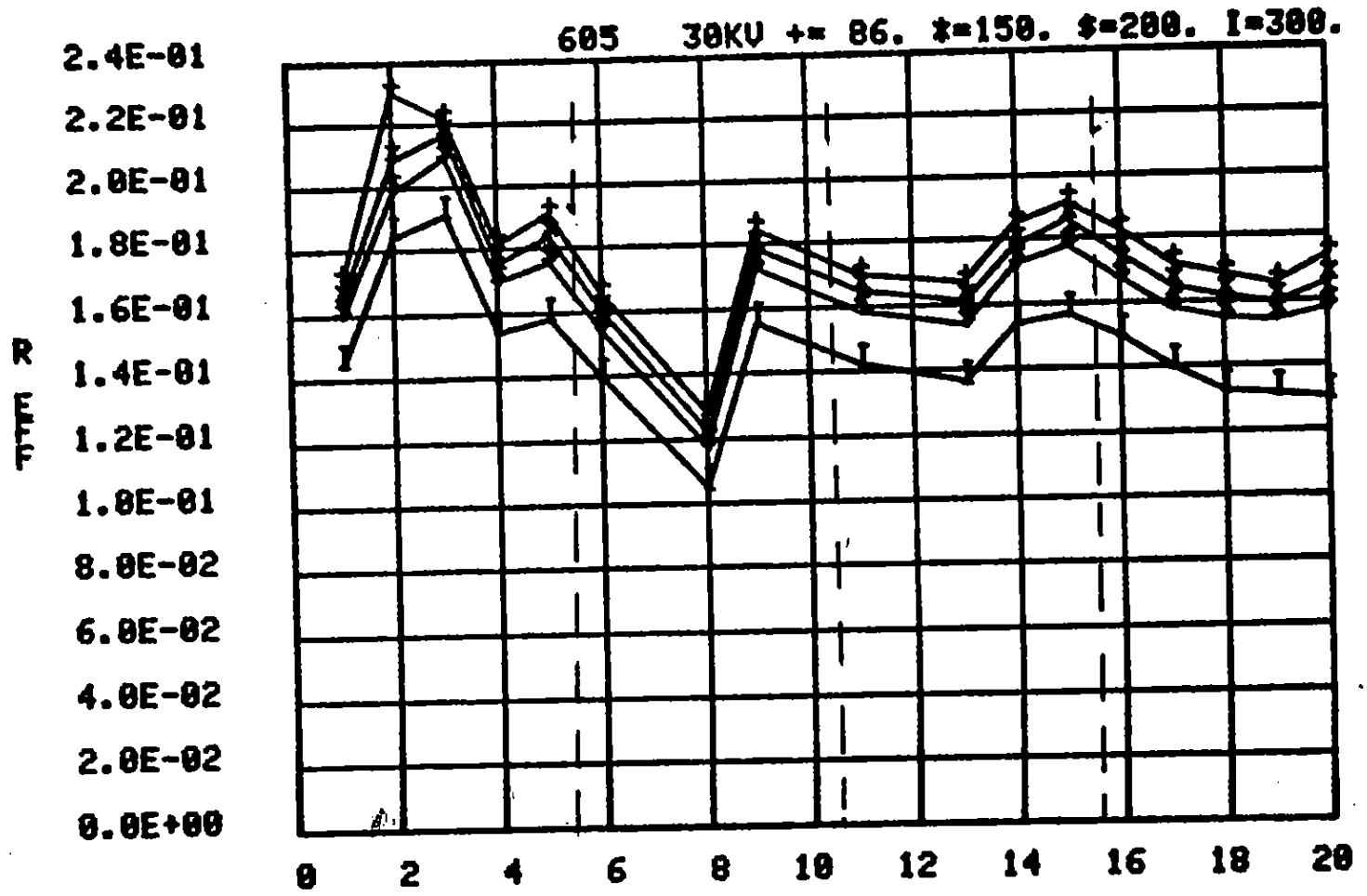

Figure 95. Azimuthal-axial resistance profile with conducting rods. (300 Ωm sand mix 360° x 1 mL)

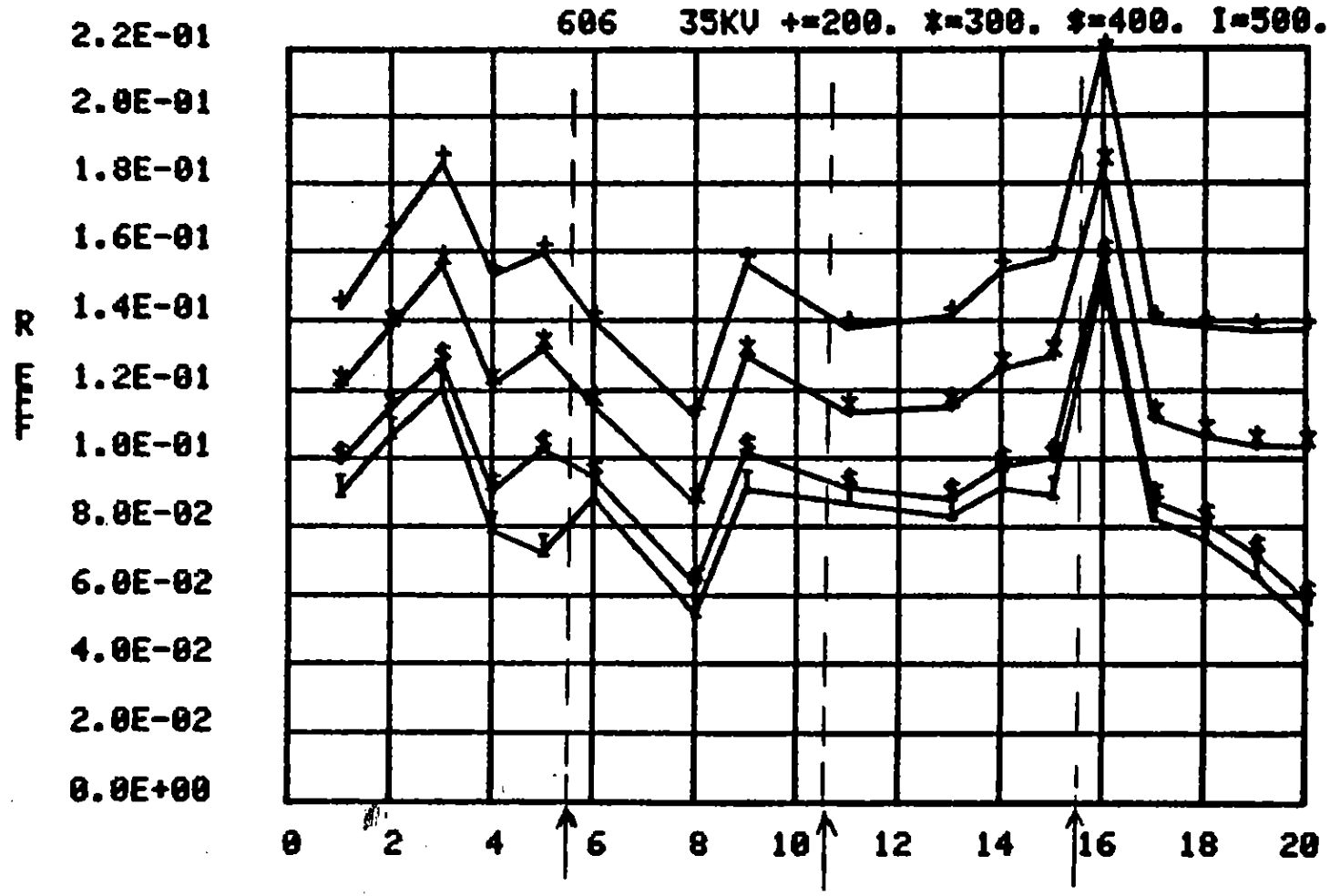

Figure 96. Azimuthal-axial resistance profile with conducting rods. (300 Ωm sand mix 360° x 1 mL)

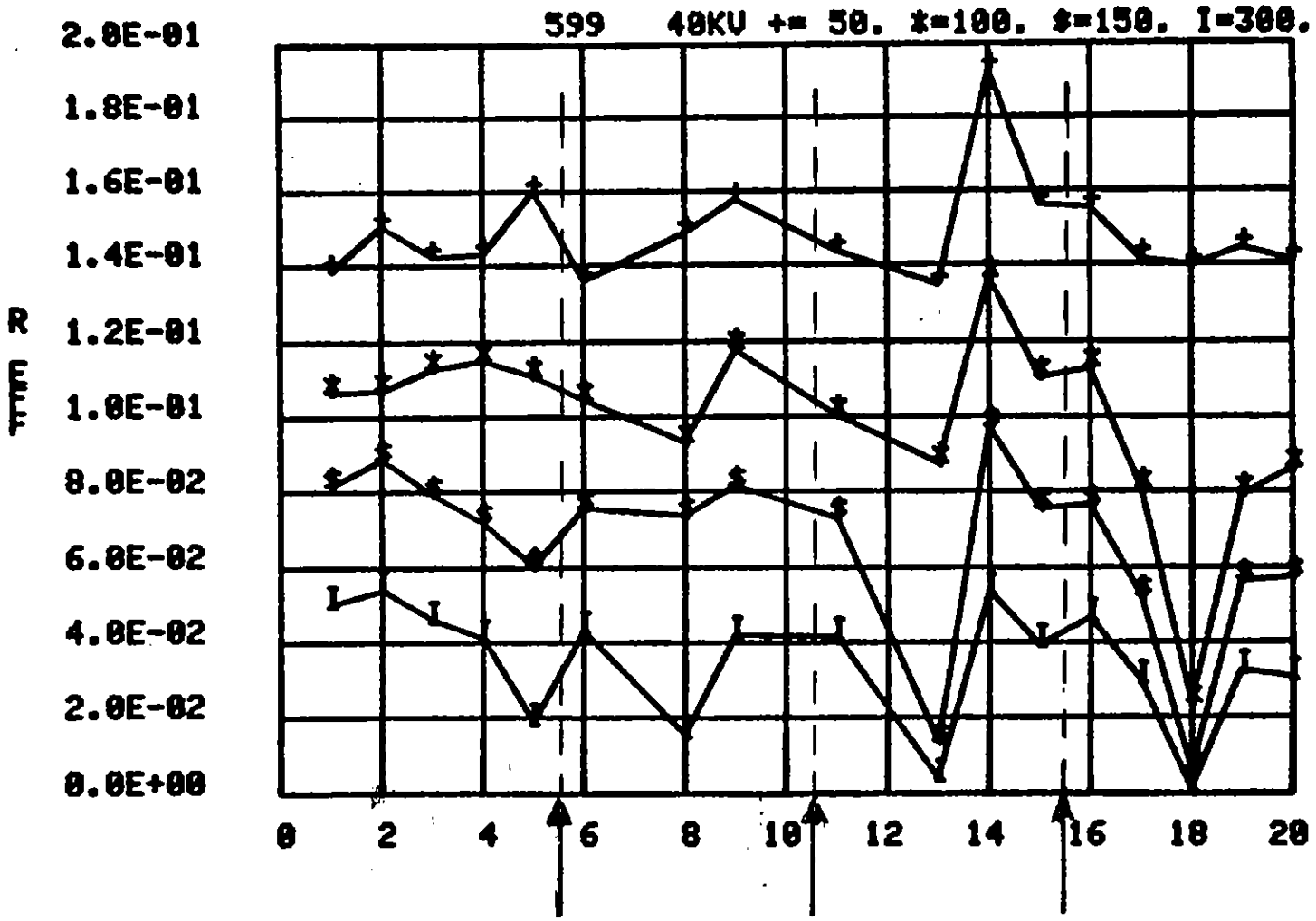

Figure 97. Azimuthal-axial resistance profile with conducting rods. (300 Ωm sand mix 360° x 1 mL)

along their length. Therefore, breakdown between rods adjacent vertically could occur without exhibiting branching of the incident streamer.

Following these measurements, a series of shots were fired with all of the rods in each vertical line electrically connected together. The recording channels were used to measure the voltage on all 20 lines of vertical cylinders. Figures 98 through 101 present the results from four successive shots at 32 kV in this configuration. The number of streamer attachment points varies from 2 to 3 and the location of the attachment point is different for each of the shots. In addition to these 32-kV shots, there exist data at 51 and 60 kV, which resulted in relatively early arc-over. These data have not yet been reduced.

These observations indicate that in the 360° × 1 mL geometry at an applied voltage just above threshold, streamers occur at an average angular separation of 120 to 180°, and an axial separation of 0.5-1 m. These results are in reasonable agreement with the decoration of conducting plastic discussed in Section III, paragraph 4b.

5. COMBINED STRESS EXPERIMENTS

The experiments in which combined axial and radial electric stresses were applied were performed at McAir in 300-Ωm sand mix with a 344 Ω resistor on the axis of the sample. The voltage at the top, bottom, and all but one of the resistor interconnections, was measured with high impedance voltage probes. Three electrical configurations were used with this geometry:

a. Axial. Positive voltage was applied to the top of the resistor, the ground returned at the bottom, and the outer cylinder was not connected. Its potential was measured with a voltage probe.

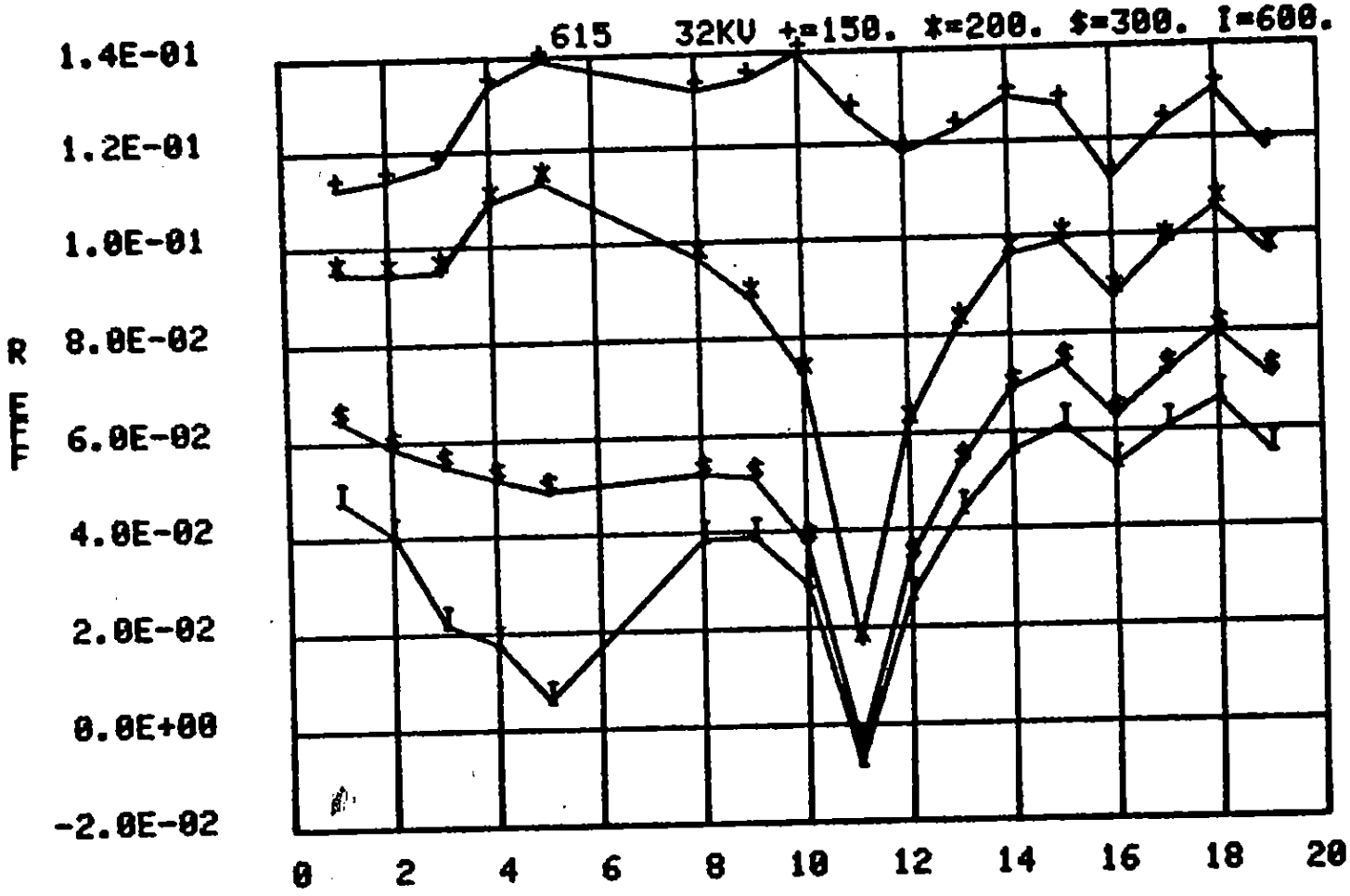

Figure 98. Azimuthal-axial resistance profile with conducting rods. (300 Ωm sand mix 360° x 1 mL)

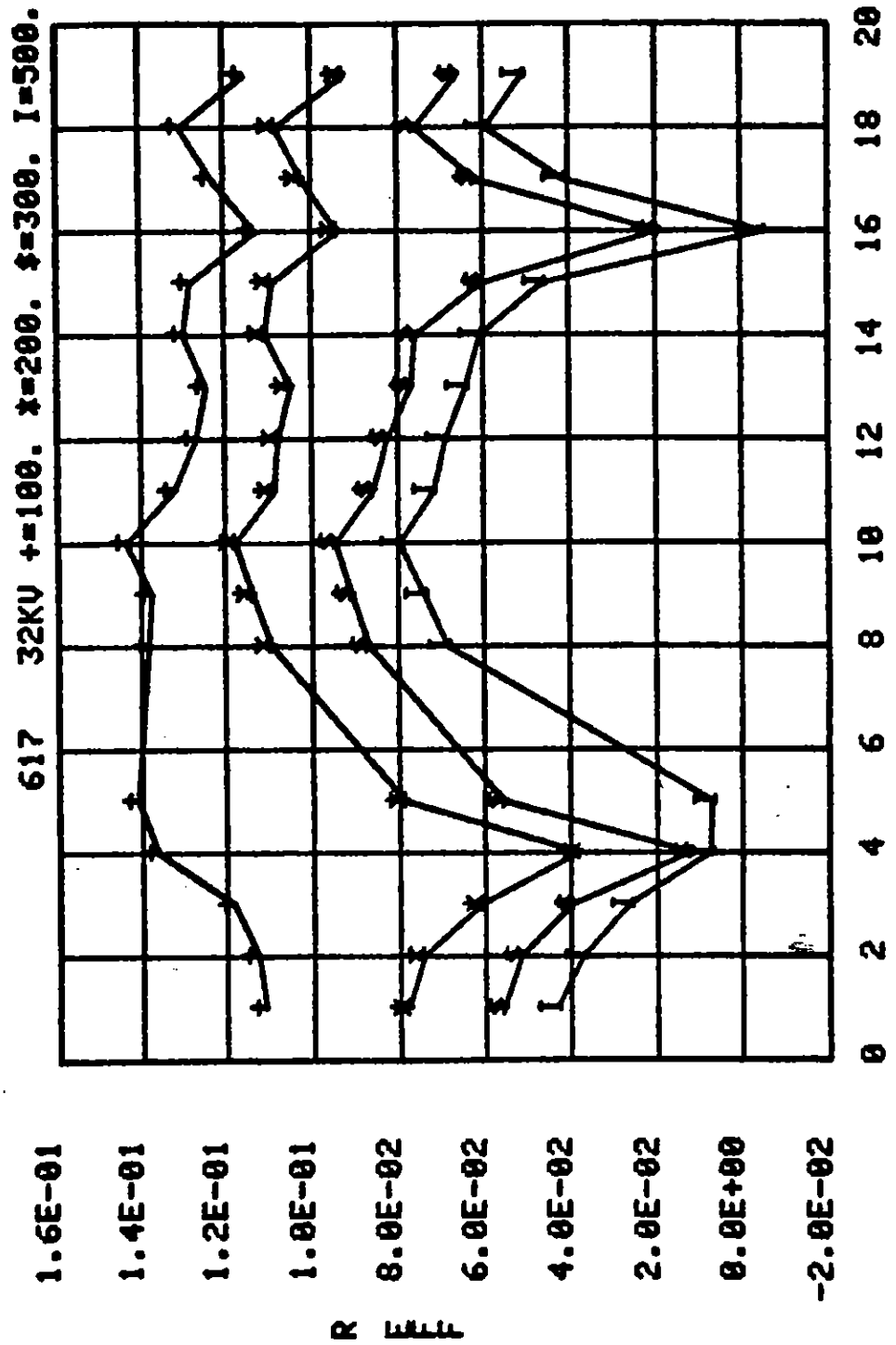

Figure 99. Azimuthal-axial resistance profile with conducting rods. (300 Ωm sand mix 360° x 1 mL)

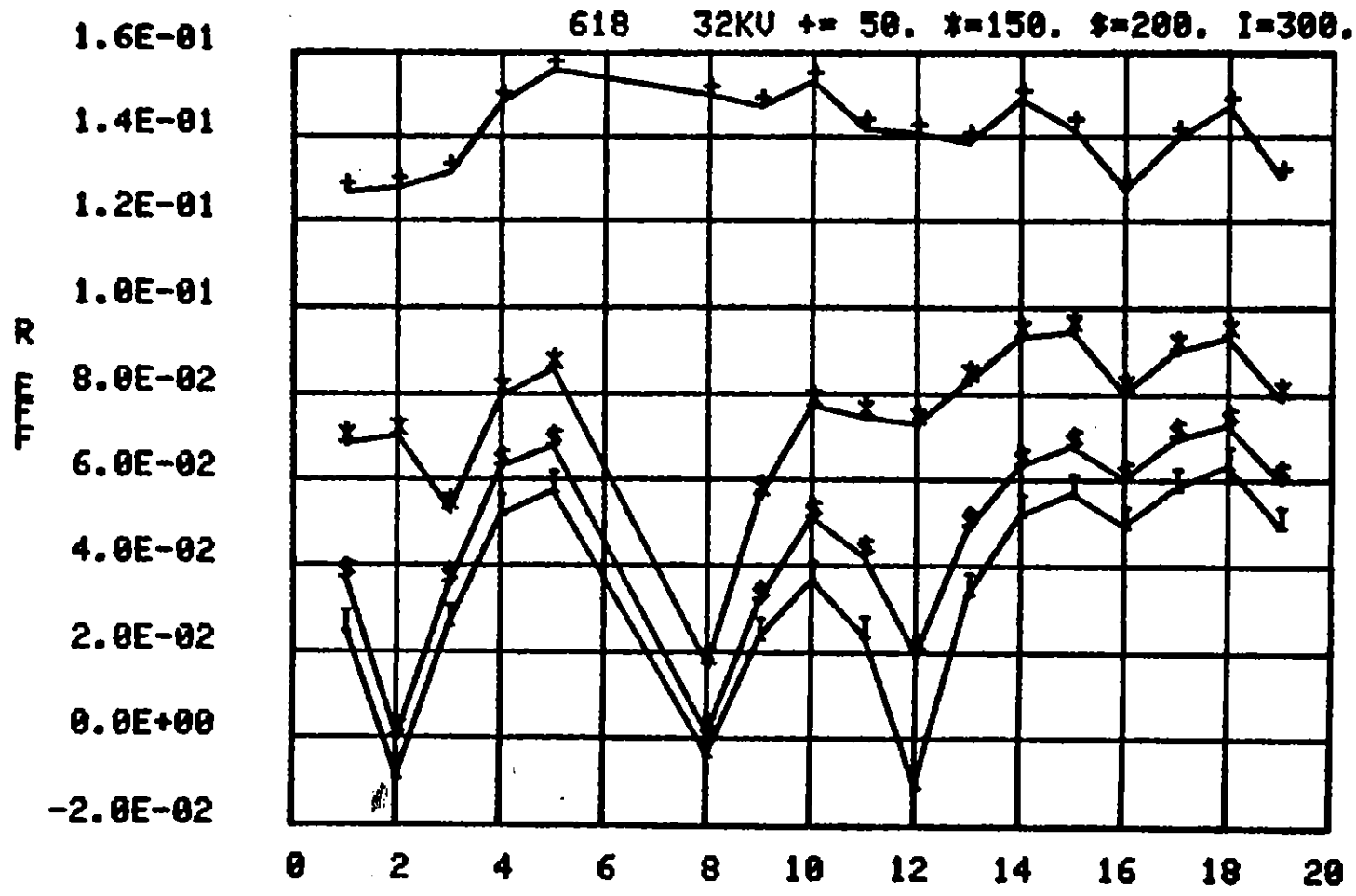

Figure 100. Azimuthal-axial resistance profile with conducting rods. (300 Ωm sand mix 360° x 1 mL)

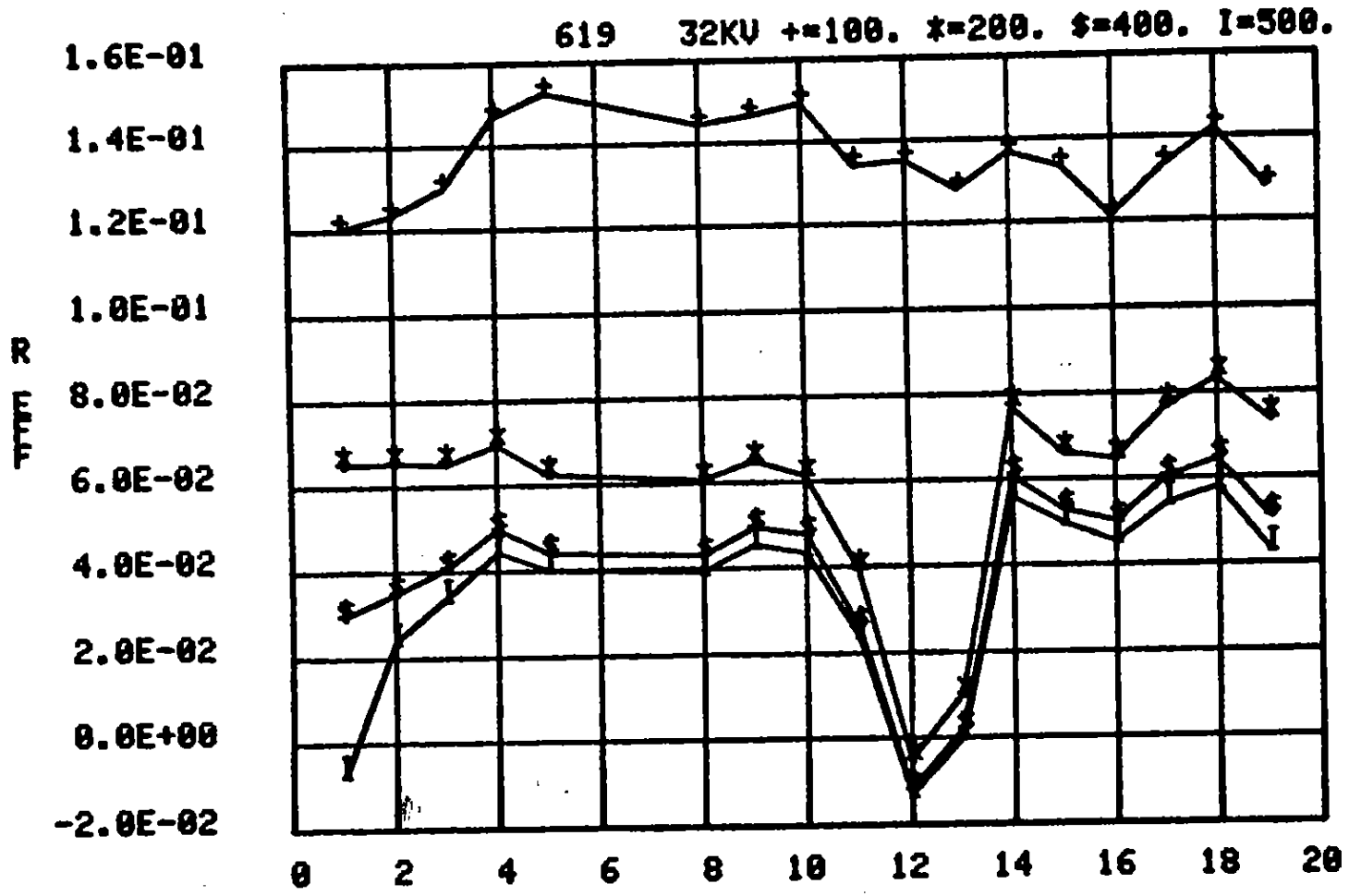

Figure 101. Azimuthal-axial resistance profile with conducting rods. (300 Ωm sand mix 360° x 1 mL)

b. Self-bias. Positive voltage was applied to the top of the resistor string with the ground return to the outer cylinder. The bottom of the resistor string was not connected and its voltage was measured with a voltage probe.

c. Combined stress. Positive voltage from one capacitor bank was applied to the top of the resistor string; negative voltage from the second capacitor bank was applied to the outer cylinder; the ground returns for both capacitor banks were connected to the bottom of the resistor string.

Considerable difficulties were encountered with the pulsers during this experiment series. Various inadvertent interconnections resulted in unwanted external arcs and premature discharges of the capacitor banks. It was also desired in the combined configuration (c) to apply the axial voltage (positive bank) some tens of microseconds after the radial negative voltage. But, the only delays that were actually achieved were ones in which the radial pulser was delayed from the axial generator. It appeared that crosstalk between the power supplies produced uncommanded triggering.

Nevertheless, some important data were acquired from a series of 35 shots and attempted shots in these three configurations. The majority of these data have not been processed due to lack of resources. It is clear that digitizing of the voltage records, particularly on the electrodes and resistors, will produce important indications of possible nonlinear axial conduction.

Figure 102 summarizes some results deduced from visual inspection of the voltage records. With 20-kV axial stress, the resistor voltages decreased approximately linearly with distance along the resistor chain. Since the resistance of the resistors is much less than the axial resistance through the earth, this behavior is expected. With 20 kV applied under self-bias, a similar behavior is observed. The magnitude of the voltage at

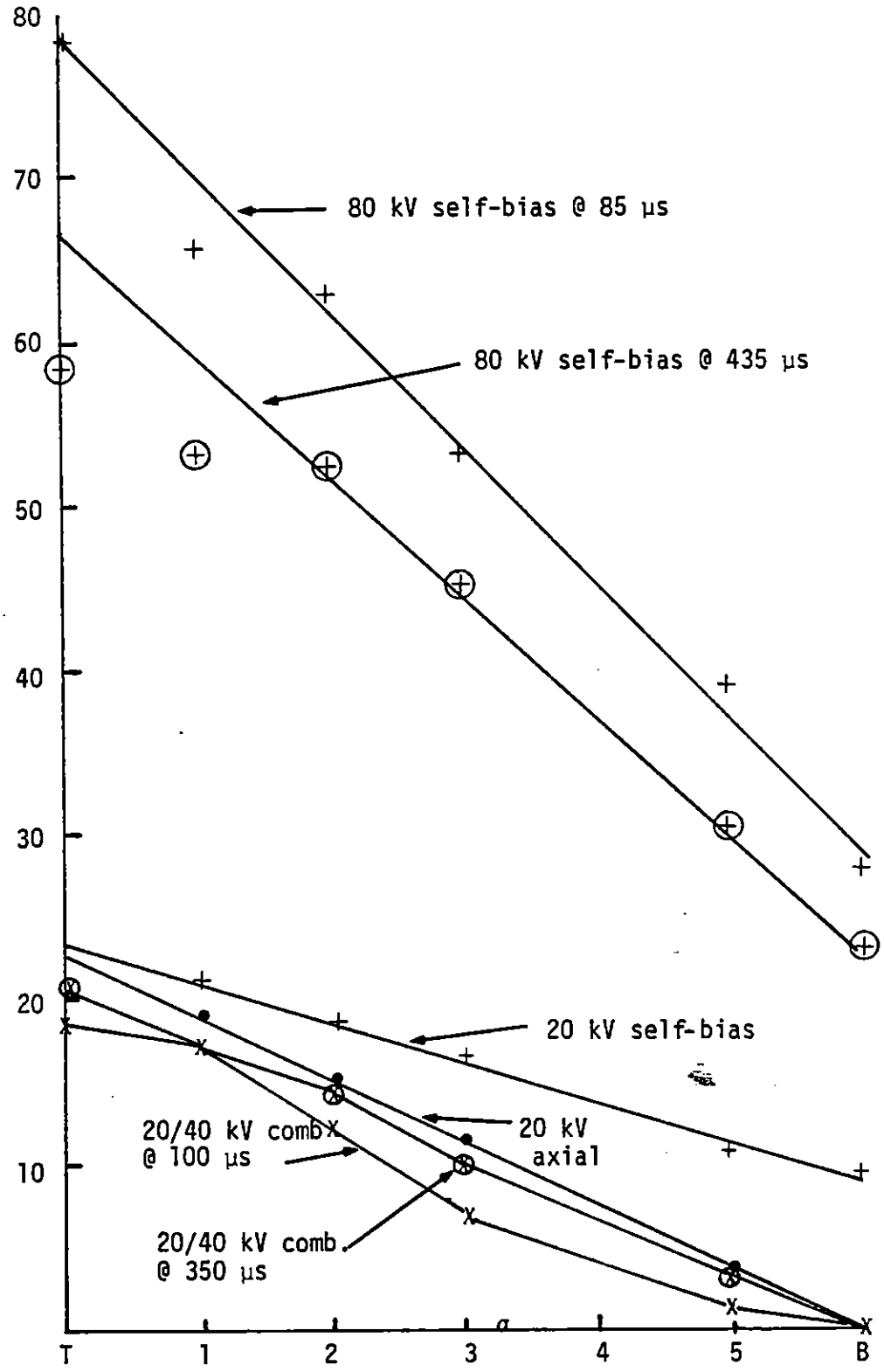

Figure 102. Resistor voltages.

the bottom of the resistor chain is in reasonable agreement with that expected for the combination of the axial resistance and surrounding earth resistivity.

Under combined excitation with 20-kV axial voltage and 40-kV radial voltage, the axial profile is changed somewhat to produce a concave upward plot. This is in general agreement with expectations, since under combined stress, the current flowing radially off the resistor will be manifested by a larger current at the top of the resistor string than near the bottom. This will produce a higher voltage gradient at the top of the string than near the bottom. Later in the pulse, when the radial current has decreased, because of the discharge of the radial power supply, the voltage profile relaxes back toward that produced by axial stress alone. Unfortunately, arc-over occurred frequently, even with only 40 kV applied radially. Therefore, the time available for measurement under combined stresses in configuration (c) was considerably reduced with the larger radial voltages. Fortunately, arc-over did not occur under self-bias excitation, even at 80 kV.

One of the principal purposes of the experiments with both axial and radial electric field was to detect any enhanced axial conduction in the presence of radial streamers. Detailed analysis of the experimental data and calculations of the expected voltage profile will be required to draw firm conclusions. A crude indication of such nonlinear behavior can be deduced from the voltage profiles presented in Figure 102. Under low-field excitation, the measured current in the external circuit for either axial or self-bias configuration agrees with the voltage drop along the top of the resistor chain. This is illustrated in Table 7. For 20-kV axial or self-bias excitation, the observed electric field along the top of the resistor chain agrees well with the measured current. However, under 80-kV excitation, the apparent resistance along the resistor chain has been reduced by approximately a factor of 2. The axial electric field at which this occurs

is approximately 40 kV/m. The radial voltage is approximately 30 kV at the bottom, 70 kV at the top. This behavior can be understood without invoking enhanced axial conduction if a large fraction of the input current flows from the center conductor outward above the first resistor. If this is the case, it should be manifested in the radial voltage profiles, which have not yet been analyzed. One additional supporting datam is that upon this assembly the top half of the top resistor exhibited pitting at all azimuths. The only other pitting appeared on the copper conductor at the bottom of the resistor chain at an azimuth of 300°. This is the direction in which arc-over near the bottom of the sample chamber occurred preferentially. There was no evidence of arc-over near the top of the sample chamber; therefore, the pitting on the upper resistor is probably the result of a number of stable streamers.

TABLE 7. RESISTOR VOLTAGE PROFILE

Shot No.	Configuration	Applied Voltage(kV)	t(μs)	I(A)	ΔV RI
551	Axial	20	50	65	1.03
554	Self-bias	20	50	45	0.95
584	Self-bias	80	85	255	0.57
			435	255	0.50

During the course of the combined stress experiments, there were a number of examples of oscillatory behavior in the voltage probe waveforms. These will be discussed in the next subsection.

6. OSCILLATORY BEHAVIOR

Figure 103 illustrates oscillatory behavior observed in the bottom voltage probes during excitation with 80 kV in the self-bias configuration.

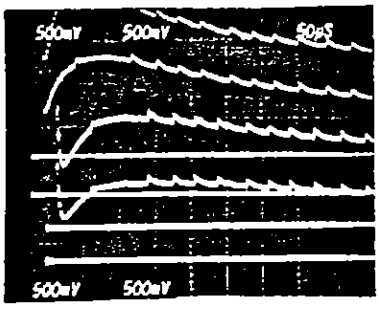

V_{BOT} - 0°

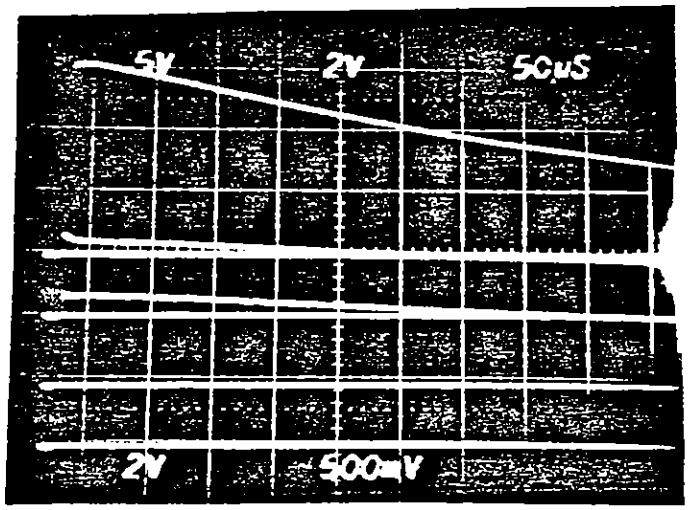

V_{TOP} - 0°

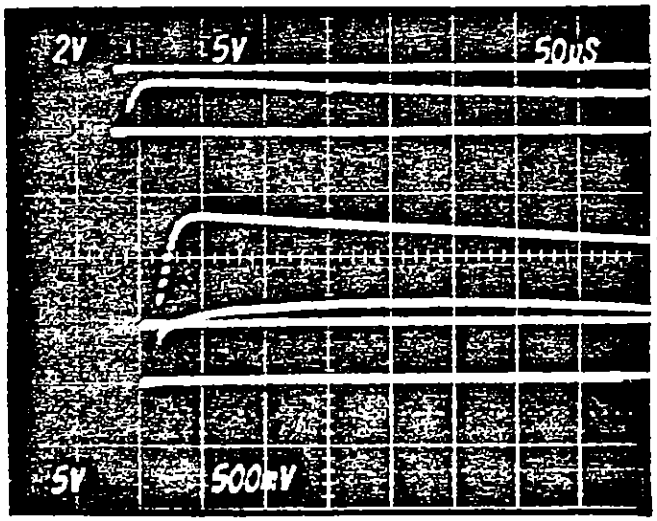

V_a

I

Figure 103. Shot 584 (80 kV self-bias).

The second and third photographs in Figure 103 illustrate that the oscillatory behavior is not apparent in the top voltage probes at the same azimuth, nor in the total sample voltage and current. Table 8 presents a summary of the combined drive experiments with comments on the occurrence of oscillations. It is apparent that oscillations occur intermittently under both self-bias and axial/radial stresses. Both for zero delays and delays of some tens of microseconds in the radial pulser. Figure 105 presents voltage probe records for axial/radial excitation. In this record a hint of oscillatory behavior is exhibited by the top voltage probes as well as the total current. Probably of greater significance is the fact that the spikes in the bottom voltage profiles now correspond to more negative voltages, as distinct from the more positive voltages displayed under self-bias in Figure 103. A more positive voltage in both cases would correspond to the sensing point potential approaching that of the center conductor; a more negative spike means that the voltage approaches that of the outer conductor.

It is tempting at this point to ascribe the oscillations to a transient behavior of the voltage probes, since the spikes on the oscillations appear to increase the magnitude of the voltage on the probe independent of sign. This interpretation is unlikely because the spikes on all of the voltage probes appear to be in synchronism, and there is a systematic difference in their appearance depending upon the location of the probe.

After these observations, a search of the records of previous shots revealed some evidence of similar oscillatory behavior. Figure 105 is an example of temporary oscillatory behavior in a 90° × 0.3 mL geometry in 1500-Ωm sand. The same behavior is displayed in Figure 106 on a faster sweep. The transients do not appear in the first probe, presumably because its potential is very close to that of the center conductor due to streamers. It also does not appear in the outermost probe whose potential continues to increase for 300 μs as the streamer approach it. A number of negative spikes, appear on the intermediate probes. Note that the polarity

TABLE 8. OSCILLATORY BEHAVIOR

Shot No.	Drive	Va(kV)	Radial Delay(μs)	Oscillations	Period(μs)	Arc-over μs
549	Axial	20		No		
550	"	"		"		
551	"	"		"		
552	Self-bias	"		"		
553	"	"		"		
554	"	"		"		
555	Axial/Radial	+20/-20	0	Pulser shorted		
556	"	+15/-15	"	" "		
557	"	+20/-20	"	Misfire		
558	"	+20/-20	"	Pulser shorted		
559	"	+20/-20	"	No		
560	"	"	"	Yes	60	
561	"	+20/-20	45	Yes	130	
562	"	+20/-20	0	No		
563	"	+20/-20	0	Irregular	20-70	
564	"	+20/-20	30	Yes	80-110	
565	"	+20/-20	30	No		
566	"	+20/-20	0	Misfire		
567	"	+20/-40	0	No		
568	"	+20/-40	20	No		
569	"	+20/-40	0	Yes	40	250
570	"	+20/-40	15	Yes	30-70	550
			(oscillations during recovery)			
571	"	"	0	No		250
572	"	"	0	Yes	50-70	550
			(oscillations continue after arc-over)			
573	"	"	40	Yes	50	130
574	"	"	0	No		100
575	Self-bias	40		Yes	50	
576	"	40		Yes	30	
577	"	60		Irregular	20-30	
578	"	"		"	20-30	
579	Axial/Radial	+20/-60	0	Pulser shorted		
580	"	+20/-60	0			35
581	"	+15/-42	0	No		70
582	"	Open?/-60	0			25
583	"	+20/-60	0			25
584	Self-bias	+80		Yes	30	
585	"	+80		Briefly	10-30	

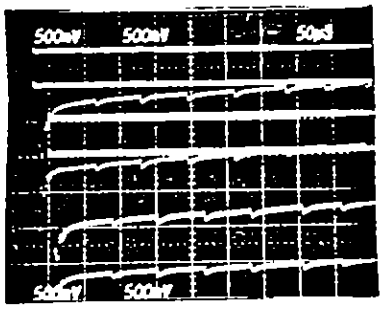

V_{BOT} - 0°

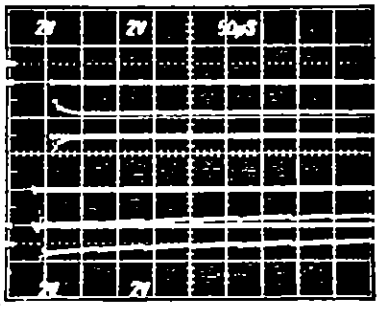

V_{TOP} - 0°

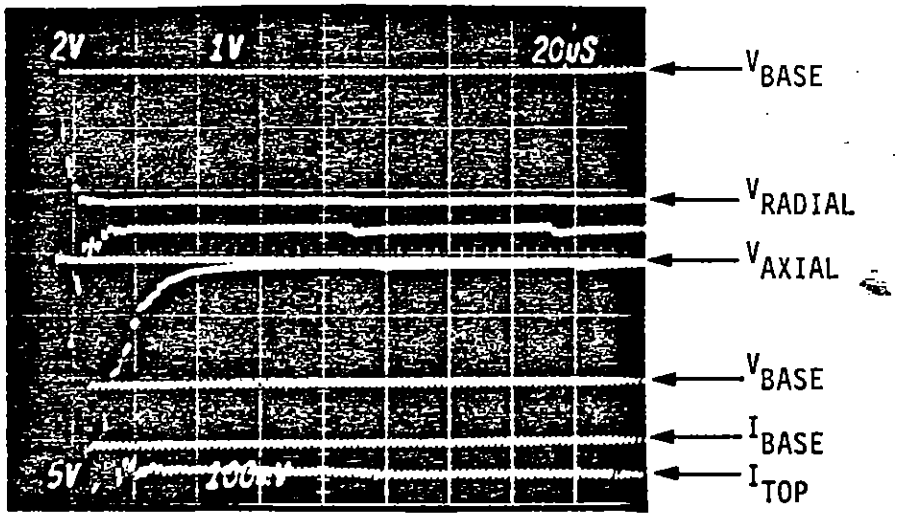

Figure 104. Shot 560 (V_a = +20 kV axial, -20 kV radial).

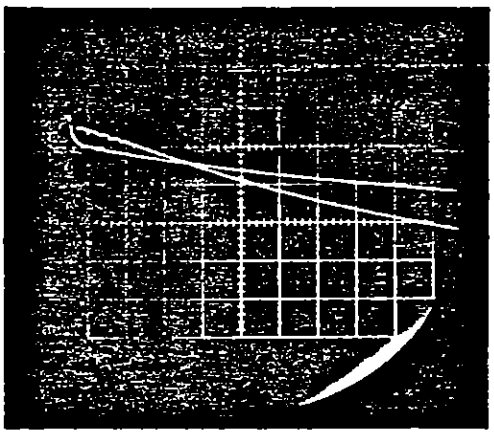

Upper (late) - Probe 1

Lower (late) - Probe 2

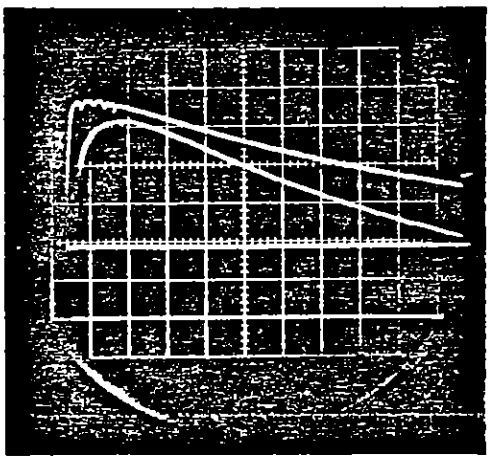

Upper - Probe 3

Lower - Probe 4

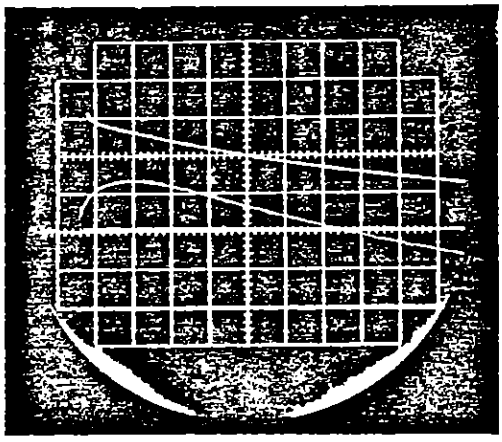

Upper - V_a

Lower - I

Figure 105. Shot 38 (1500 Ωm sand, 100 kV applied, Sweep = 200 μs/div).

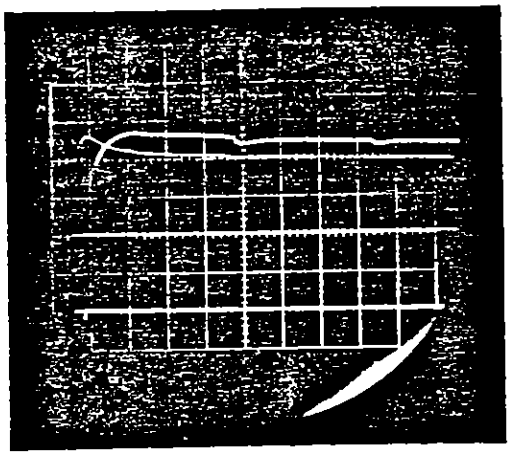

Upper (late) Probe 2

Lower (late) Probe 1

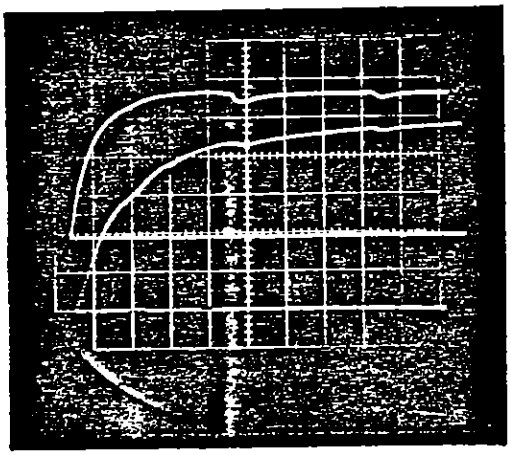

Upper - Probe 3

Lower - Probe 4

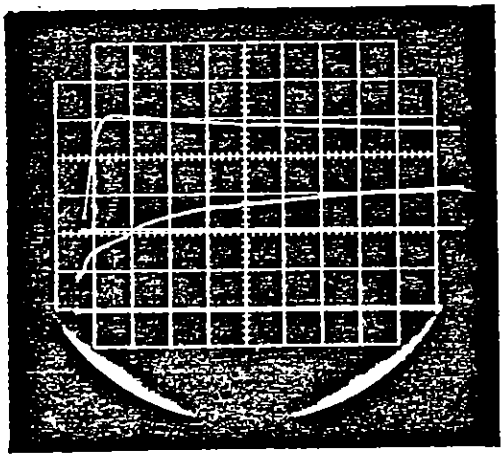

Upper: V_a

Lower: I

Figure 106. Shot 40 (1500 Ωm sand, 100 kV applied, Sweep = 20 μs/div).

of these spikes corresponds to decreasing magnitude of the voltage, as distinct from that in Figures 103 and 104.

Another example in the 360° × 1 mL sample under radial stress alone is shown in Figure 107. In this case, two spikes, again with decreasing absolute magnitude of voltage, appeared in voltage probes on the bottom of the sample. In this case, the timing of the spikes is different in the voltage probes at two different azimuths. The other voltage probes at these azimuths were not recorded, due to a camera shutter malfunction.

In the combined stress experiments, it is tempting to attribute the oscillatory behavior to a change in the direction of the net electric field as a result of the time dependent development of enhanced conduction. It is possible to postulate a mechanism by which streamers would oscillate between two locations as a result of this nonlinear behavior. This mechanism cannot explain the somewhat different oscillatory observed under radial excitation alone at both PI and McAir. For the present, these results must indicate the need for further experimentation with additional diagnostic information.

No explanation of this behavior, based upon instrumentation malfunction that is consistent with all the data, has been postulated. The oscillatory behavior is not localized on a given oscilloscope. The occurrence of spikes appears to be at the same time along a given radial vector in the sample. In one case (Fig. 107) the spikes occurred at different times along different radial vectors. In many cases, they occurred at a given radial vector on the bottom but not on the top. Since the voltage probes are essentially independent up to the oscilloscopes, it is difficult to postulate any malfunction mechanism that would exhibit this behavior.

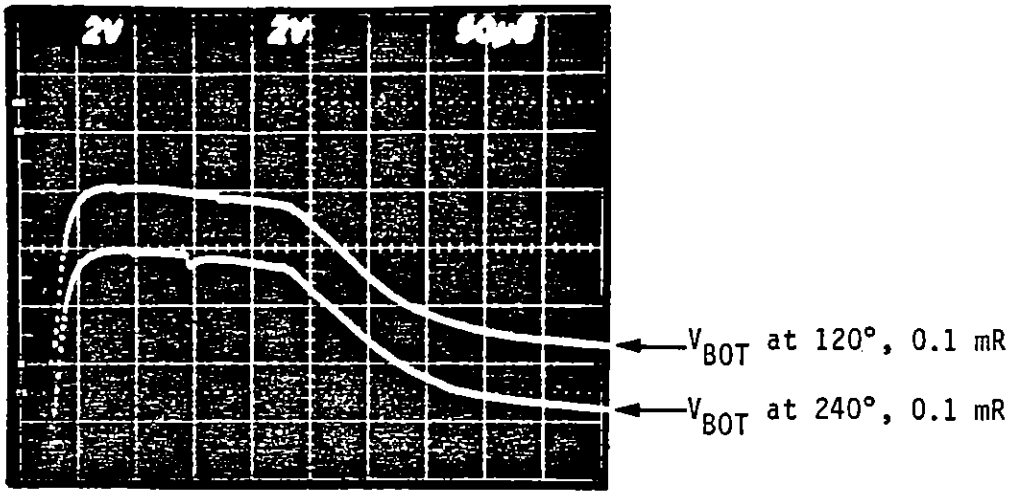

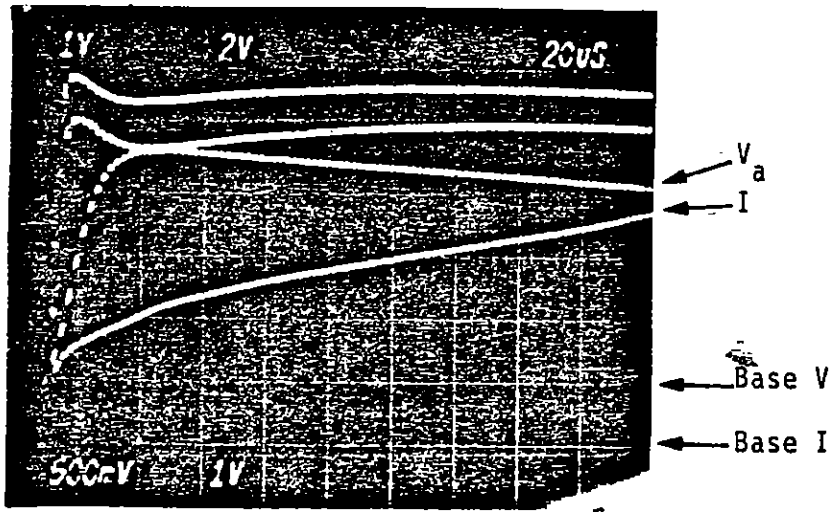

Figure 107. Shot 578 (350 Ωm sand mixture, 70 kV applied).

7. DEPENDENCE ON SOIL TYPE

The principal comparisons of the behavior of different soils under high electric stresses were performed during the PI experiments using the 90° × 0.1 mL geometry with a central conductor of 0.01-m radius and an outer conductor of 0.5 m.

Figures 108 to 113 present the voltage profiles for a variety of soil samples, measured under applied stresses that did not produce arc-over between conductors. In general, the data were chosen from shots with an applied voltage of the highest value before arc-over occurred. The soil samples in Figures 108 through 113 are in order of decreasing resistivity from 7700-Ωm to 130-Ωm.

In reviewing these data it must be remembered that the decrease in sample resistance has a direct consequence in the relaxation of the applied voltage with time. For example, in the high resistance sample illustrated in Figure 108, the applied voltage decreased by only 20% in 1 ms. At the other limit, illustrated in Figure 113, the applied voltage decayed with an effective exponentiation time of 800 μs.

Apart from the trend in the voltage at which these records are displayed, which reflects the dependence of arc-over voltage on resistivity (to be discussed later), there are no dramatic trends in these voltage profiles. The effective impedance within the nonlinear region in the highest resistivity material appears to remain rather large and stable during the entire measurement period from 80 to 1900 μs. In the lowest resitivity materials, illustrated in Figures 111 through 113, there is strong evidence that, at the intermediate voltage probes (0.05 to 0.2 m radii), the effective impedance continues to decrease at least up to 500 μs.

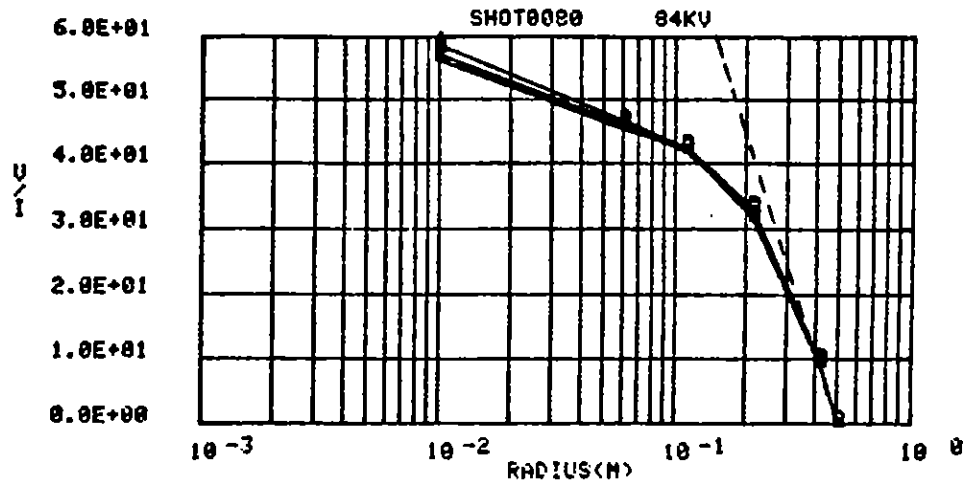

Code	A	B	C	D
Time	40 s	70 s	110 s	190 s
Current	1.55	1.55	1.53	1.50

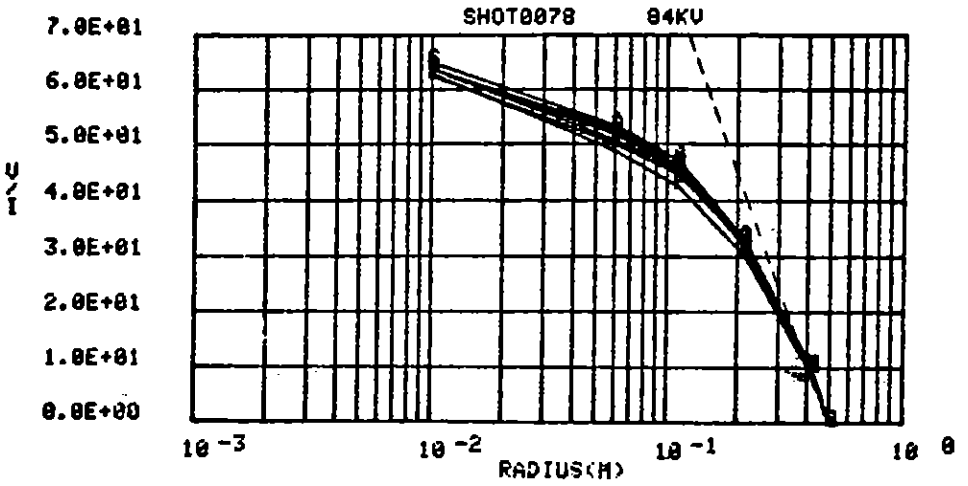

Code	A	B	C	D	E	F
Time	100 s	200 s	300 s	500 s	900 s	1900 s
Current	1.40	1.35	1.30	1.30	1.25	1.10

Figure 108. Voltage profile.
(7700 Ωm sand
90° x 0.1 mL)

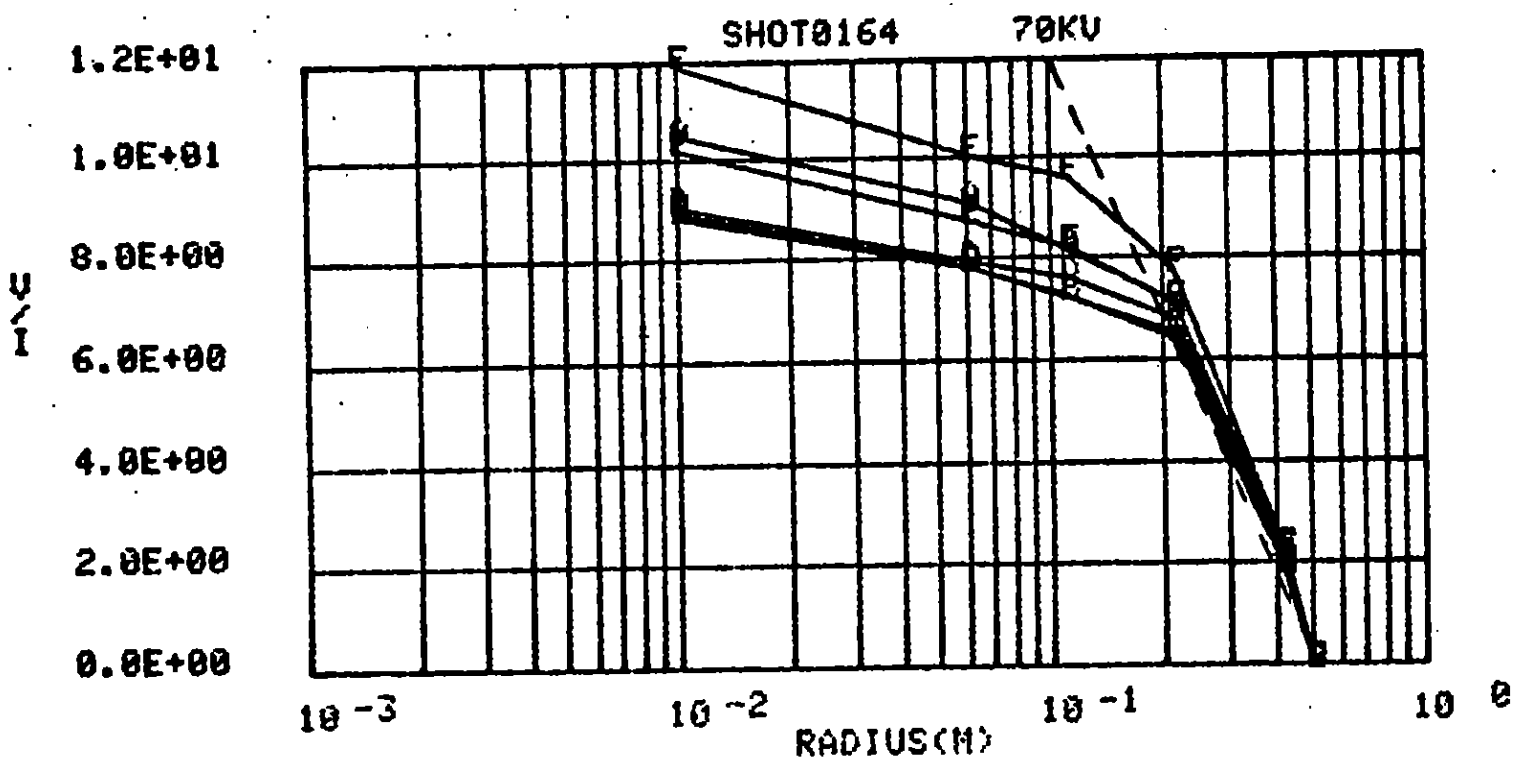

CODE	A	B	C	D	E	F
TIME	100 µs	200 µs	300 µs	500 µs	900 µs	1900 µs
CURRENT	7.00	8.00	7.75	7.13	6.00	4.00

Figure 109. Voltage profile.
(100 Ωm SDF soil
90° x 0.1 mL)

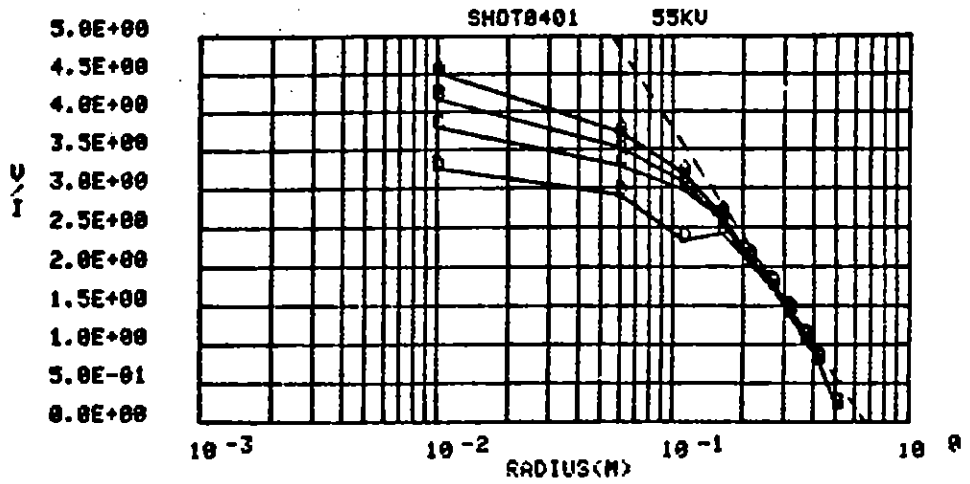

Code	A	B	C	D
Time	40 µs	70 µs	110 µs	190 µs
Current	13.50	14.25	15.25	16.75

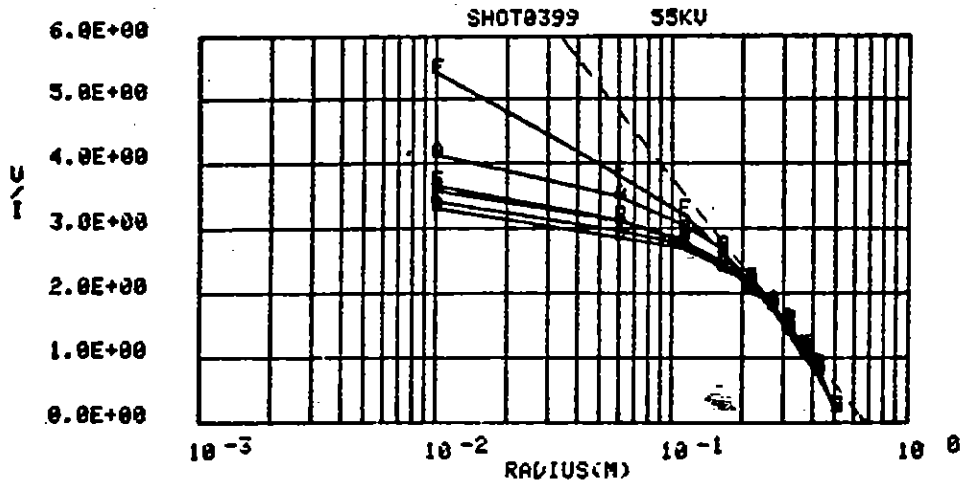

Code	A	B	C	D	E	F
Time	100 µs	200 µs	300 µs	500 µs	900 µs	1900 µs
Current	14.00	15.25	15.00	14.00	10.75	5.00

Figure 110. Voltage profile.
(350 Ωm sand mix
90° x 0.1 mL)

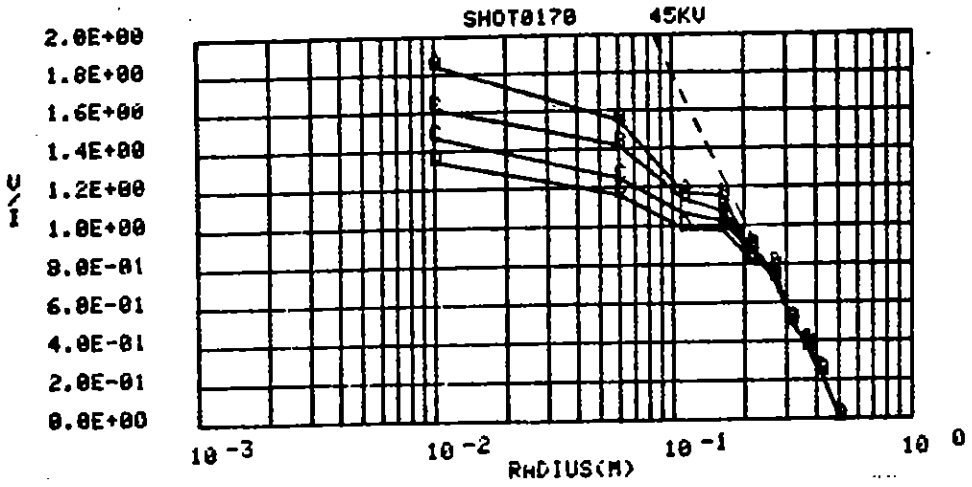

Code	A	B	C	D	E
Time	40 µs	70 µs	110 µs	190 µs	0 µs
Current	27.00	29.50	31.00	31.00	0.00

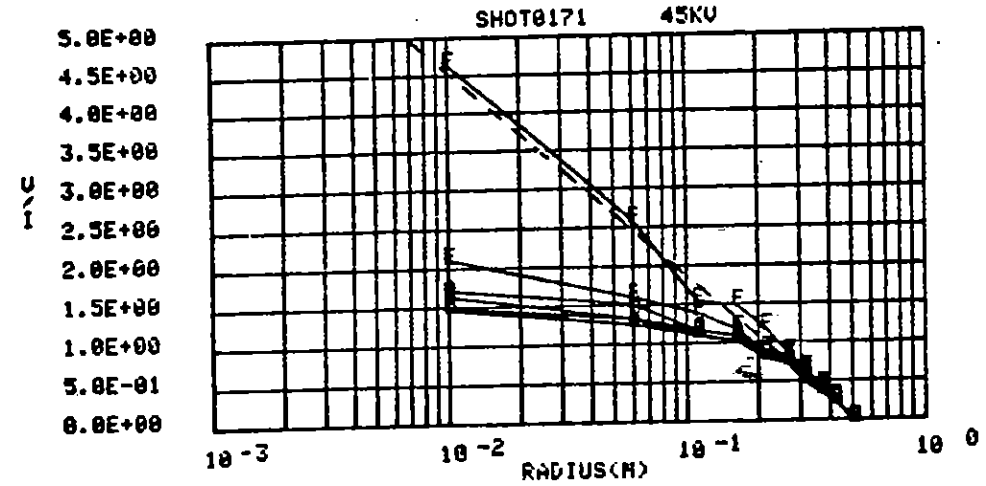

Code	A	B	C	D	E	F
Time	100 µs	200 µs	300 µs	500 µs	900 µs	1900 µs
Current	28.00	29.00	24.50	21.00	11.00	3.00

Figure 111. Voltage profile.
(170 Ωm sand
90° x 0.1 mL)

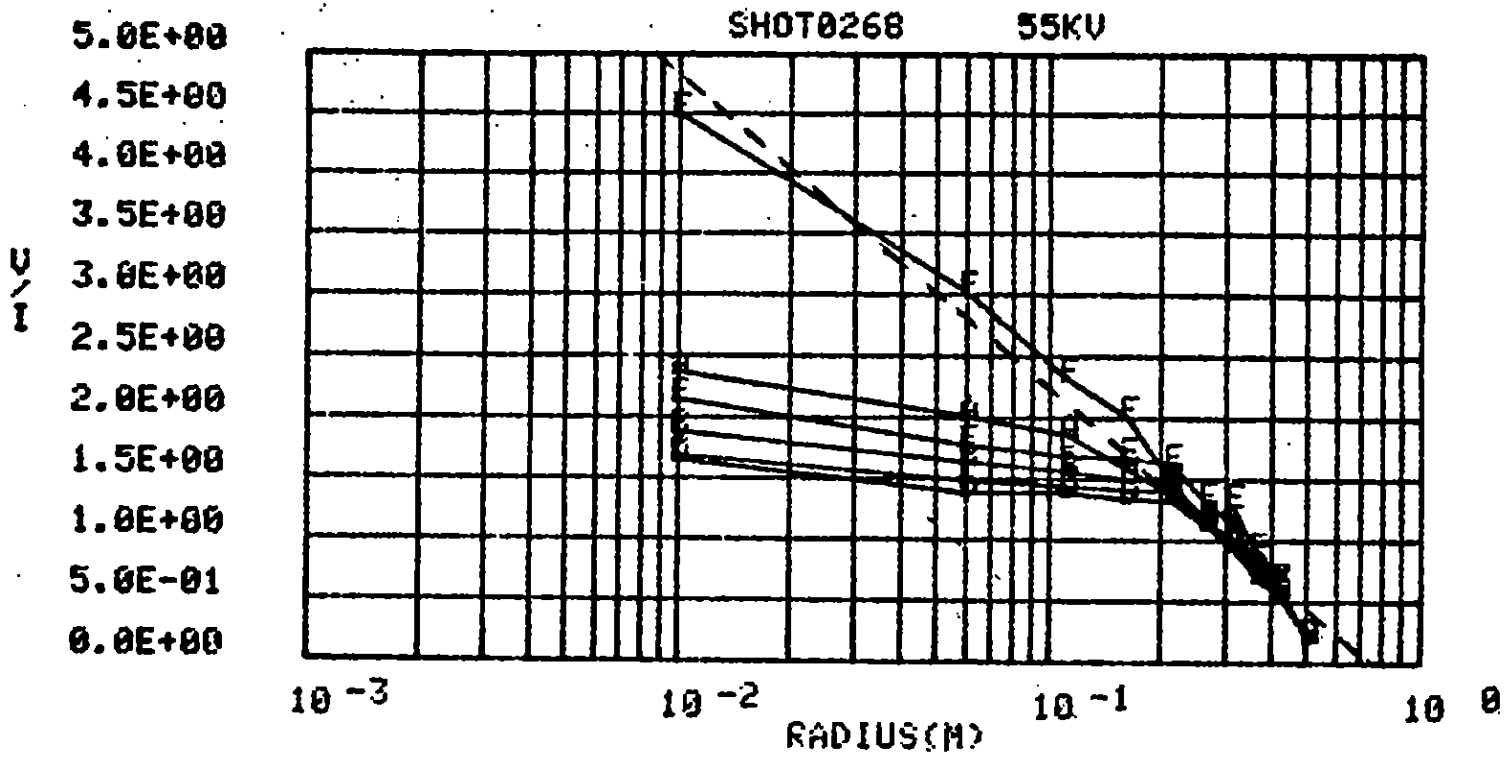

CODE	A	B	C	D	E	F
TIME	100 µs	200 µs	300 µs	500 µs	900 µs	1900 µs
CURRENT	25.00	29.00	29.50	26.00	14.00	4.00

Figure 112. Voltage profile.
(170 Ωm MX-B soil, untamped
90° x 0.1 mL)

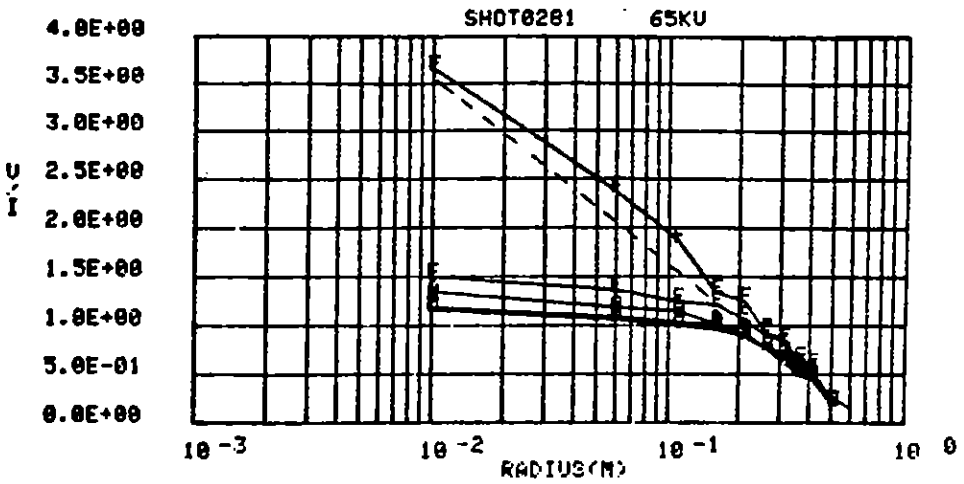

Code	A	B	C	D	E	F
Time	100 µs	200 µs	300 µs	500 µs	900 µs	1900 µs
Current	50.00	50.00	45.00	35.00	17.50	3.75

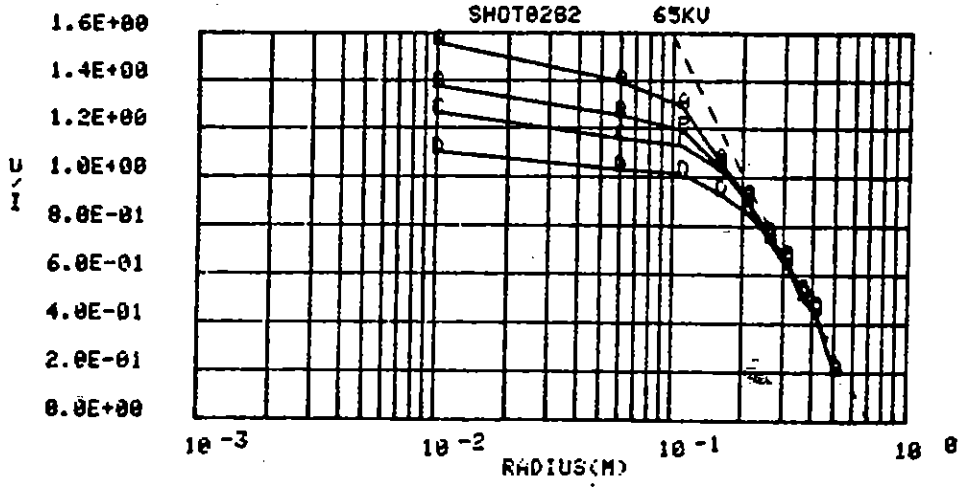

Code	A	B	C	D
Time	40 µs	70 µs	110 µs	190 µs
Current	45.00	48.75	50.00	52.50

Figure 113. Voltage profile.
(130 Ωm MX-B soil, tamped
90° x 0.1 mL)

The inner contact impedance, shown by the voltage between the voltage probe at 0.05-m radius and the central conductor, also is apparent. Some of these samples also appear to exhibit a significant nonlinear impedance at the outermost electrode. This is exhibited most strongly in Figure 110, which corresponds to a 310-Ωm sand mixture. The larger drop than expected from ohmic behavior between the outermost probe and the outer conductor is apparent in comparing the dashed line with the measured data.

With the exception of the extremely high resistance material illustrated in Figure 108, the apparent resistance of the medium in the nonlinear region continues to decrease to about 500 μs, whether the current has peaked prior to this point or not.

The strong similarity in behavior prior to arc-over is noteworthy because it occurs over a range of resistivities of more than a factor of 50. This implies that the energy deposition averaged over the entire volume of the soil sample is varying by more than an order of magnitude, while maintaining reasonably similar behavior. For the sand samples, the resistivity was changed only by adding water. Therefore, it can be expected that the actual energy deposition per unit volume of water filament is almost the same even though the gross resistivity of the sample is much different.

The marked difference in the time during which the streamer impedance continues to decrease between the high resistivity sand and lower resistivity soils may possibly be explained by differences in effective thermal relaxation times. The only difference between most of the sand samples used for these experiments is the water content. It might be expected, therefore, that the sample conductivity might be proportional to the average cross-sectional area of the conducting water filaments in the soil. One can also expect that the area of the individual conducting filaments might be less for higher resistivity materials. Consider a thermal relaxation process in which heat is generated in conducting filaments that are in contact

with nonconducting sand grains. At early times, the temperature of the filament will rise in response to the energy dissipation. Once the thermal diffusion distance into the adjacent sand grains becomes comparable with the dimensions of the conducting filament, the temperature of the conducting filament will stop rising or rise much more slowly for constant heat generation. Smaller filaments will achieve thermal equilibriation with adjacent heat-sinking sand grains at earlier times. While the evidence is insufficient to demonstrate this interpretation, it is consistent with it.

The dependence of the time for initiation of first evidence of a streamer on the soil material was discussed in Section III, paragraph 2. The time at which arc-over from inner to outer electrodes is observed is shown in Figure 114. Unfortunately, the resolution used between applied voltages was not small enough to achieve the same arc-over time in all of the different materials; however, the trend of exhibiting arc-over at lower voltages in lower resistivity materials is apparent. This trend is illustrated more clearly in Figure 115, in which the arc-over voltage is plotted as a function of soil resistivity. The values plotted in Figure 115 are the voltages corresponding to an average arc-over time of 100 μs using a relatively steep slope to correct the longer arc-over times to this reference value. The error introduced by this extrapolation procedure is small compared to the trend exhibited in Figure 115. The data have been plotted versus the applied voltage and versus the voltage existing at the time of arc-over. The apparent turn up in the top curve at low resistivities is due to the more rapid decay of the voltage from the pulser with the lower resistance load. If these experiments were done with an absolutely stiff power supply, a curve intermediate between these two would be expected.

Adding this result to those depicted in Figures 108 through 113 leads to the conclusion that the variation with soil type can be represented approximately by scaling the electric field as a weak function of soil resistivity and scaling the nonlinearities in the soil impedance proportionately to the low field value of the soil resistance.

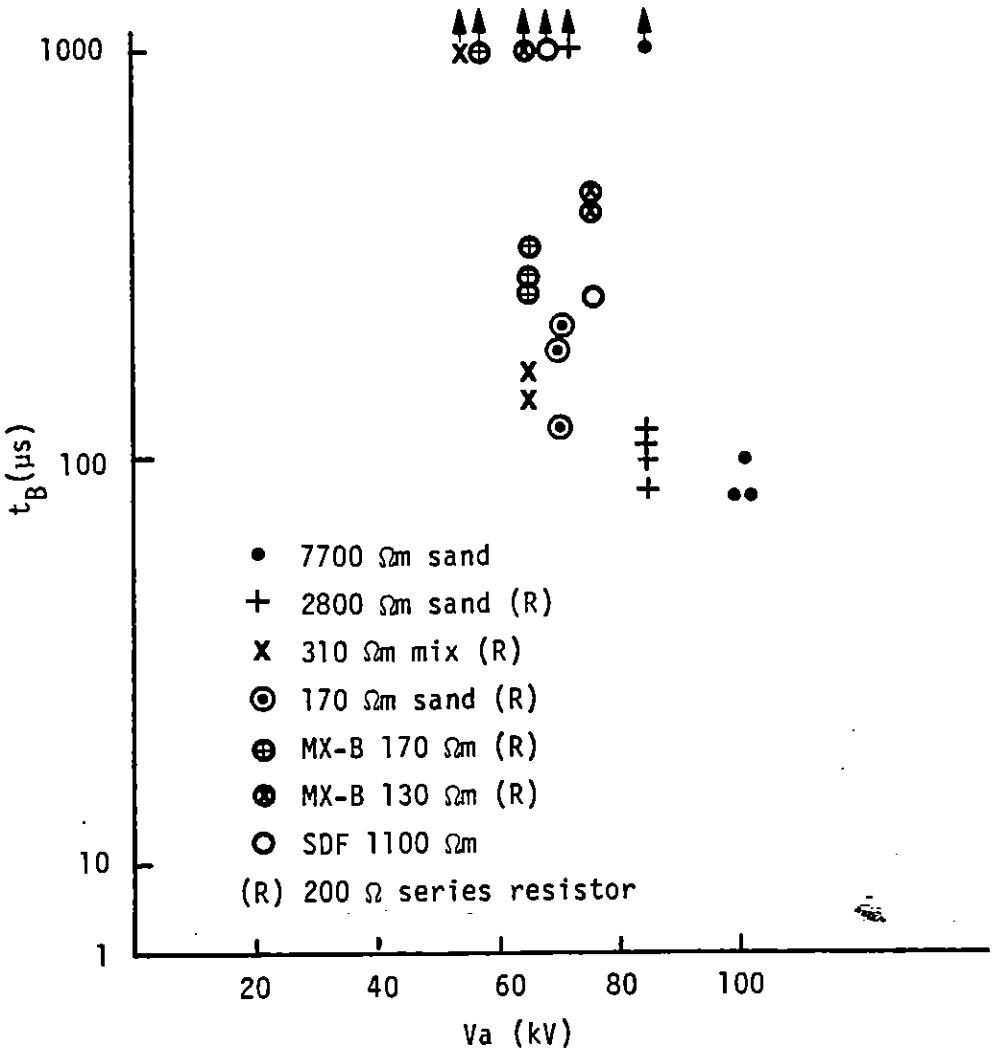

Figure 114. Arc-over time.

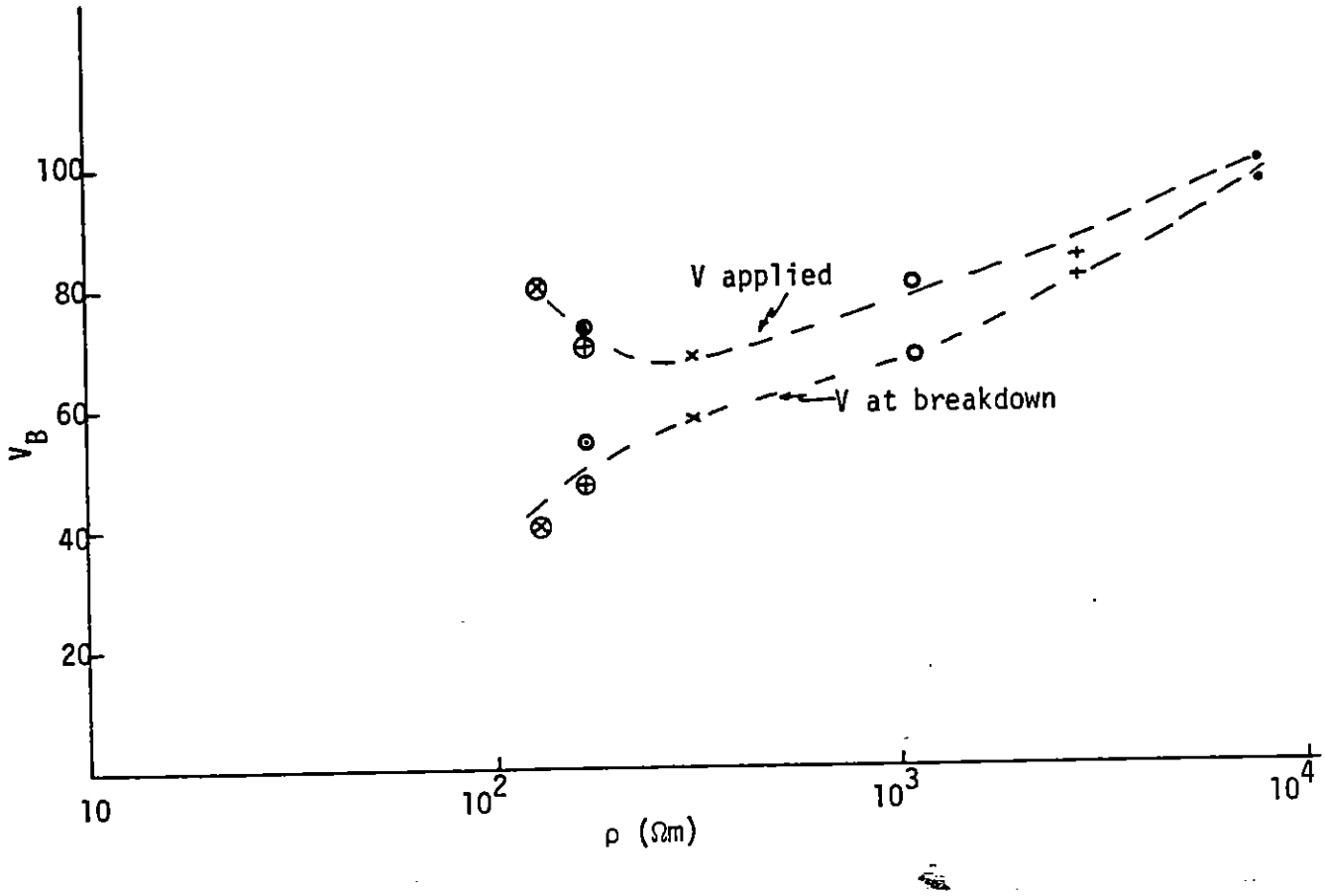

Figure 115. Arc-over voltage for t_B = 100 μs.

In comparing the data on the various resistivity sands with those for the SDF soil and the MX-B soil, there is no obvious difference between the behavior of the realistic soils and a sand of equivalent bulk resistivity. The data for the MX-A soil, which contained extremely fine particulate and had totally different characteristics from any of these other soils, have not been processed for comparison with these results.

As noted, the apparent earth impedance observed with the radial voltage probes appears to be proportional to the low field earth resistance at scaled values of the electric field, as long as arc-over does not occur. The behavior of many of these same materials at a higher voltage, at which arc-over occurred, is illustrated in Figures 116 through 120. The behavior prior to arc-over is similar to that shown in Figures 108 through 113. After arc-over, however, the impedance appears to fall to a similar low value. This is illustrated in Figure 121, which presents a rough estimate of the sample resistance as a function of time after the initiation of arc-over. Within the accuracy of this determination, including the contribution of the apparent voltage drop at the two electrodes, these curves appear to be the same over the entire range of soil resistivities. These data are all taken with a 200-Ω resistor in series between the pulser and the soil sample to limit the current. The sample resistance appears to decrease to a value of near one-half to three-fourths of the series resistance. The increase in sample resistance at late times is the consequence of the decaying voltage of the pulser. The effective decay time of the pulser capacitance into a 200-Ω series resistance would be 200 μs.

8. DEPENDENCE ON EXPERIMENT GEOMETRY

Inner Conductor Radius

Two experiments were performed in which the inner conductor radius was changed with no other intentional parameter changes. The first of these

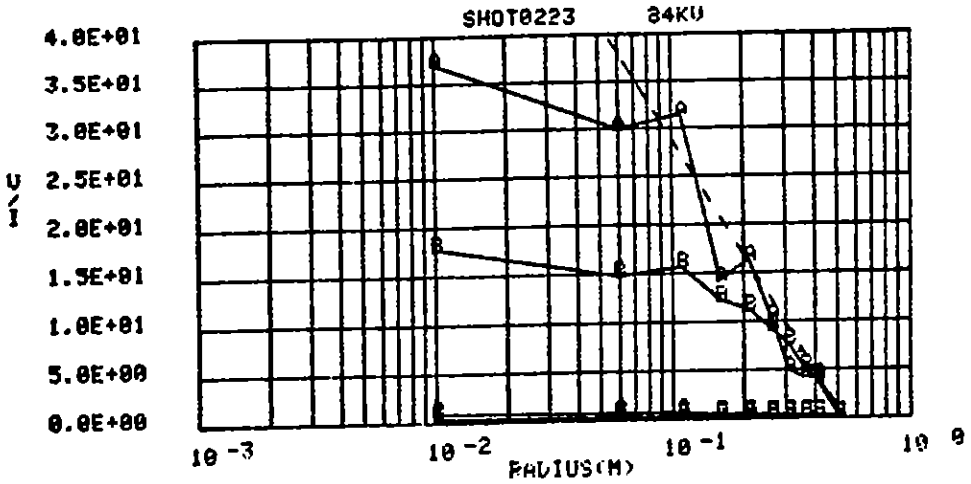

Code	A	B	C	D	E	F
Time	25 µs	75 µs	125 µs	175 µs	225 µs	450 µs
Current	2.5	5.0	110.0	200.0	190.0	60.0

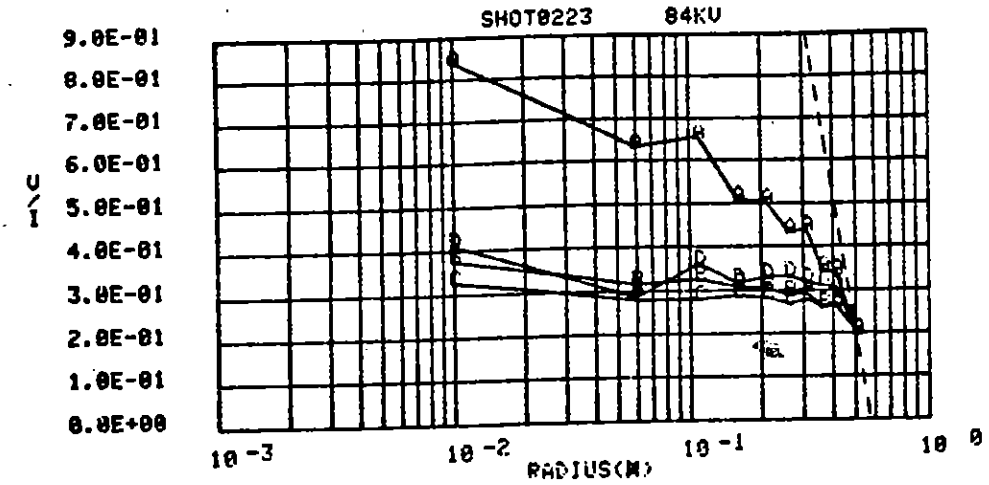

Code	A	B	C	D
Time	125 µs	175 µs	225 µs	450 µs
Current	110.0	200.0	190.0	60.0

Figure 116. Voltage profile.
(2800 Ωm sand
90° x 0.1 mL)

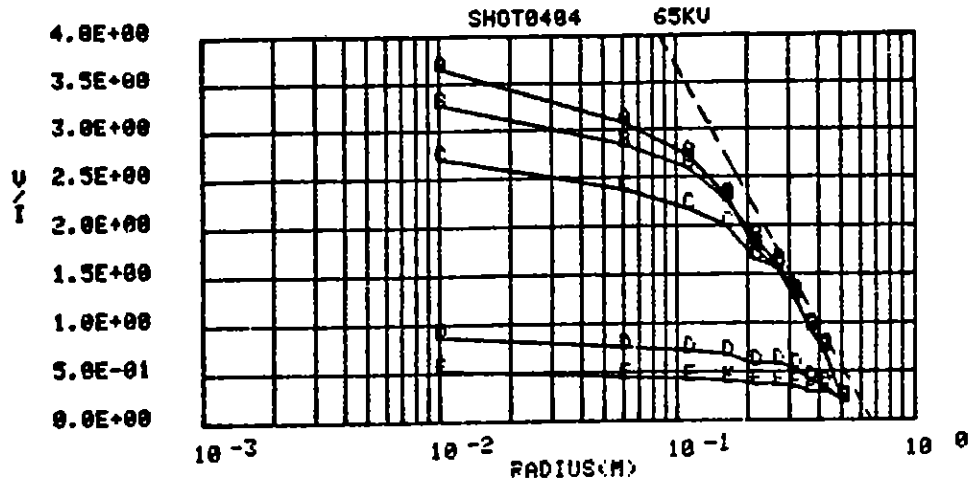

Code	A	B	C	D	E
Time	40 µs	70 µs	110 µs	170 µs	190 µs
Current	20.0	21.3	25.0	75.0	125.0

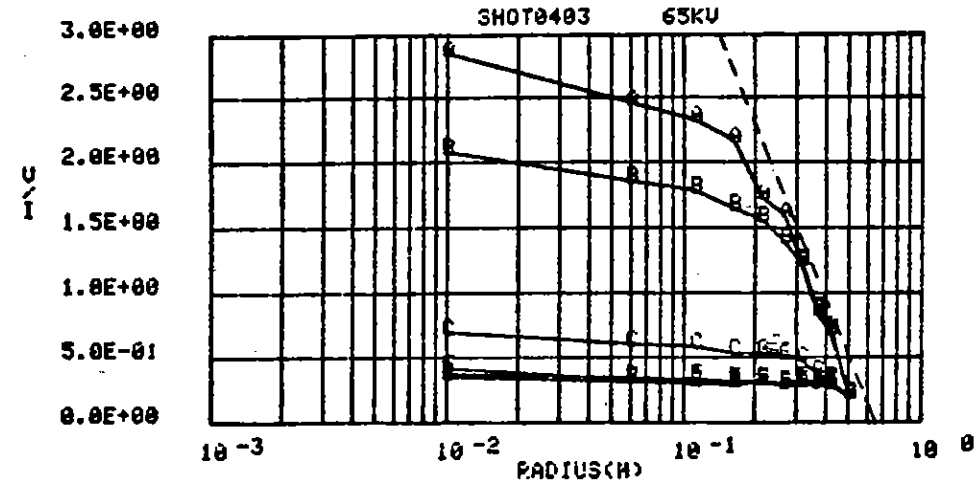

Code	A	B	C	D	E	F
Time	50 µs	100 µs	150 µs	200 µs	275 µs	475 µs
Current	25.0	32.5	95.0	153.8	130.0	52.5

Figure 117. Voltage profile.
(310 Ωm sand mix
90° x 0.1 mL)

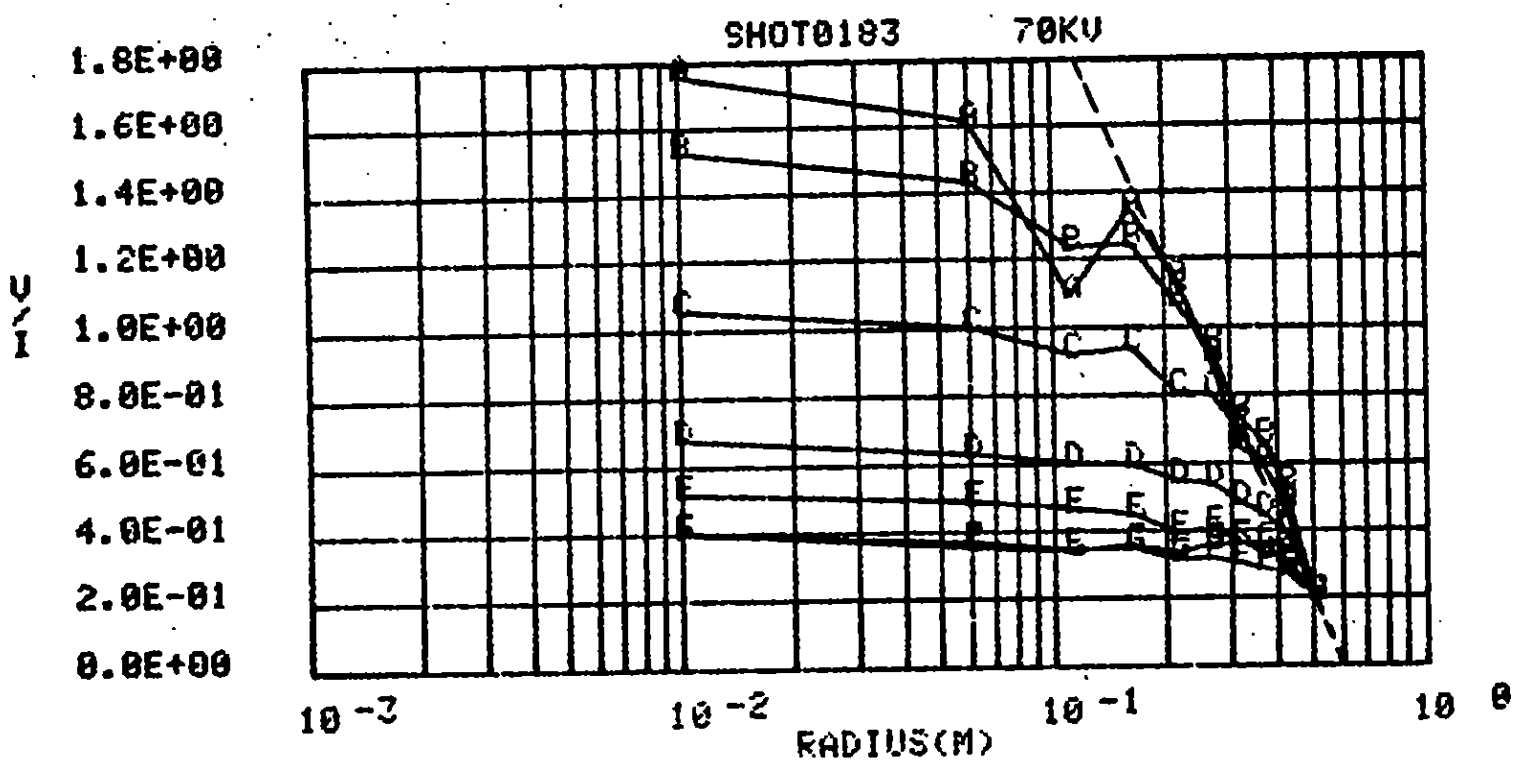

CODE	A	B	C	D	E	F	G
TIME	25 µs	50 µs	125 µs	215 µs	250 µs	300 µs	475 µs
CURRENT	42.5	50.0	65.0	90.0	107.5	120.0	65.0

Figure 118. Voltage profile.
(170 Ωm sand
90° x 0.1 mL)

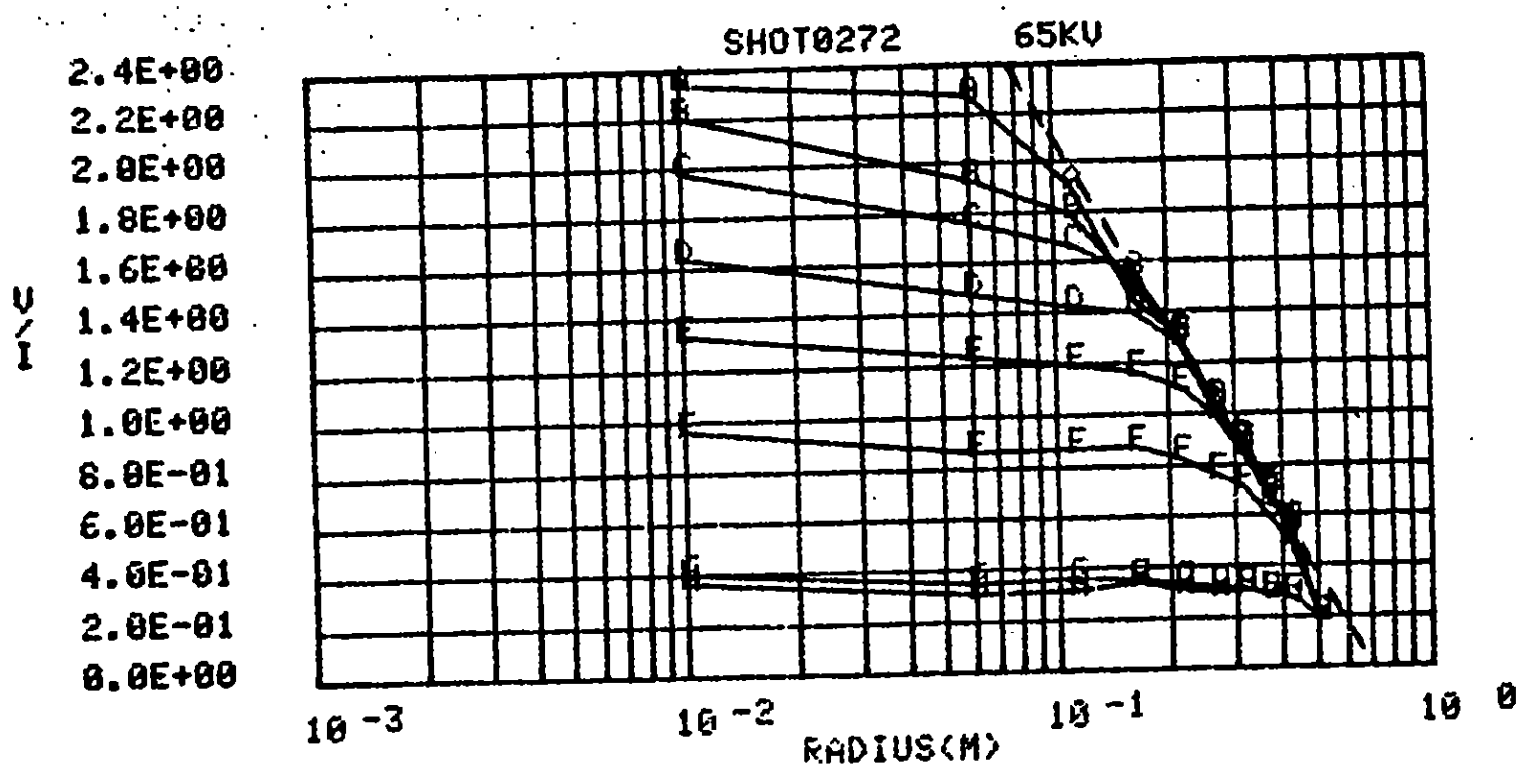

CODE	A	B	C	D	E	F	G	H
TIME	25 µs	50 µs	75 µs	125 µs	225 µs	325 µs	375 µs	475 µs
CURRENT	30.0	32.5	35.0	40.0	45.0	55.0	117.5	93.8

Figure 119. Voltage profile.
(170 Ωm MX-B soil, untamped
90° x 0.1 mL)

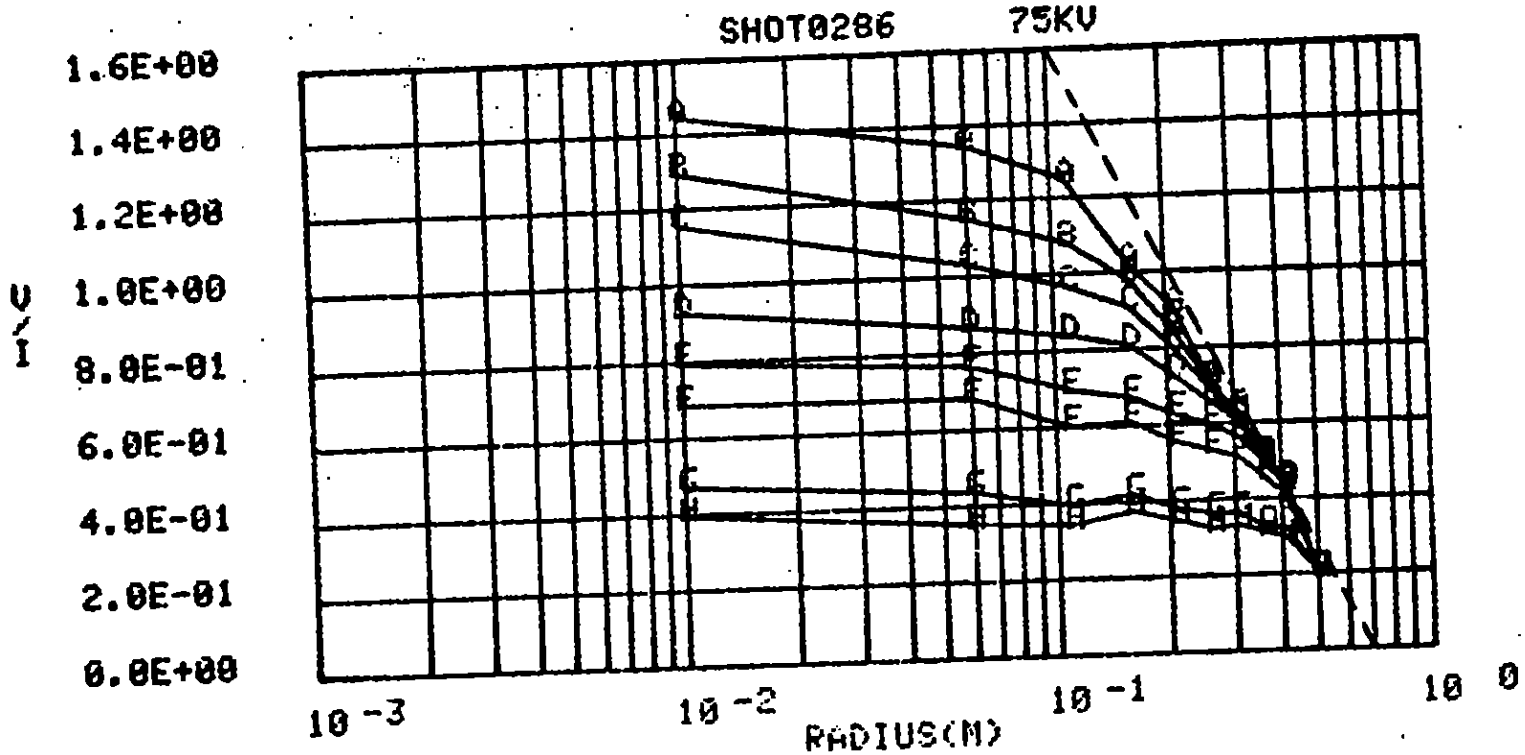

CODE	A	B	C	D	E	F	G	H
TIME	25 µs	50 µs	75 µs	175 µs	275 µs	410 µs	425 µs	475 µs
CURRENT	55.0	62.5	67.5	72.5	72.5	65.0	95.0	95.0

Figure 120. Voltage profile.
(130 Ωm MX-B soil, tamped
90° x 0.1 mL)

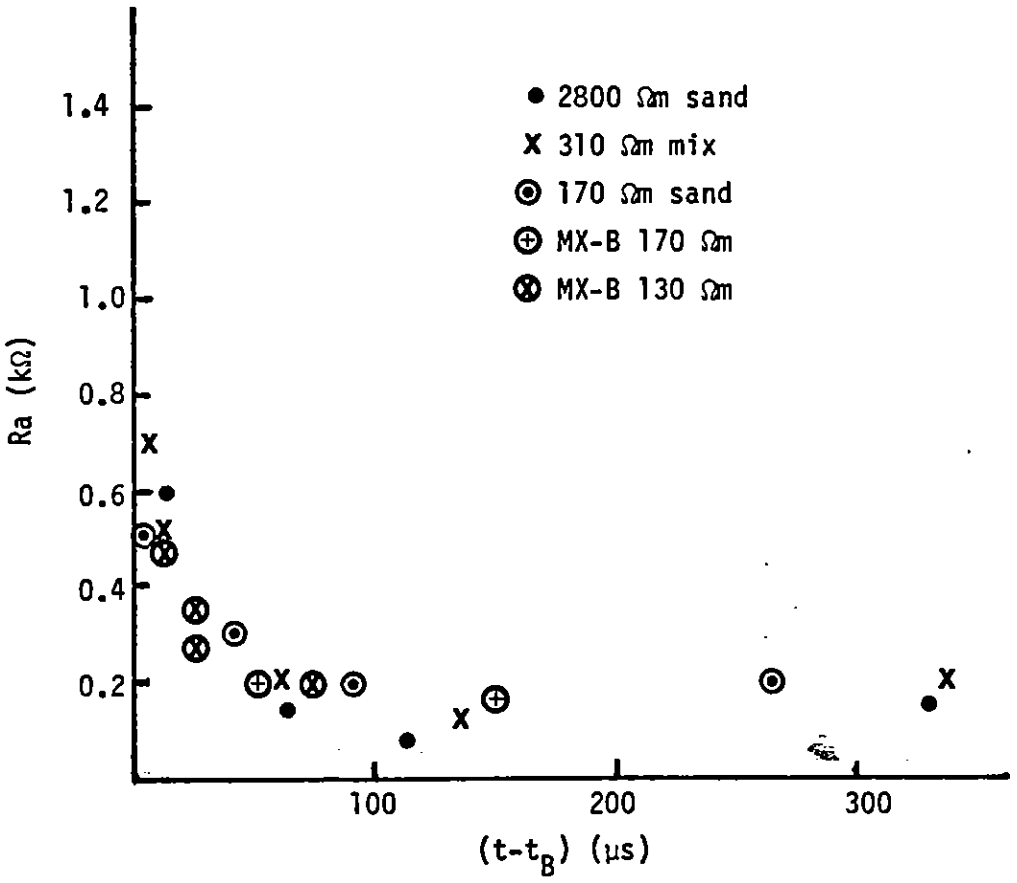

Figure 121. Apparent arc resistance.

occurred during the PI 90° × 0.1 mL sector experiments, with a 170-Ωm sand sample. The second occurred during the McAir experiments with 300-Ωm sand mixture in 360° × 1 mL geometry. Figures 122 through 125 present comparisons between the voltage profiles generated in the PI experiments for 0.01-m-radius and 0.0025-m-radius center conductors. At the lowest measured (Fig. 122), the onset of streamers near the center conductor is apparent in both geometries. The voltage measured at 0.05 m radius falls above the ohmic line for shot 191, apparently indicating a concentration of current in the vicinity of this probe for the smaller diameter center conductor. Whether this is accidental due to the random choice of streamer location, or whether it is a direct consequence of the radius of the center conductor, is not known. At intermediate voltages of 45, 50, and 55 kV the streamer development and behavior appear to be very similar. Even the voltage drop between the center conductor and the innermost voltage probe appear to be the same. At 70 kV, the time of arc-over is the same for the two geometries within the spread of values encountered in otherwise identical experiments. The development of the impedance prior to and after arc-over is also indistinquishable within the reproducibility of these responses. If anything, the impedance of the arc generated by the smaller diameter conductor is a little bit less at equivalent times, but that could be a consequence of the fact that the arc occurred earlier, at which point more voltage was available to it.

Figure 126 presents four radial profiles for the McAir experiment with 0.01-m-radius central conductor and an applied voltage of 60 kV. On four sucessive shots at the same applied voltage, arc-over occurred at 50, 50, 52, and 106 μs. The profiles prior to arc-over are shown in Figure 126. They indicate that, just before arc-over occurred, less than a proportionate share of the current was flowing in the 0° top sector, a proportionate share was flowing in the 120° bottom sector, and more than a proportionate share was flowing in the 0° and 240° bottom sectors. Immediately after these experiments, during a shot at V_a = 80 kV, physical evidence of an arc terminating on the outer cylinder at approximately 300° was produced. Therefore, it is reasonable to assume that the arc-over occurred in that same

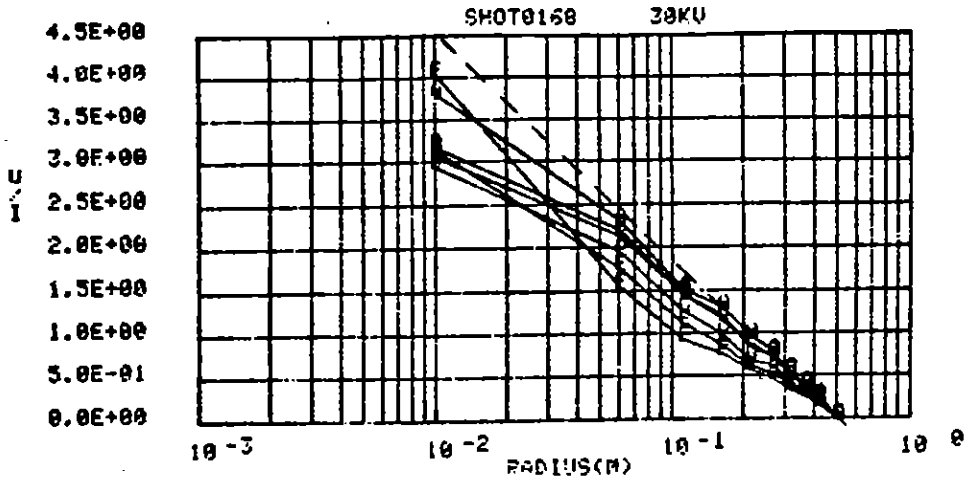

CODE	A	B	C	D	E	F
TIME	100US	200US	300US	500US	900US	1300US
CURRENT	9.0	10.0	9.0	9.5	8.0	5.0

(a) 0.01 mR center conductor

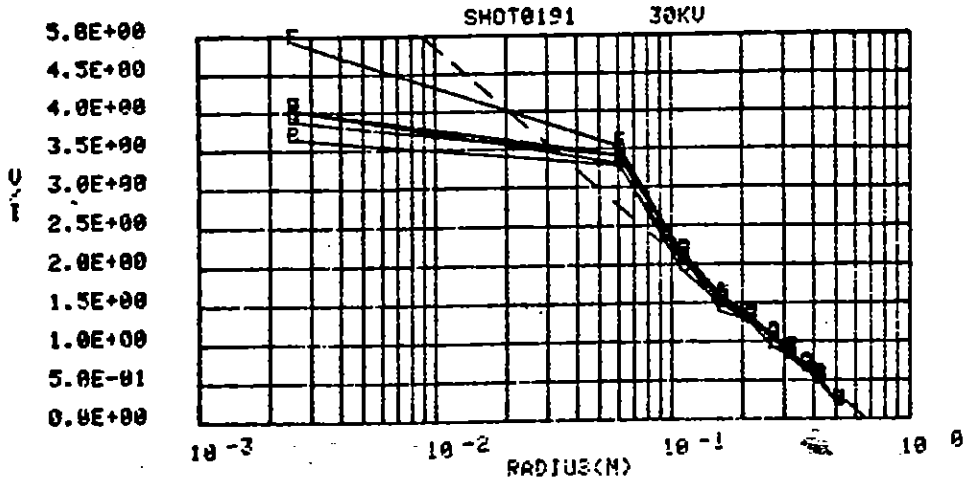

CODE	A	B	C	D	E	F
TIME	100US	200US	300US	500US	900US	1300US
CURRENT	8.3	8.0	7.3	6.5	5.5	3.0

(b) 0.0025 mR center conductor

Figure 122. Voltage profile.
(90° x 0.1 mL)

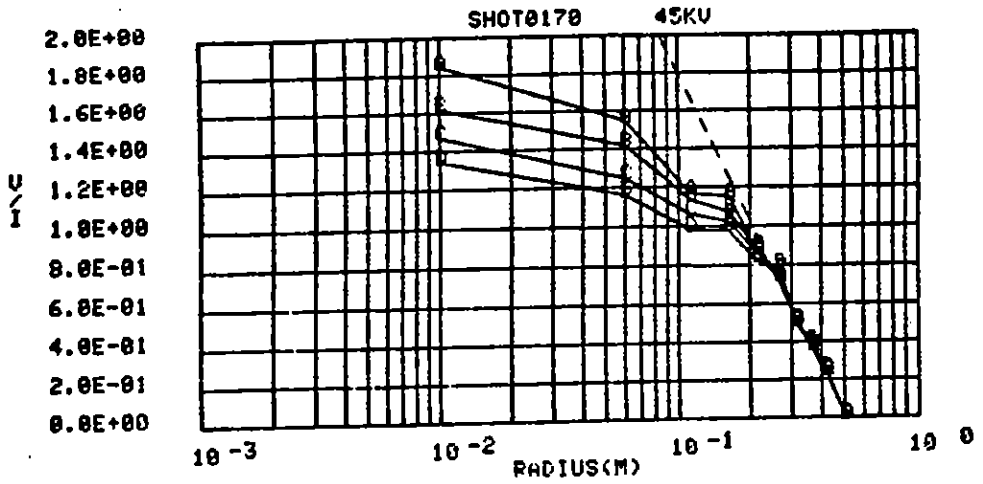

Code	A	B	C	D
Time	40 µs	70 µs	110 µs	190 µs
Current	27.00	29.50	31.00	31.00

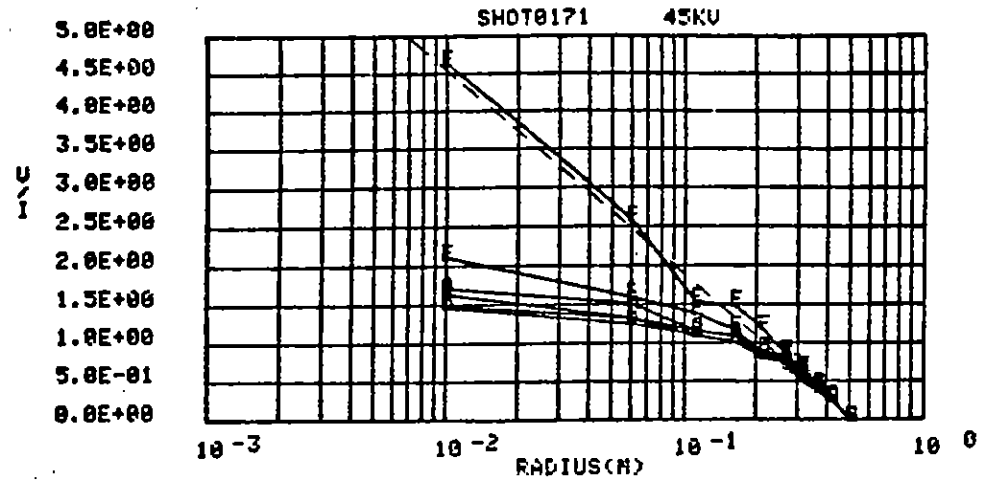

Code	A	B	C	D	E	F
Time	100 µs	200 µs	300 µs	500 µs	900 µs	1900 µs
Current	28.00	29.00	24.50	21.00	11.00	3.00

(a) 0.01 mR center conductor

Figure 123. Voltage profile (200 Ωm sand, 90° x 0.1 mL)

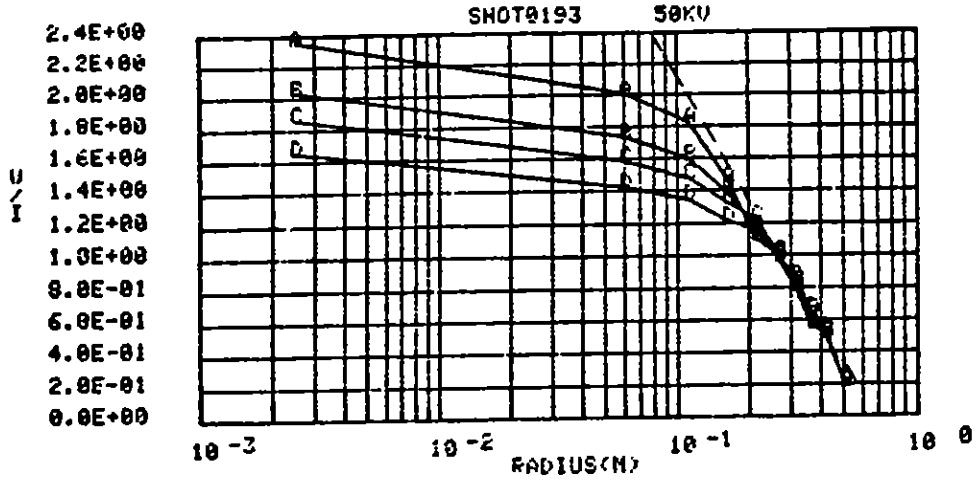

Code	A	B	C	D
Time	40 μs	70 μs	110 μs	190 μs
Current	23.5	26.0	27.5	29.0

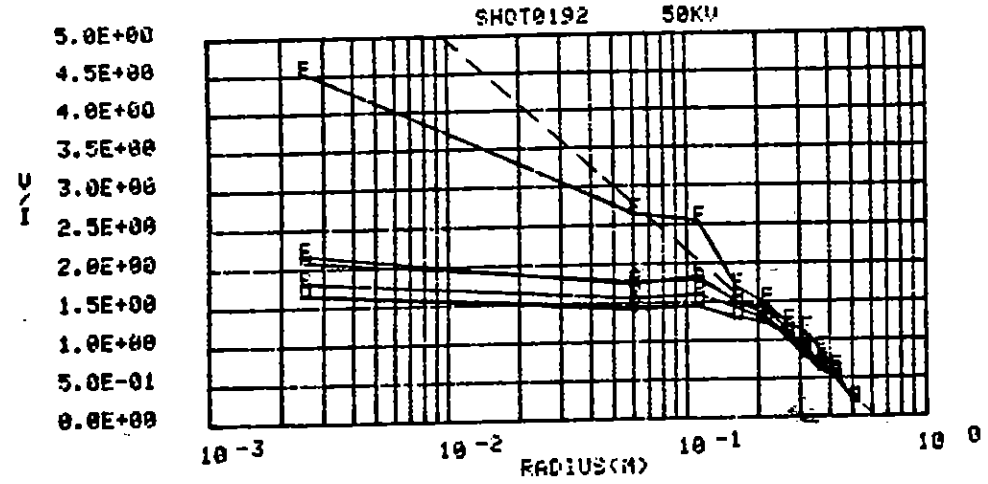

Code	A	B	C	D	E	F
Time	100 μs	200 μs	300 μs	500 μs	900 μs	1900 μs
Current	25.0	26.0	26.5	22.0	12.5	3.5

(b) 0.0025 mR center conductor

Figure 123. Concluded.

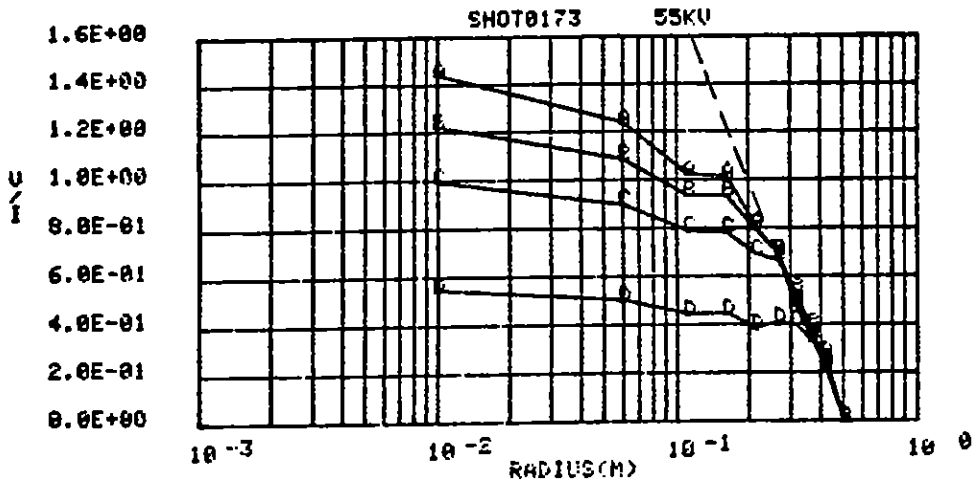

Code	A	B	C	D
Time	40 μs	70 μs	110 μs	174 μs
Current	42.5	47.5	55.0	90.0

(a) 0.01 mR center conductor

Figure 124. Voltage profile. (200 Ωm sand 90° x 0.1 mL)

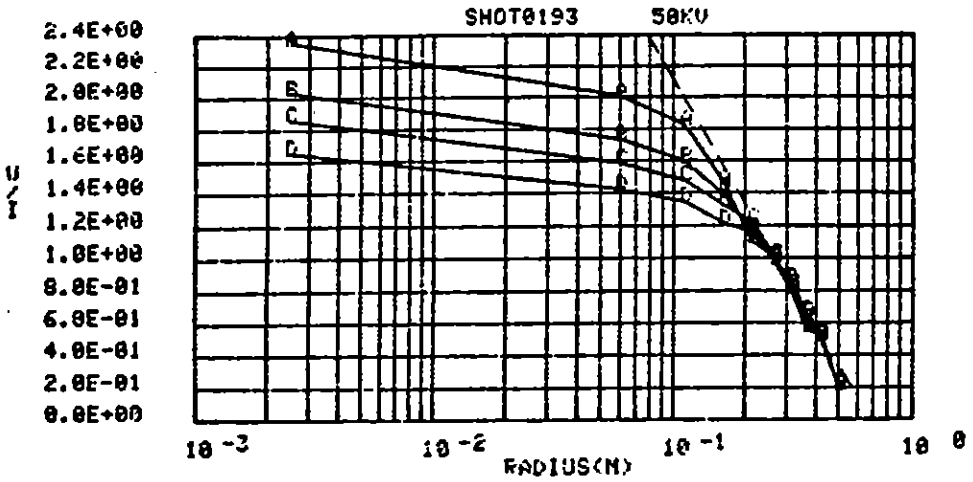

Code	A	B	C	D
Time	40 μs	70 μs	110 μs	190 μs
Current	23.5	26.0	27.5	29.0

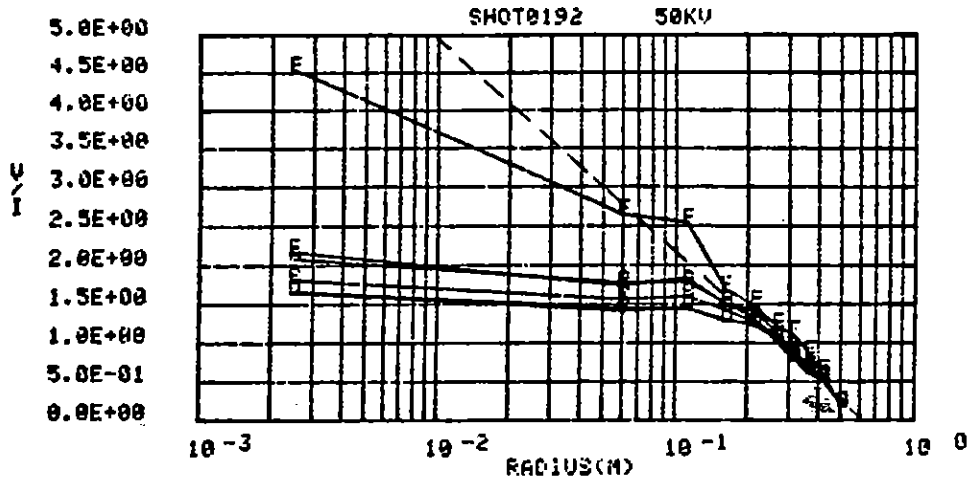

Code	A	B	C	D	E	F
Time	100 μs	200 μs	300 μs	500 μs	900 μs	1900 μs
Current	25.0	26.0	26.5	22.0	12.5	3.5

(b) 0.0025 mR center conductor

Figure 124. Concluded.

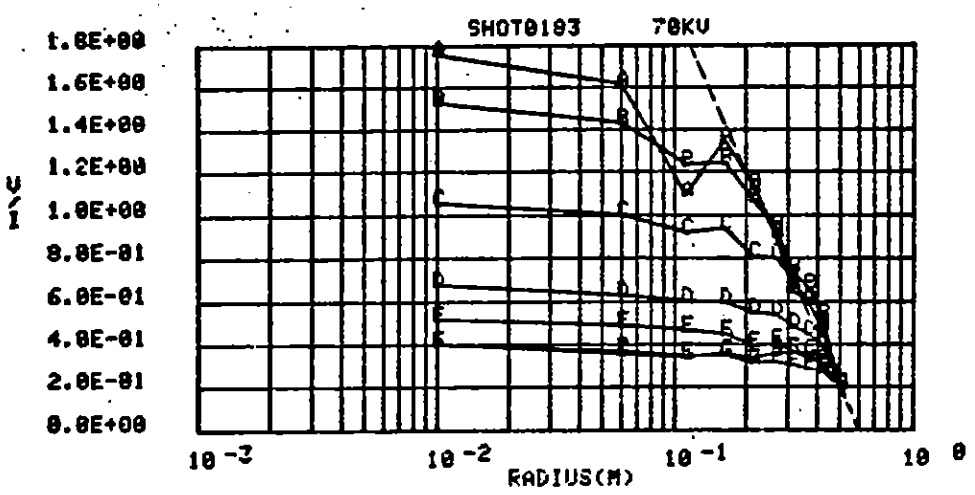

Code	A	B	C	D	E	F	G
Time	25 µs	50 µs	125 µs	215 µs	250 µs	300 µs	475 µs
Current	42.5	50.0	65.0	90.0	107.5	120.0	65.0

(a) 0.01 mR center conductor

Figure 125. Voltage profile.
(200 Ωm sand
90° x 0.1 mL)

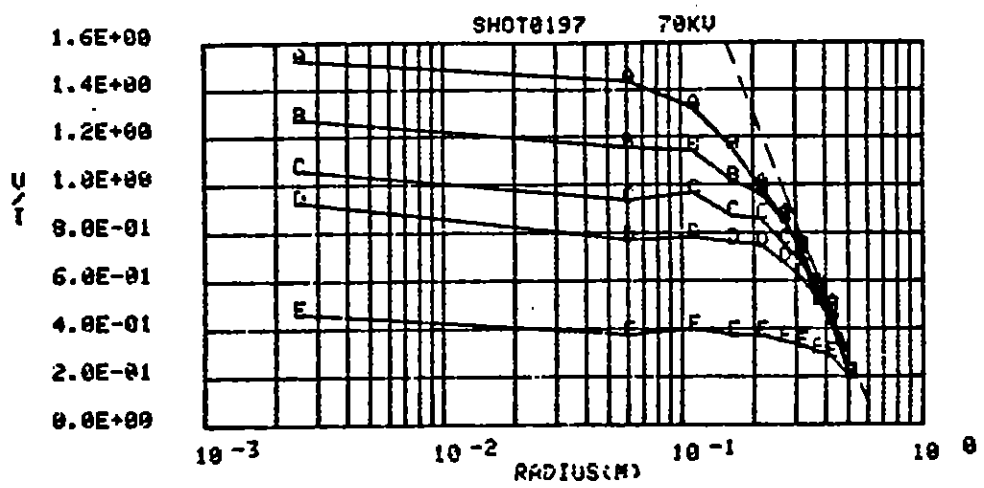

Code	A	B	C	D	E
Time	40 μs	70 μs	110 μs	150 μs	190 μs
Current	50.0	57.5	65.0	72.5	132.5

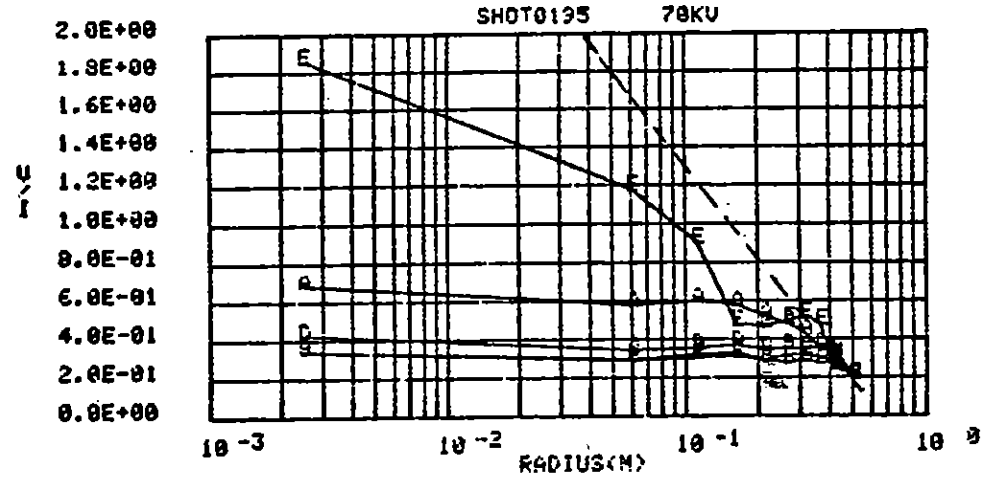

Code	A	B	C	D	E
Time	100 μs	200 μs	300 μs	500 μs	900 μs
Current	105.0	155.0	105.0	42.5	5.0

(b) 0.0025 mR center conductor

Figure 125. Concluded.

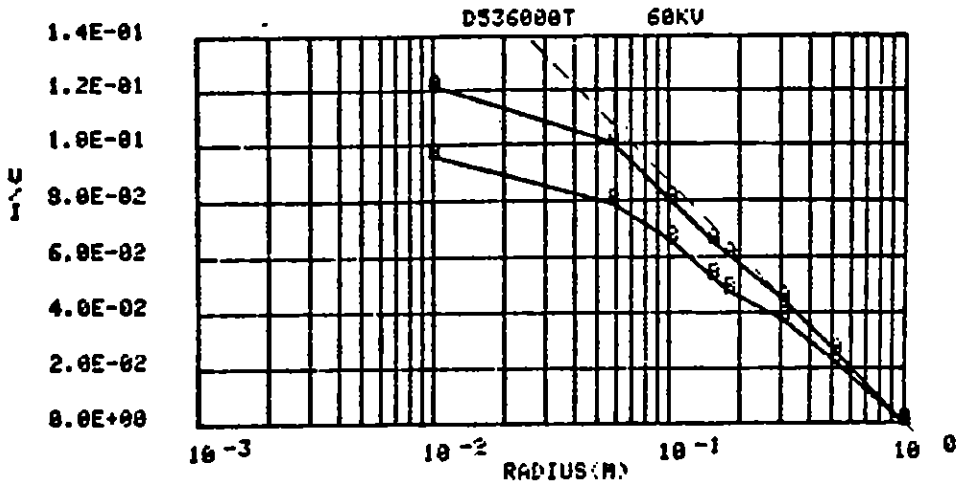

Code	A	B
Time	30 µs	50 µs
Current	500.0	625.0

(a) 0° top

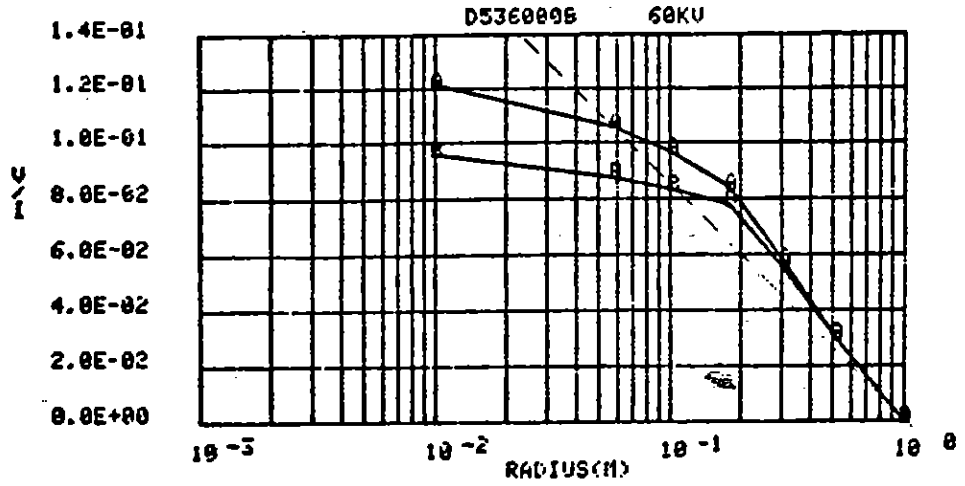

Code	A	B
Time	30 µs	50 µs
Current	500.0	625.0

(b) 0° bottom

Figure 126. Voltage profile. (300 Ωm sand mix 360° x 1 mL)

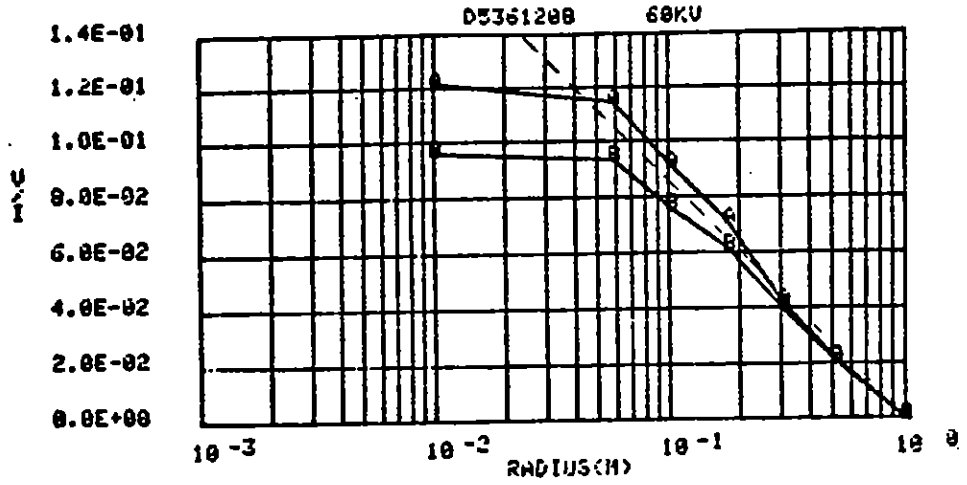

Code	A	B
Time	30 μs	50 μs
Current	500.0	625.0

(c) 120° bottom

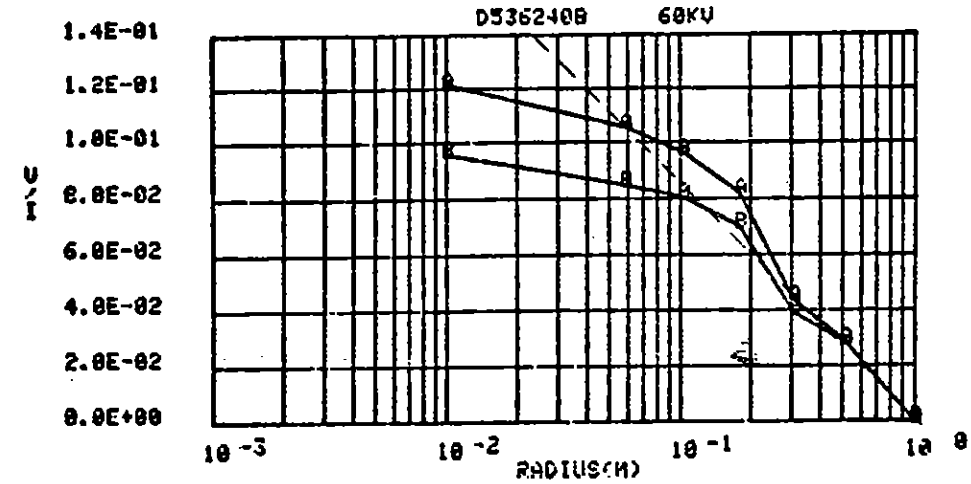

Code	A	B
Time	30 μs	50 μs
Current	500.0	625.0

(d) 240° bottom

Figure 126. Concluded.

sector during the 60-kV shots. That interpretation is supported by the voltage probes. Crude indications from the curvature of the voltage probe records are that the nonlinear conductivity is evidenced in the 0° top and 120° bottom sectors out to about 0.05 m, and in the 0° and 240° bottom sectors out to about 0.2 m.

The voltage profiles observed with 60 kV applied and a 0.003-m-radius center rod are shown in Figure 127. In this case, the time to arc-over was 1200 μs, which was much greater than the values given above. Even at 72-kV arc-over occurred at 270 μs; therefore, the evidence indicates that, with the smaller diameter center conductor, the streamer structure is stable up to higher voltages and longer times than with the larger diameter central rod. The voltage profiles shown in Figure 127 are somewhat similar to those in Figure 126 in that the 0° top sector appears to be drawing less than its share of current. The 120° bottom sector has its share, and the 0° and 240° bottom sectors carry more than their proportionate share. It is noteworthy that, at the later times, the impedance within the inner regions (< 0.1 m) is falling to an extremely low value at all positions. This is probably responsible for the increased stability, since a uniform streamer structure extending out to distances of less than 0.3 m would be expected to be stable, but an isolated conducting protrusion would be unstable at much shorter lengths.

This comparison indicates that, with the smaller-diameter central rod in the larger area McAir experiments, a more uniform density of streamering was produced, even though there is still an obvious bias toward producing an arc in the 300° sector near the bottom of the sample.

Sample Holder Size

During the PI experiments, a number of comparisons of response were made for different size soil-containing sectors. In order to conserve

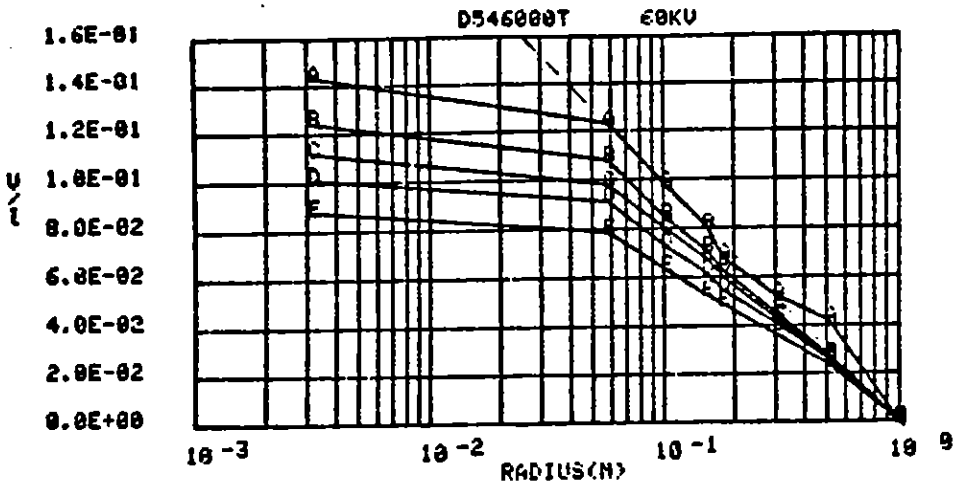

Code	A	B	C	D	E
Time	20 μs	40 μs	70 μs	110 μs	160 μs
Current	400.0	475.0	512.5	550.0	612.5

(a) 0° top

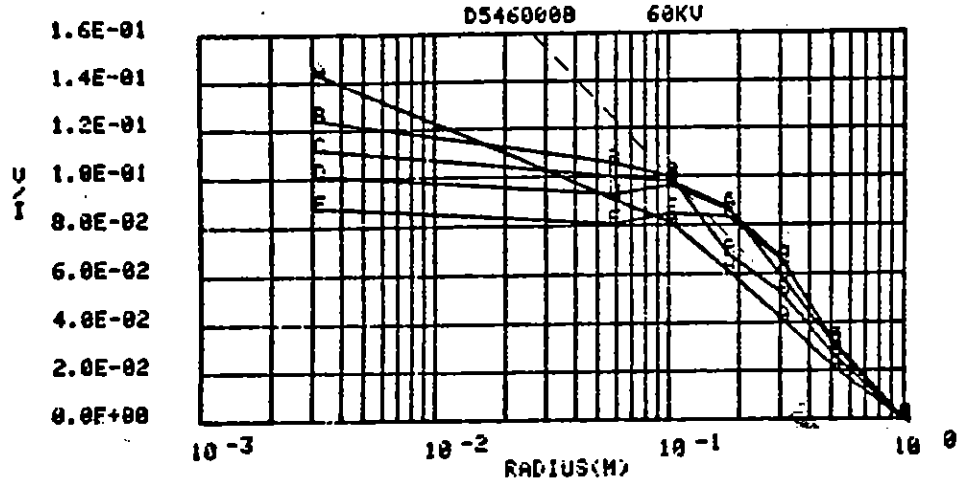

Code	A	B	C	D	E
Time	20 μs	40 μs	70 μs	110 μs	160 μs
Current	400.0	475.0	512.5	550.0	612.5

(b) 0° bottom

Figure 127. Voltage profile.
(300 Ωm sand mix
360° x 1 m x (0.003-1) mR
t_B = 1200 μs)

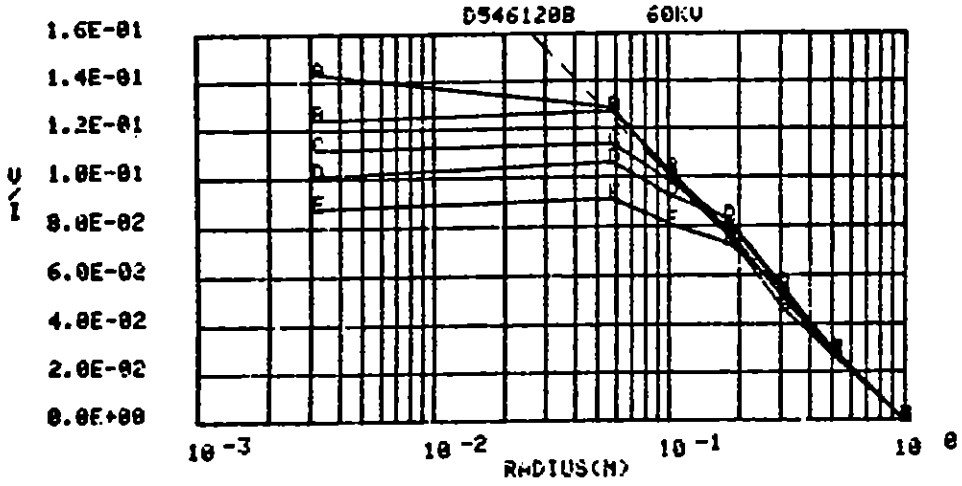

Code	A	B	C	D	E
Time	20 s	40 s	70 s	110 s	160 s
Current	400.0	475.0	512.5	550.0	612.5

(c) 120° bottom

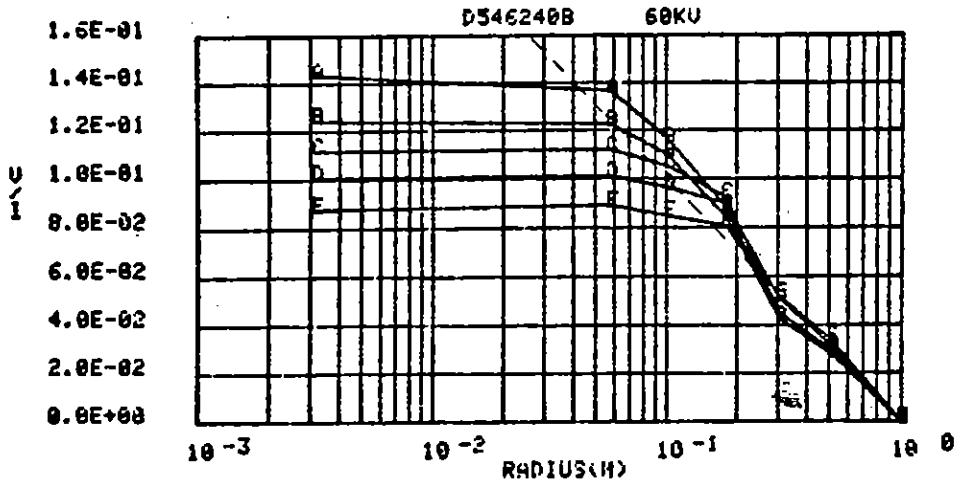

Code	A	B	C	D	E
Time	20 s	40 s	70 s	110 s	160 s
Current	400.0	475.0	512.5	550.0	612.5

(d) 240° bottom

Figure 127. Concluded.

the charge available from the pulser and to be able to use limited soil sample sizes, it was desirable to conduct experiments with the smallest possible sector. However, there is a danger that, in constraining the streamer structure to a small geometry, its characteristics might be different from those exhibited by a larger sample. The majority of the comparisons were performed in high resistivity sand (2,000 to 10,000 Ωm). One comparison between two different sector lengths of sample was performed with the 350 Ωm sand mixture.

Figures 128 through 133 illustrate the voltage profiles for a variety of sectors in high-resistivity sand. Figures 134 and 135 present the profiles for the 350 Ωm sand mixture for a 90° sector with 0.5 m outer radius and a length of 0.3 and 0.1 m, respectively. During some of the earlier experiments with high-resistivity soil, the resistivity gradually increased with time. Therefore, some of the geometry comparisons are confused by resistivity changes.

Comparing Figures 128 and 129, it can be seen that the potential profile is slightly more rounded with the longer sample; other than that, the apparent streamer impedance appears essentially the same. The increased rounding could be a manifestation of a possible increased separation between the voltage probes and the streamer location in the larger geometry.

Turning to the 30° sectors illustrated in Figures 130 and 131, it is clear that the effective impedance, even in the streamer region, is considerably greater than in the 90° geometries illustrated in Figures 128 and 129. Also, in the 0.1-m-long sample, there appears to be a very high contact impedance. For these reasons no further experiments were performed with 30° sectors.

Figures 132 and 133 represent profiles in the geometry that were used for the majority of the experiments, namely a 90° sector with 0.5 m

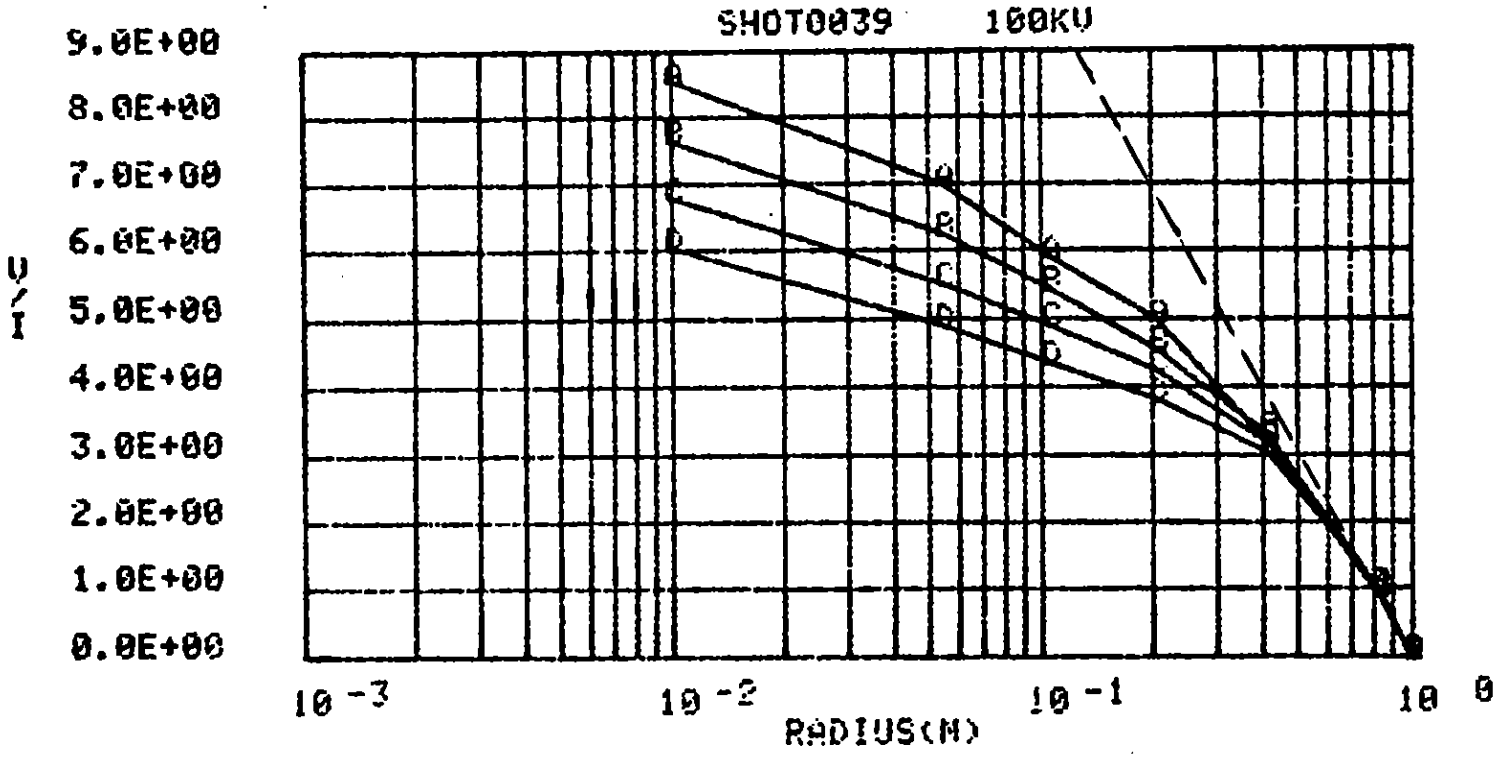

CODE	A	B	C	D
TIME	40 μs	70 μs	110 μs	190 μs
CURRENT	13.0	14.0	15.3	16.5

Figure 128. Voltage profile.
(2000 Ωm sand
90° x 0.3 mL x (0.01-1) mR)

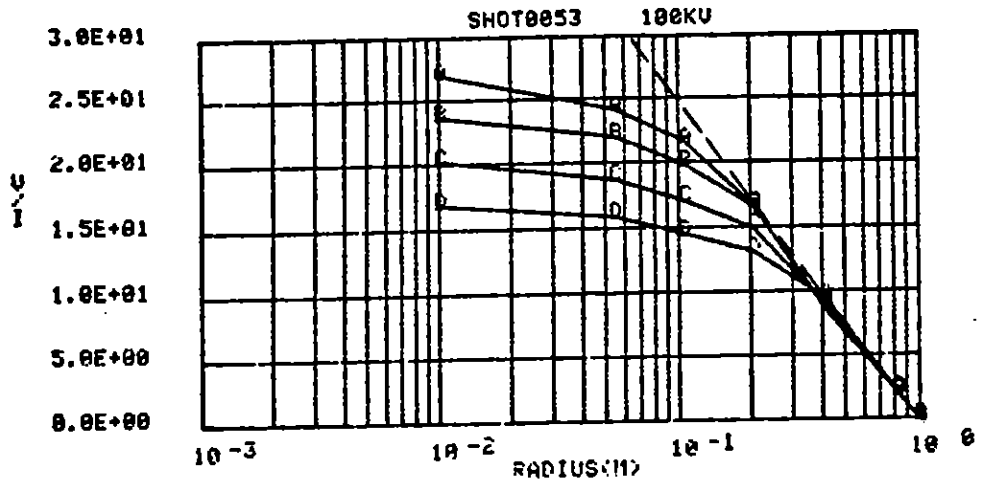

Code	A	B	C	D
Time	40 µs	70 µs	110 µs	190 µs
Current	3.8	4.1	4.8	5.5

Figure 129. Voltage profile.
(3400 Ωm sand
90° x 0.1 mL x (0.01-1) mR)

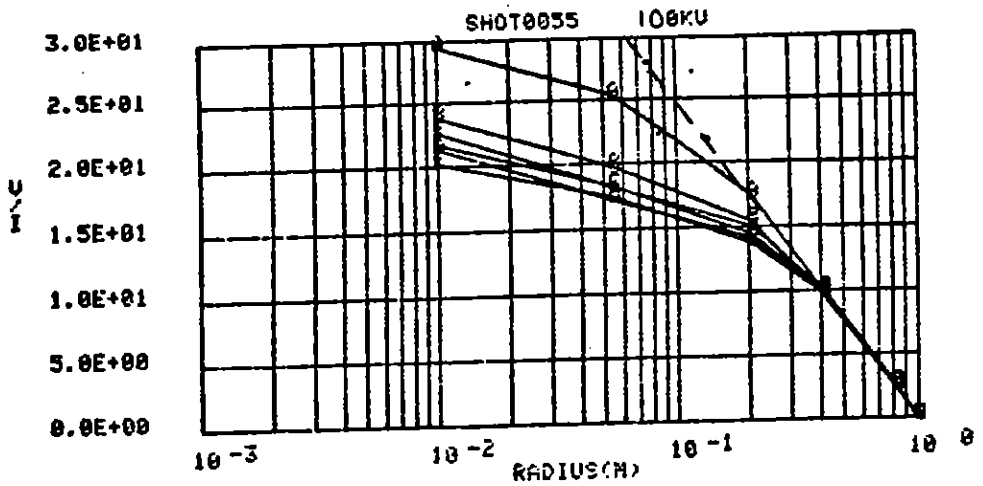

Code	A	B	C	D	E	F
Time	100 s	200 s	300 s	500 s	900 s	1900 s
Current	3.5	4.3	4.5	4.5	4.3	3.3

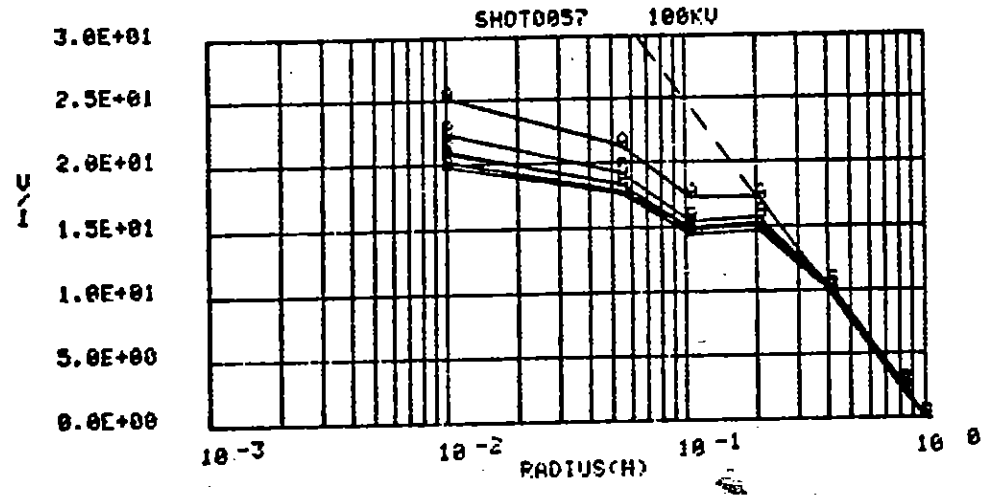

Code	A	B	C	D	E	F
Time	100 s	200 s	300 s	500 s	900 s	1900 s
Current	4.3	4.6	4.8	4.8	4.3	3.5

Figure 129. Concluded.

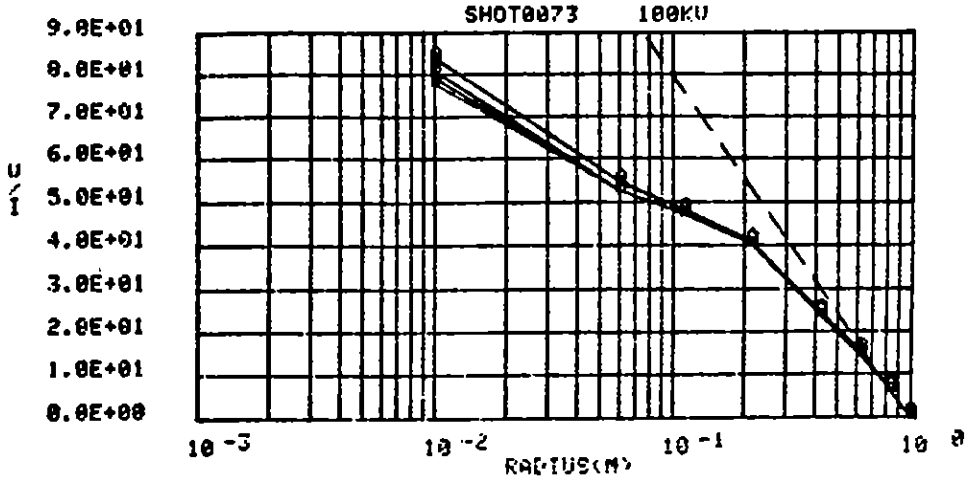

Code	A	B	C	D
Time	40 µs	70 µs	110 µs	190 µs
Current	1.3	1.4	1.4	1.4

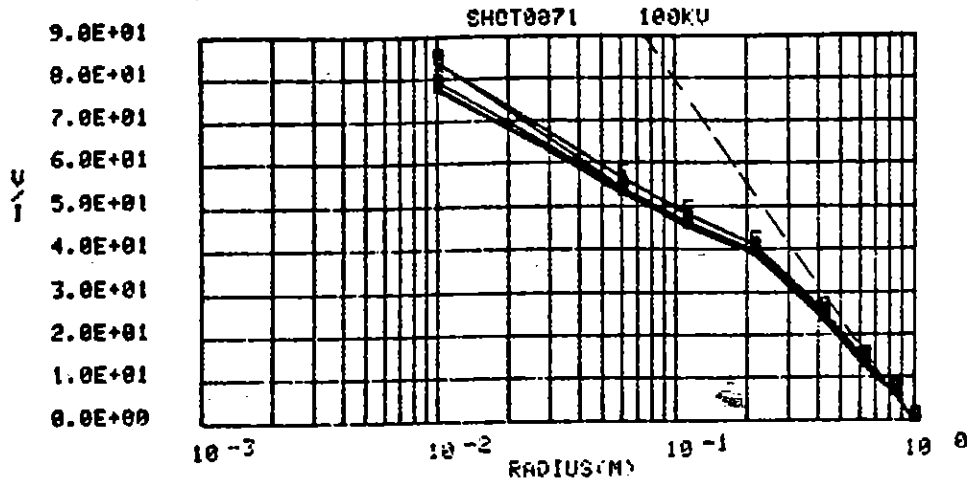

Code	A	B	C	D	E	F
Time	100 µs	200 µs	300 µs	500 µs	900 µs	1900 µs
Current	1.3	1.3	1.3	1.3	1.2	0.9

Figure 130. Voltage profile.
(5500 Ωm sand
30° x 0.1 mL x (0.01-1) mR)

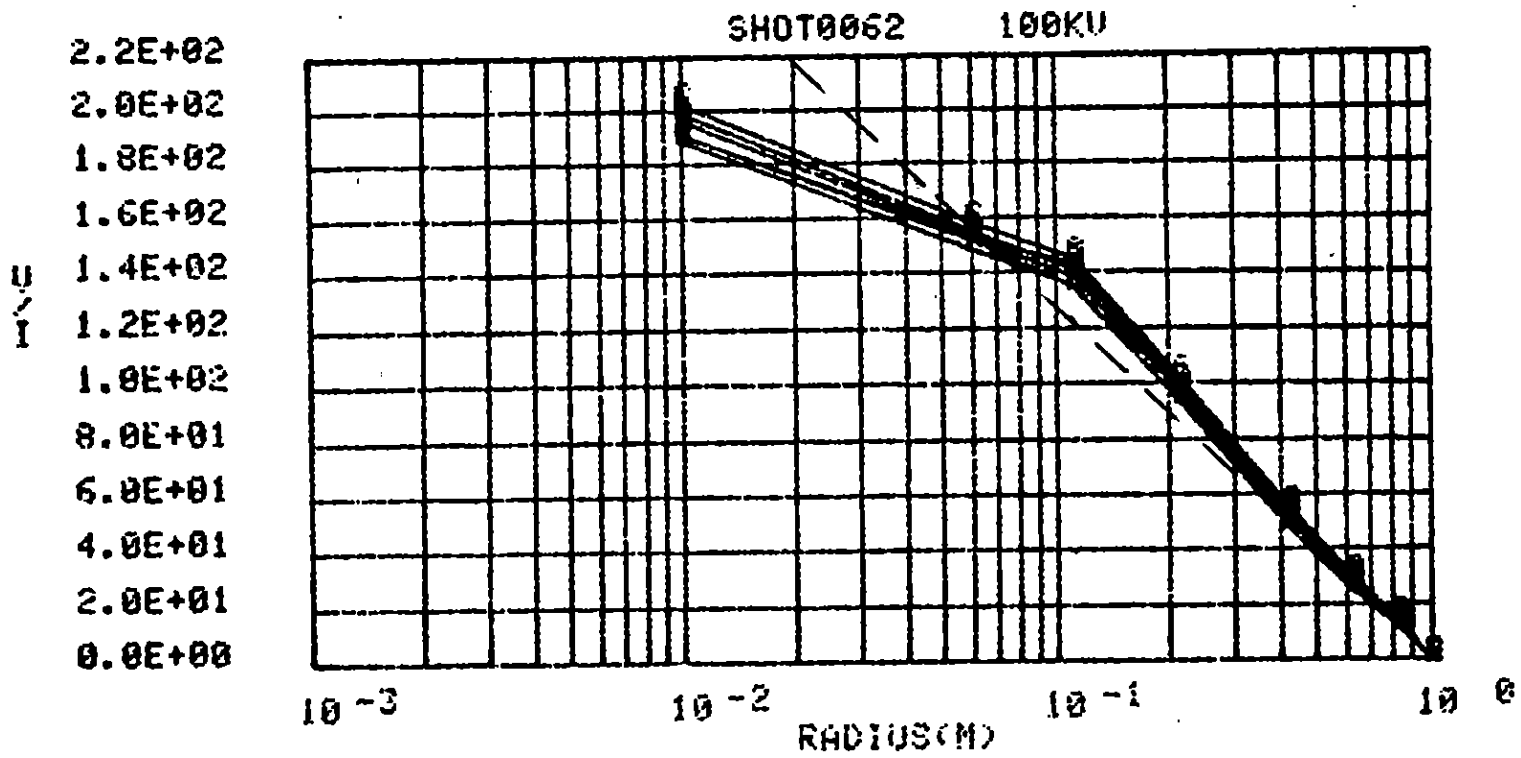

CODE	A	B	C	D	E	F
TIME	100 µs	200 µs	300 µs	500 µs	900 µs	1900 µs
CURRENT	0.6	0.5	0.5	0.5	0.5	0.4

Figure 131. Voltage profile.
(2800 Ωm sand
30° x 0.1 mL x (0.01-1) mR)

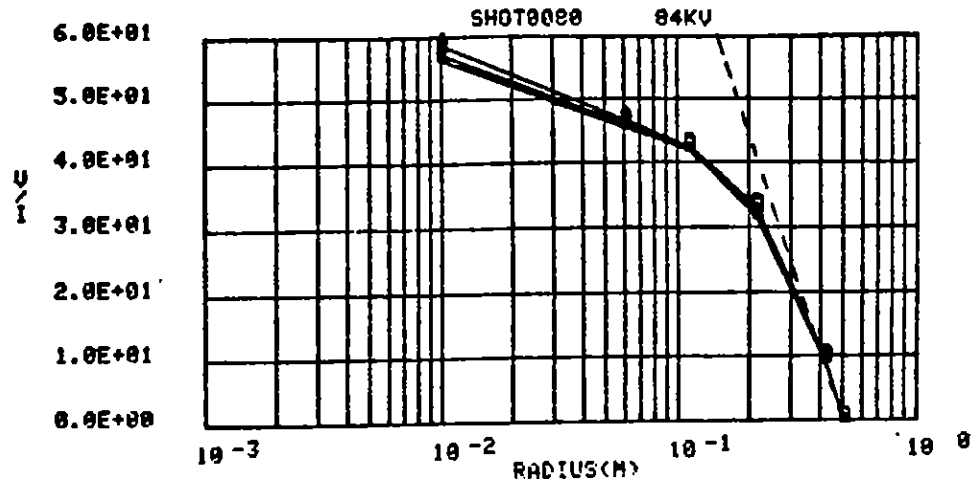

Code	A	B	C	D
Time	40 µs	70 µs	110 µs	190 µs
Current	1.55	1.55	1.53	1.50

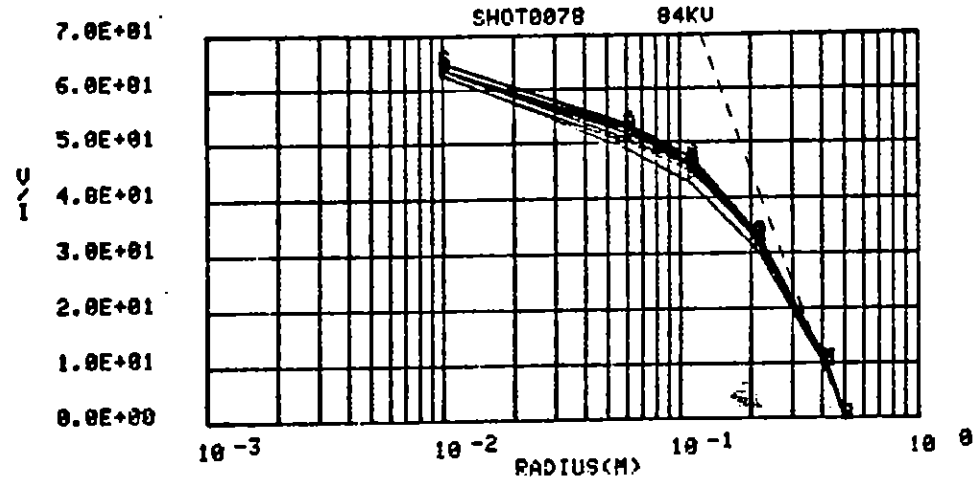

Code	A	B	C	D	E	F
Time	100 µs	200 µs	300 µs	500 µs	900 µs	1900 µs
Current	1.40	1.35	1.30	1.30	1.25	1.10

Figure 132. Voltage profile.
(7700 Ωm sand
90° x 0.1 mL x (0.01-1) mR)

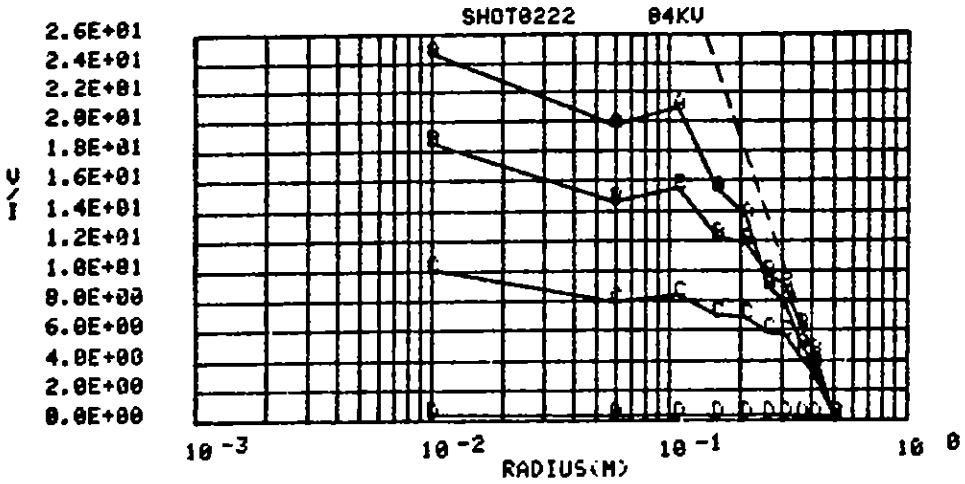

Code	A	B	C	D
Time	40 µs	70 µs	90 µs	150 µs
Current	3.8	5.0	0.8	190.0

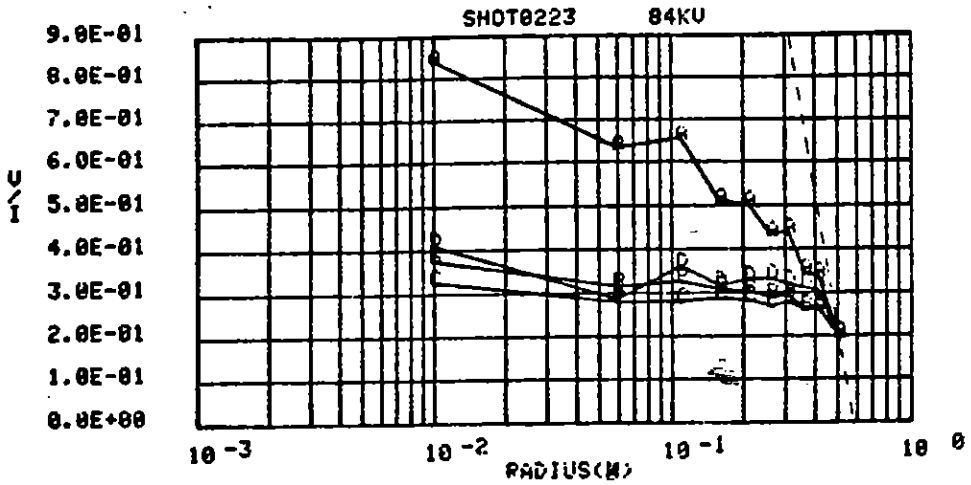

Code	A	B	D	D
Time	125 µs	175 µs	225 µs	450 µs
Current	110.0	200.0	190.0	60.0

Figure 133. Voltage profile.
(3300 Ωm sand
90° x 0.1 mL x (0.01-0.5) mR)

outer radius and 0.1 m length. By the time shot 78 was fired (Fig. 132), the resistivity of the sample had increased to 7,000 Ωm. Another sample of the same sand was mixed with water to a resistivity of 3,000 Ωm and the profile of this sample is shown in Figure 133. It is obvious that the lower resisitivity medium exhibits much faster arc-over, as was observed in the materials comparisons discussed in Section III, paragraph 7. In general, the geometry with the 0.5-m outer radius exhibits very similar behavior to the 1-m-radius experiments shown in Figures 128 and 129.

Another comparison between a 0.3-m-long and 0.1-m-long sample is shown for the 350-Ωm sand mix in Figures 134 and 135. It appears that the 0.1-m sample arcs over slightly more easily than the 0.3-m sample, although the difference in behavior is no greater than that produced by a 10% change in applied voltage.

The conclusion from these comparisons is that within the range of sectors investigated at PI, the 30° sectors are unacceptable because of the large change in apparent impedance of the region in which streamers exist. The differences in response between the other variables (0.5-m versus 1-m outer-conductor radius, 0.1-m versus 0.3-m length) were judged to be small enough to justify the use of the 0.5-m-radius, 0.1-m-long sector for the majority of the PI experiments.

Comparison of the results at PI with those at McAir indicates, as discussed in previous subsections, that the fundamental impedance characteristics of the local earth are well represented by the small sector experiments with the following qualifications:

1. With small area electrodes, there appears to be a variable delay time before the initiation of the first detectable streamer. As the electrode area is increased, this delay appears to become shorter than the resolution time in these experiments.

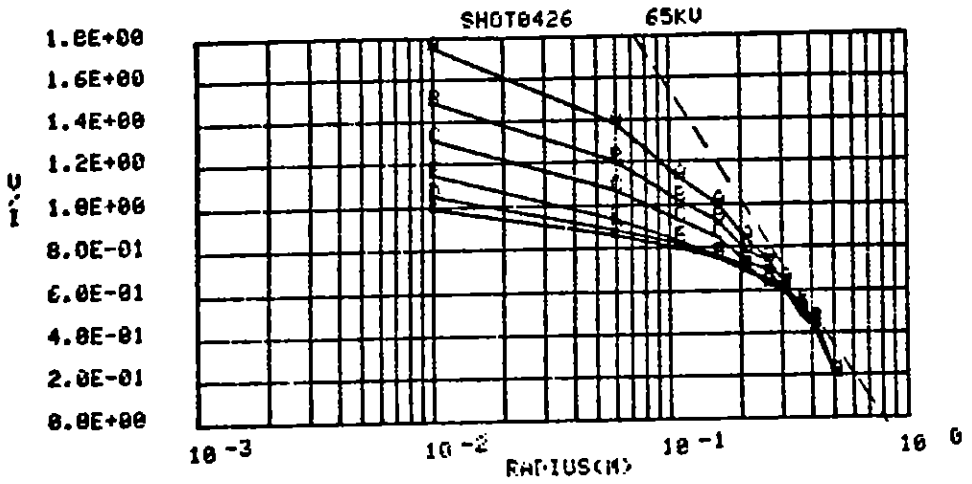

Code	A	B	C	D	E	F
Time	25 µs	50 µs	75 µs	175 µs	275 µs	475 µs
Current	40.0	45.0	50.0	55.0	50.0	35.0

Figure 134. Voltage profile.
(350 Ωm sand mix
90° x 0.3 mL x (0.01-0.5) mR)

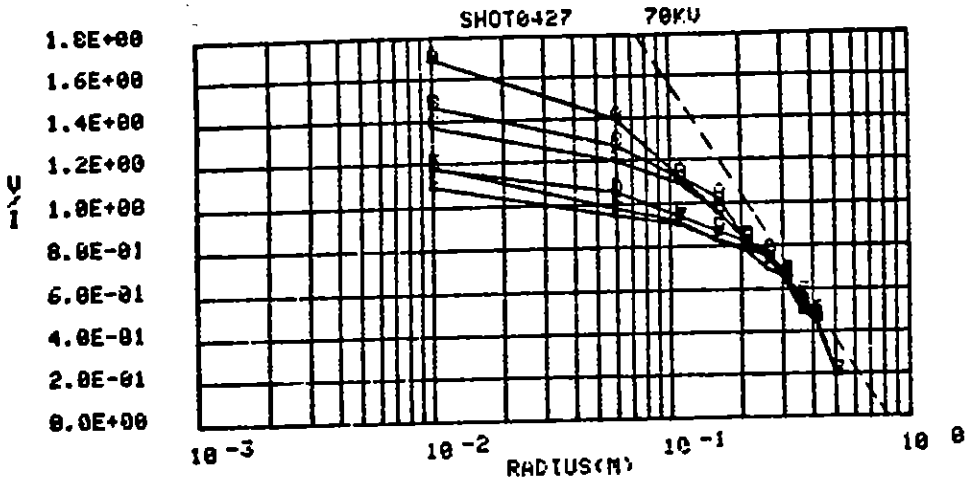

Code	A	B	C	D	E	F
Time	25 μs	50 μs	75 μs	175 μs	275 μs	475 μs
Current	45.0	50.0	51.3	52.5	50.0	37.5

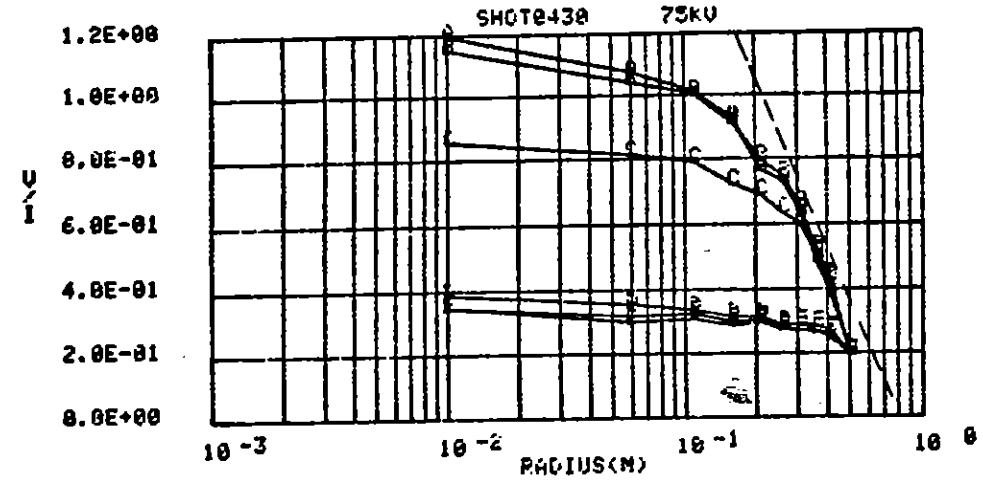

Code	A	B	C	D	E	F
Time	50 μs	75 μs	175 μs	225 μs	275 μs	475 μs
Current	65.0	65.0	75.0	150.0	140.0	70.0

Figure 134. Concluded.

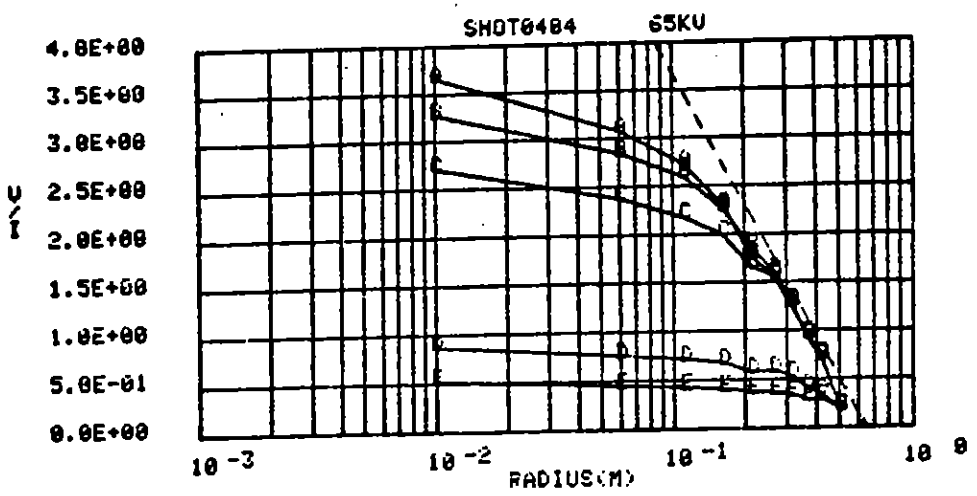

Code	A	B	C	D	E
Time	40 µs	70 µs	110 µs	170 µs	190 µs
Current	20.0	21.3	25.0	75.0	125.0

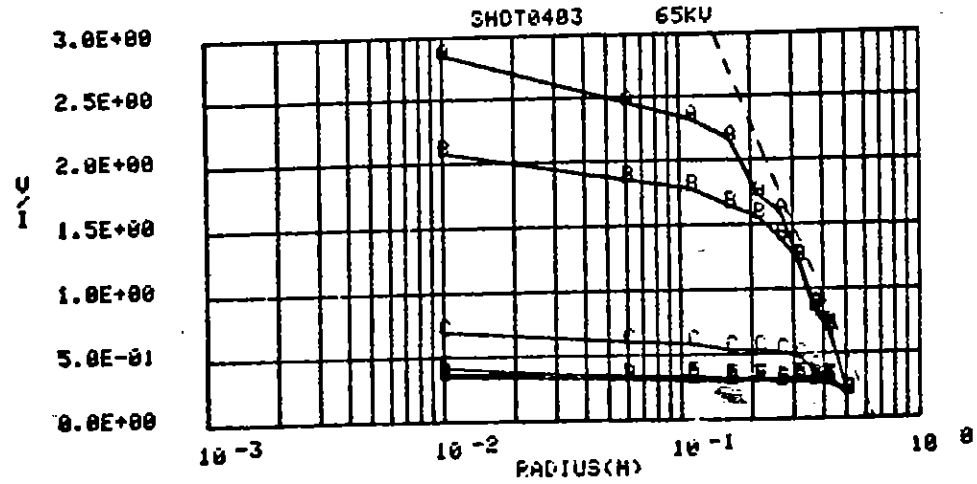

Code	A	B	C	D	E	F
Time	50 µs	100 µs	150 µs	200 µs	275 µs	475 µs
Current	25.0	32.5	95.0	153.0	130.0	53.5

Figure 135. Voltage profile.
(350 Ωm sand mix
90° x 0.1 mL x (0.01-0.5) mR)

2. In the large area 360° experiments, the inhomogeneity in the soil samples appeared to produce instability with respect to arc-over between electrodes at significantly lower applied voltages than observed in the sector experiments. When streamering was encouraged along the entire length of the center conductor by decreasing its radius, the instability behavior of the larger samples approached that of the sectored samples.

For these reasons, it is expected that:

1. The comparison of streamer characteristics between materials observed in the PI sectored experiments can be extrapolated to larger area geometries.
2. The circumstances existing in the application of a power line at a missile base, i.e., of a buried conductor with much larger voltage separated from other conductors by extremely large distances, is likely to be one in which there is a great deal of relatively uniform streamering around the conductor. The total current fed into the earth is likely to be shared among a very large number of streamers, thereby promoting stability. At present, this speculation does not have convincing evidence to support it; therefore, experiments on larger geometries at higher voltages will be required.
3. Experiments at larger geometry should allow significant increases in applied voltage for two reasons:

    a. An increase in ratio of outer and inner conductor radii produces an increase in distance for a streamer to move before it creates an instability.
    b. As the voltage is increased on the center conductor, the increased streamering tends to approximate more closely the case of a uniformly expanding cylindrical conductor.

APPENDIX A

CIRCUITS USED AT PI AND MCAIR

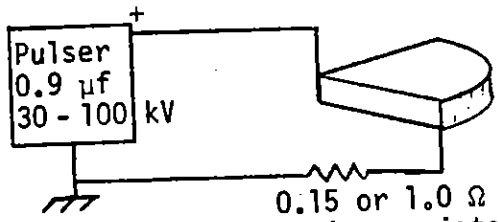

CIRCUIT USED AT PI

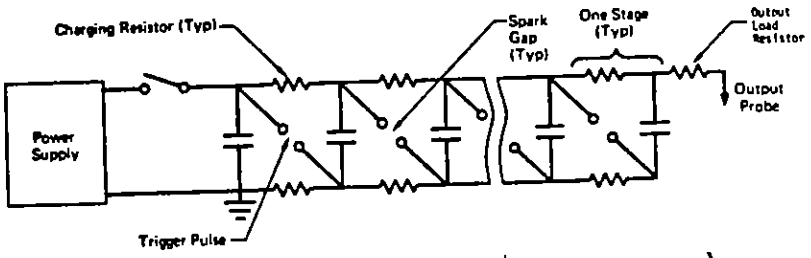

Basic MARX Generator Circuit (in Stages)
used at PI and McAir

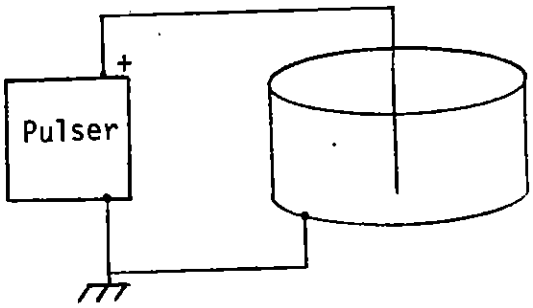

Circuit for radial drive
at McAir

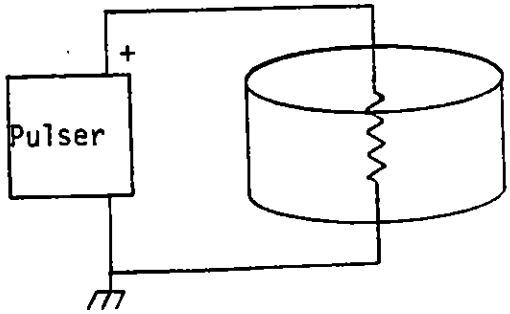

Circuit for axial drive
at McAir

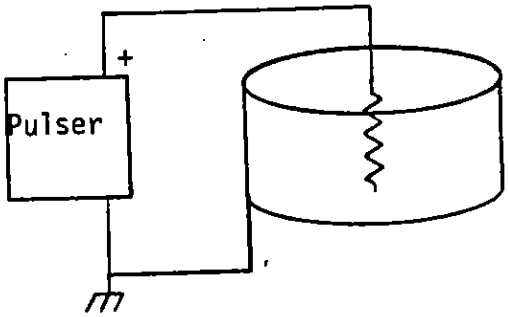

Circuit for self-bias
at McAir

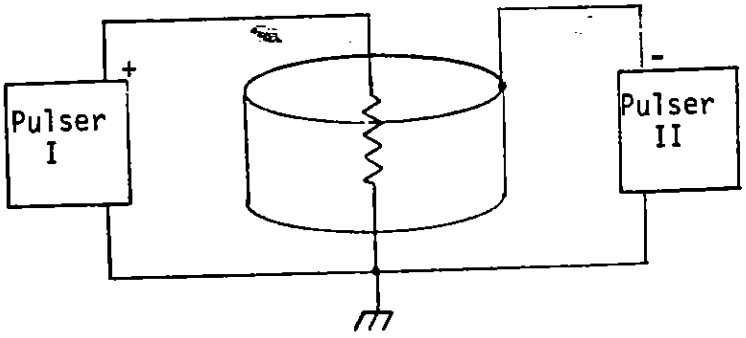

Circuit for combined drive at McAir

APPENDIX B
VOLTAGE PROBE RESPONSE TIME

Consider a voltage probe consisting of N series resistors of value R_S, terminated in a shunt resistor, R_T. The probe sensitivity is:

$$G = \frac{V_{OUT}}{V_{IN}} = \frac{R_T}{NR_S + R_T} \approx \frac{R_T}{NR_S}$$

Assume that the stray capacitance between the probe body and the external environment (assumed to be at ground potential) can be represented as a capacitance, C_S, per series resistor. There may also be a termination capacitance, C_T, which can be effectively eliminated by terminating the resistor string in a cable terminated in its characteristic impedance. Otherwise, the termination resistor and capacitance increases the response time by R_TC_T.

The resistor string can be represented by its equivalent circuit in Equation B1. Conservation of current at node(i) can be written as

$$\frac{\left(V_i - V_{i-1}\right)}{R_S} + C_S \frac{dV_i}{dt} = \frac{\left(V_{i+1} - V_i\right)}{R_S} \qquad \text{(B1)}$$

where V_i is the voltage at node(i). Rewriting

$$R_SC_S \frac{dV_i}{dt} - \left(V_{i+1} - 2V_i + V_{i-1}\right) = 0 \qquad \text{(B2)}$$

This equation is very similar to the discrete element approximation to a differential equation:

$$\tau_o \frac{\partial V_i}{\partial t} - \frac{\partial^2 V_i}{\partial x^2} = 0 \qquad \text{(B3)}$$

where
$$\frac{\partial^2 V_i}{\partial x^2} \approx \frac{V(x_{i+1}) - 2V(x_i) + V(x_{i-1})}{(\Delta x)^2} \qquad \text{(B4)}$$

The equations become identical as $\Delta x \to 1$, $\tau_o = R_S C_S$.

Equation B3 is the standard diffusion equation. Consider the initial condition $V(x,0) = 0$, subject to a step function input $V(0,t) = V_0$, $V(x = N,t) = 0$ (approximately the condition where $R_T \ll R_S$). The solution is

$$V = V_0 \left(1 - \frac{X}{N}\right) - \frac{2V_0}{\pi} \sum_{n=1}^{\infty} \frac{1}{n} \sin \frac{n\pi X}{N} \exp\left[-\frac{n^2\pi^2 t}{N^2 \tau_o}\right] \qquad \text{(B5)}$$

The first term is the steady state asymptotic solution; the second represents the transient. This transient is represented by an infinite series of response times, the longest of which determines the probe response τ_p,

$$\tau_p = \frac{N^2 R_S C_S}{\pi^2} \qquad \text{(B6)}$$

The tradeoffs in probe design are:

1. The voltage per resistor must be limited to the maximum value at which the resistor value is reproducible (not necessarily constant), $V_R(\max)$. Therefore, the number of resistor stages, N, is determined from the maximum voltage to be measured: $N = V_{IN}(\max)/V_R(\max)$.

2. The total resistance of the probe must be large enough that the probe diverts a negligible fraction of the current flowing past it. In other words, the probe resistance, NR_s, must be large compared to the spreading resistance around the probe in the earth. For a spherical probe tip of radius, r_t, in earth of resistivity, ρ_0,

$$R_s = \frac{k\rho_0}{4\pi N r_t}, \text{ where } k \gg 1 \qquad (B7)$$

3. The value of stray capacitance, C_s, is determined mostly by probe geometry and the dielectric constant of surrounding material.

Therefore, the probe response time is essentially determined by its maximum voltage capability and earth resistance.

$$\tau_p = \frac{V_{IN}(max)}{V_R(max)} \frac{k\rho_0}{4\pi^3 r_t} C_s \qquad (B8)$$

For a typical probe:

$V_{IN}(max) = 200$ kV
$V_R(max) = 5$ kV
$\rho_0 = 10^3$ Ωm
$r_t = 2 \times 10^{-3}$ m
$k = 10$
$C_s = 0.5$ pF

and thus

$R_s = 20\ k\Omega$

$N = 40$

$\tau_p = 1.6\ \mu s$